Characterisation of the effective thermal conductivity in the near-wall region of a packed pebble bed

M de Beer

orcid.org / 0000-0003-4072-0494

Thesis accepted in fulfillment of the requirements for the degree *Doctor of Philosophy* in *Mechanical Engineering* at the North-West University

Promoter: Prof CG du Toit
Co-promoter: Prof PG Rousseau

Graduation: August 2021
Student number: 21707588

Acknowledgements

Firstly, I would like to thank my Heavenly Father for the opportunities, abilities, strength, endurance, and His unending love. I know that it is only by His grace that the completion of this study was possible. I would also like to thank my two supervisors Prof. C.G. (Jat) Du Toit and Prof. P.G. (Pieter) Rousseau, thank you for your guidance, patience, and support throughout the study. I am very grateful for the experience and knowledge gained from such insightful leaders. Finally, I would like to thank my husband and parents for their unconditional love, support and understanding. They always showed an interest in my work and helped in whichever way they could.

"Action is the foundational key to all success."
Pablo Picasso

Abstract

The effective thermal conductivity is an important parameter that is representative of the overall heat transfer in a packed bed of spheres. An accurate prediction of the effective thermal conductivity is necessary for the design and analysis of packed pebble bed gas-cooled reactors, especially when considering the safety case. The wall effect present in the near-wall region affects the conduction and radiation heat transfer in this region.

Various correlations and models exist to predict the effective thermal conductivity. However, most of these are only applicable to the bulk region and fail to accurately predict the heat transfer in the near-wall region. The effective thermal conductivity trend is marked by a prominent reduction in the near-wall region followed by a characteristic “peaks-and-dip” trend which can be observed in the High Temperature Test Unit (HTTU) and SANA-I experimental results.

The objective of this study is to develop a methodology which can be used to gain insight into the characteristics of the conduction and radiation heat transfer in the near-wall region of a packed pebble bed. The methodology entails experimental and numerical work to separate the conduction and radiation components of the heat transfer. This allows one to observe the interplay between the heat transfer phenomena and the resulting effect on the overall effective thermal conductivity trend.

The Near-wall Thermal Conductivity Test Facility (NWTCTF) was used to gather the temperature and heat transfer distributions through a packed bed for different packing configurations namely Simple Cubic (SC), Body Centred Cubic (BCC) and random. From the experimental results the effective thermal conductivity was derived. A Computational Fluid Dynamics (CFD) model was set up for a numerically packed bed that is representative of the experimental packed bed. The numerical heat transfer results were obtained by using the CFD model. The CFD model can be calibrated by adjusting the contact resistance values at the solid-solid interfaces of the pebble-pebble and pebble-wall contact points in the packed bed.

Results were obtained by applying the developed methodology and separating the conduction and radiation components of the effective thermal conductivity. From the results, one can observe the interplay between the contributing heat transfer phenomena and the resulting effect on the “peaks-and-dip” trend of the overall effective thermal conductivity.

Keywords: Effective thermal conductivity, Packed pebble bed, Near-wall effect, Thermal conduction, Thermal radiation, Experimental investigation, Computational Fluid Dynamics

Preface

This is to state the I, Maritza de Beer, have chosen the article format for submitting my thesis.

The work was done by myself, Maritza de Beer, with editing done and suggestions given by Prof CG Du Toit and Prof PG Rousseau as promoters of my PhD and co-authors of all the papers.

Author affiliations:

- *Maritza de Beer*
  School of Mechanical Engineering, North-West University, Potchefstroom, South Africa

- *Prof CG Du Toit*
  Unit for Energy and Technology Systems, North-West University, Potchefstroom, South Africa

- *Prof PG Rousseau*
  Department of Mechanical Engineering, University of Cape Town, Rondebosch, South Africa

Articles 1 to 3 have been published in the journal, **Nuclear Engineering and Design**, and article 4 has been prepared for submission to the same journal.

List of publications:

1. Article 1 - De Beer, M., Rousseau, P.G. & Du Toit, C.G. 2018. A review of methods to predict the effective thermal conductivity of packed pebble beds, with emphasis on the near-wall region. *Nuclear Engineering and Design*, 331:248-262.

2. Article 2 - De Beer, M., Du Toit, C.G. & Rousseau, P.G. 2018. Experimental study of the effective thermal conductivity in the near-wall region of a packed pebble bed. *Nuclear Engineering and Design*, 339:253-268.

3. Article 3 - De Beer, M., Du Toit, C.G. & Rousseau, P.G. 2017. A methodology to investigate the contribution of conduction and radiation heat transfer to the effective thermal conductivity of packed graphite pebble beds, including the wall effect. *Nuclear Engineering and Design*, 314:67-81.

Guidelines for authors available at:
https://www.elsevier.com/journals/nuclear-engineering-and-design/0029-5493/guide-for-authors

For the sake of uniformity of the thesis, the text is not in the preferred font and size of the journal. The thesis is written in South African English, whereas all the articles were written in American English.

Permissions:

I, Prof CG Du Toit, hereby give my permission to Maritza de Beer, to submit the publications of which I am the co-author for degree purposes.

I, Prof PG Rousseau, hereby give my permission to Maritza de Beer, to submit the publications of which I am the co-author for degree purposes.

Acknowledgement of articles:

The following acknowledgement is omitted from the articles presented in the thesis for the ease of reading.

This work is based upon research supported by the South African Research Chairs Initiative of the Department of Science and Technology and National Research Foundation (Grant No. 61059). Any opinion, finding and conclusion or recommendation expressed in this material is that of the author(s) and the NRF does not accept any liability in this regard.

Table of Contents

1. Introduction

1.1 Background

The world will continuously be faced with an increasing energy demand in the future due to the growth in its population and economy, together with the effect of rapid urbanisation. A need especially exists to produce clean energy and there is an increased interest in the expansion of nuclear power's role in the development of sustainable future energy systems (World Nuclear Association, 2020a). High temperature gas-cooled reactors (HTGRs) are generation IV type reactors that form an important part of the nuclear technology solution, as they can provide electricity cost effectively and efficiently and produce high-temperature process heat which can be used for various thermal-fluid industrial applications (World Nuclear Association, 2020b).

Pebble bed gas-cooled reactors (PBRs) and fluoride salt-cooled high-temperature reactors (FHRs) are two generation IV type reactors that utilize energy transfer through randomly packed beds in their design. One of the key design features of these reactors are their inherent safety characteristics which do not rely on active engineered safety systems during accident conditions (World Nuclear Association, 2020b). The effective thermal conductivity is an important parameter that is representative of the overall heat transfer through a packed pebble bed. In order to obtain a PBR design with the desired safety characteristics one must have a thorough understanding of the contributing heat transfer phenomena as well as the interaction between the heat transfer mechanisms for different temperatures and packing structures, to be able to accurately predict amongst others the effective thermal conductivity (Van Antwerpen *et al.*, 2010; Zhou *et al.*, 2007; Zhou *et al.*, 2010; You *et al.*, 2017).

Conduction and thermal radiation become the dominant heat transfer mechanisms for decay heat removal when considering the safety case of a PBR during a depressurized loss of forced coolant incident (Van Antwerpen *et al.*, 2010; You *et al.*, 2017). The effective thermal conductivity consists of four components: (1) conduction through the pebble material itself, k_e^s, (2) conduction through the stagnant gas, k_e^g, (3) conduction through physical contact points and contact surfaces of the solid materials, k_e^c, and (4) thermal radiation between solid surfaces, k_e^r (Van Antwerpen *et al.*, 2010). The total effective thermal conductivity of the packed bed can be given by the super positioning of the four components as shown in Eq. (1):

$$k_{eff} = k_e^s + k_e^g + k_e^c + k_e^r \tag{1}$$

The contribution of radiation heat transfer to the overall effective thermal conductivity becomes significant at higher temperatures, above approximately 650 °C (Breitbach & Barthels, 1980; Zhou *et al.*, 2007; Cheng & Yu, 2013; Talukdar *et al.*, 2013). Temperatures of up to 1600 °C can be expected in a PBR during accident conditions (Breitbach & Barthels, 1980; Rousseau & Van Staden, 2008). For temperatures of about 800 °C and higher radiation is the dominant heat transfer mechanism in a packed pebble bed.

Three main regions can be identified in the geometry of a randomly packed bed namely the bulk, near-wall, and wall regions. In a randomly packed pebble bed, the packing structure is disrupted in the area near any wall and as a result the porous structure in this region changes significantly (Van Antwerpen *et al.*, 2010; 2012). This variation in packing structure is known as the wall effect and influences the magnitude of the effective thermal conductivity in the wall region, which includes the pebble to reflector interface. The near-wall region forms a part of the critical path for decay heat removal during a loss of forced coolant event in a PBR. During such an event the radiative and conductive effects in the near-wall region will become prominent and an accurate prediction of the effective thermal conductivity in this region becomes important.

Van Antwerpen *et al*. (2010) presented a thorough review of literature that describes the packing structure as well as the different methodologies used to predict the effective thermal conductivity in randomly packed beds of mono-sized spherical particles. From their review they concluded that the correlations developed by Schlünder and co-workers (Zehner & Schlünder, 1970; Zehner & Schlünder, 1972; Bauer & Schlünder, 1978) as well as Breitbach & Barthels (1980) are the methods most commonly used in the nuclear field with application to high temperature gas-cooled reactors.

Experimental studies were conducted with the SANA-I test facility (Niessen & Ball, 2000) and the High Temperature Test Unit (HTTU) (Rousseau *et al.*, 2014) to investigate the effective thermal conductivity in high temperature PBRs. The randomly packed bed for both test facilities consisted of graphite pebbles with a diameter of 60 mm. The experimental tests conducted with the SANA-I test facility were performed in a helium environment at atmospheric pressure, whereas the HTTU tests were performed in a near-vacuum nitrogen environment. The results obtained for both experimental studies showed a significant reduction in the bed effective thermal conductivity in the near-wall region.

As a part of the SANA benchmark problems Niessen & Ball (2000) proposed the summation of three different existing correlations to simulate the overall effective thermal conductivity through the pebble bed in a stagnant gas environment. The three correlations used in the summation

are (1) the ZS correlation for conduction through the solid and gas phases (Zehner & Schlünder, 1970), (2) the Kaviany (1991) model to account for conduction through the contact area and (3) the Breitbach & Barthels (1980) correlation for thermal radiation. Van Antwerpen *et al*. (2012) referred to this combination of correlations as the IAEA (International Atomic Energy Agency) ZS Total model, which can be regarded as being representative of the most current version of the original ZS model.

Van Antwerpen and co-workers (2009; 2012), compared values predicted by the IAEA ZS Total correlation as a function of position with measurements from the SANA-I and HTTU test facilities. Further analyses were done in the current study to also compare values predicted by the original ZBS correlation with the measurements from the SANA-I and HTTU test facilities, as shown in Fig. 1 and Fig. 2 respectively. The effective thermal conductivity is shown as a function of the distance from the inner wall expressed in number of sphere diameters.

As can be seen in Fig. 1 both the ZBS and the IAEA ZS Total correlations failed to capture the wall effects in the SANA-I packed bed. This observation is similar to the findings of Van Antwerpen and colleagues (Van Antwerpen *et al.*, 2012), namely that the IAEA ZS Total correlation is not valid in the near-wall region. For the HTTU test facility, Fig. 2, the IAEA ZS Total predicted effective thermal conductivity values for the bulk region are in better agreement with the experimental results. However, both the ZBS and IAEA ZS Total correlations again fail to predict the correct trend of the effective thermal conductivity in the near-wall regions.

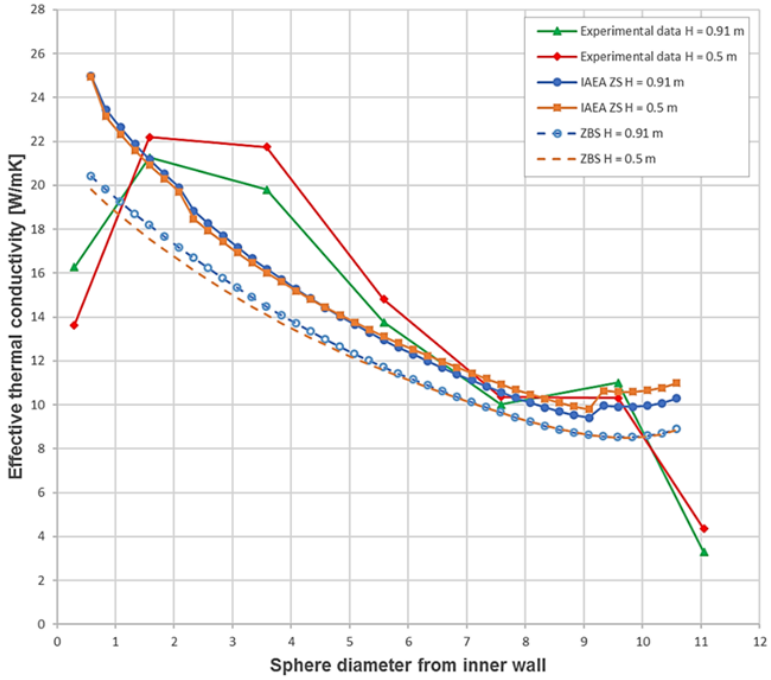

Fig. 1 Comparison between ZBS and IAEA ZS Total effective thermal conductivity correlations and the experimental results of the SANA-I experimental test facility for the 35 kW steady state test.

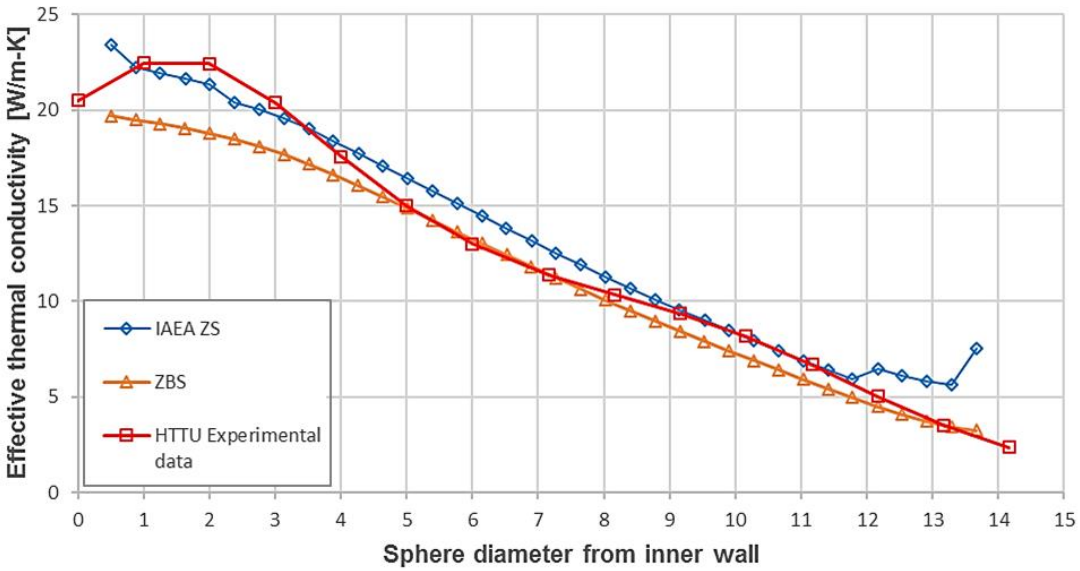

Fig. 2 Comparison between ZBS and IAEA ZS Total effective thermal conductivity correlations and the experimental results of the HTTU experimental test facility for the 82 kW steady state test.

From the results presented in Figs. 1 and 2 it is clear that the widely accepted and applied correlations from the Zehner & Schlünder collection fail to predict the correct values or correct trends of the effective thermal conductivity in the near-wall region. Thus, one should be very careful when using these correlations, which were originally intended for the bulk region, in the near-wall region.

It is therefore important to gain a better fundamental understanding of the conduction and radiation heat transfer phenomena in the near-wall region, in order to develop correlations and models which can be applied to the near-wall region and accurately represent the effective thermal conductivity trend due to the wall effects. A method that also enables one to separate out the individual contributions of conduction and radiation to the total effective thermal conductivity can be useful to gain a better understanding of the phenomena and the interaction between them.

1.2 Problem statement

Various experimental, analytical, and numerical methods have been used to study and predict the effective thermal conductivity of packed pebble beds. However, not all the studies consider the critical near-wall region in the packed bed of spheres and some studies neglect the contribution of radiation heat transfer. This is problematic when considering the PBR safety case as very high temperatures are present during upset conditions and the near-wall region forms part of the critical path for decay heat removal.

The development of a comprehensive model for the effective thermal conductivity should be based on a better understanding of the underlying phenomena and the interplay between them, especially in the near-wall region. Some studies reported in literature distinguish between the different heat transfer contributions, but do not necessarily investigate the underlying phenomena and interactions. A need exists for the ability to separate the contributions of the different heat transfer mechanisms as it can provide valuable insights into the characteristics observed due to the wall effects.

Aims of the thesis:

The primary objective of the study is to develop a methodology which can be used to gain insight into the characteristics of the conduction and radiation heat transfer in the near-wall region of a packed pebble bed. Insight into the characterisation of the effective thermal conductivity can be obtained by applying the proposed methodology to separate the conduction and radiation components of the heat transfer in the near-wall region, thus allowing one to observe the interplay between the heat transfer phenomena and the resulting effect on the overall effective thermal conductivity trend.

The current study is an extension of the work done in the dissertation by De Beer (2014). A revised version of the methodology proposed in the dissertation study is developed which combines experimental and numerical work to characterise the heat transfer in the near-wall region of a packed pebble bed. The final methodology obtained through this study can be used to perform a characterisation of the effective thermal conductivity in the near-wall region which can be used to verify and validate the applicability of effective thermal conductivity models and correlations in the near-wall region. This study will therefore contribute to a better understanding of the underlying principles regarding the design of a packed pebble bed to add to the investigation of the PBR safety case.

The enabling objectives of the study are:

- Compare effective thermal conductivity values predicted with the well-known ZBS correlation with experimental results to determine the applicability of this widely applied correlation in predicting the effective thermal conductivity in the near-wall region.
- Conduct a literature review of current methods used to predict the effective thermal conductivity and identify methods that specifically account for the near-wall region.
- Conduct experimental tests using the Near-Wall Thermal Conductivity Test Facility (NWTCTF) for packed beds with a Simple Cubic (SC) and a Body Centred Cubic (BCC) packing configuration to add to the results obtained previously for a random packed bed and

provide a more comprehensive experimental data set. Present detailed effective thermal conductivity results for all packing configurations.

- Conduct a literature review of methods and correlations used to model the conduction heat transfer though the contact areas at pebble-pebble and pebble-wall contact points including contact resistances.
- Extend and apply the CFD model that forms part of the proposed methodology and use the NWTCTF experimental results to evaluate the CFD model.
- Apply the methodology to a packed bed to demonstrate how to separate the contributions of conduction and radiation heat transfer to the overall effective thermal conductivity. Use the preliminary results of the effective thermal conductivity components to obtain better insight into the fundamental characteristics and interplay between the different heat transfer phenomena.

The scope of this study does not include the development of a new effective thermal conductivity model for the near-wall region. It does, however, focus on better understanding and providing the methodology to perform a characterisation of the heat transfer in the near-wall region. This can be used in future studies to develop an effective thermal conductivity model specifically for the near-wall region.

1.3 Methodology

The proposed methodology to characterise the heat transfer in the near-wall region will include experimental as well as numerical work. Experimental data was obtained with the NWTCTF test facility for a randomly packed bed in a previous study (De Beer, 2014). The same test facility was used to obtain further experimental data for SC and BCC packed beds in the current study. Methods similar to that used by Van Antwerpen (2009) and Rousseau et al. (2014) were used for the experimental data and uncertainty analyses as well as the derivation of the effective thermal conductivity results.

A numerical packed bed of spheres with a packing structure similar to that of the experimental setup was generated using the DEM model of STAR-CCM+. The CFD model for the heat transfer through the packed bed of spheres was developed using STAR-CCM+. As a first approximation the contact resistance model of Bahrami *et al*. (2006) will be used to define the contact resistance as a function of temperature at the various pebble-pebble and pebble-wall interfaces in the CFD model. For the final step of the methodology the conduction and radiation components of the effective thermal conductivity will be separated.

1.4 Contributions of the study

The following contributions are made in the current study:

- It is shown that the widely accepted and applied correlations from the Zehner & Schlünder collection fail to predict the correct trends of the effective thermal conductivity in the near-wall region.
- New experimental data generated via the NWTCTF test facility for structured and random packed beds is presented together with the derived effective thermal conductivity results and associated uncertainties. This clearly demonstrates the near-wall effects.
- A new methodology is developed and applied to separate the contributions of conduction and radiation to the overall effective thermal conductivity, including the wall effects.
- Valuable insights are gained regarding the trends and the interplay between the conduction and radiation components of the effective thermal conductivity in the near-wall region.

1.5 Chapter outline

Following this introduction chapter, the thesis consists of four articles which will each be presented as a separate chapter. The first three articles have been published in the international journal *Nuclear Engineering and Design*. The fourth article has been prepared and is ready for submission to the same journal.

Chapter 2 presents the first article which is a comprehensive literature review of the existing correlations and approaches used to predict the effective thermal conductivity for packed beds. The review also identifies which methods specifically account for the near-wall region. The focus is placed on reviewing studies which include the effects of conduction and thermal radiation. The widely used ZBS and IAEA-ZS correlations are applied to predict the effective thermal conductivity and the results are compared with the HTTU and SANA-I experimental results.

Chapter 3 consists of the second article. In the second article the NWTCTF test facility is introduced, and extensive experimental results obtained for structured and randomly packed beds at temperatures of up to 800 °C, together with the associated uncertainties, are presented. The focus of the NWTCTF experimental tests was to investigate the combined conduction and radiation heat transfer specifically in the near-wall region of a packed pebble bed. The results obtained demonstrate the effect of the near-wall region, the packing structure, and the presence of the wall on the effective thermal conductivity.

Chapter 4, the third article presents how the NWTCTF experimental results together with numerical work were used to develop a methodology to separate the conduction and radiation contributions to the overall effective thermal conductivity. Preliminary results are presented to demonstrate how to separate the effective thermal conductivity components. The trends observed in the preliminary results due to the interplay between the conduction and radiation heat transfer phenomena in the near-wall region are discussed.

In chapter 5, the fourth article, a comprehensive literature review of methods used to model the conduction heat transfer through the contact areas at the pebble-pebble and pebble-wall contact points in a packed bed is presented. The CFD model of the proposed methodology is adapted by adding contact resistances to the model to obtain numerical effective thermal conductivity results and are compared with the NWTCTF experimental results. The effect of the contact resistance on the overall effective thermal conductivity results as well as the conduction and radiation components are evaluated.

Lastly, chapter 6 summarises the study and provides recommendations for further work.

References

Bahrami, M., Yovanovich, M.M. & Culham, J.R. 2006. Effective thermal conductivity of rough spherical packed beds. *International Journal of Heat and Mass Transfer*, 49:3691-3701.

Bauer, R. & Schlünder, E.U. 1978. Part I: Effective radial thermal conductivity of packings in gas flow. Part II: Thermal conductivity of the packing fraction without gas flow. *International Chemical Engineering*, 18(2):189-204.

Breitbach, G. & Barthels, H. 1980. The radiant heat transfer in the high temperature reactor core after failure of the afterheat removal systems. *Nuclear Technology*, 49:392-399.

Cheng, G.J. & Yu, A.B. 2013. Particle scale evaluation of the effective thermal conductivity from the structure of a packed bed: Radiation heat transfer. *Industrial & Engineering Chemistry Research*, 52(34):12202-12211.

De Beer, M. 2014. Characterisation of thermal radiation in the near-wall region of a packed pebble bed. Potchefstroom: North-West University. (M Dissertation).

Kaviany, M. 1991. Principles of heat transfer in porous media. (New York, USA: Springer-Verlag. p. 126-127).

Niessen, H.F. & Ball, S. 2000. IAEA-TECDOC-1163: Heat Transport and Afterheat Removal for Gas Cooled Reactors Under Accident Conditions.

Rousseau, P.G., Du Toit, C.G., Van Antwerpen, W. & Van Antwerpen, H.J. 2014. Separate effects tests to determine the effective thermal conductivity in the PBMR HTTU test facility. *Nuclear Engineering and Design*, 271(2014):444-458.

Rousseau, P.G. & Van Staden, M. 2008. Introduction to the PBMR heat transfer test facility. *Nuclear Engineering and Design*, 238(2008):3060-3072.

Talukdar, P., Mendes, M.A.A., Parida, R.K., Trimis, D. & Ray, S. 2013. Modelling of conduction-radiation in a porous medium with blocked-off region approach. *International Journal of Thermal Sciences*, 72(2013):102-114.

Van Antwerpen, W. 2009. Modelling the effective thermal conductivity in the near-wall region of a packed pebble bed. Potchefstroom Campus, South Africa: North-West University. (PhD Thesis).

Van Antwerpen, W., Du Toit, C.G. & Rousseau, P.G. 2010. A review of correlations to model the packing structure and effective thermal conductivity in packed beds of mono-sized spherical particles. *Nuclear Engineering and Design*, 240:1803-1818.

Van Antwerpen, W., Rousseau, P.G. & Du Toit, C.G. 2012. Multi-sphere Unit Cell model to calculate the effective thermal conductivity in packed pebble beds of mono-sized spheres. *Nuclear Engineering and Design*, 247:183-201.

World Nuclear Association. 2020a. The Nuclear Debate. https://www.world-nuclear.org/information-library/current-and-future-generation/the-nuclear-debate.aspx Date of access: 1 March. 2021.

World Nuclear Association. 2020b. Generation IV Nuclear Reactors. https://www.world-nuclear.org/information-library/nuclear-fuel-cycle/nuclear-power-reactors/generation-iv-nuclear-reactors.aspx Date of access: 1 March. 2021.

You, E., Sun, X., Chen, F., Shi, L. & Zhang, Z. 2017. An improved prediction model for the effective thermal conductivity of compact pebble bed reactors. *Nuclear Engineering and Design*, 2017(323):95-102.

Zehner, P. & Schlünder, E.U. 1970. Wärmeleitfähigkeit von Schüttungen bei mäβigen Temperaturen. *Chemie Ingenieur Technik*, 42:933-941.

Zehner, P. & Schlünder, E.U. 1972. Einfluss der Wärmestrahlung und des Druckes auf den Wärmetransport in nicht durchströmten Schüttungen. *Chemie Ingenieur Technik*, 44:1303-1308.

Zhou, J., Yu, A. & Zhang, Y. 2007. A boundary element method for evaluation of the effective thermal conductivity of packed beds. *Journal of Heat Transfer*, 129:363-371.

Zhou, Z.Y., Yu, A.B. & Zulli, P. 2010. A new computational method for studying heat transfer in fluid bed reactors. *Powder Technology*, 197:102-110.

2. Article 1: A review of methods to predict the effective thermal conductivity of packed pebble beds, with emphasis on the near-wall region

M. De Beer *, P.G. Rousseau, C.G. Du Toit

Abstract

The effective thermal conductivity is an important parameter that is representative of the overall heat transfer in a packed bed of spheres. It includes the effects of conduction through the solid material and contact areas between spheres, conduction through the stagnant gas phase as well as thermal radiation between the surfaces of the spheres. An accurate prediction of the effective thermal conductivity is necessary for the design and analysis of packed pebble bed gas-cooled and solid fuel molten salt-cooled generation IV reactors, especially when considering the safety case. This includes the near-wall region where the packing structure is altered significantly. The well-known ZBS correlation is widely applied to predict the effective thermal conductivity and it is often implicitly assumed that it is equally applicable in the near-wall region. This paper presents an analysis of the validity of the ZBS correlation in this regard. In addition to this, an up-to-date review of methods used to predict the effective thermal conductivity is presented and methods that specifically account for the near-wall region are identified. It is noted that the contributions of the various heat transfer mechanisms are not yet fully understood and therefore the ability to separate the different mechanisms can be useful for understanding the characteristics in the near-wall region.

Keywords: Effective thermal conductivity, Packed pebble bed, Thermal conduction, Thermal radiation, Near-wall effect

1. Introduction

Energy transfer through randomly packed beds is important for various thermal-fluid industrial applications, including catalytic reactors, drying processes, thermal insulation, heat storage systems, hydrogen production and gas-cooled nuclear reactors (Asakuma *et al.*, 2016; Ren *et al.*, 2017; Van Antwerpen *et al.*, 2010; Zhou *et al.*, 2007). A thorough understanding of the thermal properties and the heat transfer phenomena in packed beds is essential to achieve an optimal design (Zhou *et al.*, 2007; Zhou *et al.*, 2010).

Pebble bed gas-cooled reactors (PBRs) are generation IV type reactors that are favoured because of the inherent safety characteristics of the reactor design (Wu *et al.*, 2016). The effective thermal conductivity is an important parameter that is representative of the overall heat transfer through a packed pebble bed. In order to achieve a PBR design with the desired safety characteristics one must be able to accurately predict the effective thermal conductivity (Van Antwerpen *et al.*, 2010; Zhou *et al.*, 2007; Zhou *et al.*, 2010). This is also true for another generation IV type reactor namely the fluoride salt-cooled high-temperature reactor (FHR). It is a variant of a molten salt reactor (MSR) that has solid fuel with a core structure similar to the PBR, but instead of helium gas it has molten liquid FLiBe salt as the coolant (World Nuclear Association, 2017). Liquid salts used in the FHR are semi-transparent and can be a participating medium for radiative heat transfer during the removal of decay heat.

When considering the safety case of a PBR during a depressurized loss of forced coolant incident, the effective thermal conductivity consists of three components: (1) conduction through the pebble material itself and through the stagnant fluid, k_e^g, (2) conduction through physical contact points and contact surfaces of the solid materials, k_e^c, and (3) thermal radiation between solid surfaces, k_e^r (Van Antwerpen *et al.*, 2010). Thus, the total effective thermal conductivity of the packed bed can be given by the super-positioning of the three components as shown in Eq. (1):

$$k_{eff} = k_e^g + k_e^c + k_e^r \tag{1}$$

The geometry of a randomly packed bed consists of three main regions namely the bulk, wall, and near-wall regions (Van Antwerpen, 2009). The porous structure changes significantly in the region near any wall as the packing geometry is disrupted in this area (Van Antwerpen *et al.*, 2010; 2012). This variation in packing structure is known as the wall effect and influences the magnitude of the effective thermal conductivity in the wall region, which includes the pebble to reflector interface. During normal operation, the conductive effects in the near-wall region will be negligible compared to convective transport. However, during a loss of coolant event the near-wall region forms part of the critical path for decay heat removal. Thus, an accurate prediction of the effective thermal conductivity in this region is important.

2. Background

Various studies have been conducted in which the effective thermal conductivity was investigated using different analytical, numerical, and experimental methods (Slavin *et al.*, 2002; Tsotsas & Martin, 1987; Van Antwerpen *et al.*, 2010). Van Antwerpen *et al.* (2010) presented a thorough review of literature that describes the packing structure as well as the different

methodologies used to predict the effective thermal conductivity in randomly packed beds of mono-sized spherical particles. They concluded that the correlations developed by Schlünder and co-workers (Zehner & Schlünder, 1970; Zehner & Schlünder, 1972; Bauer & Schlünder, 1978) as well as Breitbach & Barthels (1980) are the methods most commonly used in the nuclear field with application to high temperature gas-cooled reactors.

Fig. 1 shows a schematic representation that summarises the various correlations developed by Schlünder and co-workers, as well as the refinement of the original correlations into the commonly used ZBS model. As this is one of the most widely used approaches it is important to have a thorough understanding of the phenomena characterised by the different correlations together with the potential limitations of the different variations of the correlations.

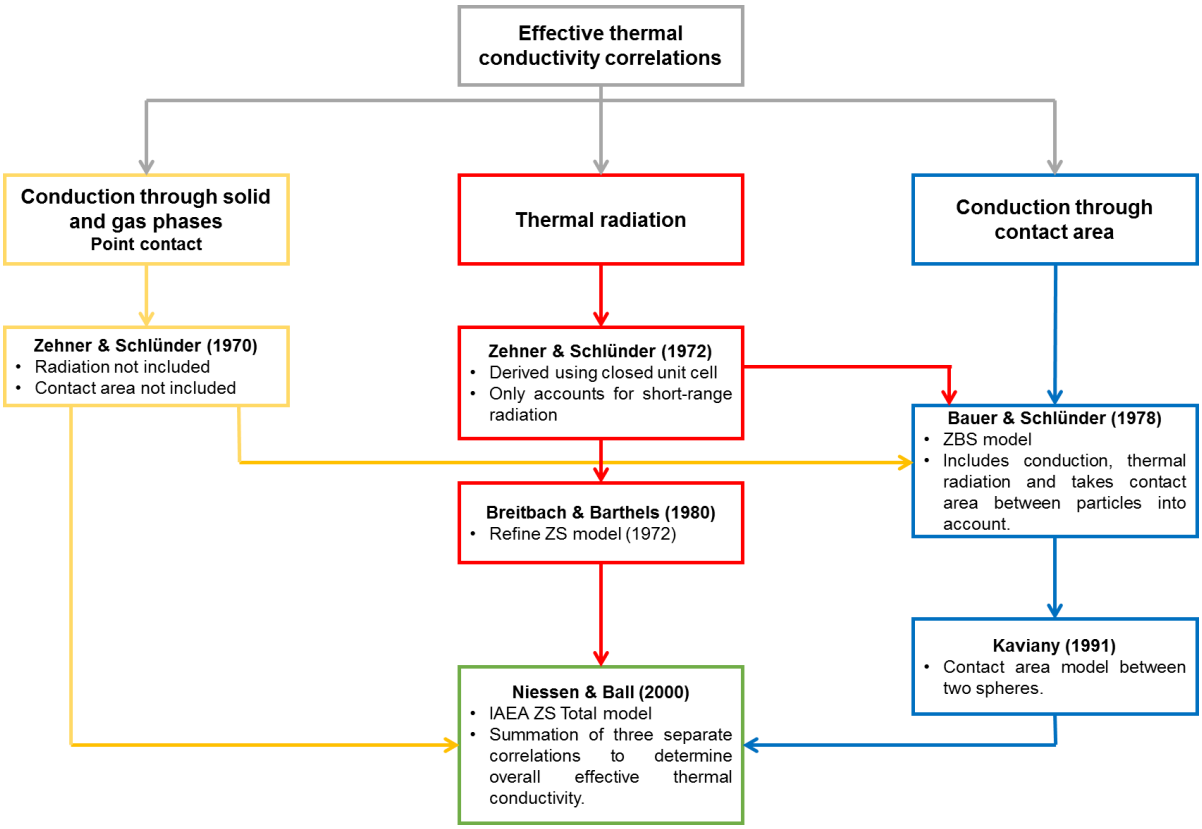

Fig. 1 Summary of the effective thermal conductivity correlations originating from the research of Schlünder and co-workers.

Zehner & Schlünder (1970) presented the first correlation in the series which considered a cylindrical unit cell consisting of two half spheres. The unit cell contained both solid and fluid phases and only conduction heat transfer was accounted for. An analogy was drawn between mass transfer experiments and thermal conduction to obtain an empirical curve to describe the effective thermal conductivity. The mass transfer experiments that were used to obtain the

empirical curve were done for the bulk region of a packed bed with specific porosities. For this reason, Van Antwerpen *et al.* (2010) concluded that the Zehner & Schlünder (ZS) (1970) correlation is not valid in the near-wall region of a packed bed as an analogy between a bulk porosity of a specific value and a near-wall porosity of the same value cannot be made.

Zehner & Schlünder (1972) continued by adding the effect of radiation heat transfer to their original model. However, the unit cell considered in the model was a closed cell and therefore the radiation from the spheres outside of the unit cell was not taken into account.

The original ZS model was later improved by Bauer & Schlünder (1978) by accounting for thermal radiation, considering the Smoluchowski effect and including heat transfer through the contact areas by defining a surface fraction parameter. The surface fraction parameter is a function of the contact area. They noted that the surface fraction parameter is a function of various undetermined limiting quantities such as material elasticity, external mechanical stress, material surface properties as well as the contact area. The contact area must therefore be obtained experimentally. This improved correlation is commonly known as the Zehner, Bauer and Schlünder (ZBS) model.

Bauer & Schlünder (1978) stated that one can expect the wall effect to have an influence on the effective thermal conductivity in the wall region due to the increase in the porosity. They reasoned that the increase in the porosity in the wall region is associated with a simultaneous decrease in the number of contact points between particles in this area. This simultaneous increase in porosity together with the decrease in the number of contact points will affect both the radiation and conduction heat transfer. They concluded that since these are two opposing effects with the same order of magnitude, the net effect due to the wall on the effective thermal conductivity may be neglected. Thus, the reasoning was that with a reduction in the number of contact points in the wall region the conduction heat transfer will decrease. At the same time the increase in porosity in the wall region will result in an increase in the radiation heat transfer, due to less shielding from adjacent pebbles.

However, results from carefully controlled experiments conducted by the current authors have shown that this is not necessarily the case and that the effective thermal conductivity is actually significantly reduced in the near-wall region. The first tests were conducted in the non-nuclear High Temperature Test Unit (HTTU) in South Africa on behalf of the PBMR company (Rousseau *et al.*, 2014). The HTTU consisted of an annular test section holding approximately 25 000 randomly packed graphite spheres with a diameter of 60 mm each. In order to reduce the effects of convection a near-vacuum nitrogen environment was maintained inside the test

facility. A temperature gradient was induced through the packed bed of spheres by heating the inner graphite reflector walls and cooling the outer reflector wall. The heated inner reflector wall was positioned at a radius of 0.3 m while the cooled outer reflector wall was positioned at a radius of 1.2 m. Tests were conducted for heater power levels of 20 kW and 82 kW respectively. The reduction in the effective thermal conductivity is clearly evident in the results of the 82 kW test as shown in Fig. 2.

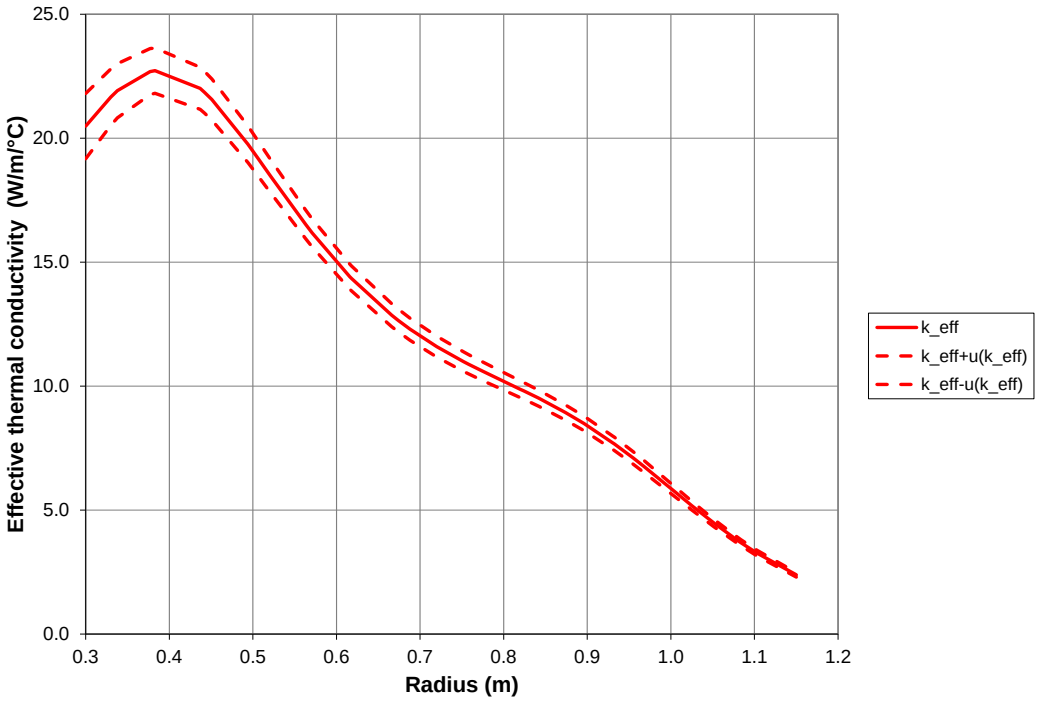

Fig. 2 Effective thermal conductivity with uncertainties as a function of radial position for the 82 kW tests conducted in the HTTU test facility (Rousseau *et al.*, 2014).

In a more recent study (De Beer *et al.*, 2017) the current authors conducted further tests in the so-called Near-Wall Thermal Conductivity Test Facility (NWTCTF). It consists of a rectangular packed bed with approximately 330 of the same graphite spheres as that of the HTTU. During the test the packed bed was again contained in a near-vacuum nitrogen environment and for the result considered here the “hot” graphite wall was maintained at a temperature of 800 °C with the “cold” graphite wall at 163 °C. Fig. 3 presents the results for the measured overall effective thermal conductivity as a function of position in the packed bed. From Fig. 3 it is again clear that there is a marked reduction in the magnitude of the effective thermal conductivity in the near-wall region, especially on the hot wall side.

This decrease observed in the effective thermal conductivity in the near-wall region contradicts the conclusion made by Bauer & Schlünder (1978). Therefore, it is important to consider

whether the conduction and radiation mechanisms and the interplay between them are indeed well understood.

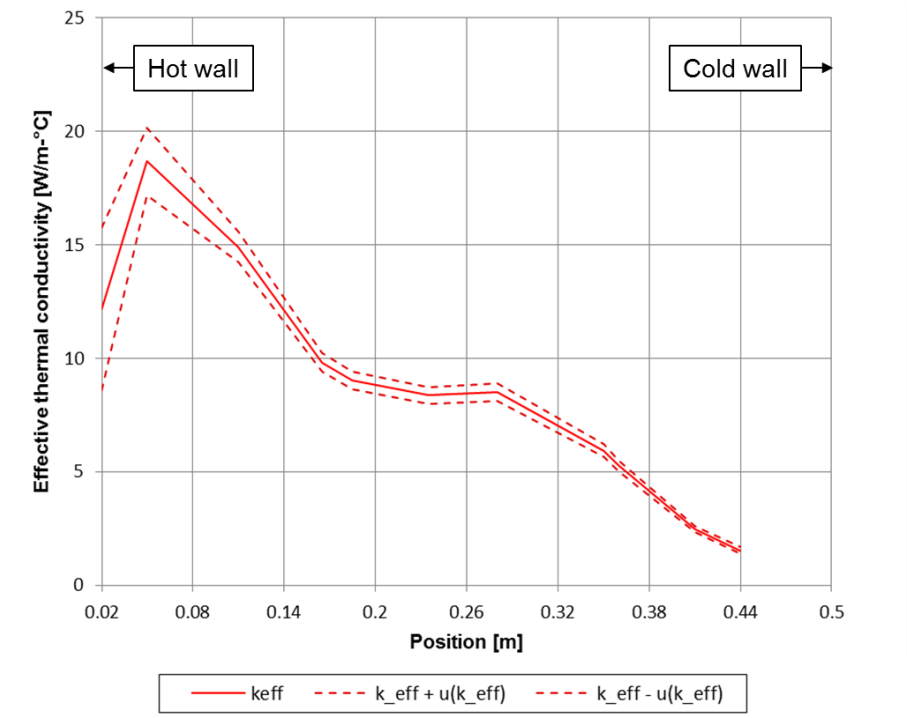

Fig. 3 NWTCTF effective thermal conductivity as a function of position (De Beer *et al.*, 2017).

The radiation correlation developed by Zehner & Schlünder (1972) was further refined by Breitbach & Barthels (1980). They modified the original ZS radiation equation by closing the base areas of the unit cell under consideration with black surfaces instead of using surfaces with the same emittance as the particles, thus solving the shortcoming of considering a closed unit cell when predicting the radiation heat transfer.

The SANA-I experimental test facility predates the HTTU and NWTCTF and was also designed and constructed to investigate the effective thermal conductivity in high temperature PBRs (Niessen & Ball, 2000). The randomly packed bed of the SANA-I test facility of interest here consisted of graphite pebbles with a diameter of 60 mm. The packed bed had a diameter of 1.5 m and a height of 1 m (Niessen & Ball, 2000). Two steady state tests were conducted for heater power inputs of 10 kW and 35 kW respectively. Both experimental tests were performed with a helium environment at atmospheric pressure inside the vessel. The developers of the SANA-I test facility specifically wanted to determine how natural convection assisted in the decay heat removal process and therefore natural convection was not suppressed during the tests.

As a part of the SANA benchmark problems Niessen & Ball (2000) proposed the summation of three different existing correlations to simulate the overall effective thermal conductivity through

the pebble bed in a stagnant gas environment. The three correlations used in the summation are (1) the ZS correlation for conduction through the solid and gas phases (Zehner & Schlünder, 1970), (2) the Kaviany (1991) model to account for conduction through the contact area and (3) the Breitbach & Barthels (1980) correlation for thermal radiation. Van Antwerpen *et al*. (2012) referred to this combination of correlations as the IAEA (International Atomic Energy Agency) ZS Total model, which can be regarded as being representative of the most current version of the original ZS model.

Van Antwerpen *et al*. (2012) used both the ZBS and the IAEA ZS Total correlations to predict the effective thermal conductivity as a function of temperature for the SANA-I experimental test facility. The predicted effective thermal conductivity values were compared with the SANA-I experimental data presented by Niessen & Ball (2000). This showed that the values obtained with the ZBS and IAEA ZS Total correlations were slightly lower than the SANA-I experimental data but followed the correct trend. They concluded that the reason for the difference between the predicted values and the experimental data is that the correlations only account for conduction and radiation heat transfer, whereas natural convection was also present in the SANA-I experimental tests.

The effective thermal conductivity values obtained with the ZBS correlation were slightly lower than that of the IAEA ZS Total correlation. The reason for the difference between the results of the two correlations was ascribed to the surface fraction parameter in the ZBS correlation that is unknown for the SANA-I packing structure (Van Antwerpen *et al.*, 2012). A first order estimate was used for the surface fraction parameter, which should ideally be determined experimentally.

3. ZBS and IAEA ZS Total correlations in the near-wall region

However, close agreement between the predicted effective thermal conductivity values with the experimental data as a function of temperature alone does not automatically mean that the correlations are valid for the near-wall region. To determine whether the ZBS and IAEA ZS Total correlations capture the effects of the altered packing structure in the wall region it must also be determined as a function of position through the packed bed. This was indeed done by Van Antwerpen *et al*. (2012) for the IAEA ZS Total correlation, but not for the ZBS correlation. The 35 kW SANA-I IAEA ZS Total results are presented in Fig. 4. The results show the reduction in effective thermal conductivity in the near-wall region and also that the IAEA ZS Total correlation fails to predict this phenomenon.

Van Antwerpen (2009) also determined the effective thermal conductivity for the HTTU using the IAEA ZS Total correlation and compared the results with the HTTU experimental data. The

82 kW HTTU IAEA ZS Total results are presented in Fig. 5. Similar to the case for the SANA-I test facility, it shows that the IAEA ZS Total correlation breaks down in the near-wall region.

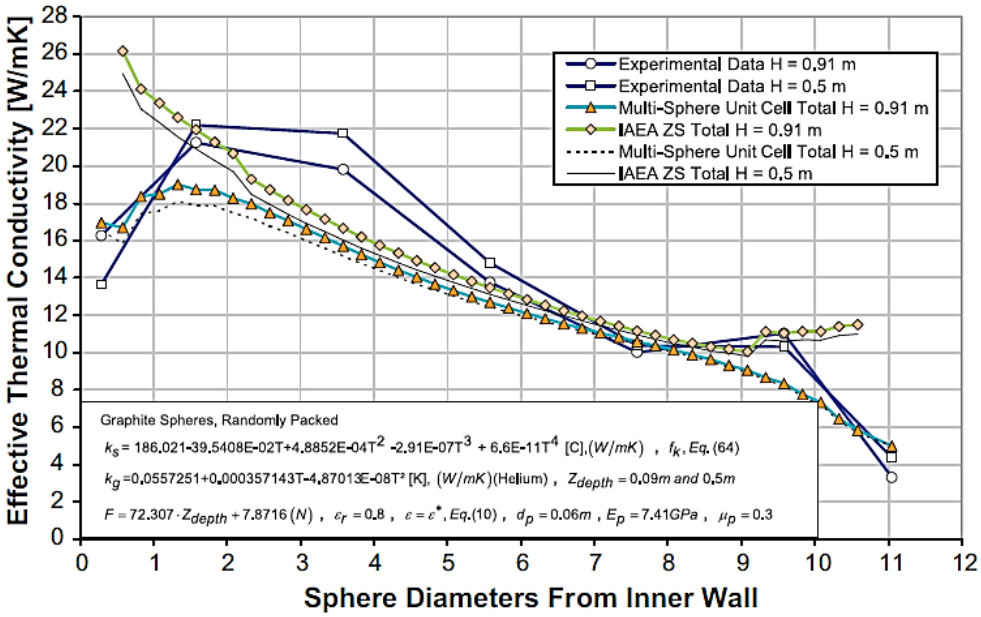

Fig. 4 Comparison between IAEA ZS Total effective thermal conductivity correlation and the experimental results of the SANA-I experimental test facility for the 35 kW steady state test (Van Antwerpen *et al.*, 2012).

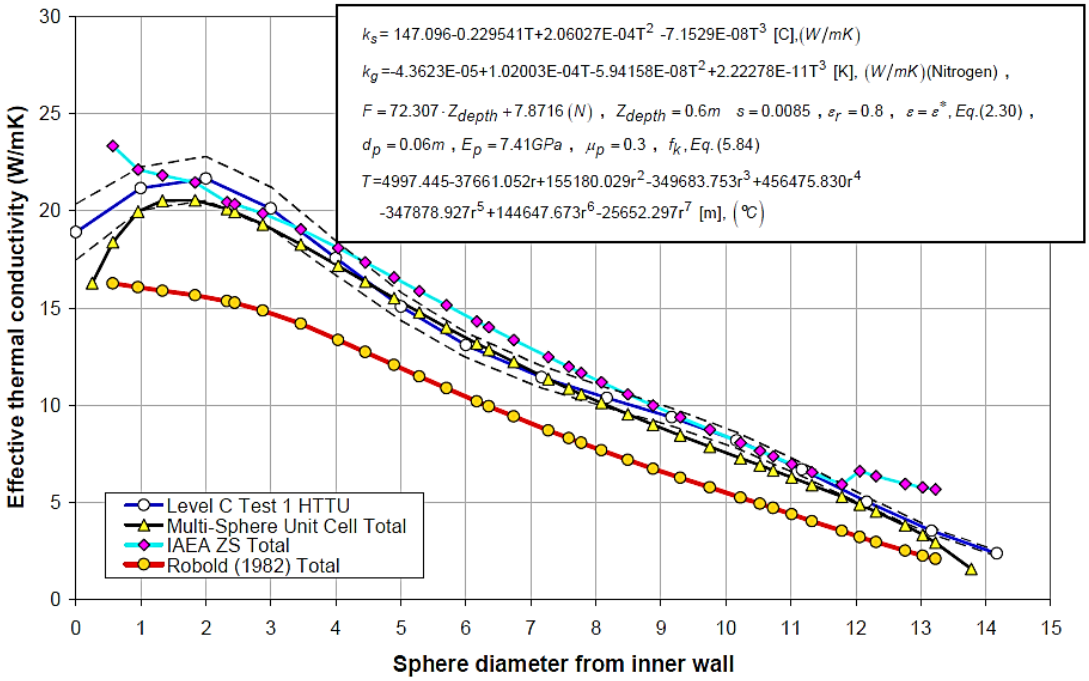

Fig. 5 Comparison between IAEA ZS Total effective thermal conductivity correlation and the experimental results of the HTTU experimental test facility for the 82 kW steady state test, Test 1 (Van Antwerpen, 2009).

Van Antwerpen and co-workers (2009; 2012), however, did not compare values predicted by the original ZBS correlation as a function of position with the measurements from the SANA-I and HTTU test facilities. Further analysis will therefore be conducted below regarding this. We

will first apply the ZBS correlation to the SANA-I test facility and thereafter to the HTTU test facility. For completeness we will also include recalculated results for the IAEA ZS Total correlation in each case, although this was also done by Van Antwerpen and co-workers.

The porosity function proposed by Van Antwerpen *et al*. (2012) for the near-wall region in a packed bed was used to determine the porosity values for the current calculations, namely:

$$\varepsilon^* = -0.0127z^2 + 0.0967z + 0.2011 \quad (2)$$

with

$$z = (r - R_i) / d_p \text{ for } R_i \le r \le (R_o + R_i) / 2 \quad (3)$$

$$z = (R_o - r) / d_p \text{ for } (R_o + R_i) / 2 \le r \le R_o \quad (4)$$

where z is the radial position in the packed bed expressed in sphere diameters from the inner wall, r is the radial position in the packed bed, d_p is the pebble diameter, and R_i and R_o are the inner and outer radii of the packed bed respectively.

For the calculations with the IAEA ZS Total correlation the contact force distribution between the pebbles must be known. Van Antwerpen (2009) derived a function for the contact force distribution in the HTTU pebble bed by using a numerically packed bed that is representative of the HTTU. The contact force distribution function is given by:

$$F = 72.307 \cdot z_{depth} + 7.8716 \quad (5)$$

where z_{depth} is the position in the z-direction of the packed bed. Van Antwerpen *et al*. (2012) assumed that the contact force distribution for the SANA-I pebble bed was the same as that of the HTTU due to the geometry of the pebbles and packed bed being similar for the two experimental test facilities. For the analysis presented in this study the same assumption was made in the calculation of the IAEA ZS Total effective thermal conductivity for the SANA-I packed bed.

The SANA-I experimental results presented here were originally extracted as a function of position by Van Antwerpen (2009) for the two temperature profiles measured by Niessen & Ball (2000) at heights of 0.5 m and 0.91 m in the packed bed. The comparison between the effective thermal conductivity results calculated with the two correlations and the SANA-I experimental results for the 10 kW and 35 kW steady state tests are shown in Fig. 6 and Fig. 7 respectively.

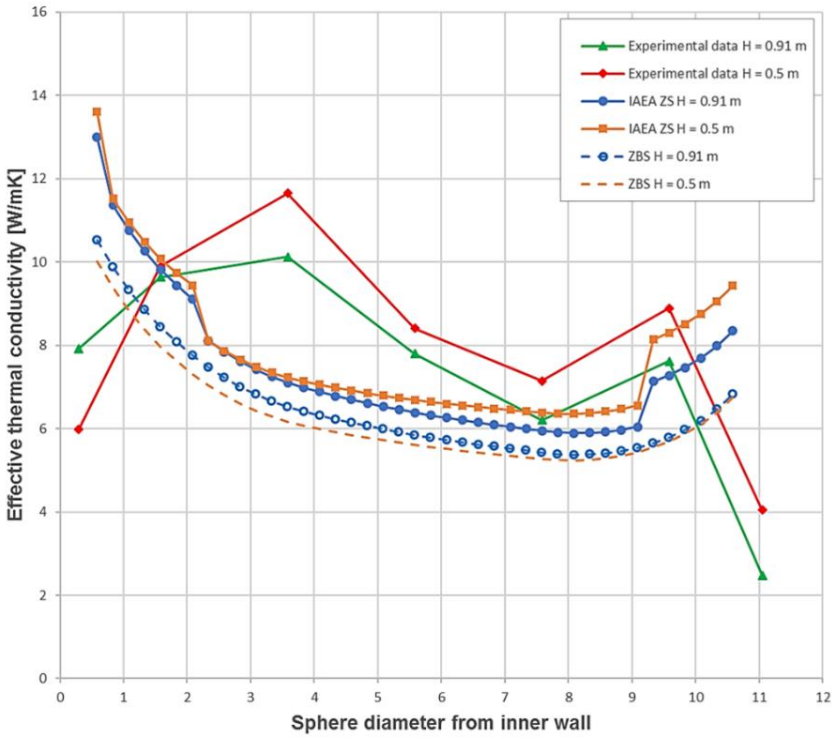

Fig. 6 Comparison between ZBS and IAEA ZS Total effective thermal conductivity correlations and the experimental results of the SANA-I experimental test facility for the 10 kW steady state test.

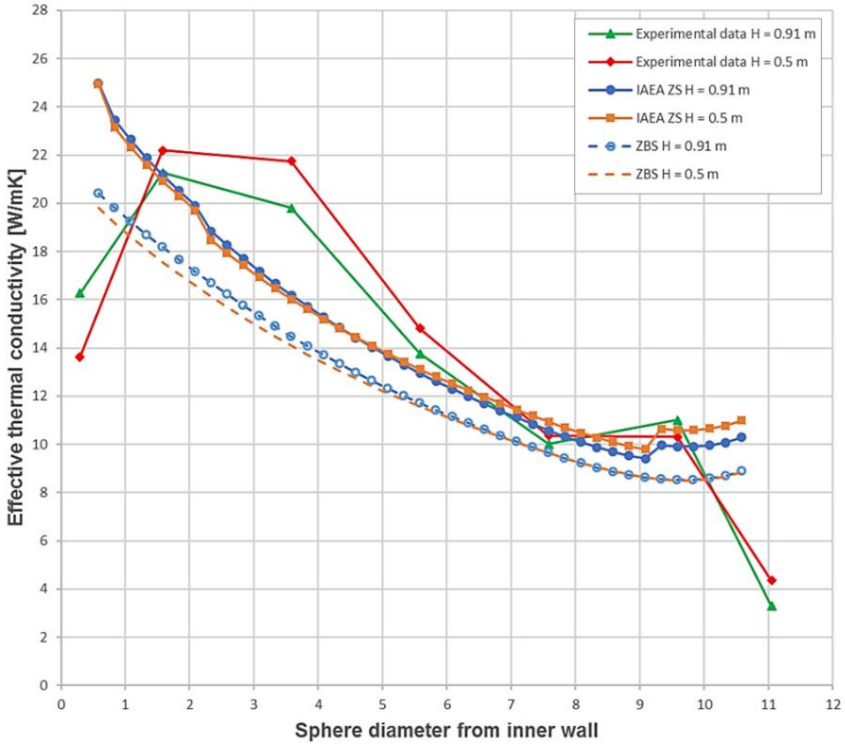

Fig. 7 Comparison between ZBS and IAEA ZS Total effective thermal conductivity correlations and the experimental results of the SANA-I experimental test facility for the 35 kW steady state test.

Both the ZBS and IAEA ZS Total results are lower than the experimental results, which can be expected due to the presence of natural convection in the experimental tests. However, the ZBS

predicted values are slightly lower than that of the IAEA ZS Total correlation due to the first order estimate of the surface fraction parameter used in the calculation of the effective thermal conductivity. As can be seen in Fig. 6 and Fig. 7, both the ZBS and the IAEA ZS Total correlations failed to capture the wall effects. This observation is similar to the findings of Van Antwerpen and colleagues (Van Antwerpen *et al.*, 2012), namely that the IAEA ZS Total correlation is not valid in the near-wall region.

Next, we will look at the HTTU test facility. The HTTU experimental results presented in the graphs were obtained from the study by Rousseau *et al*. (2014), who provided detailed experimental data together with the associated uncertainties. Fig. 8 and Fig. 9 show the comparison between the effective thermal conductivity results calculated with the ZBS and the IAEA ZS Total correlations and the HTTU experimental results for the 20 kW and 82 kW steady state tests respectively.

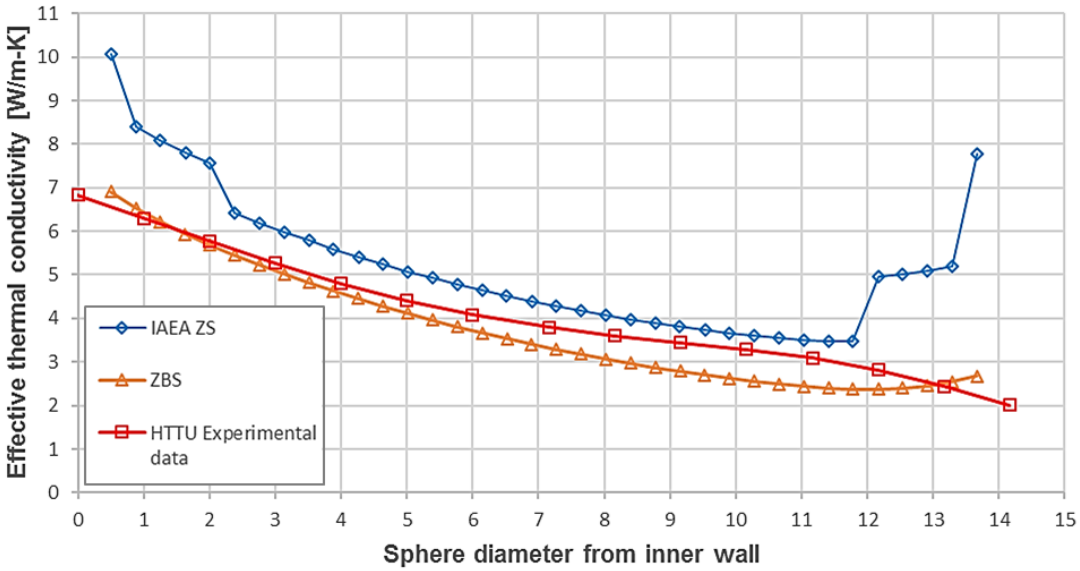

Fig. 8 Comparison between ZBS and IAEA ZS Total effective thermal conductivity correlations and the experimental results of the HTTU experimental test facility for the 20 kW steady state test.

The influence of the wall effects in the near-wall regions are visible in the experimental results for both the 20 kW and 82 kW tests, however it is the most prominent at higher temperatures. This can be seen in Fig. 9 where there is a significant reduction of the effective thermal conductivity value in the wall region next to the inner reflector.

Fig. 8 shows that the IAEA ZS Total correlation predicts values that are higher than the HTTU experimental data for the bulk region of the pebble bed, but the trend is in close agreement. For the 82 kW test, Fig. 9, the IAEA ZS Total predicted effective thermal conductivity values for the bulk region are in better agreement with the experimental results. In both cases the IAEA ZS Total correlation fails to predict the correct trend of the effective thermal conductivity in the

near-wall regions. For both the test cases the ZBS correlation predicts values that are slightly lower than that of the experimental results as well as the IAEA ZS Total results in the bulk region. However, the ZBS correlation also fails to predict the correct trend in the near-wall regions for both the 20 kW and 82 kW tests.

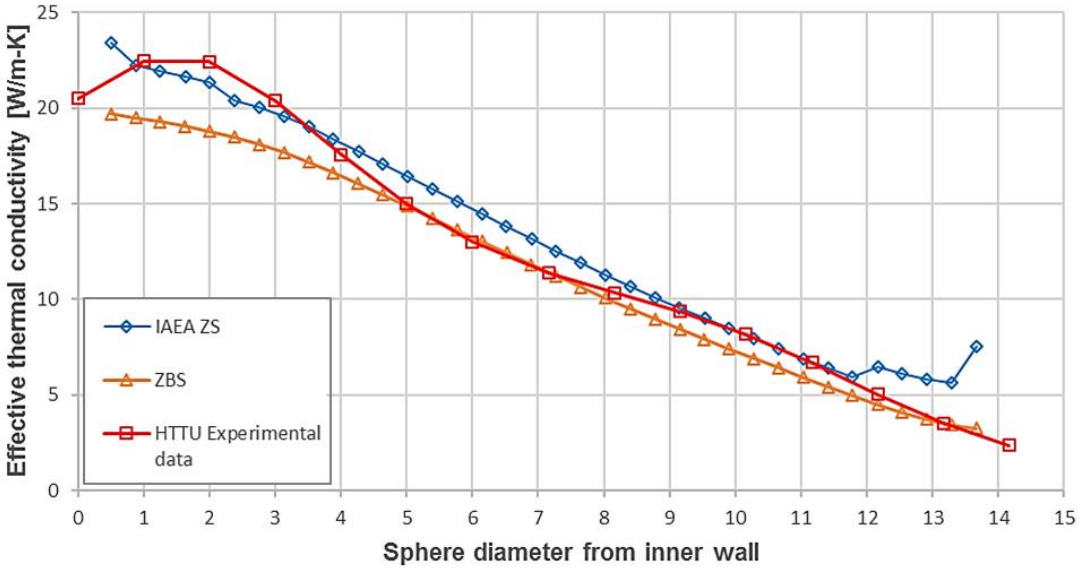

Fig. 9 Comparison between ZBS and IAEA ZS Total effective thermal conductivity correlations and the experimental results of the HTTU experimental test facility for the 82 kW steady state test.

From the analysis presented above it is clear that the widely accepted and applied correlations from the Zehner & Schlünder collection fail to predict the correct values or correct trends in the effective thermal conductivity for the near-wall region. Therefore, one should be very careful when using these correlations here which were originally intended for the bulk region of the bed. Given this the authors believe that it is important to gain a better fundamental understanding of the conduction and radiation heat transfer phenomena in the near-wall region. The authors also believe that being able to separate out the individual contributions to the total effective thermal conductivity can be useful to gain a better understanding of the phenomena and the interplay between them. This does not necessarily imply that all models should treat the phenomena separately.

This does however raise the question as to whether there are existing correlations that do account correctly for the phenomena in the near-wall region, or that already separate out the different phenomena and then correctly predict the interplay between them. From the 2010 review done by Van Antwerpen *et al*. (2010) it was clear that no correlations existed at that time which accurately addressed the near-wall region. However, there may have been recent advances in this regard and therefore the next section presents a review of correlations reported since the previous review.

4. Review of recent work on the effective thermal conductivity

Van Antwerpen *et al*. (2010) made important conclusions from their comprehensive review of the various effective thermal conductivity models and correlations. Firstly, the correlations and models that neglected the effect of contact area resulted in values being lower than that of the experimental results. The models that do account for the specific contact area parameter provide results that are in good agreement with the experimental data for the bulk region of the bed. This illustrates the importance of the inclusion of a suitable contact resistance associated with the contact area between pebbles to ensure a more accurate prediction.

They concluded that the quality of the experimental results reported in literature cannot easily be evaluated since the associated measurement uncertainties are rarely reported. It was also noted that the use of purely empirical correlations has become less popular. The use of numerically simulated packed beds has become the preferred approach to determine the effective thermal conductivity, as researchers can more easily distinguish between the effects of the different contributing phenomena.

Since the review of Van Antwerpen *et al*. (2010) various new studies have been performed that address the prediction of the effective thermal conductivity. The various effective thermal conductivity models and correlations reviewed by them were divided into different categories according to the heat transfer mechanisms and wall effects accounted for in the models. A similar categorization will be used here to review the more recently published work.

In the first category the solid and stagnant fluid effective thermal conductivity models will be discussed. Correlations in this category considered the effective thermal conductivity through the solid phase as well as the stagnant fluid phase of the packed bed. Conduction through point contacts were also taken into account, however the effects of thermal radiation were neglected by these models. In the second category the research of authors that accounted for heat transfer through the contact areas, particle surface roughness or a combination of these phenomena will be presented.

The third category will present the models and correlations used to predict the effective thermal conductivity due to thermal radiation in a packed pebble bed. Due to the importance of considering the wall effects, the correlations applicable in the near-wall region will be specifically addressed in the fourth category.

The main focus for this review will be on identifying which of the models and approaches actually account specifically for contact resistance, which account for the near-wall effects and

which use the separation of the conduction and radiation components to gain a better understanding of the heat transfer phenomena. The conduction components of the various models and approaches will be discussed in sections 4.1 and 4.2, whilst the radiation components will be discussed in section 4.3. A summary of the models and approaches included in the current review is provided in Table 1.

Table 1: A summary of the categorization of the models and approaches used to predict the effective thermal conductivity.

Reference	Account for contact resistance	Account for near-wall effects	Separate conduction & radiation components
Models and approaches that account for conduction-only			
Panchal *et al*. (2016)	-	-	-
Suárez *et al.* (2017)	-	-	-
Dixon *et al*. (2013)	-	-	-
Chen *et al*. (2016)	✓	-	-
Liang & Li (2014); Liang *et al*. (2016)	✓	-	-
Tsory *et al.* (2013)	✓	-	-
Models and approaches that account for radiation-only			
Wu *et al*. (2016)	-	-	-
Models and approaches that account for conduction and radiation			
Wu *et al*. (2017)	-	-	✓
Van Antwerpen *et al.* (2012)	✓	✓	✓
Zhou *et al*. (2007)	✓	-	✓
Zhou *et al*. (2010)	✓	-	-
Cheng & Yu (2013)	✓	-	✓
Wang *et al.* (2016a; 2016b)	✓	-	✓
Yamoah *et al*. (2012)	✓	-	-
Ren *et al*. (2017)	✓	-	-
Asakuma *et al*. (2014; 2016)	✓	-	-
Gan & Kamlah (2010)	✓	✓	-
De Beer *et al*. (2017)	-	✓	✓

4.1. Solid and stagnant fluid effective thermal conductivity with the consideration of point contact

In this section all the correlations and approaches which define the conduction component in the packed bed with consideration of a point contact will be discussed. No contact area is thus included in the approaches discussed here.

Conduction-only models

The effective thermal conductivity due to conduction heat transfer was determined numerically by Panchal *et al*. (2016). A DEM method was used to generate the packed pebble bed. For the investigation of the heat transfer the Finite Element Analysis (FEA) code COMSOL was used, and the DEM geometry was manually imported into the FEA model. The effect of contact area

on the conduction through the particle-particle contact points was considered to be negligible. The effective thermal conductivity was determined for packed beds with a simple cubic (SC), body centred cubic (BCC), face centred cubic (FCC) and a random packing structure. The numerical results for the randomly packed bed agreed reasonably well with the results predicted by the ZBS model (Bauer & Schlünder, 1978).

Suárez *et al.* (2017) derived new expressions to predict the effective thermal conductivity due to conduction in a fixed bed consisting of mono-sized spheres. The approach used by them focused on capturing the underlying characteristics of the conduction heat transfer phenomenon. The effective thermal conductivity was evaluated based on estimations of the number of contacts, the spreading or constriction of the flux lines inside the particles and the concentration of particles in the packed bed. No correction factor or adjustable parameter was included in the effective thermal conductivity expressions that would ensure the predicted values correlate well with experimental data.

The effective thermal conductivity component describing the conduction through the solid material of the spheres in the core region, $\lambda_{es,c}$, was calculated using Eq. (6):

$$\lambda_{es,c}/k_f = (1-\varepsilon_c)\, n_e \left(0.8\theta^0 + 0.2\theta^{0.01}\right) \tag{6}$$

where k_f is the fluid thermal conductivity, ε_c is the average porosity of the core region and n_e is the effective number of contacts in the solid core region with thermal parameters θ^0 and $\theta^{0.01}$. The expression was derived by considering 80 % of real contacts and 20 % of near contacts in the packed bed. Near contacts were defined as contact points where the physical separation distance between the particles, ℓ_o , was equal to $0.01d_p$ where d_p is the particle diameter.

Eq. (7) was used to predict the conduction contribution through the stagnant fluid in the bed voids between spheres, $\lambda^0_{e,c}$:

$$\lambda^0_{e,c}/k_f = \varepsilon_c + (1-\varepsilon_c)\, n_e \left(0.8\theta^0 + 0.2\theta^{0.01}\right) \tag{7}$$

The results obtained with the proposed expressions were compared with experimental data from literature and were found to be in good agreement without using any fitting parameters. The authors concluded that future work must be performed to address conduction through finite contact areas when compression forces between particles are accounted for.

Dixon *et al*. (2013) conducted a study to evaluate if the ZBS cell model for conduction heat transfer can be used on a pointwise basis to predict local values of the overall stagnant effective thermal conductivity due to conduction using the local bed void fraction. A 3D CFD model of an annular test bed was used to calculate the local void fraction of the packed bed. The

temperature profile of the packed bed was calculated with a one-dimensional pseudo-continuum FEA model that made use of the ZBS model and the CFD void fraction results. Conduction through the finite contact areas were neglected in the study. The results obtained showed that the ZBS model predicted the temperature profile of the packed bed well, thus the use of the ZBS model can be extended from global to local if a detailed void fraction profile of the packed bed is known.

Conduction-radiation models

Wu *et al*. (2017) used a coupled computational fluid dynamics (CFD) and discrete element method (DEM) approach to investigate the combined conduction and radiation heat transfer in a PBR core during a depressurized loss of forced coolant incident. A Fourier conduction rate equation was used to simulate the conduction heat transfer between two particles in contact. However, Wu *et al*. (2017) reported that the component of the total effective thermal conductivity due to conduction-only heat transfer could be obtained from existing experimental data as it was assumed that the conduction heat transfer between particles is not affected by a variation in temperature.

4.2. Solid and stagnant fluid effective thermal conductivity with the consideration of contact area

The models and approaches discussed in this section predict the conduction component of the effective thermal conductivity through the solid and fluid phases with stagnant flow in the packed bed, but with the contact area explicitly taken into account. Thus, the first two components of the effective thermal conductivity shown in Eq. (1) are combined to form one component, $k_e^{g,c}$.

Contact area refers to the contact region between two particles that can increase in size as a result of the elasticity of the particle solid material when an external load is applied to the packed bed. The effective thermal contact area is dependent on the surface roughness which is a characteristic of the two particles in contact (Van Antwerpen *et al.*, 2010).

Conduction-only models

The models and approaches discussed in this section only account for the conduction heat transfer, and not radiation.

A one-way coupled CFD-DEM method was used by Chen *et al*. (2016) to simulate the heat transfer through a packed pebble bed and determine the effective thermal conductivity. Chen *et*

al. (2016) assumed that the effects of thermal radiation could be neglected due to the relatively low temperatures that were used in their study.

The steady state temperature field for the packed bed was obtained via a CFD simulation, after which a one-dimensional Fourier conduction rate equation was used to calculate the effective thermal conductivity. The particle contact points derived from the DEM model were included in the mesh generation for the CFD model; however, some very small gaps or overlaps between particles at the contact points caused difficulty with the mesh generation. To overcome this problem, the particles causing problems were resized within ± 0.5 % and the mesh could then be rebuilt successfully. The numerical effective thermal conductivity results were compared with values predicted with the ZBS model (Bauer & Schlünder, 1978) and were found to be in good agreement.

Liang & Li (2014) developed a new parallel-column model for the conduction heat transfer through the contact network in a randomly packed pebble bed. For the parallel-column model it was assumed that the packed pebble bed can be represented by several particle columns and the contact network throughout the pebble bed consists of several parallel chains. The conduction path between contacting particles was approximated to be a particle column. Thus, the parallel-column model can be seen as a parallel connection of particle columns. (Liang & Li, 2014), as shown in Fig. 10.

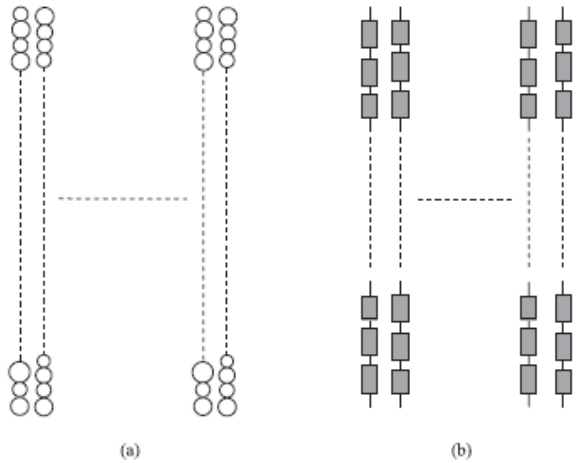

Fig. 10 (a) Schematic of particle columns in parallel-column model and (b) particle column contact resistor network (Liang & Li, 2014).

The conduction effective thermal conductivity for an ideal arrangement of a series of parallel particle columns was calculated using the analytical expression given in Eq. (8):

$$k_{eff} = 2Ck_s\xi^{1/2}L^{-1/2}\left\langle d_p^{-1/2}\right\rangle^{-1}\left\langle d_p\right\rangle^{1/2} \quad (8)$$

where C is a dimensionless fitting parameter, ξ is the compressive displacement, L is the height of the particle column and d_p is the particle diameter. An assumption was made that none of the particle columns participate in heat transfer with the neighbouring particle columns. The results obtained with the analytical expression were compared with numerical results and were found to be in good agreement. Thus, it was concluded that the parallel-column model adequately represents the heat transfer through the contact network in a pebble bed.

In a more recent study Liang *et al*. (2016) conducted further research on the parallel-column model of Liang & Li (2014). Various types of contact force models were incorporated into the existing parallel-column model. An expression for the effective thermal conductivity was derived for each of the different contact force models.

A coupled DEM-CFD model was developed by Tsory *et al*. (2013) to predict the effective thermal conductivity due to conduction through the solid and fluid material including the conduction through the contact areas for packed beds under compression. Surface roughness as well as the interstitial gas at the contact points were taken into account in the calculation of the conduction through the contact area. From the simulation results the temperature distribution in the packed bed was obtained and using Fourier's law the effective thermal conductivity was calculated. The calculated numerical results were compared with the experimental data of Widenfield *et al*. (2003). The average slope of the surface roughness was used as an adjustable parameter that was varied until a good agreement was achieved between the numerical and experimental results.

Conduction-radiation models

Van Antwerpen *et al*. (2012) developed the Multi Sphere Unit Cell (MSUC) model to provide more accurate predictions of the effective thermal conductivity in both the bulk and the near-wall regions. The MSUC model specifically accounts for the porous structure, solid and gas thermal conduction, contact area and the thermal radiation. Results obtained with the MSUC model were compared with existing experimental data including data from the SANA-I test facility.

They used a thermal resistance network approach to predict the conduction component of their newly developed MSUC model. The conduction path between two contacting spheres were divided into three regions namely an inner, middle, and outer region, as shown in Fig. 11. Each of these regions accounted for specific heat transfer mechanisms represented by an arrangement of parallel and series thermal resistances. Combining the various thermal resistances resulted in a joint thermal resistance that could be used to predict the effective

thermal conductivity due to conduction. It was assumed that the two contacting spheres are made of the same material.

The joint thermal resistance can account for either a rough or a smooth surface thermal resistance depending on the surface roughness of the sphere material. According to Van Antwerpen *et al*. (2012) the smooth contact network is used when the conduction component does not need to be simulated in such detail. Therefore, the joint thermal resistance for the rough contact network, R_j, is presented in Eq. (9), which is used for the bulk region of the pebble bed:

$$R_j = \left(\left(R_{L,1,2} + \left(\frac{1}{R_g} + \frac{1}{R_s} \right)^{-1} \right)^{-1} + \frac{1}{R_\lambda} + \frac{1}{R_G} \right)^{-1} + \left(\frac{1}{R_{in,1,2}} + \frac{1}{R_{mid,1,2}} + \frac{1}{R_{out,1,2}} \right)^{-1} \tag{9}$$

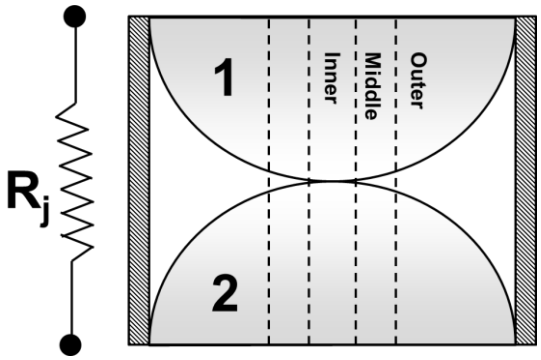

Fig. 11 Multi Sphere Unit Cell model for conduction (Van Antwerpen *et al*., 2012).

The contact area component of the inner conduction region consists of three thermal resistances namely the macro-contact and micro-contact constriction/spreading resistances, $R_{L,1,2}$ and R_s respectively, as well as the interstitial gas resistance in the micro-gap, R_g. All three of these thermal resistances are calculated using models developed by Bahrami *et al*. (2006). The thermal resistance $R_{in,1,2}$ represents the conduction through the solid material in the inner region assuming one dimensional heat transfer and is calculated using Eq. (10):

$$R_{in,1,2} = \frac{\left(d_p - \omega_o \right)}{k_s \pi r_a^2} \tag{10}$$

where k_s is the thermal conductivity of the solid material, r_a is the radius of the micro-contact area and ω_o is the material deformation depth as defined by Bahrami *et al*. (2006).

The middle conduction region consisted of two thermal resistance components namely the conduction through the interstitial gas, R_λ, and the conduction through the solid material in the middle region, $R_{mid,1,2}$. The thermal resistance R_λ was developed by Van Antwerpen (2009) to account for the Smoluchowski effect in the middle region. Using the mean free path radius, r_λ, the thermal resistance $R_{mid,1,2}$ can be calculated with Eq. (11):

$$R_{mid,1,2} = \frac{\left(d_p - \omega_0\right)}{k_s \pi \left(r_\lambda^2 - r_a^2\right)} \tag{11}$$

The two thermal resistance components that describe the conduction heat transfer through the outer region is the resistance through the interstitial gas in the macro-gap, R_G, and the resistance of the outer solid material, $R_{out,1,2}$. Fourier's law for conduction is used to calculate R_G. The expression to calculate $R_{out,1,2}$ was also derived and is shown in Eq. (12):

$$R_{out,1,2} = \frac{ln\left|\left(A_{out} + B_{out}\right)/\left(A_{out} - B_{out}\right)\right|}{k_s \pi B_{out}} \tag{12}$$

where $A_{out} = r_p - 2\left(0.5\omega_0 + 5\lambda\right)$ and $B_{out} = \sqrt{r_p^2 - r_\lambda^2}$ with r_p the sphere radius and λ the mean free path of the gas molecules.

Finally, the conduction effective thermal conductivity vector is calculated using Eq. (13):

$$\bar{k}_e^{g,c} = \frac{L_j}{R_j A_j} \tag{13}$$

where $L_j = (d_p - \omega_0)$ is the distance between the centres of the two spheres in contact and $A_j = d_p^2$ is the joint conduction area. A conduction effective thermal conductivity component can be calculated in both the radial and the axial coordinate directions. The results obtained with the MSUC model were compared with the experimental data of various studies and were found to be in good agreement.

A boundary element method (BEM) was developed by Zhou *et al*. (2007) to predict the effective thermal conductivity due to conduction-radiation heat transfer in a two-dimensional packed bed. Conduction differential equations with a continuous temperature and heat flux boundary condition for the solid and gas phases were solved to obtain the temperature distribution in the packed bed. From the temperature field the effective thermal conductivity was calculated using a Fourier conduction rate equation. The BEM converted the partial differential equation into a boundary integral equation that was solved using an iterative procedure to reduce the computational resources needed. The conduction through particle-particle contact areas was taken into account in the calculations by defining the void fraction of the structured packed beds as a function of the ratio of contact radius to the particle radius.

The BEM method produced good results for square and hexagonal packing structures when compared with existing theoretical models. The temperature distribution results in the local regions of the packed beds indicated that the heat flux constriction effect due to the contact area between particles was adequately captured by the BEM model.

Zhou *et al*. (2010) used a coupled discrete particle simulation (DPS) and CFD approach to study the heat transfer in a packed pebble bed on a particle scale level and from that determine the effective thermal conductivity. For the particle-fluid-particle conduction the model of Cheng *et al*. (1999) was used with some modifications. A shortcoming of the approach by Cheng *et al*. (1999) was that the coordinates of the packing structure had to be obtained in order to determine the Voronoi polyhedron parameters required for their model. However, Zhou *et al*. (2010) addressed this shortcoming in one of their previous studies (Zhou & Yu, 2009) and therefore this model could be used.

Secondly Zhou *et al*. (2010) included the conduction through the contact area between two static contacting particles in their DPS-CFD approach. The equation for conduction through the contact area derived by Batchelor & O'Brien (1977), which was slightly modified by Cheng *et al*. (1999), was used as shown in Eq. (14).

$$Q_{i,j} = \frac{4r_c^{'}\left(T_j - T_i\right)}{\left(1/k_{si} + 1/k_{sj}\right)} \tag{14}$$

In Eq. (14) $Q_{i,j}$ is the conduction heat transfer between the contacting particles *i* and *j*, with *T* the surface temperature and k_s the solid thermal conductivity of each of the particles *i* and *j*. The reduced particle-particle contact radius, $r_c^{'}$, was introduced by Zhou *et al*. (2010) to ensure an accurate prediction of the conduction by accounting for the overestimation of the particle-particle contact radius, r_c, due to the use of a low Young's modulus in the DPS simulation.

A separate conduction effective thermal conductivity was not provided in the results by Zhou *et al*. (2010), instead the overall effective thermal conductivity of the packed bed is calculated by determining an overall heat flux through the bed that included the effects of conduction and radiation. From the CFD results the simple Fourier conduction rate equation was used to infer the effective thermal conductivity. Zhou *et al*. (2010) did express the relative contributions of the various contributing heat transfer mechanisms as a percentage of the total heat flux in the packed bed at a certain temperature. The results obtained with the DPS-CFD approach were validated with measured and predicted results reported in literature.

The particle-fluid-particle conduction model of Cheng *et al*. (1999) was also used in their more recent study, Cheng & Yu (2013), in which they extended their reported approach to also include the effects of radiation heat transfer.

Wang *et al*. (2016a) proposed an effective thermal conductivity model to predict conduction, radiation, and convection heat transfer in a pebble bed. Their model is based on the same thermal resistance approach as that of Van Antwerpen *et al*. (2012). The minimum unit cell of

the packed bed was also divided into inner, middle, and outer regions accounting for different conduction heat transfer mechanisms in each of these regions, similar to the approach of Van Antwerpen *et al*. (2012). The conduction path through the inner region consists of two thermal resistance components, i.e., the resistance of the conduction through the solid material, R_c, and the contact resistance in the contact region, R_{cont}. It was assumed that the spheres have smooth surfaces, therefore the empirical correlation derived by Chen & Tien (1973), shown in Eq. (15), was used to determine R_{cont}.

$$R_{cont} = \frac{0.64}{k_s r_o} \tag{15}$$

A method to couple the contact area between the spheres with bed strain was presented by Wang *et al*. (2016a), by expressing the radius of the contact area, r_o, as a function of the bed strain, ε. Eq. (16) shows the expression used to calculate the radius of the contact area:

$$r_o = R_o \sqrt{2\zeta \cdot \varepsilon} \tag{16}$$

where R_o is the initial sphere radius before radial deformation and ζ is a correction factor. A method to obtain a preliminary estimation of the correction factor is given by Wang *et al*. (2016a). However, a DEM method can be used to predict the parameter in detail.

The thermal resistance for the middle region, R_m, of the unit cell accounts for the conduction through the solid and gas materials, as shown in Eq. (17):

$$R_m = \frac{\beta^2}{\pi R_o k_f \left(ln\left(k_s/k_f\right) - \beta \right)} \tag{17}$$

with $\beta = 1 - k_f/k_s$. Conduction through the outer gas material is represented by the thermal resistance for the outer region, R_{out}. The proposed model was used to study the effects of various parameters on the effective thermal conductivity, including the effect of contact area (Wang *et al.*, 2016b). From the results it was evident that the effective thermal conductivity increased significantly with an increase in bed strain as a result of the larger contact areas, thus effectively increasing the conduction component.

Yamoah *et al*. (2012) proposed a mathematical model to investigate the fluid flow as well as the heat transfer in a PBR. Both conduction and radiation heat transfer were addressed in the calculation of the effective thermal conductivity. Ren *et al*. (2017) performed theoretical calculations to predict the effective thermal conductivity in a full-size pebble bed representative of the heat transfer test facility that has been constructed as a part of the Chinese HTR-PM demonstration project. The results obtained will be used for the optimization of the test facility and to determine which future experimental tests are required.

Yamoah *et al*. (2012) and Ren *et al*. (2017) used the same mathematical models to calculate the effective thermal conductivity. The conduction component of the effective thermal conductivity consists of two components. Firstly, for the conduction through the solid pebble material and stagnant fluid the model of Zehner & Schlünder (1970) was used. The second component describes conduction through the solid material and contact area between pebbles, for which an existing model defined by Kaviany (1991) was used. This is similar to the approach of the IAEA ZS Total correlation.

Asakuma *et al*. (2016) used a numerical approach and presented a homogenization method that can be used to perform a thermal analysis of a packed pebble bed. The advantage of the proposed method is that it evaluates exact changes in microstructure and temperature by using a three-dimensional finite element method. For the prediction of the conduction component of the effective thermal conductivity specific attention was given to the contact resistances at the contact surfaces between two adjacent spheres. Conduction through the contact areas due to the rough surfaces of the spheres as well as the conduction through the interstitial gas in the micro-gap were considered. Parameters that are accounted for in the calculation of the contact resistance include surface roughness, contact pressure and micro-hardness of the material. A parallel resistance network was used to calculate the overall contact resistance due to the resistances of each of the conduction paths.

The effective thermal conductivity was then calculated for a pebble bed with a BCC packing structure. Asakuma *et al*. (2016) concluded from their results that the effect of contact resistance becomes less significant at higher temperatures and larger particle sizes. It is however important to note that the effect of porosity was ignored in the study.

4.3. Effective thermal conductivity due to thermal radiation

The contribution of the radiation component to the effective thermal conductivity of a packed bed of spheres becomes significant at higher temperatures, i.e., above approximately 650 °C (Breitbach & Barthels, 1980; Zhou *et al.*, 2007; Cheng & Yu, 2013; Talukdar *et al.*, 2013). For temperatures of about 800 °C and higher radiation becomes the dominant heat transfer mechanism in a packed pebble bed. Therefore, it is essential to include the effects of radiation when predicting the effective thermal conductivity, especially when considering potential upset conditions as very high temperatures may be reached under these conditions.

An investigation to determine the effects of mean temperature, particle size and surface emissivity on the effective thermal conductivity was included in the study done by Zhou *et al*. (2007). Their proposed method was also used by Cheng & Yu (2013) to understand the effect of

these variables on the calculation of the effective thermal conductivity as well as radiation heat transfer in a packed bed of spheres.

Radiation heat transfer is directly influenced by the mean temperature in the packed bed as well as the size of the spherical particles. Results showed that an increase in mean temperature and particle size causes an increase in the effective thermal conductivity. Asakuma *et al*. (2014) noted that for larger particles radiation becomes the dominant heat transfer mechanism and the effective thermal conductivity becomes dependent on the emissivity. The radiation heat transfer component only becomes negligible for particle diameters smaller than 0.001 m.

Thus, the contribution of the radiation heat transfer mechanism becomes more important in instances where larger particles are used, and the effective thermal conductivity also increases with an increase in the solid surface emissivity. These conclusions are in agreement with the findings of Chen and Churchill (1963) and Talukdar *et al*. (2013).

According to Lee *et al*. (2001) the various methods to simulate the radiation heat transfer in a packed bed of spheres can be grouped into three different approaches namely the Radiative Transfer Equation (RTE) approach, the unit cell method and Radiative Transfer Coefficient (RTC) approach. Van Antwerpen *et al*. (2010) reviewed and grouped the existing thermal radiation models according to these three approaches. The conduction component of the models that will be discussed in the following section was reviewed in section 4.1 and 4.2. In this section only the radiation component of these models will be discussed.

Van Antwerpen *et al*. (2012) addressed both conduction and radiation in their MSUC model. The effective thermal conductivity due to radiation in the MSUC model was divided into two components: a short-range and a long-range radiation component, $k_e^{r,S}$ and $k_e^{r,L}$ respectively, as shown in Eq. (18):

$$k_e^r = k_e^{r,S} + k_e^{r,L} \tag{18}$$

Short-range radiation was defined as the radiation exchange between two neighbouring spheres that are in contact. The long-range radiation component referred to the radiation exchange through the voids in the packed bed with spheres not in contact with the sphere under consideration.

The short-range radiative conductivity vector was derived based on the assumption that the two contacting spheres can be approximated by two grey diffuse parallel plates and is given by Eq. (19):

$$\bar{k}_e^{r,S} = \frac{4 d_p \sigma A_s \bar{T}^3}{A_r \left(\left(2 - 2\varepsilon_r\right) / \varepsilon_r + 1 / F_{1-2} \right)} \tag{19}$$

with σ the Stephan-Boltzmann constant for radiation, A_s the surface area of a sphere, ε_r the solid emissivity of a sphere, A_r the radiation conduction area and $\bar{T}$ the average of the sphere surface temperatures. It is assumed that the surface areas and emissivities of the spheres are the same. The diffuse view factor between the two spheres, $F_{1\text{-}2}$, was calculated based on the diffuse view factor between two hemispheres in contact as defined by Wakao *et al.* (1969).

Eq. (20) was derived by Van Antwerpen *et al*. (2012) to predict the long-range radiation component of the effective thermal conductivity, $k_e^{r,L}$.

$$k_e^{r,L} = \frac{4\left(1.33 d_p\right) \sigma A_s \bar{T}^3 \bar{n}_{long}}{A_r \left(\left(2 - 2\varepsilon_r\right) / \varepsilon_r + 1 / F_{1-2,avg}^{L} \right)} f_k \tag{20}$$

The long-range coordination flux number, $\bar{n}_{long}$, represents the number of spheres participating in the long-range radiation and was determined empirically and the parameter f_k is a non-isothermal correction factor. The unweighted average long-range diffuse view factor, $F_{1-2,avg}^{L}$, shown in Eq. (20) was derived based on the findings of Pitso (2011).

Pitso (2011) studied the distribution of the long-range diffuse view factor in the bulk region of a numerically packed bed using the built-in ray tracing view factor calculator of a CFD package. From the results it was concluded that the long-range view factor decreases to zero at a distance of approximately 2.25 sphere diameters from the sphere under consideration. Thus, a sphere in the bulk region of a randomly packed bed does not have a view of spheres with centre points 2.25 sphere diameters or more away from the sphere under consideration.

The long-range radiation is a complex phenomenon to model because of the difficulty to characterise the porous structure. Van Antwerpen *et al*. (2012) focused on the bulk region in the characterisation of the long-range radiation due to the complex nature of the characterisation of the long-range diffuse view factor in the near-wall region. Results obtained for the radiation component of the MSUC model were compared with the experimental data from various studies and were found to be in good agreement for temperatures up to 1200 °C. It was concluded that the long-range radiation should be investigated further in future studies to improve the MSUC model specifically for temperatures above 1200 °C.

Wang *et al*. (2016a) incorporated the radiation model as proposed by Van Antwerpen *et al*. (2012) to predict the radiation heat transfer component of their proposed effective thermal conductivity model. The results obtained were compared with various available theoretical

models, CFD numerical simulations as well as experimental data and it was shown that good agreement was obtained.

Zhou *et al.* (2007) combined a net radiation method with the BEM to determine the radiation heat exchange between solid surfaces. As mentioned previously the method was applied to square array and hexagonal array ordered packing configurations. Thus, the voids in the packed bed were enclosed by the boundaries of the solid surfaces surrounding it. As a result, the radiation was solved for a closed cavity. For a random packing of spherical particles, the radiation problem becomes more complex as radiation rays can travel through other voids in the packed bed of spheres. The radiation component of the effective thermal conductivity is determined by deducting the conduction component from the overall effective thermal conductivity value, similar to Eq. (1).

The radiative effective thermal conductivity results were compared with the results obtained using theoretical radiation models found in current literature. Although there were large variations between the existing theoretical models, the results obtained with the BEM model fell within the range of the results predicted by the models. The BEM method can be applied to a random packed bed; however, the packing structure has to be known.

In the DPS-CFD approach used by Zhou *et al*. (2010) an overall heat flux through the packed bed was determined to calculate the overall effective thermal conductivity of the packed bed as discussed in section 4.2. The radiation heat transfer was calculated in their model using an approach used in a previous study (Zhou & Yu, 2009), where a local environmental temperature is assumed to represent the surface temperature of the particles and fluid in the enclosed cell that surround the particle under consideration.

A new numerical macroscopic approach to calculate the radiation heat transfer in a packed bed of uniform spheres was proposed by Cheng & Yu (2013) to extend their existing conduction model as mentioned in section 4.2. The difference between the proposed approach and existing studies was that the packing structure was used directly in the calculation of the effective thermal conductivity. This was done by using a Voronoi network model and it resulted in a particle scale approach for the calculation of the effective thermal conductivity. The results obtained using the proposed approach were in good agreement with the results presented in existing publications. Although the structural approach of the proposed method was general, the model and results were case specific and further studies must be done for the development of a more comprehensive model.

The effect of spatial scale on the modelling of thermal radiation in packed pebble beds were investigated numerically with a discrete element method by Wu *et al*. (2016). Three models of different scales were used namely (1) the short-range model, (2) the long-range model and (3) the microscopic model. The short-range model is a partial integral scale model that takes into account only the radiation to all neighbouring spheres in direct contact with the sphere under consideration. This is similar to the short-range radiation component derived by Van Antwerpen *et al*. (2012). For the short-range model the radiant heat flux between a pair of Voronoi neighbouring spheres as well as the temperature of each sphere was calculated. The sphere temperatures were then used to determine the radiative effective thermal conductivity and the radiation exchange factor.

The long-range model is a full integral scale model that takes into account all possible radiation between surrounding spheres, even if the spheres participating in the radiation is not in direct contact. This is similar to the combined short-range and long-range radiation models derived by Van Antwerpen *et al*. (2012). For the long-range model the net radiative heat flux was calculated for each sphere. The view factors were calculated using a Monte Carlo ray tracing method. It was found that for the calculation of the view factors it was sufficient to only consider the interaction between the sphere under consideration and three layers of surrounding spheres. This is similar to the findings of Pitso (2011).

The microscopic model is a sub-particle scale model for which each particle surface is divided into a series of meshes and each mesh is considered as an isothermal surface. This model has a high computational cost and is impractical for the prediction of the heat transfer in a complete packed bed; therefore, it will not be discussed in further detail. The radiative effective thermal conductivity results obtained with both the short-range and long-range models were compared with the results predicted by existing correlations. It was concluded that the short-range model delivered results in good agreement with the results predicted by the correlations for temperatures lower than 1200 °C; however, it is not suitable for packed beds where the solid material conductivity of the packed bed is much larger than the radiative effective thermal conductivity.

For the long-range model to be applicable it was assumed that all the spheres in the packed bed were isothermal bodies with an infinite solid thermal conductivity. The results of the long-range model were also compared with the experimental data of the HTTU (Rousseau *et al.*, 2014). An average conduction component for the effective thermal conductivity was assumed based on the HTTU results and the total effective thermal conductivity was determined by the summation of the average conduction and long-range radiative components. Although the

results for the long-range model were in good agreement with the theoretical correlations, when compared with experimental data it overestimated the total effective thermal conductivity.

Wu *et al*. (2017) continued their investigation of radiation in packed beds by using a CFD-DEM approach coupled with their short-range model (Wu *et al.*, 2016) to determine the effective thermal conductivity in a randomly packed bed due to conduction and radiation. A randomly packed bed that is representative of the HTR-10 reactor core was simulated. Similar to Zhou *et al*. (2007) the total effective thermal conductivity was considered equal to a summation of the conduction and radiation components. This approach together with the least squares method for post-processing of the simulation data were used to calculate the radiative effective thermal conductivity for the packed bed. The results obtained were compared with the values predicted by existing correlations and were found to be in good agreement for temperatures up to 1200 °C.

The Zehner & Schlünder (1972) model as modified by Breitbach & Barthels (1980) was used to predict the radiation component of the effective thermal conductivity in the studies conducted by Yamoah *et al*. (2012) and Ren *et al*. (2017).

The thermal radiation component in the study by Asakuma *et al*. (2016) was modelled using a thermal radiation model developed in one of their previous studies. Thermal radiation was added to an existing model for a packed bed by using a combination of the homogenization method and conventional methods (Asakuma *et al.*, 2014). The radiative effective thermal conductivity was then calculated for pebble beds with simple cubic and body centred cubic packing structures. The results obtained were in good agreement with the values predicted by an empirical conventional model for body centred cubic geometries but did not provide good results for a simple cubic packed bed.

4.4. Effective thermal conductivity in the near-wall region

Despite the importance of the near-wall region the majority of studies still neglect wall effects in the prediction of the effective thermal conductivity. To eliminate the wall effects, some studies increase the number of particles in the packed bed under consideration and then ignore the wall regions of the packed bed in the prediction of the effective thermal conductivity (Cheng *et al.*, 1999; Zhou *et al.*, 2007; Cheng & Yu, 2013). Others eliminate the wall effects in DEM generated packed pebble beds by cutting off the wall regions and only considering the remaining bulk region in their heat transfer analysis (Chen *et al.*, 2016).

After the review done by Van Antwerpen *et al*. (2010) they developed the MSUC model (Van Antwerpen *et al.*, 2012) to specifically address the shortcoming of the studies that do not address the wall effects in a packed pebble bed. The effect of the changes in the packing structure of the pebble bed in the wall regions was clearly visible in the effective thermal conductivity results of the MSUC model.

The MSUC model for the wall region uses a similar thermal resistance network approach as was used for the bulk region as described in section 4.2 and 4.3. For the derivation of the component of the MSUC model applicable to the wall region a half sphere in contact with a flat wall was considered. The unit cell for the wall region was also divided into an inner, middle, and outer region. The joint thermal resistance, $R_{j,W}$, for a rough contact network that can be used to predict the conduction component of the effective thermal conductivity in the wall region is given in Eq. (21):

$$R_{j,W} = \left(\left(R_{L,1,2} + \left(\frac{1}{R_g} + \frac{1}{R_s} \right)^{-1} \right)^{-1} + \frac{1}{R_{\lambda,W}} + \frac{1}{R_{G,W}} \right)^{-1} + \left(\frac{1}{R_{in,1,W}} + \frac{1}{R_{mid,1,W}} + \frac{1}{R_{out,1,W}} \right)^{-1} \tag{21}$$

All the thermal resistances were calculated with the same methods as discussed in section 4.2 with small changes in some of the equations in order to account for the change in the geometry of the conduction path from two spheres to a half sphere and a flat wall. The reader is referred to the paper by Van Antwerpen *et al*. (2012) for the detailed expressions of the thermal resistances. Eq. (13) can be used to calculate the conduction effective thermal conductivity for the wall region; however, it will only consist of a component in the radial coordinate direction.

In the MSUC model the total effective thermal conductivity due to radiation in the wall region is equal to the summation of the short-range and long-range radiation components in the wall region, similar to Eq. (18). The short-range radiation component of the effective thermal conductivity for the wall region was predicted using Eq. (22):

$$k_e^{r,S,W} = \frac{2 d_p \sigma \bar{T}^3}{A_r \left(\left(1 - \varepsilon_{r,1} \right) / \left(\varepsilon_{r,1} A_1 \right) + 1 / \left(A_1 F_{1-2}^W \right) + \left(1 - \varepsilon_{r,2} \right) / \left(\varepsilon_{r,2} A_2 \right) \right)} \tag{22}$$

where A_1 is the surface area of the sphere, A_2 is the effective surface area of the wall and F_{1-2}^W is the diffuse radiation view factor from a single sphere to the wall. An approximation for the view factor F_{1-2}^W was obtained using the results from the study done by Pitso (2011).

Van Antwerpen *et al.* (2012) assumed that the long-range radiation component of the effective thermal conductivity is the same in both the bulk and the near-wall regions, due to the complexity of modelling the long-range radiation in the near-wall region. It was concluded that

as the model for the long-range radiation was only a first approximation, further study in this area should be done to refine the proposed model. Specifically, the long-range diffuse view factor should be defined as a function of radial position in a randomly packed bed to account for the wall effect in the near-wall region. The average long-range view factor must also be weighted to include radiation from the number of spheres that explicitly contribute to the long-range radiation.

The results for the conduction and radiation components of the MSUC model in the wall region were compared with experimental data from literature. The results of the MSUC model were found to be in good agreement with the experimental data. They also concluded that short-range radiation is the dominant radiation heat transfer mechanism in the wall region. It must also be noted that the radiation component of the MSUC model in the wall region is only valid if the curvature of the wall is large compared to the sphere diameter.

Gan & Kamlah (2010) investigated the heat transfer at the pebble bed-wall interface by modelling a heat transfer coefficient that is representative of the thermal contact conductance of the interface. The model is based on a basic unit cell of the contact region which includes the wall, a pebble, and the interstitial gas. Three different heat transfer mechanisms were accounted for in the calculations namely (1) conduction through the solid-solid contact point, (2) conduction through the gas gap between the pebble and the wall and (3) thermal radiation. A thermal resistance network approach was used to determine the heat transfer from the pebble bed through the contact area to the wall. The interfacial heat transfer coefficient can be considered as a resultant thermal resistance that is a combination of the three thermal resistances representing the various heat transfer mechanisms connected in parallel.

The predicted values for the interfacial heat transfer coefficient were compared with experimental data and the results were in reasonable agreement. A detailed explanation of the differences between the predicted value and the experimental data was provided by Gan & Kamlah (2010). The proposed model can be implemented into a finite element code that can then be used to perform a full thermo-mechanical analysis of a pebble bed. The effective thermal conductivity for the near-wall region is required to determine the heat transfer through the wall region. Thus, the approach proposed by Gan & Kamlah (2010) does not predict the effective thermal conductivity for the near-wall region but can be useful to predict a contact resistance value for the pebble bed-wall interface.

4.5. Separation of the conduction and radiation components of the effective thermal conductivity

From the experimental results presented in section 2 and 3, it is clear that the near-wall effects significantly influence the effective thermal conductivity trend in the near-wall region. It is not only important to accurately predict the effective thermal conductivity in the near-wall region of a pebble bed, but it is also important to gain a better understanding as to why and how the wall effects change the trend of the effective thermal conductivity curve. By investigating the underlying phenomena and the characteristics of the resultant values of the effective thermal conductivity, such an understanding can possibly be achieved.

During loss of forced cooling accidents in a PBR the main contributing heat transfer mechanisms are conduction and radiation for the removal of decay heat. The experimental results for the SANA-I test facility showed a prominent reduction in the effective thermal conductivity values in the near-wall region. Whilst natural convection played a role in the SANA-I experimental tests, the HTTU tests were conducted under near-vacuum conditions to eliminate the effects of natural convection. Thus, conduction and radiation were the only heat transfer phenomena present in the HTTU packed bed that could influence the effective thermal conductivity trend.

A possible method to investigate the underlying phenomena of the effective thermal conductivity can be to separate the conduction and radiation components of the overall effective thermal conductivity result. By using a separation method, one would be able to evaluate and understand the effect of each of the contributing heat transfer phenomena to the overall effective thermal conductivity trend. In this section studies that attempt to separate the effective thermal conductivity contributions will be discussed.

Some studies distinguish between the conduction and radiation components of the overall effective thermal conductivity by assuming that the heat transfer phenomena can be superimposed, as shown in Eq. (1). This approach was used by Zhou *et al*. (2007), Cheng & Yu (2013) and Wu *et al.* (2017).

Zhou *et al*. (2007) and Cheng & Yu (2013) determined the overall effective thermal conductivity due to combined conduction-radiation. After which the conduction contribution to the effective thermal conductivity was calculated using a pure conduction model. The radiation component of the effective thermal conductivity was then calculated using Eq. (1). Wu *et al.* (2017) used the same method, but instead of determining the conduction component using a pure conduction model, the conduction component was obtained from existing experimental data in literature.

None of these studies considered the influence of the wall effects on the effective thermal conductivity and its radiation and conduction components.

Van Antwerpen *et al*. (2012) also distinguished between the conduction and radiation components in the MSUC model, by assuming that the heat transfer phenomena can be superimposed. The conduction and radiation components as well as the overall effective thermal conductivity results predicted with the MSUC model were presented as a function of temperature. Thus, one could easily distinguish between the contributions of the different phenomena. Their study took into account the wall effects in the near-wall region.

The MSUC model was used to determine the conduction and radiation components of the effective thermal conductivity for the SANA-I test facility, as can be seen in Fig. 12 (Van Antwerpen *et al.*, 2012). Van Antwerpen and co-workers noted that the conduction component showed a slight increase in the region next to the inner wall, whereas the radiation component showed a slight decrease. For the near-wall region both the radiation and conduction components showed a decrease. From the results it is evident that the altered packing structure has a definite influence on both the radiation and conduction components of the effective thermal conductivity. The cause of the decrease in the trends of the effective thermal conductivity components was not investigated in further detail.

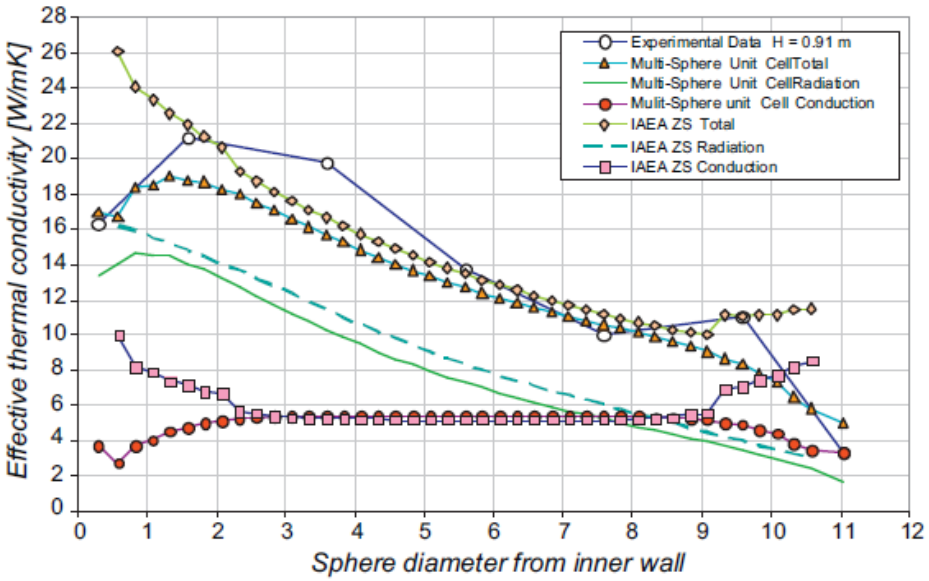

Fig. 12 Comparison between the effective thermal conductivity components predicted by the MSUC model and the experimental results of the SANA-I test facility for the 35k W steady state test (Van Antwerpen *et al.*, 2012).

Although the MSUC model accounted for the near-wall effects the long-range radiation component used in the model is only valid for the bulk region and not the near-wall region. Thus, the results obtained for the radiation component with the MSUC model will be a first

approximation as further work needs to be done to develop a long-range radiation component that is valid for the near-wall region. A more fundamental understanding of the radiation contribution of the effective thermal conductivity in the near-wall region would be beneficial in developing such a long-range radiation model.

The radiation model of Van Antwerpen *et al*. (2012) was used by Wang *et al*. (2016a; 2016b) to predict the radiation component of the effective thermal conductivity. However, the conduction and radiation component results were not presented separately, but each of the components were expressed as a ratio of the overall effective thermal conductivity.

5. Conclusion

The effective thermal conductivity in the near-wall region of a packed pebble bed reactor forms part of the critical heat flow path during the decay heat removal process. Therefore, for the design of pebble bed gas-cooled and solid fuel molten salt-cooled generation IV reactors, it is imperative to properly understand and assess this phenomenon.

The ZBS (Bauer & Schlünder, 1978) and the IAEA ZS Total (Niessen & Ball, 2000) correlations are commonly used to predict the effective thermal conductivity in packed pebble beds. These widely used correlations are valid for the bulk region but breaks down in the near-wall region. The comparison between the results of these correlations and experimental results prove that the conclusion of Bauer & Schlünder (1978), that the wall effects can be neglected, is not valid. Thus, a better understanding of how the wall effects impact the characteristics of the heat transfer is essential.

From the review presented in this paper it is evident that none of the current methods that account for conduction and radiation heat transfer properly addresses the near-wall effects. The MSUC model is the closest to a comprehensive model. However, its long-range radiation component is only applicable to the bulk region and should be developed further. Therefore, a need still exists for a complete model of the effective thermal conductivity that takes into account the effects of the altered packing structure in the near-wall region.

The review also showed that there has been a shift from using implicit models to using explicit models. Some of the explicit models reported recently, such as the one by Wu *et al.* (2016; 2017), has the potential to be used in the near-wall region. However, the simulation of the thermal-hydraulic behaviour of a full reactor is really only practical with the aid of implicit models of the effective thermal conductivity phenomenon.

The development of a comprehensive model for effective thermal conductivity should be based on a better understanding of the underlying phenomena and the interplay between them, especially in the near-wall region. Some studies reported in literature do distinguish between the different components, but do not necessarily investigate the underlying phenomena and interactions. The authors believe that the ability to separate the contributions of the different mechanisms can provide valuable insight into the characteristics observed due to the wall effects.

Nomenclature

A_j	Joint conduction area [m^2]
A_r	Radiation conduction area [m^2]
A_s	Surface area of sphere [m^2]
C	Fitting parameter [-]
d_p	Particle diameter [m]
f_k	Non-isothermal correction factor [-]
F	Contact force [N]
F_{1-2}	Diffuse view factor between two surfaces [-]
$F^L_{1-2,avg}$	Average long-range diffuse view factor [-]
k_e^c	Effective thermal conductivity through contact area [W/m-K]
k_e^g	Effective thermal conductivity through fluid/gas and point contact [W/m-K]
$k_e^{g,c}$	Effective thermal conductivity through fluid/gas, point contact and contact area [W/m-K]
k_e^r	Effective thermal conductivity due to radiation [W/m-K]
$k_e^{r,L}$	Effective thermal conductivity due to long-range radiation [W/m-K]
$k_e^{r,S}$	Effective thermal conductivity due to short-range radiation [W/m-K]
k_{eff}	Total effective thermal conductivity [W/m-K]
k_f	Fluid thermal conductivity [W/m-K]
k_s	Thermal conductivity of solid material [W/m-K]
ℓ_o	Physical separation distance between particles [m]
L	Height of particle column [m]

L_j	Length between centres of two spheres [m]
n_e	Effective number of contacts in solid core region [-]
$\bar{n}_{long}$	Average coordination flux number for long-range radiation [-]
r	Radial position in packed bed [m]
r_a	Radius of the micro-contact area [m]
r_c	Particle-particle contact radius [m]
$r_c^{'}$	Reduced particle-particle contact radius [m]
r_o	Radius of contact area [m]
r_p	Sphere radius [m]
r_λ	Mean free path radius between two spheres [m]
R_{cont}	Contact resistance [K/W]
R_g	Resistance of the interstitial gas in the micro-gap [K/W]
R_i	Inner radius [m]
$R_{in,1,2}$	Inner solid material resistance [K/W]
R_j	Thermal resistance of joint [K/W]
$R_{L,1,2}$	Macro-contact constriction/spreading resistance [K/W]
R_m	Resistance through middle region [K/W]
$R_{mid,1,2}$	Middle solid material resistance [K/W]
R_o	Initial radius [m] / Outer radius [m]
R_{out}	Resistance through outer region [K/W]
$R_{out,1,2}$	Outer solid material resistance [K/W]
R_s	Micro-contact constriction/spreading resistance [K/W]
T	Temperature [K]
$\bar{T}$	Average surface temperature of interacting spheres [K]
Q	Heat flux [W]
z	Sphere diameters from wall [-]
z_{depth}	Z coordinate in packed bed [m]
ε	Bed porosity [-]
ε^*	Porosity correction factor [-]
ε_c	Average porosity of core region [-]

ε_r	Emissivity [-]
ζ	Correction factor [-]
θ	Thermal parameter [-]
λ	Mean free path of gas molecules [m]
$\lambda_{es,c}$	Effective thermal conductivity of the solid core region [W/m-K]
$\lambda_{e,c}^{0}$	Effective thermal conductivity of a stagnant bed [W/m-K]
ξ	Compressive displacement [m]
σ	Stephan-Boltzmann constant [W/m^2-K^4]
ω_o	Deformation depth at origin [m]

Abbreviations

BCC	Body Centred Cubic
BEM	Boundary Element Method
CFD	Computational Fluid Dynamics
DEM	Discrete Element Method
DPS	Discrete Particle Simulation
FCC	Face Centred Cubic
FEA	Finite Element Analysis
FHR	Fluoride salt-cooled High-temperature Reactor
HTTU	High Temperature Test Unit
IAEA	International Atomic Energy Agency
MSR	Molten Salt Reactor
MSUC	Multi Sphere Unit Cell
NWTCTF	Near-wall Thermal Conductivity Test Facility
PBR	Pebble Bed Gas-cooled Reactor
RTC	Radiative Transfer Coefficient
RTE	Radiative Transfer Equation
SC	Simple Cubic
ZBS	Zehner, Bauer & Schlünder
ZS	Zehner & Schlünder

References

Asakuma, Y., Asada, M., Kanazawa, Y. & Yamamoto, T. 2016. Thermal analysis with contact resistance of packed bed by a homogenization method. *Powder Technology*, 291:46-51.

Asakuma, Y., Kanazawa, Y. & Yamamoto, T. 2014. Thermal radiation analysis of packed bed by a homogenization method. *International Journal of Heat and Mass Transfer*, 73(2014):97-102.

Bahrami, M., Yovanovich, M.M. & Culham, J.R. 2006. Effective thermal conductivity of rough spherical packed beds. *International Journal of Heat and Mass Transfer*, 49:3691-3701.

Batchelor, G.K. & O'Brien, R.W. 1977. Thermal or electrical conduction through a granular material. *Proceedings of the Royal Society of London. Series A - Mathematical and Physical Sciences*, 355(1682):313-333.

Bauer, R. & Schlünder, E.U. 1978. Part I: Effective radial thermal conductivity of packings in gas flow. Part II: Thermal conductivity of the packing fraction without gas flow. *International Chemical Engineering*, 18(2):189-204.

Breitbach, G. & Barthels, H. 1980. The radiant heat transfer in the high temperature reactor core after failure of the afterheat removal systems. *Nuclear Technology*, 49:392-399.

Chen, L., Chen, Y., Huang, K. & Liu, S. 2016. Investigation of effective thermal conductivity for pebble beds by one-way coupled CFD-DEM methods for CFETR WCCB. *Fusion Engineering and Design*, 106(2016):1-8.

Chen, J.C. & Churchill, S.W. 1963. Radiation heat transfer in packed beds. *American Institute of Chemical Engineers*, 9(1):35-41.

Cheng, G.J. & Yu, A.B. 2013. Particle Scale Evaluation of the Effective Thermal Conductivity from the Structure of a Packed Bed: Radiation Heat Transfer. *Industrial and Engineering Chemistry Research*, 52:12202-12211.

Cheng, G.J., Yu, A.B. & Zulli, P. 1999. Evaluation of effective thermal conductivity from the structure of a packed bed. *Chemical Engineering Science*, 54:4199-4209.

Chen, C.K. & Tien, C.L. 1973. Conductance of packed spheres in vacuum. *Journal of Heat Transfer*, 95(1973):302-308.

De Beer, M., Du Toit, C.G. & Rousseau, P.G. 2017. A methodology to investigate the contribution of conduction and radiation heat transfer to the effective thermal conductivity of packed graphite pebble beds, including the wall effect. *Nuclear Engineering and Design*, 314(2017):67-81.

Dixon, A.G., Gurnon, A.K., Nijemeisland, M. & Stitt, E.H. 2013. CFD testing of the pointwise use of the Zehner-Schlünder formulas for fixed-bed stagnant thermal conductivity. *International Communications in Heat and Mass Transfer*, 42(2013):1-4.

Gan, Y. & Kamlah, M. 2010. Thermo-mechanical modelling of pebble bed-wall interfaces. *Fusion Engineering and Design*, 85(2010):24-32.

Kaviany, M. 1991. Principles of heat transfer in porous media. (New York, USA: Springer-Verlag. p. 126-127).

Lee, S.H.-K., Ip, S.C.-H. & Wu, A.K.C. 2001. Sphere-to-Sphere Radiative Transfer Coefficient for packed sphere system. (*In* Proceedings of 2001 ASME International Mechanical Engineering Congress and Exposition. New York. p. 105-110.)

Liang, Y. & Li, X. 2014. A new model for heat transfer through the contact network of randomly packed granular material. *Applied Thermal Engineering*, 73(2014):984-992.

Liang, Y., Niu, H. & Lou, Y. 2016. Expression for ETC of the solid phase of randomly packed granular materials. *Applied Thermal Engineering*, 109(2016):44-52.

Niessen, H.F. & Ball, S. 2000. IAEA-TECDOC-1163: Heat Transport and Afterheat Removal for Gas Cooled Reactors Under Accident Conditions.

Panchal, M. Chaudhuri, P., Van Lew, J.T. & Ying, A. 2016. Numerical modelling for the effective thermal conductivity of lithium meta titanate pebble bed with different packing structures. *Fusion Engineering and Design*, 112(2016):303-310.

Pitso, M.L. 2011. Characterisation of long range radiation heat transfer in packed pebble beds. Potchefstroom Campus, South Africa: North-West University. (M Dissertation).

Ren, C., Yang, X., Jia, H., Jiang, Y. & Xiong, W. 2017. Theoretical analysis of effective thermal conductivity for the Chinese HTR-PM heat transfer test facility. *Applied Sciences*, 7(1)

Rousseau, P.G., Du Toit, C.G., Van Antwerpen, W. & Van Antwerpen, H.J. 2014. Separate effects tests to determine the effective thermal conductivity in the PBMR HTTU test facility. *Nuclear Engineering and Design*, 271(2014):444-458.

Slavin, A.J., Arcas, V., Greenhalgh, C.A., Irvine, E.R. & Marshall, D.B. 2002. Theoretical model for the thermal conductivity of a packed bed of solid spheroids in the presence of a static gas, with no adjustable parameters except at low pressure and temperature. *International Journal of Heat and Mass Transfer*, 45:4151-4161.

Suárez, F., Luzi, C.D., Mariani, N.J. & Barreto, G.F. 2017. Effective parameters for conductive contributions to radial heat transfer in fixed beds under stagnant conditions. *Chemical Engineering Research and Design*, 119(2017):245-262.

Talukdar, P., Mendes, M.A.A., Parida, R.K., Trimis, D. & Ray, S. 2013. Modelling of conduction-radiation in a porous medium with blocked-off region approach. *Journal of Thermal Sciences*, 72(2013):102-114.

Tsory, T., Ben-Jacob, N., Brosh, T. & Levy, A. 2013. Thermal DEM-CFD modeling and simulation of heat transfer through packed bed. *Powder Technology*, 244(2013):52-60.

Tsotsas, E. & Martin, H. 1987. Thermal Conductivity of Packed Beds: A Review. *Chemical Engineering Processes*, 22:19-37.

Van Antwerpen, W. 2009. Modelling the effective thermal conductivity in the near-wall region of a packed pebble bed. Potchefstroom Campus, South Africa: North-West University. (PhD Thesis).

Van Antwerpen, W., Du Toit, C.G. & Rousseau, P.G. 2010. A review of correlations to model the packing structure and effective thermal conductivity in packed beds of mono-sized spherical particles. *Nuclear Engineering and Design*, 240:1803-1818.

Van Antwerpen, W., Rousseau, P.G. & Du Toit, C.G. 2012. Multi-sphere Unit Cell model to calculate the effective thermal conductivity in packed pebble beds of mono-sized spheres. *Nuclear Engineering and Design*, 247:183-201.

Wakao, N., Kato, K. & Furuya, N. 1969. View factor between two hemispheres in contact and radiation heat transfer coefficient in packed beds. *International Journal of Heat and Mass Transfer*, 12:118-120.

Wang, X., Zheng, J. & Chen, H. 2016a. A prediction model for the effective thermal conductivity of mono-sized pebble beds. *Fusion Engineering and Design*, 103(2016):136-151.

Wang, X., Zheng, J. & Chen, H. 2016b. Application of a model to investigate the effective thermal conductivity of randomly packed fusion pebble beds. *Fusion Engineering and Design*, 106(2016):40-50.

Widenfield, G., Weiss, Y. & Kalman, H. 2003. The effect of compression and preconsolidation on the effective thermal conductivity of particulate beds. *Powder Technology*, 133(2003):15-22.

World Nuclear Association. 2017. Molten Salt Reactors. http://www.world-nuclear.org/information-library/current-and-future-generation/molten-salt-reactors.aspx Date of access: 13 September. 2017.

Wu, H., Gui, N., Yang, X., Tu, J. & Jiang, S. 2016. Effect of scale on the modeling of radiation heat transfer in packed pebble beds. *International Journal of Heat and Mass Transfer*, 101:562-569.

Wu, H., Gui, N., Yang, X., Tu, J. & Jiang, S. 2017. Numerical simulation of heat transfer in packed pebble beds: CFD-DEM coupled with particle thermal radiation. *International Journal of Heat and Mass Transfer*, 110(2017):393-405.

Yamoah, S., Akaho, E.H.K., Ayensu, N.G.A. & Asamoah, M. 2012. Analysis of fluid flow and heat transfer model for pebble bed high temperature gas cooled reactor. *Research Journal of Applied Sciences, Engineering and Technology*, 4(12):1659-1666.

Zehner, P. & Schlünder, E.U. 1970. Wärmeleitfähigkeit von Schüttungen bei mäβigen Temperaturen. *Chemie Ingenieur Technik*, 42:933-941.

Zehner, P. & Schlünder, E.U. 1972. Einfluss der Wärmestrahlung und des Druckes auf den Wärmetransport in nicht durchströmten Schüttungen. *Chemie Ingenieur Technik*, 44:1303-1308.

Zhou, Z.Y. & Yu, A.B. 2009. Particle scale study of heat transfer in packed and bubbling fluidized beds. *AIChe Journal*, 55(4):868-884.

Zhou, J., Yu, A. & Zhang, Y. 2007. A boundary element method for evaluation of the effective thermal conductivity of packed beds. *Journal of Heat Transfer*, 129:363-371.

Zhou, Z.Y., Yu, A.B. & Zulli, P. 2010. A new computational method for studying heat transfer in fluid bed reactors. *Powder Technology*, 197:102-110.

3. Article 2: Experimental study of the effective thermal conductivity in the near-wall region of a packed pebble bed

M. De Beer *, C.G. Du Toit, P.G. Rousseau

Abstract

The effective thermal conductivity is an important parameter that represents the overall heat transfer in packed beds, including packed pebble beds. Experimental test facilities have been used to determine the effective thermal conductivity of packed pebble beds; however, the experimental results are often case specific and do not account for wall effects in the near-wall region. Recently the Near-Wall Thermal Conductivity Test Facility (NWTCTF) was developed at the North-West University in Potchefstroom, South Africa to perform detailed investigations of the conduction and radiation heat transfer phenomena in the near-wall region of a packed bed of spheres. The experimental test facility was introduced in a previous paper and some results were presented. This paper provides a short description of the test facility and then presents extensive experimental results obtained for structured and randomly packed beds consisting of 60 mm diameter graphite spheres at temperatures of up to 800 °C, together with the associated uncertainties. Results obtained demonstrate the effect of the near-wall region and the packing structure on the effective thermal conductivity.

Keywords: Effective thermal conductivity, Experimental investigation, Near-wall effect, Packed pebble bed, Thermal conduction, Thermal radiation

1. Introduction

A thorough understanding and an accurate prediction of the heat transfer through packed pebble beds are essential for the design of various thermal-fluid systems such as catalytic reactors, drying processes, thermal insulation, heat storage systems, packed bed regenerators, hydrogen production and generation IV type nuclear reactors (Asakuma *et al.*, 2016; Ren *et al.*, 2017; Van Antwerpen *et al.*, 2010; Yang *et al.*, 2012; Zhou *et al.*, 2007). Two generation IV type reactors which are favoured for the inherent safety characteristics of their designs are pebble bed gas-cooled reactors (PBRs) and fluoride salt-cooled high-temperature reactors (FHRs) (Wu *et al.*, 2016; World Nuclear Association, 2017; You *et al.*, 2017).

The overall heat transfer through a packed pebble bed is represented implicitly by a single parameter known as the effective thermal conductivity. When considering upset conditions in a PBR during a depressurized loss of forced coolant incident, conduction and radiation become

the dominant heat transfer mechanisms for decay heat removal (Van Antwerpen *et al.*, 2010; You *et al.*, 2017). In order to ensure that an optimal reactor design is achieved it is important to have a thorough understanding of the contributing heat transfer phenomena as well as the interplay between the heat transfer mechanisms for different temperatures and packing structures (Van Antwerpen *et al.*, 2010; You *et al.*, 2017).

The geometry of a randomly packed bed consists of three main regions namely the bulk, wall, and near-wall regions (Van Antwerpen, 2009). The porous structure changes significantly in the region near any wall as the packing geometry is disrupted in this area. This variation in packing structure is known as the wall effect and influences the magnitude of the effective thermal conductivity in the wall region, which includes the pebble to reflector interface. During normal operation, the conductive effects in the near-wall region will be negligible compared to convective transport. However, during a loss of coolant event the near-wall region forms part of the critical path for decay heat removal.

It is important to consider higher temperatures when investigating the effective thermal conductivity as the contribution of radiation heat transfer to the overall effective thermal conductivity increases significantly at temperatures above 650 °C (Breitbach & Barthels, 1980; Zhou *et al.*, 2007; Cheng & Yu, 2013; Talukdar *et al.*, 2013; Ren *et al.*, 2017). Implicit effective thermal conductivity models are often used in practice to predict the heat transfer in full-scale reactors due to the excessive computational resources required by explicit models. For the development and testing of new and existing models it is necessary to have good quality experimental data that can be used to validate the predicted values of the effective thermal conductivity.

Various experimental studies have been done for the investigation of heat transfer in packed pebble beds. Van Antwerpen (2009) concluded that far more experimental work has been done for packed pebble beds at low temperatures with small particle diameters than at higher temperatures with larger particles. When focusing on the safety case for a PBR design, which is the motivation for this study, the experimental test conditions should be similar to what can be expected during actual upset conditions; namely a packed pebble bed consisting of larger particle sizes at higher temperatures, in a stagnant gas environment with limited convective heat transfer.

Researchers that conducted experimental work to predict the effective thermal conductivity in packed pebble beds at higher temperatures for larger sphere diameters include Breitbach & Barthels (1980), Stöcker & Niessen (1997) and Rousseau *et al.* (2014).

Breitbach & Barthels (1980) conducted experimental work using the High Temperature Oven (HTO) test facility at temperatures of up to 1500 °C. Experimental tests were conducted with zirconium-oxide pebbles and graphite pebbles with a particle diameter of 45 mm and 40 mm respectively. A least-squares regression function was fitted to the temperature distribution to obtain a smooth temperature function. The authors used a transient method to determine the effective thermal conductivity from the temperature distribution.

Stöcker & Niessen (1997) used the SANA-I test facility to investigate the heat transfer phenomena inside a High Temperature Gas-cooled Reactor (HTGR) core. Two steady state experimental tests were conducted for a randomly packed pebble bed with graphite pebbles with diameters of 60 mm and 30 mm. Both experimental tests were performed within a helium environment at atmospheric pressure with heater power inputs of 10 kW and 35 kW respectively. The effective thermal conductivity for the packed pebble bed was calculated using the heat transfer and temperature measurements.

The High Temperature Test Unit (HTTU) test facility was used by Rousseau *et al.* (2014) to determine the effective thermal conductivity through a randomly packed bed of graphite spheres with a diameter of 60 mm. The experimental tests were conducted at near-vacuum conditions in a nitrogen environment at temperatures of up to 1200 °C. The effective thermal conductivity was determined by using a simple Fourier conduction rate equation, as shown in Eq. (1):

$$\dot{Q} = -k_{eff} A \frac{dT}{dr} \tag{1}$$

with $\dot{Q}$ the heat transfer rate, k_{eff} the effective thermal conductivity, T the temperature, A the applicable area in the pebble bed through which the heat transfer is taking place and Δr the path length associated with the relevant area in the pebble bed.

Rousseau *et al.* (2014) proposed and applied a comprehensive method to the HTTU experimental data to derive the effective thermal conductivity of the pebble bed together with the associated uncertainties. Therefore, the HTTU results could be used with confidence in the verification and validation of new models. The HTTU results showed that the near-wall effects had a significant influence on the resultant effective thermal conductivity values at higher temperatures and it was concluded that further studies are required to investigate the near-wall effects in more detail (Rousseau *et al.*, 2014).

In support of the Chinese High Temperature gas-cooled Reactor Pebble bed Module (HTR-PM) demonstration project; a full-scale heat transfer test facility has been developed to conduct effective thermal conductivity tests for a randomly packed pebble bed of machined graphite

spheres with a diameter of 60 mm (Ren *et al.*, 2017). The test section is annular with an inner radius of 0.5 m, an outer radius of 2 m and a height of 1 m. Although no experimental results have been published yet it is planned that experimental tests will be conducted at atmospheric conditions in a helium environment for temperatures of up to 1600 °C. Due to the similarity between the HTR-PM and the SANA-I test facilities the SANA-I experimental data were used for a theoretical analysis of the pebble bed of the HTR-PM test facility. The results of the theoretical analysis were used to aid the design and optimization of the test facility and additional experimental tests.

None of the experimental investigations discussed here focused specifically on the characterization of the heat transfer in the near-wall region of a packed pebble bed. Furthermore, not all of the reported experimental data provide the associated uncertainties, thus limiting the use of the data to validate new models. The purpose of this paper is to attempt to fill some of this gap in the available knowledge by presenting an extensive data set of experimental results for the near-wall region obtained for structured and randomly packed beds consisting of 60 mm graphite spheres at temperatures of up to 800 °C, together with the associated uncertainties.

2. Near-wall Thermal Conductivity Test Facility

A new test facility, the Near-wall Thermal Conductivity Test Facility (NWTCTF), was introduced in recent papers by the current authors (Rousseau *et al.*, 2015; De Beer *et al.*, 2017) and will therefore only be described briefly here. The purpose of the NWTCTF, shown in Fig. 1 (a), is to perform detailed experimental investigations of the combined conduction and radiation heat transfer in the near-wall region at temperatures of up to 1600 °C. The NWTCTF test section has a cubical configuration with side lengths of 420 mm in which spheres are placed to form the packed bed. The packed bed consists of no more than 343 machined graphite spheres, but the exact number depends on the packing configuration used. Each sphere has a diameter of 60 mm and was inherited from the PBMR HTTU test facility. Fig. 1 (b) shows an exploded view of the NWTCTF test unit and its various components.

The packed bed has an inner “radiator” graphite wall (heated wall) and an outer reflector graphite wall (cooled wall) on opposite sides. These can each be maintained at a constant near-homogenous temperature. The inner radiator wall is heated by a set of heater elements positioned next to it, while the outer reflector wall is cooled by a water jacket positioned right up against it. A temperature gradient is induced through the packed bed of spheres between the

heated and cooled wall. The test section is enclosed in layers of insulation material to minimize heat losses to the surroundings.

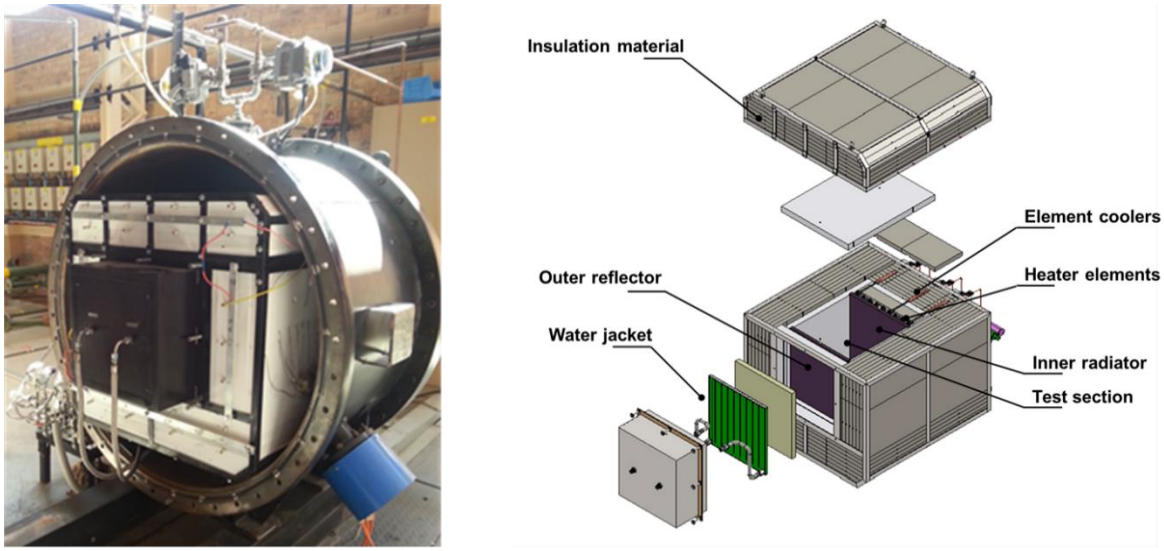

Fig. 1 (a) Photograph of NWTCTF test unit positioned inside pressure vessel and (b) exploded view of NWTCTF test unit.

All experimental tests were conducted with a near-vacuum nitrogen environment maintained in the test section in order to ensure that the effects of convection could be neglected. The temperature of the inner radiator wall was controlled at a constant temperature and the temperature difference between the water inlet and outlet temperatures of the water jacket was controlled at approximately 10 °C for all the tests. Temperature measurements were taken along the length of the test section from the inner radiator to the outer reflector wall. The effective thermal conductivity was calculated using the temperature and heat transfer measurements. For a more detailed description of the NWTCTF experimental test facility as well as the experimental method used to conduct the tests the reader is referred to the paper by De Beer *et al.* (2017).

In the two previous papers referenced above only some of the experimental results gathered with the NWTCTF for a randomly packed bed (De Beer *et al.*, 2017) and for ordered packing structures (De Beer *et al.*, 2016) at 800 °C were presented. However, the full set of NWTCTF experimental data obtained for a randomly packed bed includes test cases for temperatures ranging from 400 °C to 800 °C in increments of 100 °C. Since publication of the previous papers additional tests were also completed for packed beds with ordered Simple Cubic (SC) and Body Centred Cubic (BCC) packing configurations with the heated wall temperature controlled at 400, 500, 600, 700 and 800 °C respectively. A detailed data and uncertainty analysis was also

performed for all the experimental tests at the different temperatures and the various packing structures.

The aim of this paper is to present a more comprehensive set of experimental results of all the tests conducted with the NWTCTF, providing the various effective thermal conductivity results together with the associated uncertainties. A comparison of the temperature and effective thermal conductivity results for the SC, BCC and random packing configurations at different temperatures will be presented. The NWTCTF experimental data can be used to gain a better understanding of the heat transfer phenomena and the resulting effective thermal conductivity in the near-wall region of packed beds with different packing configurations.

3. Results

The methodology proposed by Rousseau *et* al. (2014) for data reduction and uncertainty analysis was applied to the NWTCTF experimental data to extract the effective thermal conductivity results. The methodology is based on the relationship shown in Eq. (1). The measured temperature and heat transfer distribution results as well as the derived effective thermal conductivity results for the various temperature cases are presented in the following sections.

3.1 Temperature results

The measured temperatures for the random, BCC and SC packed beds are shown in Fig. 2 to Fig. 6 for the 400, 500, 600, 700 and 800 °C test cases respectively. The graphs also contain error bars indicating the measurement uncertainties for each of the measured data points. However, since the maximum measurement uncertainty for all the tests is ± 5 °C, the plotted error bars are barely visible. The temperature at which the heated wall surface was maintained during the experiment together with the resultant cooled wall temperature for each packing structure and test case are presented in Table 1Table .

The temperature distributions for the different packing structures appear to be quite similar. However, the structured packings clearly exhibit “smoother” distributions than that of the random packing.

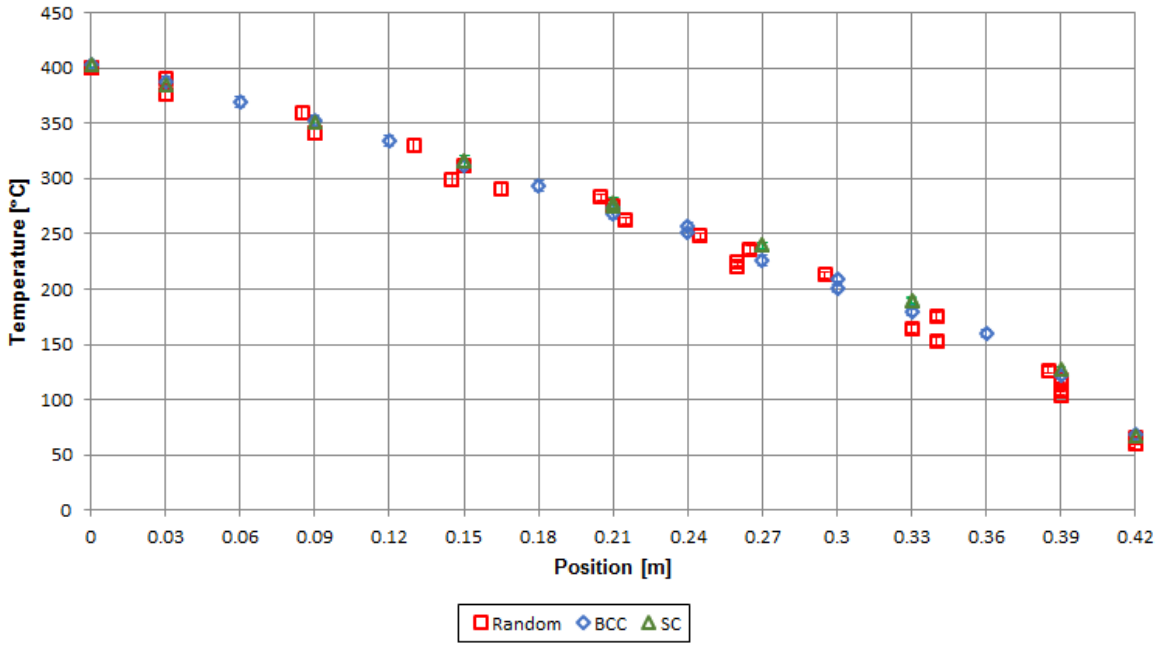

Fig. 2 Measured temperatures for the random, BCC and SC packed beds for the 400 °C test case.

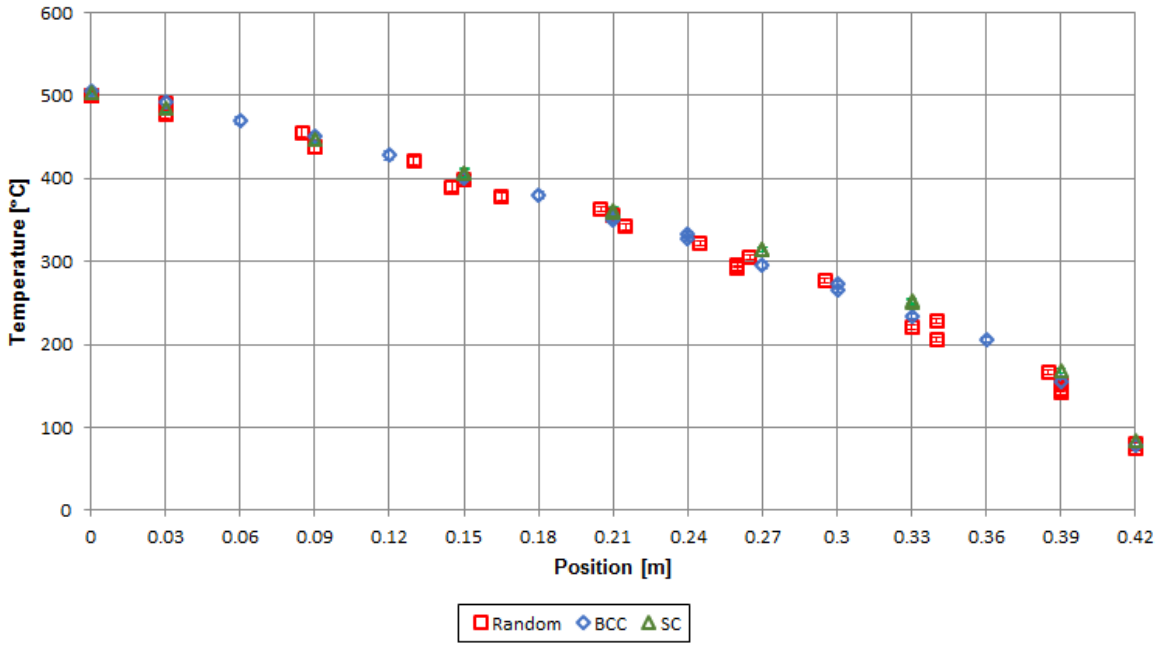

Fig. 3 Measured temperatures for the random, BCC and SC packed beds for the 500 °C test case.

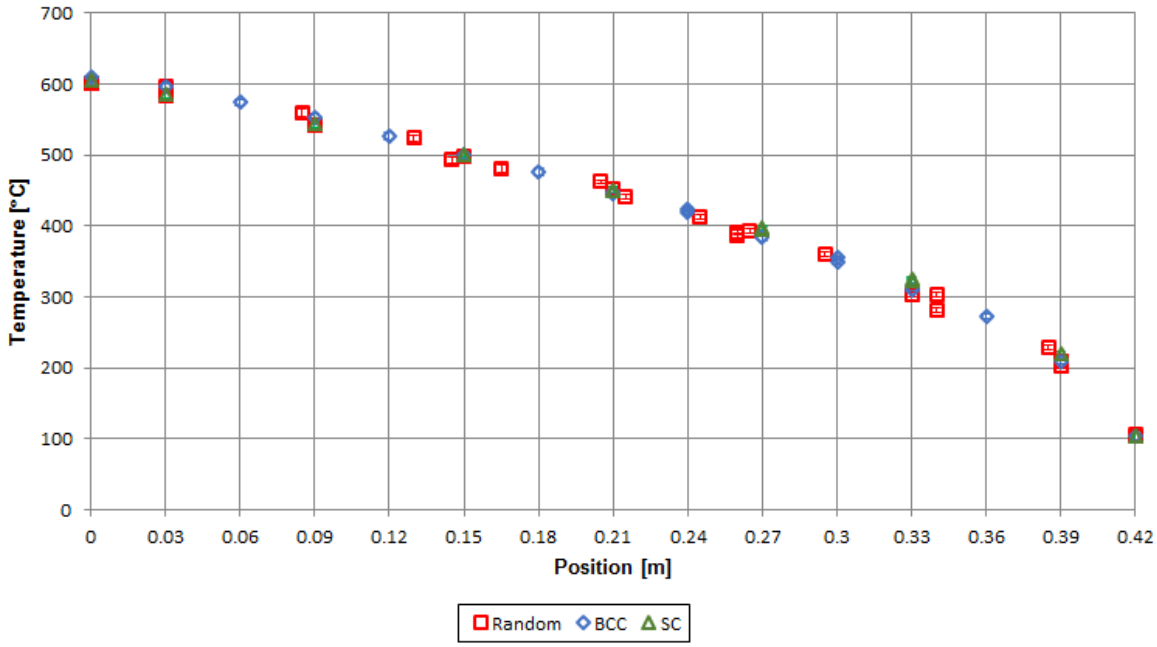

Fig. 4 Measured temperatures for the random, BCC and SC packed beds for the 600 °C test case.

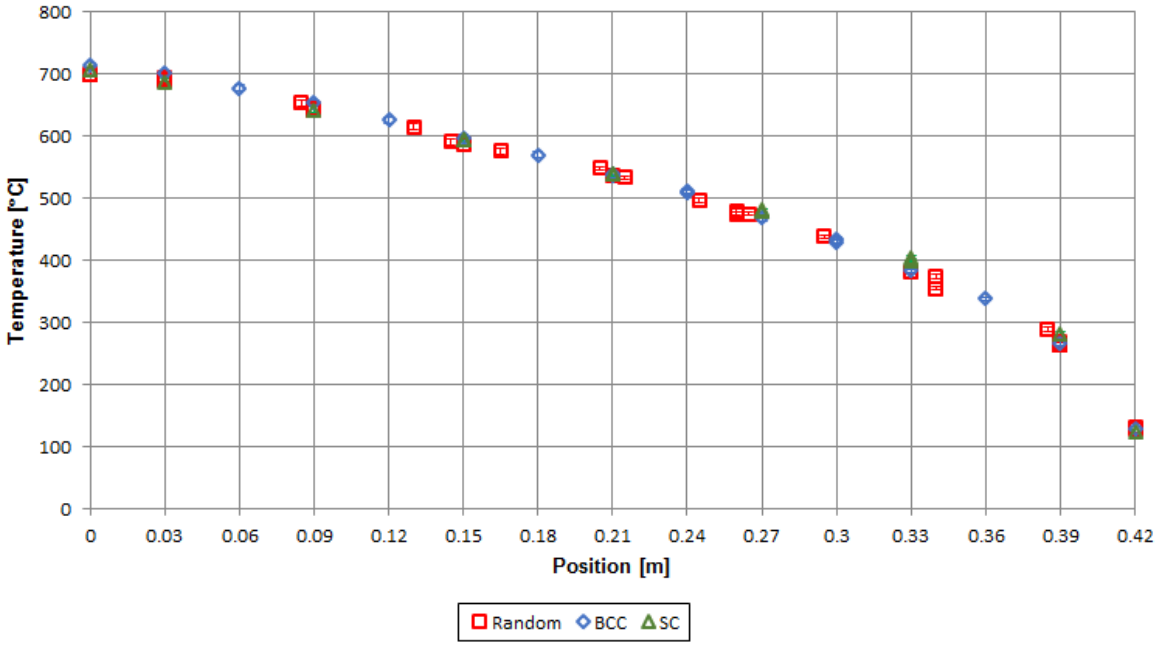

Fig. 5 Measured temperatures for the random, BCC and SC packed beds for the 700 °C test case.

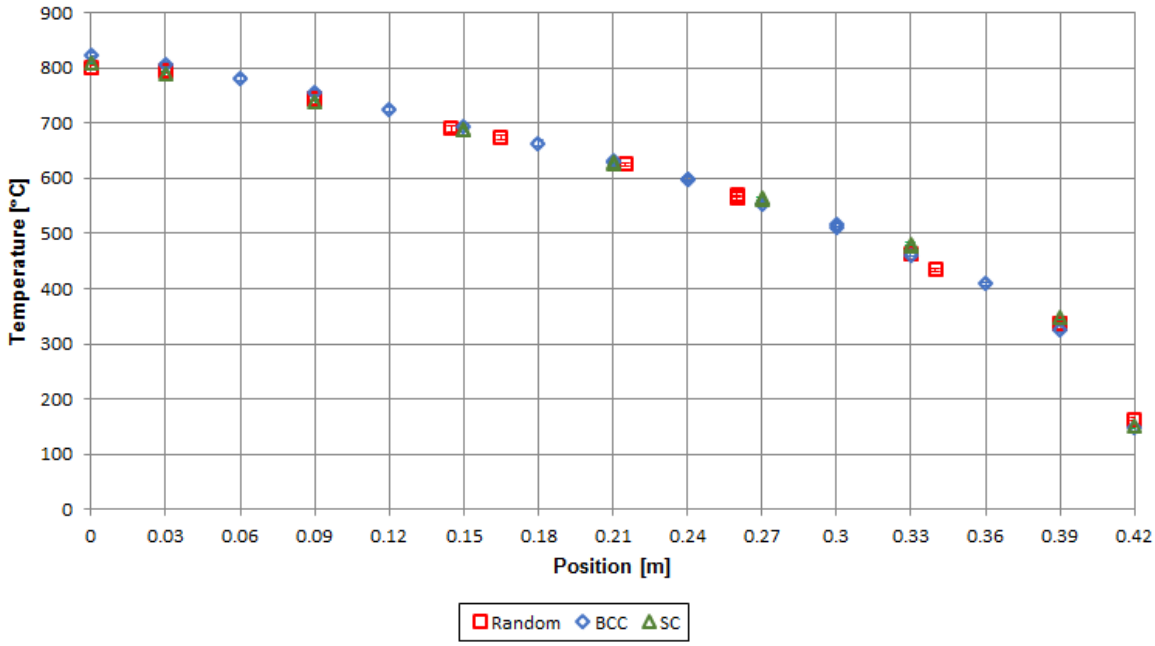

Fig. 6 Measured temperatures for the random, BCC and SC packed beds for the 800 °C test case.

Table 1: Surface temperatures at which the heated wall was maintained together with resultant cooled wall temperatures for each of the test cases.

Packing structure	Random	BCC	SC
400 °C Test case			
Heated wall surface temperature [°C]	400	403	403
Cooled wall surface temperature [°C]	63	68	67
500 °C Test case			
Heated wall surface temperature [°C]	500	506	504
Cooled wall surface temperature [°C]	77	78	83
600 °C Test case			
Heated wall surface temperature [°C]	600	609	605
Cooled wall surface temperature [°C]	105	105	105
700 °C Test case			
Heated wall surface temperature [°C]	700	715	707
Cooled wall surface temperature [°C]	131	129	124
800 °C Test case			
Heated wall surface temperature [°C]	800	824	810
Cooled wall surface temperature [°C]	163	149	150

3.2 Heat transfer and temperature distribution results

In order to derive the effective thermal conductivity values the heat transfer distribution along the length of the test section must be determined and matched with the relevant temperature gradient at each position (Rousseau *et al.*, 2014; Rousseau *et al.*, 2015). The heat transfer distribution through the packed bed was determined by discretizing the packed bed into smaller increments and accounting for all the heat inflow and outflow paths for each of the increments. This includes the heat losses to the outside of the test unit through the various insulation layers.

These losses were calculated based on additional measurements on the outside of the insulation and the known heat conduction characteristics of the insulation. The derived function describing the heat transfer through the packed bed, $Q_{bed}(y)$, is shown in Eq. (2):

$$Q_{bed}(y) = c_0 y^3 + c_1 y^2 + c_2 y + c_3 \pm u(Q_{bed}) \quad (2)$$

with $c_0 - c_3$ the polynomial coefficients specific to each test case, y the position in the packed bed measured from the heated wall and $u(Q_{bed})$ the uncertainty associated with the heat flux through the bed.

The calculated values of the polynomial coefficients as well as the values of the heat extracted via the cooled wall and the heat losses through the insulation walls with associated uncertainties for each of the test cases are presented in Table 2. For each of the test cases the heat losses through the insulation is nearly the same for the different packing structures. This can be expected since the temperature distributions are very similar and therefore the temperature differences between the test section and the outside of the test unit are very similar for the different packing structures. The variation in the number of contact points between the spheres and the walls may amongst others account for the differences.

Table 2: Heat transfer results for the various packing configurations and temperature test cases.

Packing structure	Random	BCC	SC
400 °C Test case			
c_0	235	273	315
c_1	283	298	269
c_2	-451	-426	-428
c_3	377	424	386
$u(Q_{bed})$	± 13.4 W	± 14.2 W	± 11.6 W
$Q_{cooled\ wall}$	255.8 ± 13.3 W	317.9 ± 14.0 W	277.4 ± 11.4 W
Q_{losses}	114.4 ± 1.6 W	108.4 ± 2.3 W	110.9 ± 2.5 W
500 °C Test case			
c_0	447	508	573
c_1	319	341	281
c_2	-632	-608	-599
c_3	646	676	646
$u(Q_{bed})$	± 22.0 W	± 18.6 W	± 17.6 W
$Q_{cooled\ wall}$	470.8 ± 21.9 W	518.6 ± 18.2 W	487.1 ± 17.1 W
Q_{losses}	166.5 ± 2.5 W	160.7 ± 3.4 W	162.7 ± 4.3 W
600 °C Test case			
c_0	850	810	894
c_1	215	319	248
c_2	-814	-784	-777
c_3	945	916	1045
$u(Q_{bed})$	± 24.1 W	± 23.2 W	± 27.3 W
$Q_{cooled\ wall}$	703.8 ± 36.5 W	703.9 ± 22.5 W	829.7 ± 26.3 W

Q_{losses}	229.8 ± 3.5 W	216.8 ± 5.4 W	220.1 ± 7.1 W
700 °C Test case			
c_0	1196	1008	1249
c_1	155	353	201
c_2	-1012	-979	-973
c_3	1497	1487	1475
$u(Q_{bed})$	± 45.2 W	± 39.5 W	± 40.7 W
$Q_{cooled\ wall}$	1185.8 ± 44.9 W	1213.1 ± 38.7 W	1194.7 ± 39.2 W
Q_{losses}	296.4 ± 4.6 W	279.0 ± 8.0 W	285.5 ± 11.1 W
800 °C Test case			
c_0	1409	1434	1580
c_1	139	301	168
c_2	-1212	-1197	-1170
c_3	2042	2024	2022
$u(Q_{bed})$	± 74.0 W	± 54.5 W	± 53.4 W
$Q_{cooled\ wall}$	1657.6 ± 73.1 W	1681.1 ± 52.9 W	1677.5 ± 51.1 W
Q_{losses}	366.7 ± 11.2 W	349.3 ± 13.0 W	350.7 ± 15.7 W

Following the methodology proposed by Rousseau *et al.* (2014) a fifth order polynomial was fitted through the measured temperature data, presented in Fig. 2 to Fig. 6, to derive a function describing the temperature distribution through the packed bed for each of the experimental tests. The function describing the temperature distribution through the packed bed, $T(y)$, is shown in Eq. (3):

$$T(y) = a_0 + a_1 y + a_2 y^2 + a_3 y^3 + a_4 y^4 + a_5 y^5 \quad (3)$$

with $a_0 - a_5$ the polynomial coefficients specific to each test case. Table 3 presents the calculated values of the polynomial coefficients for the temperature distribution functions of each of the test cases.

Table 3: Temperature distribution function results for the various packing configurations and temperature test cases.

Packing structure	Random	BCC	SC
400 °C Test case			
a_o	414	420	418
a_1	-720	-868	-826
a_2	2236	5336	4475
a_3	-15867	-38161	-30630
a_4	44650	108666	87553
a_5	-47760	-110593	-92449
500 °C Test case			
a_o	517	522	521
a_1	-816	-813	-943
a_2	3640	4403	5767
a_3	-29345	-37785	-41437
a_4	86832	115899	121238
a_5	-93180	-125052	-130495

600 °C Test case			
a_o	618	626	629
a_1	-836	-811	-1293
a_2	5667	4654	10758
a_3	-49168	-43173	-73807
a_4	150831	137811	210046
a_5	-163843	-154569	-219510
700 °C Test case			
a_o	722	738	740
a_1	-1058	-1138	-1816
a_2	9517	9125	18711
a_3	-78304	-72584	-126404
a_4	238701	219502	357221
a_5	-256949	-237335	-367139
800 °C Test case			
a_o	829	856	853
a_1	-1433	-1690	-2450
a_2	15644	16682	27881
a_3	-119792	-120518	-185044
a_4	353861	350519	517458
a_5	-370541	-367327	-524339

3.3 Effective thermal conductivity results

The effective thermal conductivity for the various temperature cases as well as the porosity of the random, BCC and SC packed bed as a function of position are shown in Fig. 7, Fig. 8 and Fig. 9 respectively. The dashed lines in the figures indicate the error bands showing the expanded uncertainty at a 95 % confidence interval associated with the effective thermal conductivity values. For all three packing structures there is a marked reduction in the magnitude of the effective thermal conductivity in the near-wall region followed by a “peak” indicating the maximum value. There also seems to be a slight dip in the effective thermal conductivity values at a position between 0.15 m and 0.3 m. This “peaks-and-dip” trend can be seen in the results for all the test cases and packing configurations, however, it becomes more notable for the higher temperature cases. A similar “peaks-and-dip” trend was observed in the HTTU effective thermal conductivity results presented by Rousseau *et al*. (2014).

The packed beds consist only of wall and near-wall regions as wall effects were present on each side of the bed. The method proposed by Du Toit (2002) was used to determine the porosity variation for a DEM generated numerically packed pebble bed which is representative of the experimental packed bed. The porosity variation of the randomly packed bed, Fig. 7, shows that at the inner wall region, between 0 m and 0.06 m, and at the outer wall region, between 0.36 m and 0.42 m, the wall effects force the packing structure to be more ordered. As

we move further away from the inner and outer wall the packing structure becomes more disordered.

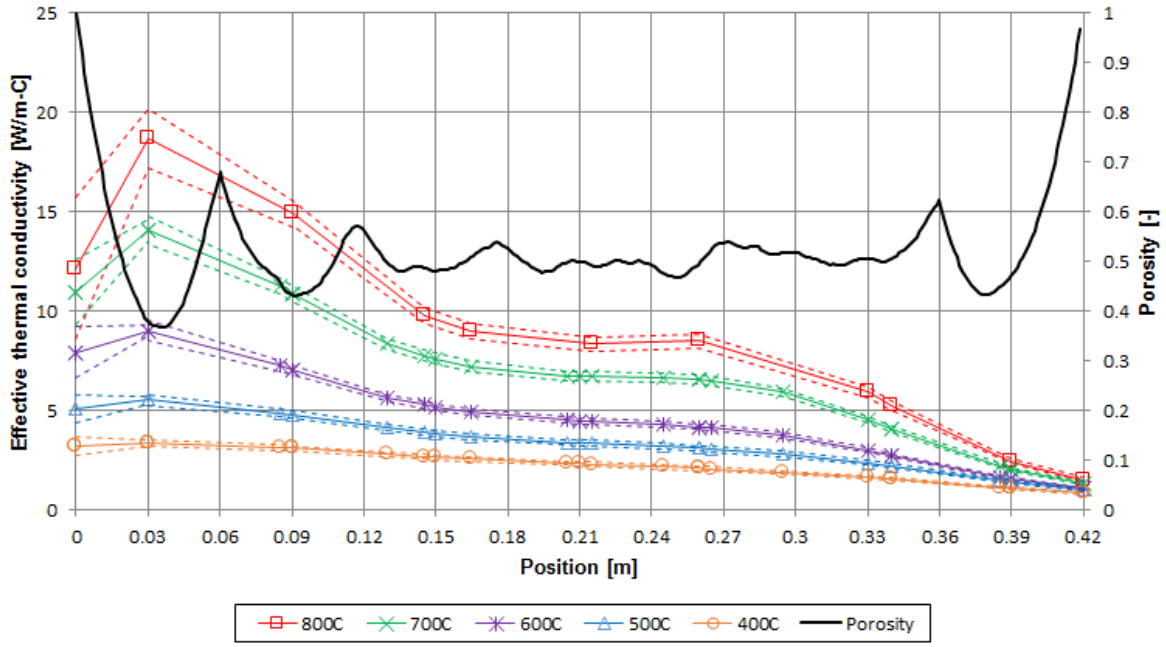

Fig. 7 Effective thermal conductivity with uncertainties and porosity as a function of position for the randomly packed bed.

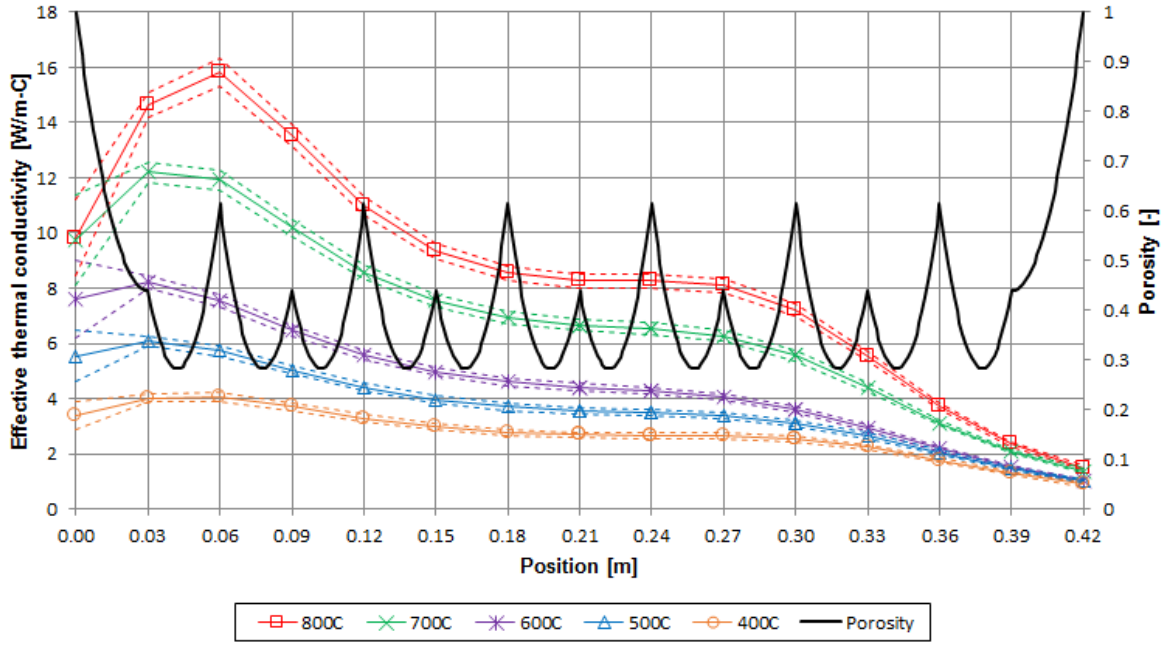

Fig. 8 Effective thermal conductivity with uncertainties and porosity as a function of position for the BCC packed bed.

For all the temperature cases of the randomly packed bed the maximum value of the effective thermal conductivity is found at a position of 0.03 m, which is half a sphere diameter from the inner (heated) wall and coincides with the minimum porosity. The observed “peaks-and-dip” trend next to the inner wall seems to be directly influenced by the porosity variations due to the

wall effects. However, a smaller peak can also be seen at a position of 0.26 m, which is not directly next to the wall where a more ordered packing structure is observed. The smaller peak becomes more notable for the 800 °C case whereas there seems to be no smaller peak in the effective thermal conductivity for the lower temperature cases, especially the 400 °C case. Fig. 7 also shows that the influence of the wall effects becomes more significant at higher temperatures, as can be seen next to the heated wall at z = 0.0 m.

For the BCC packed bed, Fig. 8, the change in the porosity variation due to the wall effect is limited to a distance of one sphere diameter from the wall. The effect of the inner wall, which is at higher temperatures, on the effective thermal conductivity is more pronounced and different to the effect of the outer wall, which is at lower temperatures. Next to the inner wall there is a sharp reduction in the effective thermal conductivity, whereas a smaller more gradual reduction is notable next to the outer wall. The effective thermal conductivity curves for the random and SC packed beds have a similar characteristic. Also note that for the BCC packed bed the “peak” indicating the maximum value of the effective thermal conductivity moves from a position of half a sphere diameter from the inner wall for lower temperatures to one sphere diameter for higher temperatures. This is in contrast to the “peak” for the random packing that appears at half a sphere diameter from wall for all the temperature cases. The inflection point in the porosity at 0.03 m coincides with the minimum porosity associated with first layer of spheres next to the wall. The maximum porosity at 0.06 m coincides with the centres of the first layer of central spheres from the wall in the BCC packing.

The smaller “peak” is also not as prominent for the BCC packed bed as it is for the random packing. The effective thermal conductivity decreases more “smoothly” for the BCC packing compared to the random packing. A change in the gradient of the effective thermal conductivity curve can be noted at a position of 0.27 m followed by a sharp decrease in the thermal conductivity. The decrease is more significant for the higher temperature cases.

The walls on each side of the packed bed had no influence on the porosity variation for the SC packed bed, Fig. 9, however the “peaks-and-dip” trend is still visible in the effective thermal conductivity results. For the SC packed bed, the position of the maximum “peak” moves from half a sphere diameter from the heated wall at lower temperatures to one and a half sphere diameters from the heated wall at higher temperatures. Both positions coincide with a point of minimum porosity. The position of the maximum “peak” is the same for all the packing structures at lower temperatures but differs as temperature increases.

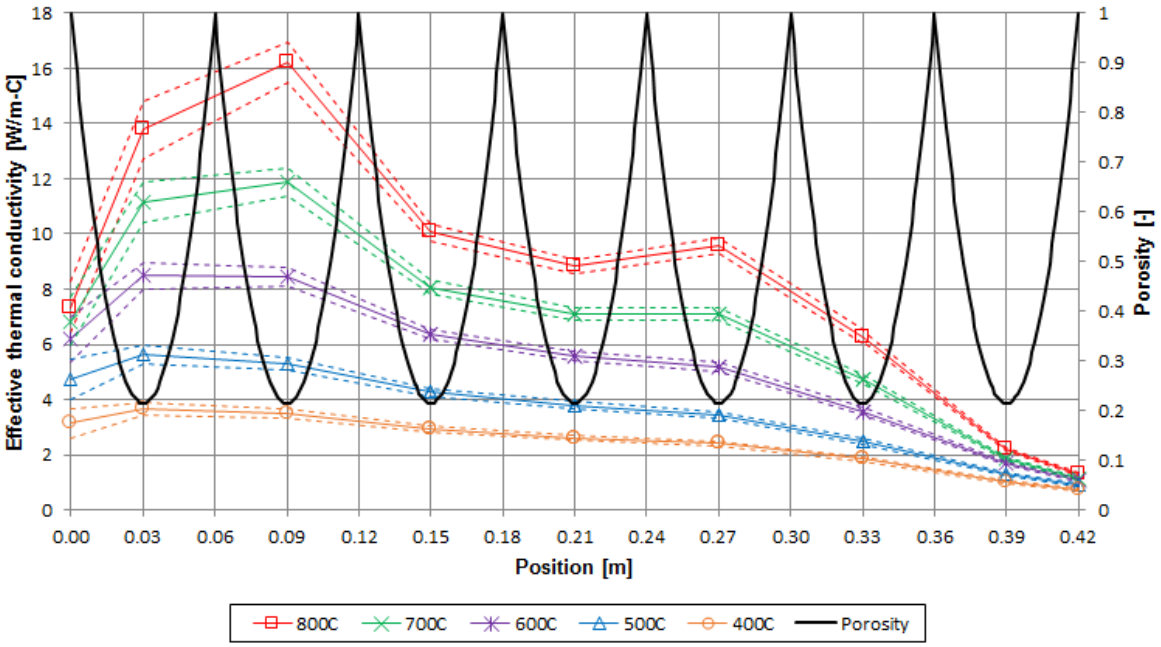

Fig. 9 Effective thermal conductivity with uncertainties and porosity as a function of position for the SC packed bed.

Fig. 9 shows the smaller “peak” for the SC packed bed at a position of 0.27 m which is the same as the BCC packed bed. Similar to the random packing the smaller “peak” for the SC packed bed becomes more prominent at higher temperatures.

During the experimental tests, thermocouples were inserted into the centre of the graphite spheres and the temperature measurements were obtained at the centre of each of the instrumented spheres. Thus, it is also important to note that the positions of the measurement points and the derived effective thermal conductivity are associated with the centres of the spheres in the packed beds. Therefore, the measurement points for the three different packing structures were not all at exactly the same positions, except for the regions directly next to the inner and outer wall, where z = 0.03 m and z = 0.39 m.

Thus, when considering the heat transfer in a packed bed the effect of the packing structure on the effective thermal conductivity cannot be characterised by the porosity alone. This is similar to the findings of Van Antwerpen *et al*. (2010); that the variation in coordination number and contact angles between adjacent spheres must amongst others also be considered when studying the effect of packing structure on the heat transfer through the packed bed.

The calculated effective thermal conductivity results with its associated uncertainties as a function of position for the different packed beds are shown together in Fig. 10 to Fig. 14 for the 400, 500, 600, 700 and 800 °C test cases respectively. This shows clearly that the reduction in

the effective thermal conductivity is more pronounced next to the heated wall for all the packings. This effect is also more significant for the higher temperature case in all the packings.

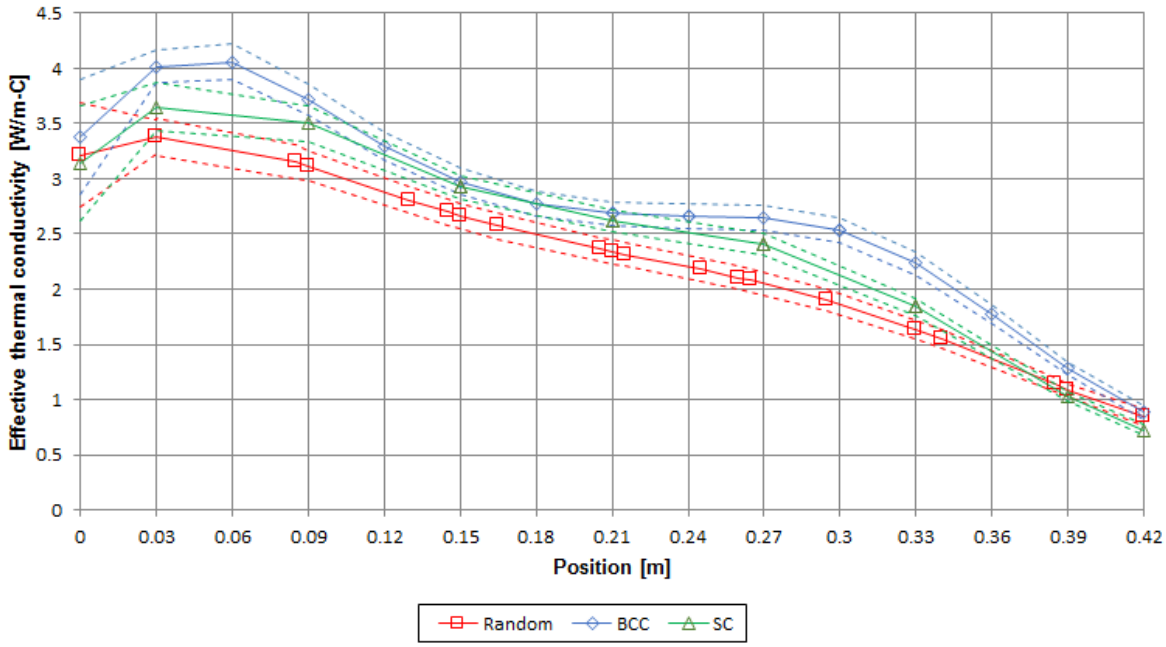

Fig. 10 Effective thermal conductivity with uncertainties as a function of position for the 400 °C test case.

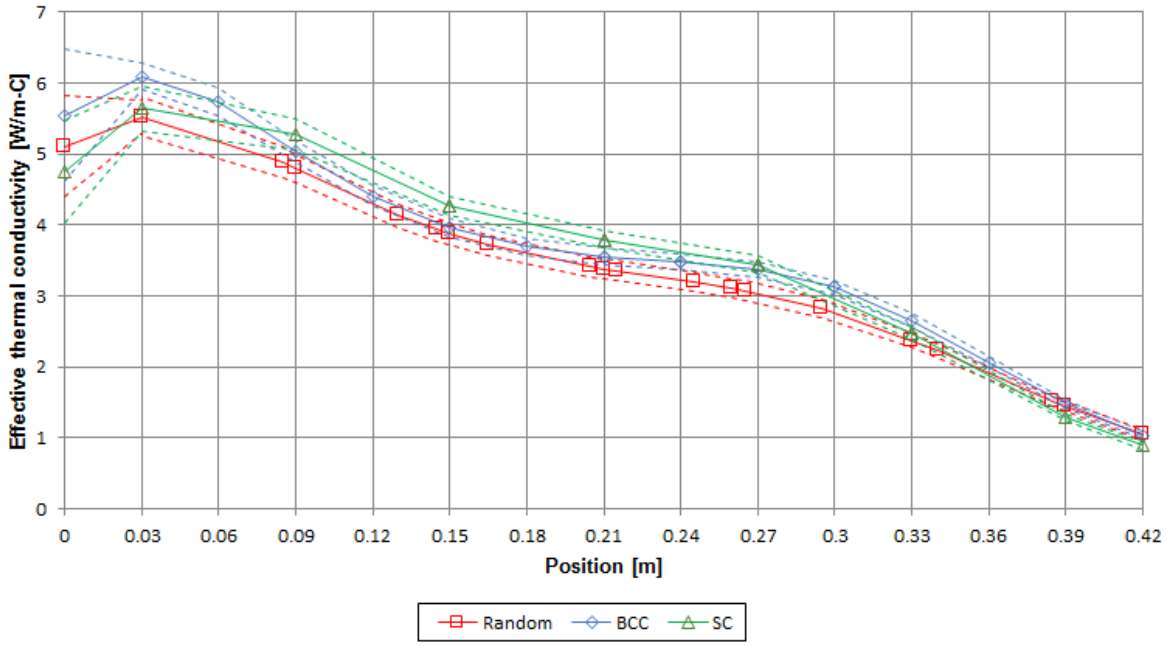

Fig. 11 Effective thermal conductivity with uncertainties as a function of position for the 500 °C test case.

The effective thermal conductivity for the different packing structures are of the same order of magnitude for the different temperature cases, but the trends observed differs. The “peak” value next to the heated wall, z = 0.03 m, for the 400 °C case of the random packing is lower than the “peaks” of the BCC and SC packed beds. As the heated wall temperature increases the “peak”

value for the random packing gradually increases at a faster rate than the values for the structured packed beds. For the 600 °C to 800 °C cases the “peak” value of the random packing becomes higher than that of the BCC and SC packed beds.

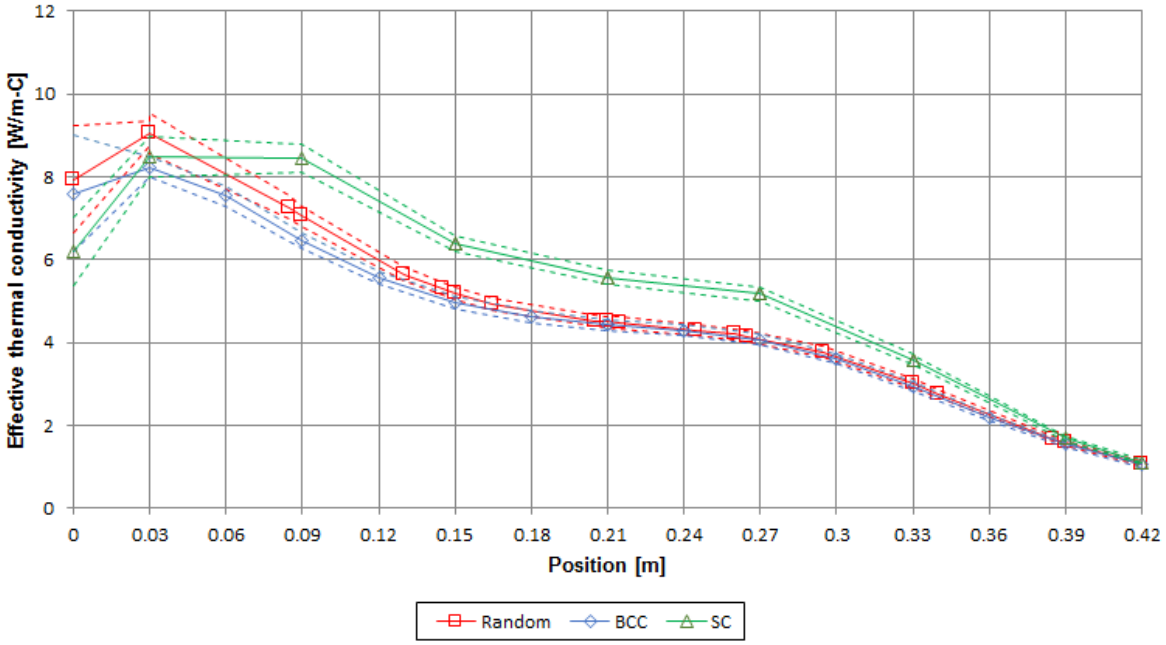

Fig. 12 Effective thermal conductivity with uncertainties as a function of position for the 600 °C test case.

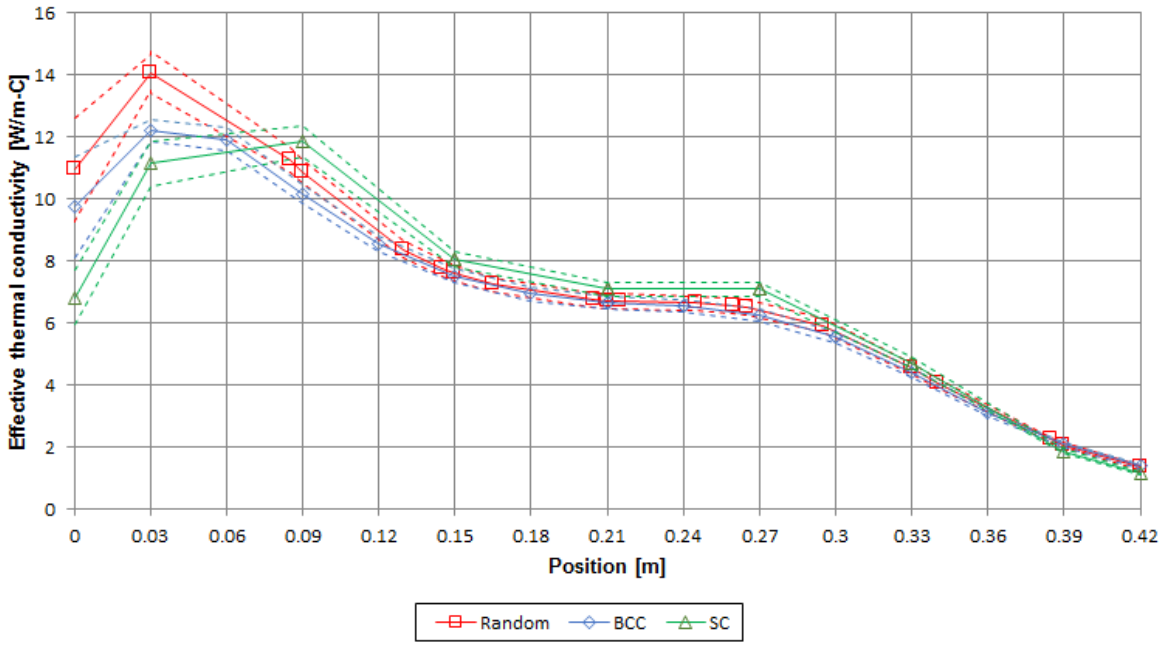

Fig. 13 Effective thermal conductivity with uncertainties as a function of position for the 700 °C test case.

As discussed previously the position of the maximum “peak” for the random packing stays at a half sphere diameter from the heated wall. However, for the BCC and SC packed beds the positions of the maximum “peaks” move away from the heated wall as the temperature increases. The position of the “peak” of the SC packing moves away from the heated wall at a

faster rate than the BCC packing for higher temperatures. The magnitude of the maximum values of the BCC and SC packed beds also becomes very similar as the temperature of the heated wall increases. The position of the smaller “peak” (nearer to the outer wall) as a function of the distance from the heated wall remains the same for all the temperature cases, regardless of the packing structure.

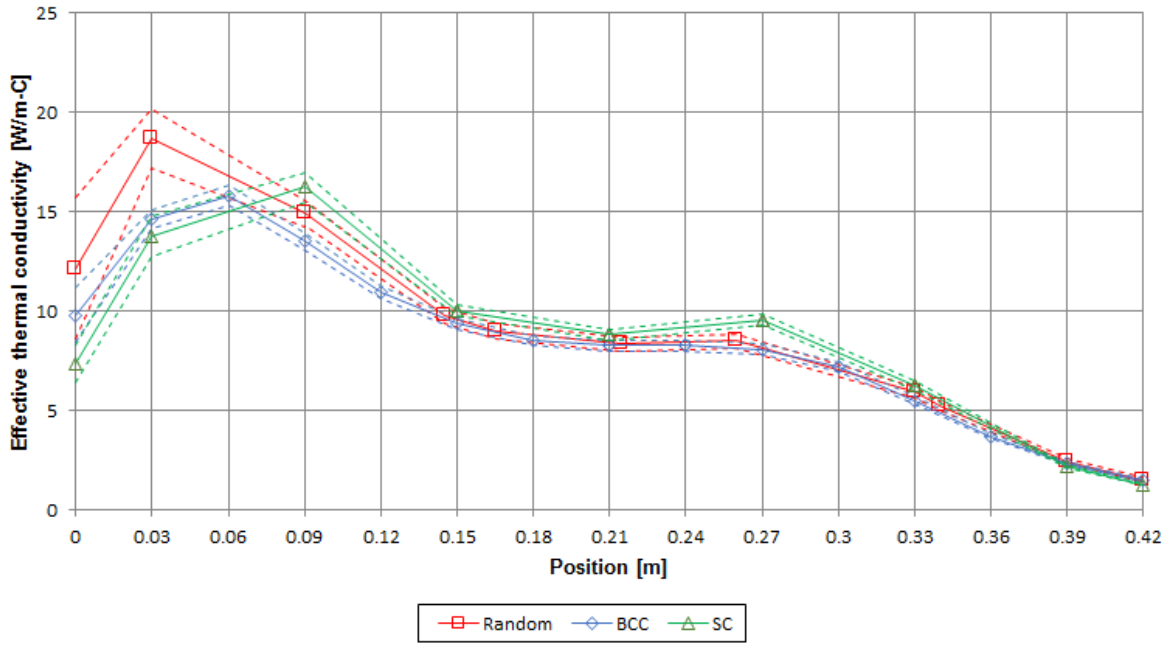

Fig. 14 Effective thermal conductivity with uncertainties as a function of position for the 800 °C test case.

For the 400 °C case the overall effective thermal conductivity curve for the BCC packed bed lies above the curves for the random and SC packings. As the temperature increases the effective thermal conductivity values for SC packed bed increases for the positions between 0.09 m and 0.36 m. At these positions for the higher temperature cases the values for the SC packing becomes slightly higher than those for the random and BCC packed beds, as can be seen in Fig. 12 to Fig. 14. Although the effective thermal conductivity for the SC packed bed is higher than the corresponding values for the other packing structures at higher temperatures for the positions 0.09 m < z < 0.36 m, the effective thermal conductivity of the SC packed bed stays lower than that of the random and BCC packings next to the inner and outer walls. It should also be noted that for the higher temperature cases, Fig. 12 to Fig. 14, the trends of the curves for the random and BCC packed beds between 0.15 m and 0.33 m become quite similar. Regardless of the different packing structures used in the experimental tests the “peaks-and-dip” trend is visible throughout the effective thermal conductivity results.

Fig. 15 to Fig. 19 show the same values of the effective thermal conductivity, but as a function of temperature for the 400 °C to 800 °C test cases respectively. The results show that the

effective thermal conductivity is a non-linear function of temperature for all the packing structures with the gradient generally increasing as the temperature increases. This trend is to be expected due to the effect of thermal radiation becoming more dominant at higher temperatures.

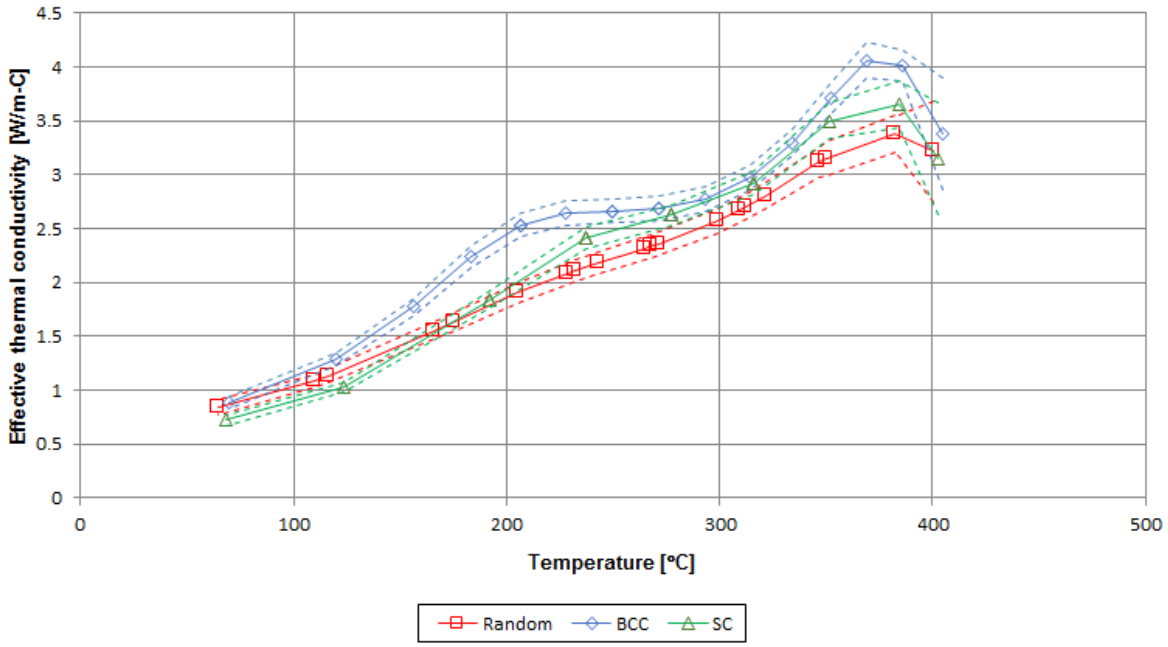

Fig. 15 Effective thermal conductivity with uncertainties as a function of temperature for the 400 °C test case.

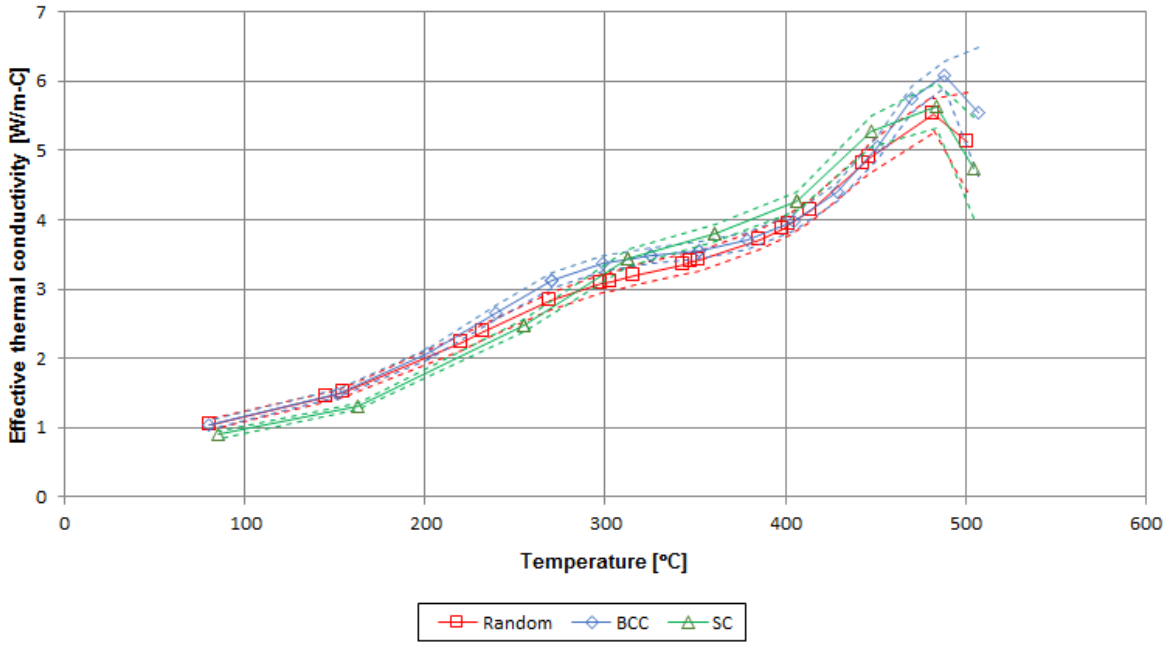

Fig. 16 Effective thermal conductivity with uncertainties as a function of temperature for the 500 °C test case.

The position of the smaller “peak” (nearer to the cooled wall) as a function of temperature gradually moves from approximately 200 °C to 550 °C as the temperature of the heated wall increases from 400 °C to 800 °C. There always seems to be about a 200 °C difference between

the “peaks” of the effective thermal conductivity curve. The influence of the wall effect at lower temperatures, next to the cooled wall, is less prominent than at higher temperatures for all the test cases.

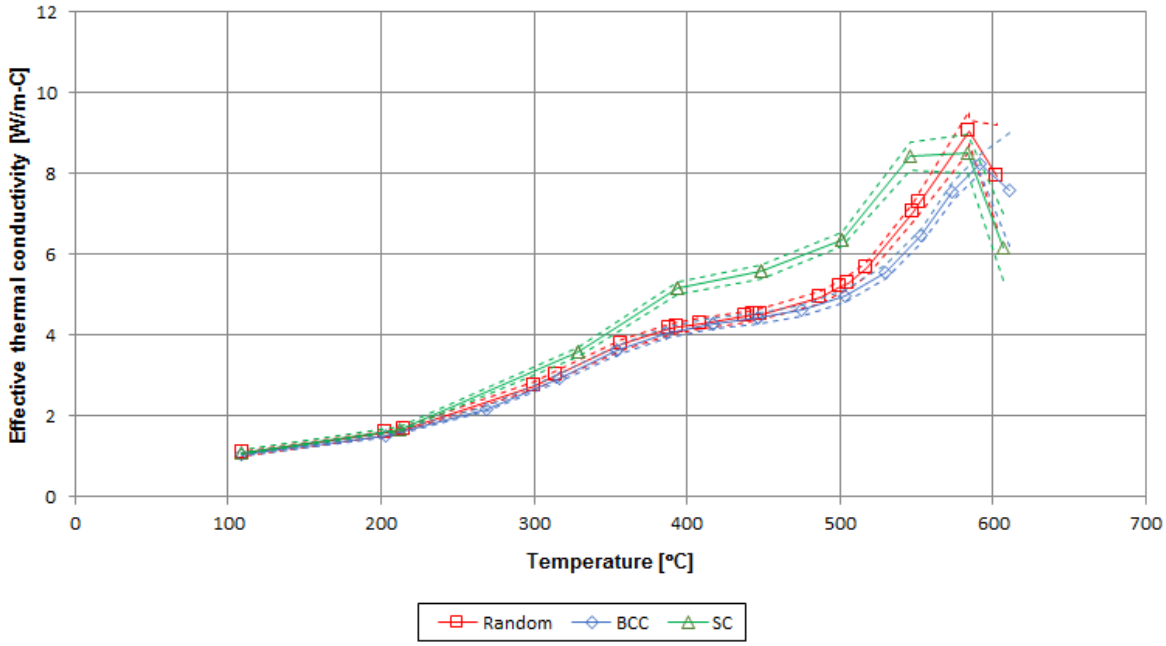

Fig. 17 Effective thermal conductivity with uncertainties as a function of temperature for the 600 °C test case.

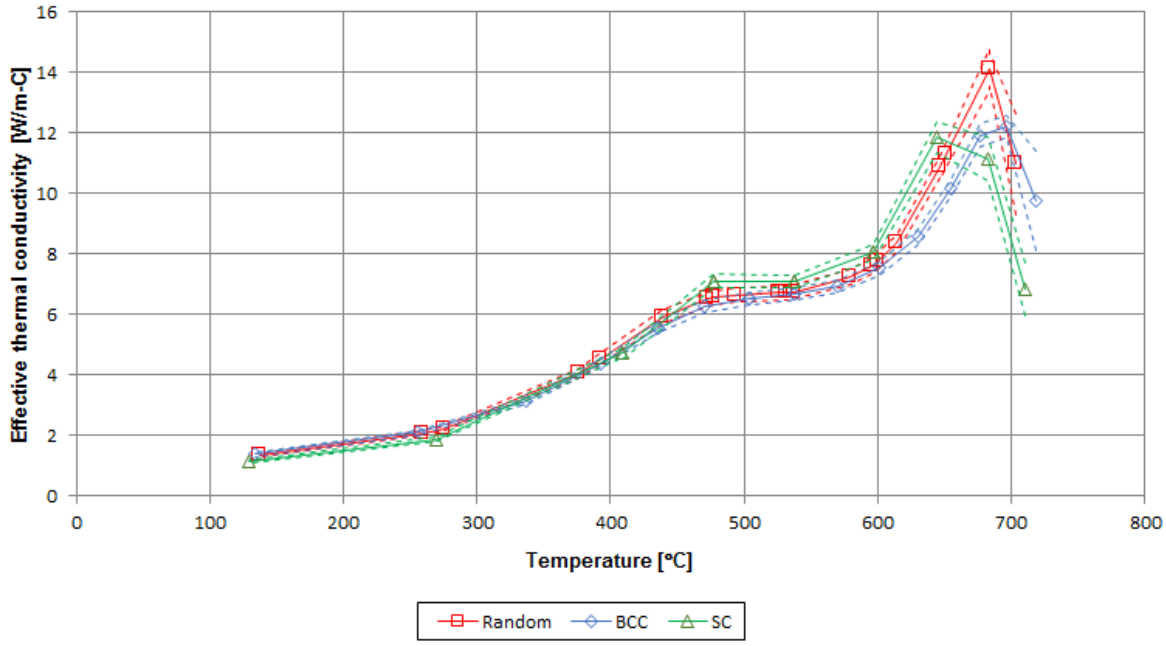

Fig. 18 Effective thermal conductivity with uncertainties as a function of temperature for the 700 °C test case.

It is important to note that the top, bottom, and side insulation walls surrounding the packed bed also had an influence on the results. Ideally one would only have the packing structure influenced by the inner radiator and/or outer reflector, which is perpendicular to the heat flux through the packed bed. However, for the current tests no special measures were taken to

eliminate the wall effects at the insulated walls. For the randomly and BCC packed beds a gap was present between the top layer of spheres and the top cover of the test section. This gap was formed due to the packing method used and the physical constraints of the geometry of the test section.

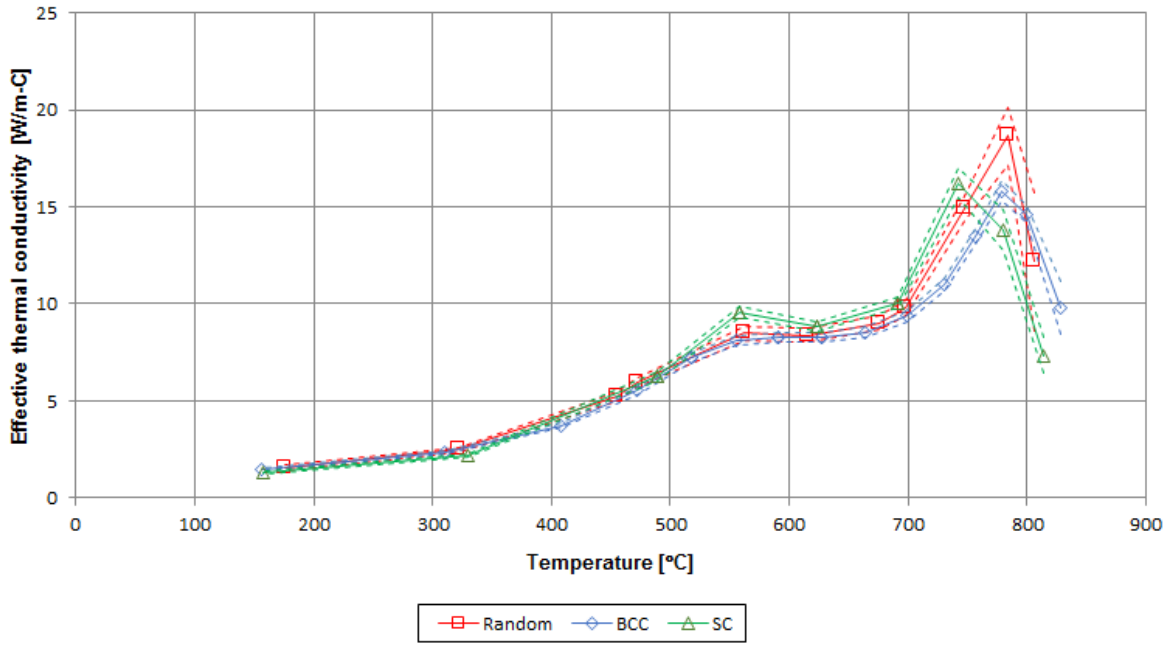

Fig. 19 Effective thermal conductivity with uncertainties as a function of temperature for the 800 °C test case.

It was also noted that irregularities were present in the SC packed bed, in which gaps existed between some of the adjacent spheres. The graphite spheres were inherited from the PBMR HTTU test facility and therefore due to the wear-and-tear of the previous experimental tests some of the spheres did not have a diameter of precisely 60 mm. It should be kept in mind that this will also have an effect on the predicted conduction heat transfer as the conduction phenomenon was essentially eliminated between the spheres where the irregularities were present. For future experimental tests, the elimination of the additional wall effects should be addressed and any irregularities in the packed bed should be minimized as far as is practically possible.

4. Conclusion

Gaining a fundamental understanding of the heat transfer phenomena in the near-wall region of a packed pebble bed can be valuable when considering the design and safety case of PBRs. Especially interesting is the interplay between the conduction and radiation heat transfer at different temperature levels and for different packing structures.

The newly built NWTCTF test facility was used to determine the influence of wall effects on the effective thermal conductivity of a packed bed consisting of graphite spheres of uniform size. Three different packing structures namely random, BCC and SC were investigated for temperatures ranging from 400 °C to 800 °C. The measured temperature and heat transfer results as well as the derived effective thermal conductivity with associated uncertainties were presented.

The results show that the wall effects have an influence on the effective thermal conductivity in the near-wall region, resulting in a notable reduction next to the both the inner and outer wall followed by a “peaks-and-dip” trend of the effective thermal conductivity curve. The influence of the wall effects is more significant for higher temperatures, where the contribution of radiation to the overall heat transfer is more pronounced. The effect of the altered packing structure in the near-wall region on the effective thermal conductivity cannot be characterized based on porosity alone.

The effective thermal conductivity is a non-linear function of temperature and the gradient of the effective thermal conductivity curve increases with an increase in temperature. For future experimental tests with the NWTCTF it would be beneficial to eliminate the effects of the altered packing structure due to the top, bottom, and side insulated walls.

Nomenclature

$a_0 - a_5$	Polynomial coefficients [-]
A	Area [m²]
$c_0 - c_3$	Polynomial coefficients [-]
k_{eff}	Effective thermal conductivity [W/m-K]
$\dot{Q}$	Heat transfer rate [W]
Q_{bed}	Heat transfer rate through packed bed [W]
$Q_{cooled\ wall}$	Heat extracted through cooled wall [W]
Q_{losses}	Heat lost through insulation walls [W]
r	Path length [m]
T	Temperature [K] / [°C]
$u(Q_{bed})$	Uncertainty of heat transfer through packed bed [W]
y	Position in the packed bed measured from the heated wall [m]

Abbreviations

BCC	Body Centred Cubic
FHR	Fluoride Salt-cooled High-temperature Reactor
HTGR	High Temperature Gas-cooled Reactor
HTO	High Temperature Oven
HTR-PM	High Temperature Gas-cooled Reactor Pebble Bed Module
HTTU	High Temperature Test Unit
NWTCTF	Near-wall Thermal Conductivity Test Facility
PBR	Pebble Bed Gas-cooled Reactor

References

Asakuma, Y., Asada, M., Kanazawa, Y. & Yamamoto, T. 2016. Thermal analysis with contact resistance of packed bed by a homogenization method. *Powder Technology*, 291:46-51.

Breitbach, G. & Barthels, H. 1980. The radiant heat transfer in the high temperature reactor core after failure of the afterheat removal systems. *Nuclear Technology*, 49:392-399.

Cheng, G.J. & Yu, A.B. 2013. Particle Scale Evaluation of the Effective Thermal Conductivity from the Structure of a Packed Bed: Radiation Heat Transfer. *Industrial and Engineering Chemistry Research*, 52:12202-12211.

De Beer, M. 2014. Characterisation of thermal radiation in the near-wall region of a packed pebble bed. Potchefstroom: North-West University. (M Dissertation).

De Beer, M., Du Toit, C.G. & Dreyer, H. 2016. Experimental investigation of the effective thermal conductivity in the near-wall region of a packed pebble bed. (Potchefstroom, South Africa: Proceedings of the 10th South African Conference on Computational and Applied Mechanics.)

De Beer, M., Du Toit, C.G. & Rousseau, P.G. 2017. A methodology to investigate the contribution of conduction and radiation heat transfer to the effective thermal conductivity of packed graphite pebble beds, including the wall effect. *Nuclear Engineering and Design*, 314(2017):67-81.

Du Toit, C.G. 2002. The numerical determination of the variation in porosity of the pebble-bed core. (Petten, Netherlands: Proceedings of 1st International Topical Meeting on High Temperature Reactor Technology: HTR-2002,)

Ren, C., Yang, X., Jia, H., Jiang, Y. & Xiong, W. 2017. Theoretical analysis of effective thermal conductivity for the Chinese HTR-PM heat transfer test facility. *Applied Sciences*, 7(1)

Rousseau, P.G., Du Toit, C.G. & De Beer, M. 2015. A methodology for the characterization of the effective thermal conductivity in the near-wall region of a packed pebble bed. (Nice, France: Proceedings of ICAPP: Paper 15167.)

Rousseau, P.G., Du Toit, C.G., Van Antwerpen, W. & Van Antwerpen, H.J. 2014. Separate effects tests to determine the effective thermal conductivity in the PBMR HTTU test facility. *Nuclear Engineering and Design*, 271(2014):444-458.

Stöcker, B. & Niessen, H.F. 1997. The SANA-I-experiments for self-acting removal of the afterheat from a pebble bed.

Talukdar, P., Mendes, M.A.A., Parida, R.K., Trimis, D. & Ray, S. 2013. Modelling of conduction-radiation in a porous medium with blocked-off region approach. *Journal of Thermal Sciences*, 72(2013):102-114.

Van Antwerpen, W. 2009. Modelling the effective thermal conductivity in the near-wall region of a packed pebble bed. Potchefstroom Campus, South Africa: North-West University. (PhD Thesis).

Van Antwerpen, W., Du Toit, C.G. & Rousseau, P.G. 2010. A review of correlations to model the packing structure and effective thermal conductivity in packed beds of mono-sized spherical particles. *Nuclear Engineering and Design*, 240:1803-1818.

Van Antwerpen, W., Rousseau, P.G. & Du Toit, C.G. 2012. Multi-sphere Unit Cell model to calculate the effective thermal conductivity in packed pebble beds of mono-sized spheres. *Nuclear Engineering and Design*, 247:183-201.

World Nuclear Association. 2017. Molten Salt Reactors. http://www.world-nuclear.org/information-library/current-and-future-generation/molten-salt-reactors.aspx Date of access: 13 September. 2017.

Wu, H., Gui, N., Yang, X., Tu, J. & Jiang, S. 2016. Effect of scale on the modeling of radiation heat transfer in packed pebble beds. *International Journal of Heat and Mass Transfer*, 101:562-569.

Yang, J., Wang, J., Bu, S., Zeng, M., Wang, Q. & Nakayama, A. 2012. Experimental analysis of forced convective heat transfer in novel structured packed beds of particles. *Chemical Engineering Science*, 2012(71):126-137.

You, E., Sun, X., Chen, F., Shi, L. & Zhang, Z. 2017. An improved prediction model for the effective thermal conductivity of compact pebble bed reactors. *Nuclear Engineering and Design*, 2017(323):95-102.

Zhou, J., Yu, A. & Zhang, Y. 2007. A boundary element method for evaluation of the effective thermal conductivity of packed beds. *Journal of Heat Transfer*, 129:363-371.

4. Article 3: A methodology to investigate the contribution of conduction and radiation heat transfer to the effective thermal conductivity of packed graphite pebble beds, including the wall effect

M. De Beer *, C.G. Du Toit, P.G. Rousseau

Abstract

The effective thermal conductivity represents the overall heat transfer characteristics of a packed bed of spheres and must be considered in the analysis and design of pebble bed gas-cooled reactors. During depressurized loss of forced cooling conditions, the dominant heat transfer mechanisms for the passive removal of decay heat are radiation and conduction. Predicting the value of the effective thermal conductivity is complex since it inter alia depends on the temperature level and temperature gradient through the bed, as well as the pebble packing structure. The effect of the altered packing structure in the wall region must therefore also be considered. Being able to separate the contributions of radiation and conduction allows a better understanding of the underlying phenomena and the characteristics of the resultant effective thermal conductivity. This paper introduces a purpose-designed test facility and accompanying methodology that combines physical measurements with Computational Fluid Dynamics (CFD) simulations to separate the contributions of radiation and conduction heat transfer, including the wall effects. Preliminary results obtained with the methodology offer important insights into the trends observed in the experimental results and provide a better understanding of the interplay between the underlying heat transfer phenomena.

Keywords: Effective thermal conductivity, Near-wall effect, Packed pebble bed, Thermal radiation, Thermal conduction, Computational Fluid Dynamics

1. Introduction

Randomly packed beds of spherical particles are used in several thermal-fluid industrial applications that involve energy transfer processes including catalytic reactors, drying processes, and pebble bed gas-cooled reactors (PBRs) (Zhou *et al.*, 2007). For the analysis and design of PBRs with inherent safety characteristics a thorough understanding of the heat transfer phenomena in packed pebble beds is essential.

The effective thermal conductivity is an important parameter that is representative of the overall heat transfer through a packed bed of spheres. When considering the safety case of a PBR, during a depressurized loss of forced coolant accident, the effective thermal conductivity consists of three components: (1) thermal radiation between solid surfaces, (2) conduction through the pebble material itself and (3) conduction through physical contact points between the surfaces of the solid materials (Van Antwerpen *et al.*, 2010). According to Rousseau *et al.* (2014) models for the effective thermal conductivity are typically based on a simple Fourier conduction rate equation as shown in Eq. (1):

$$\dot{Q} = -k_{eff} A \frac{dT}{dr} \tag{1}$$

with $\dot{Q}$ the heat transfer rate, k_{eff} the effective thermal conductivity, T the temperature, A the applicable area in the pebble bed through which the heat transfer is taking place and r the coordinate perpendicular to the area.

At higher temperatures, above approximately 650 °C, the contribution of the radiation component to the effective thermal conductivity becomes significant (Breitbach & Barthels, 1980; Cheng & Yu, 2013; Talukdar *et al.*, 2013; Zhou *et al.*, 2007). For temperatures around 800 °C and higher radiation becomes the dominant heat transfer mechanism in a packed pebble bed.

The geometry of a randomly packed bed consists of three main regions namely the bulk, wall, and near-wall regions (Van Antwerpen, 2009). The porous structure changes significantly in the region near any wall as the packing geometry is disrupted in this area (Van Antwerpen *et al.*, 2010; 2012). This variation in packing structure is known as the wall effect and influences the magnitude of the effective thermal conductivity in the wall region, which includes the pebble to reflector interface. During normal operation, the conductive effects in the near-wall region will be negligible compared to convection. However, during a loss of coolant event the near-wall region forms part of the critical path for decay heat removal, thus an accurate prediction of the effective thermal conductivity in this region is important.

2. Background

2.1 Methods to separate the conduction and radiation components of the effective thermal conductivity

Existing approaches described in literature to determine the effective thermal conductivity can be divided into three basic types namely experimental, numerical, and analytical (Slavin

et al., 2002; Tsotsas & Martin, 1987). The experimental approach includes experimental measurements of the temperature distribution and heat flux through the packed pebble bed (Abou-Sena *et al.*, 2003; Breitbach & Barthels, 1980; Rousseau *et al.*, 2014; Stöcker & Niessen, 1997). For the numerical approach, the three-dimensional packed bed is subdivided into a large number of cells with the temperatures and heat flows matched at their boundaries (Asakuma *et al.*, 2014; Cheng & Yu, 2013; Zhou *et al.*, 2007; Zhou *et al.*, 2010). The analytical approach describes the packed bed as a network of conduction paths and the effective thermal conductivity is described as a combination of the individual conduction paths connected in series, parallel or a combination of both (Slavin *et al.*, 2002; Van Antwerpen, 2009; Wang *et al.*, 2016).

In order to gain better insight into the contribution of the different heat transfer mechanisms to the effective thermal conductivity it is important to separate the conduction and radiation components. This allows a better understanding of the underlying phenomena and the characteristics of the resultant values of the effective thermal conductivity.

The separation of the conduction and radiation contributions by means of an experimental approach only is not possible since both mechanisms naturally occur simultaneously. An experimental method can be coupled with another approach in an attempt to separate the contributing phenomena. None of the experimental studies in current literature attempted to separate the conduction and radiation components (Abou-Sena *et al.*, 2003; Breitbach & Barthels, 1980; Rousseau *et al.*, 2014; Stöcker & Niessen, 1997).

In the studies done by Zhou *et al*. (2007) and Cheng and Yu (2013) the contribution of the conduction and radiation to the overall effective thermal conductivity was separated by assuming the heat transfer phenomena can be superimposed. The overall effective thermal conductivity, k_{eff}, due to combined conduction-radiation was determined after which the conduction contribution to the effective thermal conductivity, k_{cond}, was calculated using a pure conduction model. Finally, using Eq. (2), the radiation component of the effective thermal conductivity, k_{rad}, was calculated from:

$$k_{eff} = k_{cond} + k_{rad} \tag{2}$$

The effect of radiation heat transfer was isolated and examined in the model of Asakuma *et al*. (2014) by specifying a constant material thermal conductivity, instead of defining the material property as a function of temperature. Thus, the model did not separate the contributing phenomena explicitly, but rather attempted to eliminate the effect of variations in the conduction by keeping the material thermal conductivity constant throughout the analysis. Zhou *et al*. (2010) did not explicitly separate the conduction and radiation

components but did express the relative contributions of the various contributing heat transfer mechanisms as a percentage of the total heat flux in the packed bed at a certain temperature. This is similar to one of the methods used by Cheng and Yu (2013).

Slavin *et al*. (2002) modelled the packing structure of the bed by dividing the bed into two regions, (1) the region where spheres are close-packed and (2) the region where deviations from the close-packed structure occur resulting in void regions. Thus, the overall unit cell considered in the model was divided into a close-packed cell in parallel with a void cell. The total thermal conductivity of a unit cell was calculated as a summation of the thermal conductivities for the close-packed region and the void region of the unit cell. For each of the unit cell regions the contributions of the various heat transfer mechanisms were determined separately and combined by means of a network approach to determine the overall value of the thermal conductivity.

In his MSUC model Van Antwerpen (2009) also distinguished between the conduction and radiation components by assuming that the heat transfer phenomena can be superimposed, as shown in Eq. (2). The conduction and radiation components as well as the overall effective thermal conductivity results predicted with the MSUC model were presented as a function of temperature, thus one could easily distinguish between the contributions of the different phenomena (Van Antwerpen *et al.*, 2012). Wang *et al*. (2016) also investigated the relative contributions of conduction versus radiation as a function of temperature.

Although the wall effect has a significant influence on the prediction of the effective thermal conductivity, the current approaches used in most studies are only applicable to the bulk region of a packed bed and do not take into account the changes in the packing structure found in the near-wall region. Rousseau *et al*. (2014) concluded from their results that the effective thermal conductivity decreased in the near-wall region of the packed bed due to the altered packing structure of the graphite spheres in that region. None of the other experimental studies reported on the influence of the wall effect on their results.

All of the studies that used a numerical approach did not take wall effects into account. The MSUC model developed by Van Antwerpen (2009) can be used for both the bulk and the near-wall regions. It is the only study from the analytical approach category that took the wall effects into account. From the summary shown in Table 1 it can be concluded that none of the studies used an experimental method coupled with another approach in an attempt to separate the contributing phenomena.

Table 1: A summary of studies that predict the effective thermal conductivity due to conduction and radiation.

Reference	Distinguish between conduction & radiation	Account for wall effects
Experimental approach		
Breitbach and Barthels (1980)	x	x
Stöcker and Niessen (1997)	x	x
Abou-Sena *et al*. (2003)	x	x
Rousseau *et al*. (2014)	x	✓
Numerical approach		
Zhou *et al*. (2007)	✓ - Eq. (2)	x
Cheng and Yu (2013)	✓ - Eq. (2)	x
Asakuma *et al*. (2014)	✓ - constant k_{cond}	x
Zhou *et al*. (2010)	✓ - relative contributions	x
Analytical approach		
Slavin *et al*. (2002)	✓ - Parallel network	x
Van Antwerpen (2009)	✓ - Eq. (2)	✓
Wang *et al*. (2016)	✓ - Eq. (2)	x

2.2 HTTU test facility

Rousseau *et al*. (2014) used the non-nuclear High Temperature Test Unit (HTTU) test facility to conduct tests to more accurately describe the thermal fluid phenomena through an annular PBR. Fig. 1 shows a photograph of the HTTU test facility (Rousseau & Van Staden, 2008). Approximately 25 000 graphite spheres were randomly packed inside the test section. In order to ensure that the effects of convection heat transfer were negligible, a near-vacuum environment was maintained inside the vessel of the test facility during testing. A temperature gradient was induced through the packed bed of spheres by heating the inner graphite radiator wall and cooling the outer reflector graphite wall of the test section. Temperature measurements within the pebble bed were gathered from which the heat transfer distribution could be obtained in order to calculate the effective thermal conductivity.

Fig. 1 Photograph of the HTTU test facility (Rousseau & Van Staden, 2008).

The effective thermal conductivity result with the associated uncertainties as obtained by Rousseau *et al*. (2014) is shown in Fig. 2. The result clearly shows the reduction in the effective thermal conductivity due to the wall effect near the "hot" wall between 0.3 m and 0.4 m radius. The influence of the wall effect at the outer reflector is less prominent, however a slight decrease in the gradient can be observed at a radial position of approximately 0.9 m. In addition to this, there seems to be a slight dip in the value through the bulk region in-between the two near-wall regions at a radius between 0.6 m and 0.7 m.

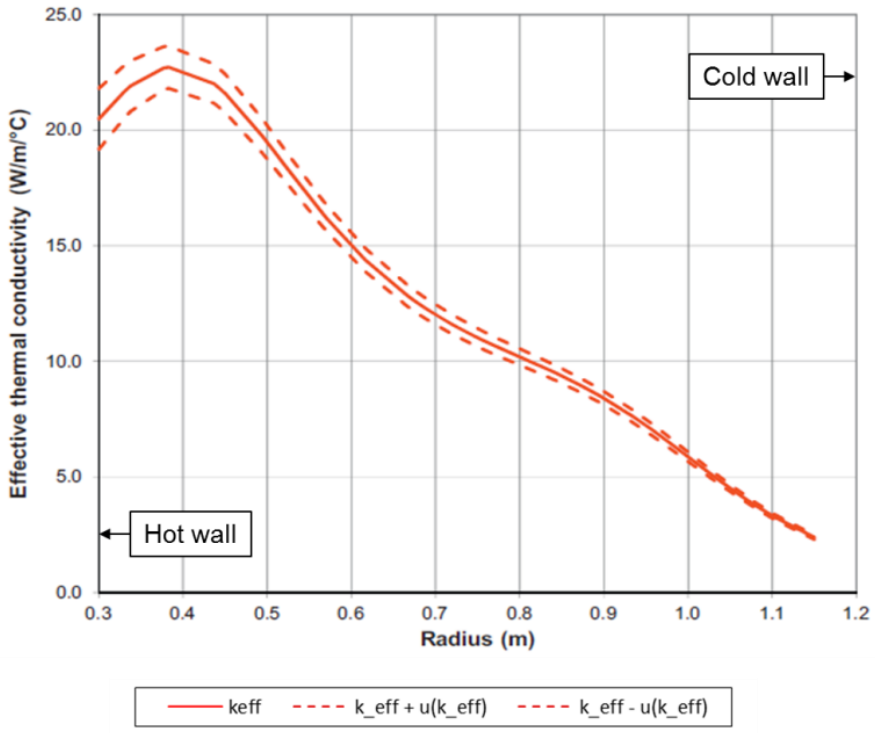

Fig. 2 HTTU effective thermal conductivity result as a function of position (Rousseau *et al.*, 2014).

The "peaks-and-dip" trend observed in the effective thermal conductivity result can only be as a result of the effect of radiation and conduction in the near-wall region since convection was negligible. It was concluded by Rousseau *et al*. (2014) that in order to gain a better understanding of the cause of the "peaks-and-dip" trend a detailed investigation of the effective thermal conductivity in the near-wall region would be required.

3. Near-wall Thermal Conductivity Test Facility

The "peaks-and dip" trend observed in the HTTU effective thermal conductivity results led to the development of the new Near-wall Thermal Conductivity Test Facility (NWTCTF). The purpose of the NWTCTF is to perform detailed investigations of the conduction and radiation heat transfer phenomena in the near-wall region of a packed pebble bed at temperatures of up to 1600 °C.

3.1 Test facility description

Fig. 3 shows a schematic representation of a vertical section through the NWTCTF test section (De Beer, 2014). The packed bed consists of approximately 330 machined virgin graphite spheres, each with a diameter of 60 mm. The spheres fit into a cubic volume with side lengths of 420 mm. On one side of the bed there is an inner graphite “radiator” wall with nine graphite electrodes (or heater elements) positioned on the outside right next to it. These were designed so that it can heat up the radiator wall to approximately 1600 °C.

On the opposite side of the bed there is an outer graphite “reflector” wall with a water jacket positioned right up against it. The water jacket was designed so that it can maintain the reflector wall temperature at an almost homogeneous temperature. A temperature gradient is induced through the packed bed of spheres in the y-coordinate direction between the heated and cooled wall. The rate of heat extracted via the water jacket can be determined by measuring the temperature difference and mass flow rate of the water flowing through the water jacket.

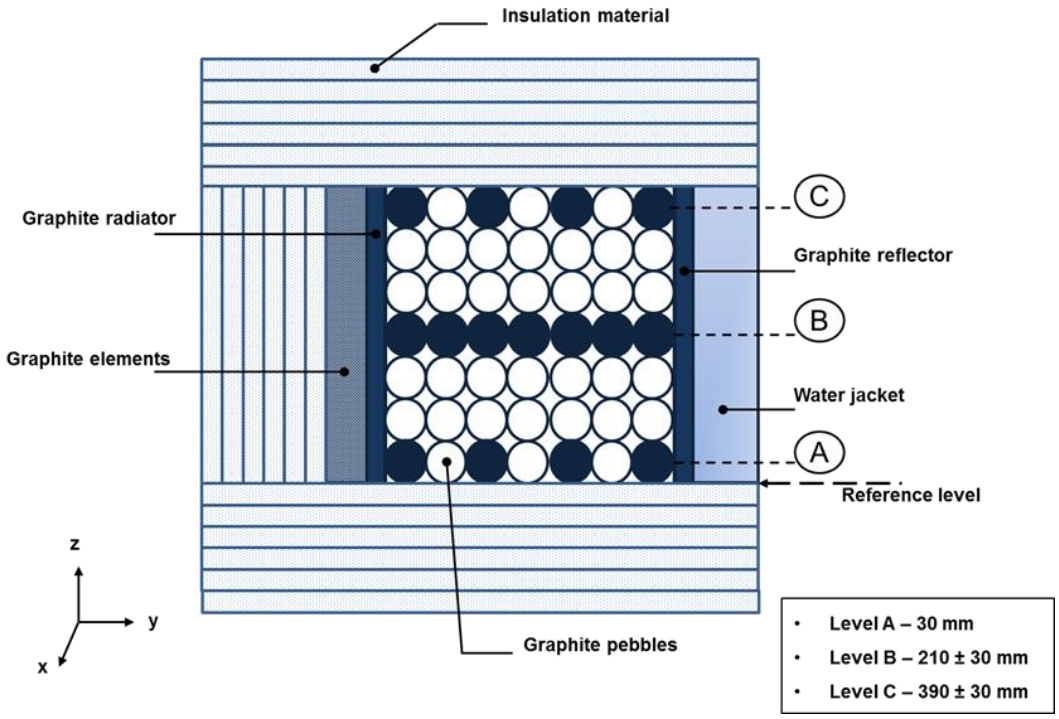

Fig. 3 Schematic representation of a vertical section through the NWTCTF test section (De Beer, 2014).

The graphite spheres used were inherited from the HTTU test facility (Rousseau & Van Staden, 2008) and were originally supplied by SGL Carbon Group in 2005 with designated grade MLRF1. Fig. 4 shows the thermal conductivity of the virgin graphite pebble material as a function of temperature.

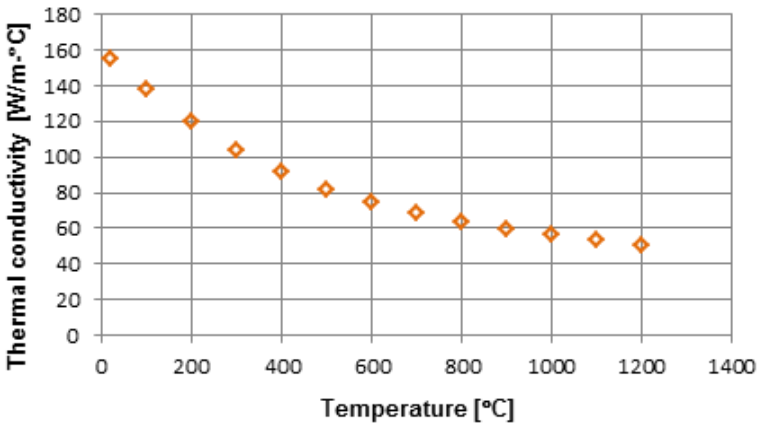

Fig. 4 Thermal conductivity of the virgin graphite pebble material as a function of temperature (Rousseau *et al.*, 2014).

As shown in Fig. 5 (a), the whole test section is enclosed in layers of insulation with a total thickness of approximately 230 mm in an effort to minimize the heat losses to the surroundings. The insulation is made up of layers of either Zircar type SALI-2 or AL-45. The test section fits into a pressure vessel, as can be seen in Fig. 5 (b), which allows for a vacuum to be drawn on the complete assembly. This is required in preparation for and during the actual tests. The preparation includes a rigorous bake-out procedure in order to remove as much as possible of the moisture naturally contained in the porous insulation material. The tests are also done at a near-vacuum condition in order to eliminate natural convection effects within the packed bed.

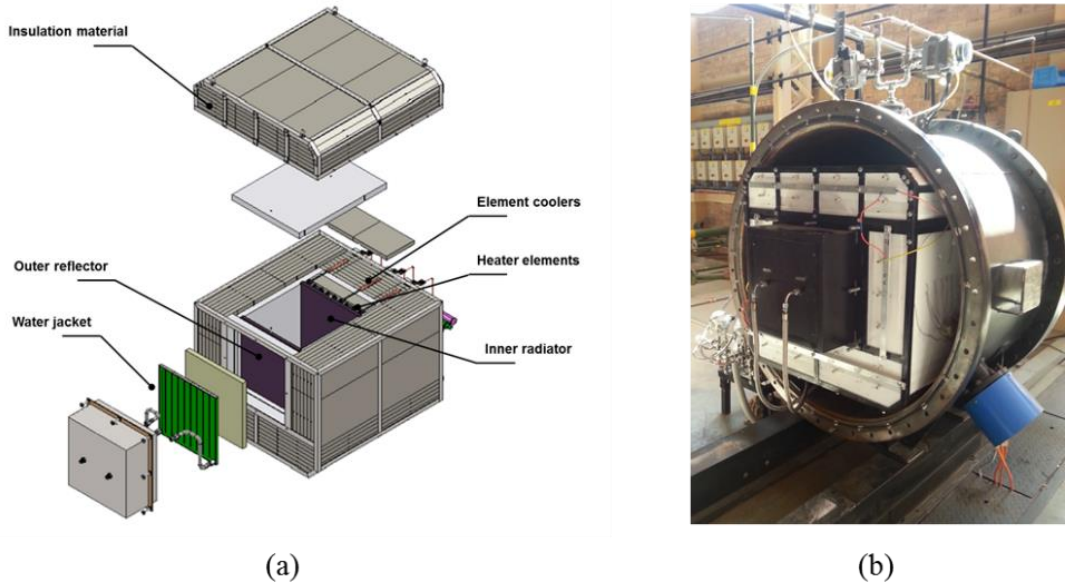

Fig. 5 (a) Exploded view of NWTCTF test section and (b) photograph of test section positioned inside pressure vessel (De Beer, 2014).

Besides the vacuum and heating systems, which include the element coolers, the test facility is also fitted with a nitrogen supply system, water cooling system and an intricate instrumentation and control system. These will not be discussed in detail here.

Thermocouples were installed inside the randomly packed bed along the y-coordinate direction, parallel to the primary heat flux direction. These were installed at three different heights, z coordinate direction, roughly in the middle along the x-coordinate direction. The levels are indicated by the dark coloured spheres in Fig. 3. For levels A and C there were two graphite spheres with thermocouples at the centre of each sphere. Since level B represents the area of primary interest for the heat transfer through the packed bed, 12 spheres instrumented with thermocouples were spaced at this level along the length of the bed.

As shown in Fig. 6 the thermocouple wires were threaded through the packed bed and inserted into the various spheres while taking care to minimize the disruption to the packing structure of the bed. In order to fit the thermocouples small holes with a depth of 30 mm and diameter of 1 mm were drilled into the graphite spheres and a tight fit was obtained once the thermocouple wires were inserted into the spheres. Two thermocouples were also embedded in the inner graphite radiator and one in the outer graphite reflector. The thermocouples were either type B Platinum-Rhodium with a maximum operating temperature of 1750 °C and an instrument uncertainty of ± 5 °C, or type K Inconel with a maximum operating temperature of 1350°C and an instrument uncertainty of ± 3 °C.

Fig. 6 Photograph of the spheres inside the test section showing the thermocouple wires (De Beer, 2014).

Once the bake-out procedure of the insulation material was completed, tests were conducted with the inner radiator wall controlled at 400, 500, 600, 700 and 800 °C (De Beer, 2014). For experimental tests that will be conducted in future it is expected that the maximum temperature can be increased up to 1600 °C. Due to space constraints only the measured temperature results for the 800 °C case will be presented in this paper. It is important to ensure that complete steady-state is reached before the data is collected for each temperature case. In order to prove the repeatability of the experimental results it is also important to perform identical tests at separate times, with the test facility shut down and restarted between tests.

It is important to note here that in order to obtain archival results regarding the wall effect using the NWTCTF one would have to eliminate the effects of the altered packing due to the presence of the walls at the top, bottom and sides that are parallel to the y-coordinate direction. This would be necessary to obtain a bed geometry that represents a section cut from a larger randomly packed bed with the packing structure altered only at the hot and cold walls that are perpendicular to the heat flux created by the temperature gradient. However, the purpose of the current paper is not to present such archival results. Rather, it is to introduce the test facility and the accompanying methodology proposed for separating the effects of conduction and radiation, as well as to demonstrate the qualitative interplay between the phenomena. Therefore, no special measures have yet been taken to eliminate the wall effects at the top, bottom, and sides. The authors are currently working towards obtaining such archival data that will be presented in subsequent papers.

3.2 Effective thermal conductivity results

The data reduction methodology proposed by Rousseau *et al*. (Rousseau *et al.*, 2014) was applied to the experimental data obtained from the NWTCTF to extract the effective thermal conductivity results. The methodology is based on the relationship shown in Eq. (1) and includes a rigorous error propagation analysis. Fig. 7 shows the effective thermal conductivity result together with the associated uncertainty bands as a function of position for the 800 °C case (De Beer, 2014; Rousseau *et al.*, 2015).

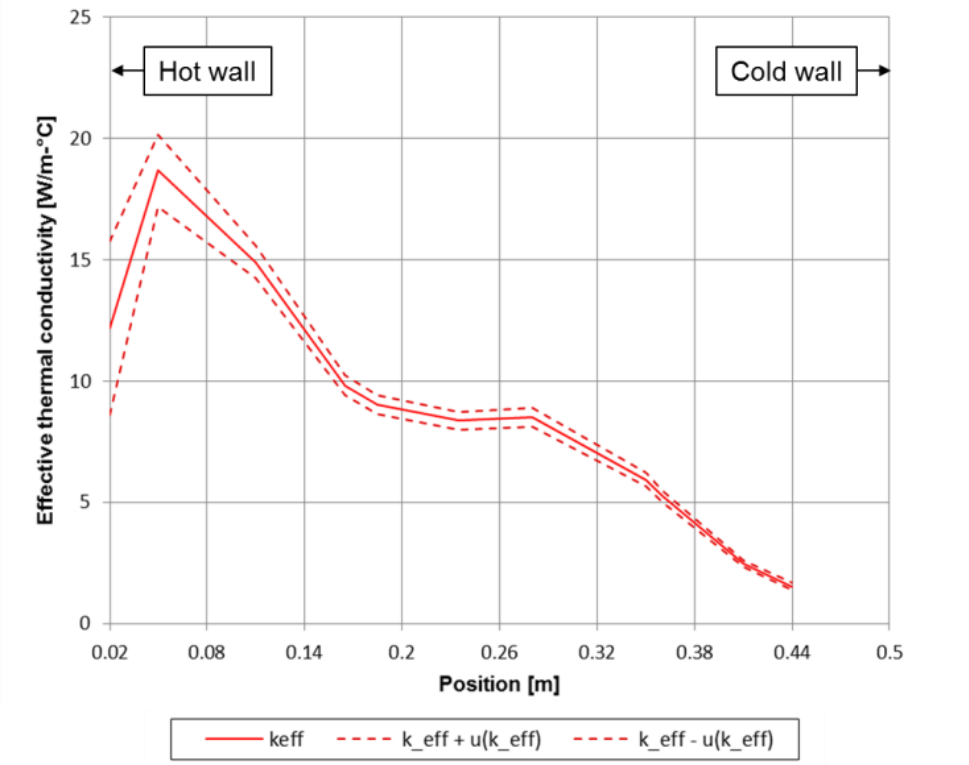

Fig. 7 NWTCTF effective thermal conductivity as a function of position.

From Fig. 7 it is clear that there is a marked reduction in the magnitude of the effective thermal conductivity in the near-wall region at the high temperature inner radiator (hot wall), and a less pronounced reduction at the lower temperature outer reflector (cold wall). This "peaks-and-dip" trend corresponds with the results reported for the HTTU test facility, shown in Fig. 2. As both test facilities were designed to eliminate convection effects, the observed trend has to be a result of the interplay between conduction and radiation heat transfer in the near-wall region and it is important to further investigate this to gain a better fundamental understanding of the phenomena. This can be done by separating the conduction and radiation components of the effective thermal conductivity. The methodology to do this is introduced and expounded upon here and is based on the idea originally proposed elsewhere by the current authors (De Beer, 2014; Rousseau *et al.*, 2015). It combines experimental measurements with the results of CFD simulations to separate the radiation and conduction heat transfer components of the effective thermal conductivity.

4. Methodology

The first two steps of the methodology entail performing experimental tests with the NWTCTF test facility and deriving the effective thermal conductivity from the experimental data, as described in more detail in section 3. The third step is to set up a suitable CFD model to simulate the test conditions and in the fourth step the two sets of results are

compared and the CFD model is calibrated. These steps will be described in more detail in sections 4.1 and 4.2. The final step is to separate the radiation and conduction components of the effective thermal conductivity, as described in section 4.3.

4.1 CFD Model

A CFD model was set up in order to simulate the radiation and conduction heat transfer through the pebble bed at the experimental test conditions and thereby numerically determine the effective thermal conductivity. The randomly packed pebble bed shown in Fig. 8 was generated using the Discrete Element Modeling (DEM) function of STAR-CCM+. Data describing the coordinates of the position of each sphere centroid in the numerically packed bed of spheres was extracted and exported from STAR-CCM+. The data was used in Solidworks to create a solid body for each of the DEM particles forming the packed pebble bed geometry that was then used for the CFD heat transfer model.

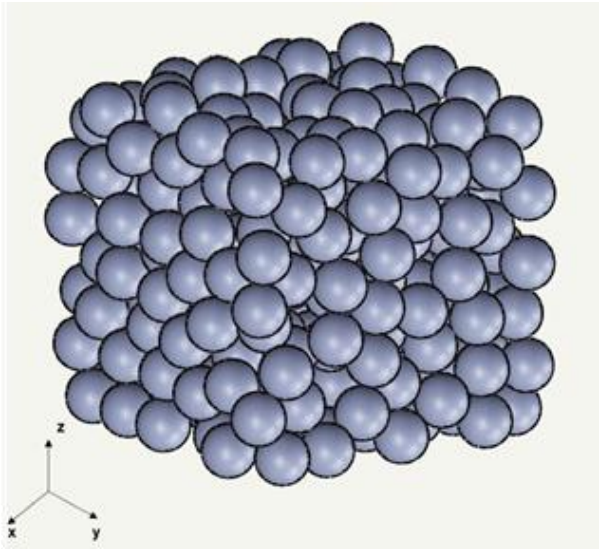

Fig. 8 Solid model of the DEM generated pebble bed (De Beer, 2014).

The porosity variation for the randomly packed DEM pebble bed was analyzed in the x-, y- and z-directions and was compared with the porosity variation of a packed bed of spheres with an ordered simple cubic (SC) packing structure. The results of the porosity variations are shown in Fig. 9.

The average porosity for the numerical pebble bed with a simple cubic packing structure is 0.477. Table 2 lists the average porosities for the wall regions and the near-wall region for each of the coordinate directions in the DEM generated pebble bed. For the x-direction the “inner” and “outer” regions are actually the two side walls, while for the z-direction the “inner” region refers to the bottom of the bed and the “outer” region refers to the top of the bed.

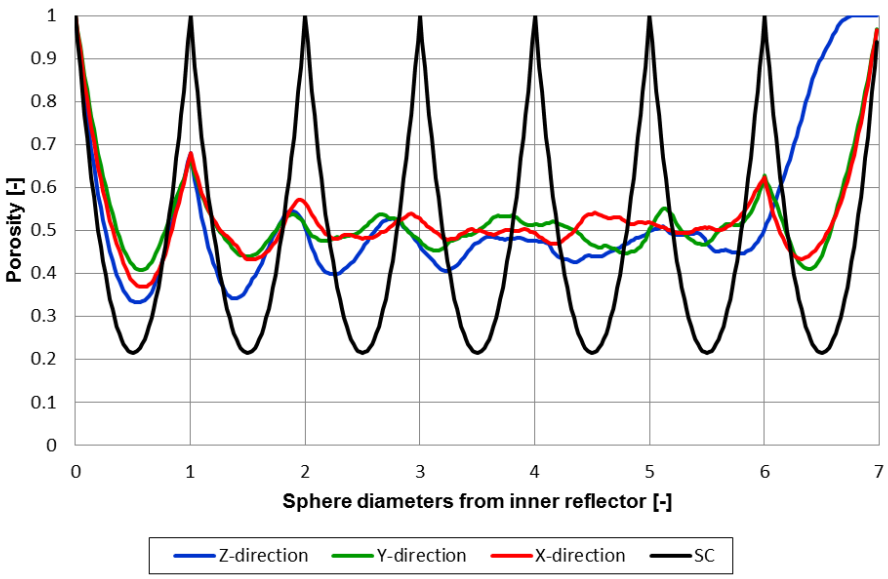

Fig. 9 Variation in porosity for the numerically generated pebble bed compared to the variation in porosity for a pebble bed with a structured packing (SC) (De Beer, 2014).

Table 2: Average porosities in the wall regions of the DEM generated pebble bed (De Beer, 2014).

Direction	Average porosity [-]		
	Inner wall region $0 \leq z \leq 0.5$	Near-wall region $0.5 < z < 6.5$	Outer wall region $6.5 \leq z \leq 7$
X	0.621	0.502	0.666
Y	0.626	0.499	0.683
Z	0.518	0.484	0.985

The effects of the insulated side walls on the porosity variation in the x-direction as well as the effects of the inner and outer reflector walls in the y-direction can be seen in Fig. 9. For both of these we obtain nearly symmetrical profiles, as can be expected. In both the randomly packed bed and the ordered bed the packing structure at the actual inner and outer walls are quite ordered. As we move further away from the inner and outer wall the packing structure of the randomly packed bed becomes more disordered whereas the packing structure of the simple cubic packed bed remains ordered. The non-symmetrical z-direction profile with a sharp increase in the porosity at approximately six sphere diameters is as a result of the gap left between the top layer of spheres and the top cover of the test section. The gap was formed due to the packing method used as well as the physical constraints of the geometry of the test section.

The DEM generated bed described above was used as the geometry for the CFD simulations of the heat transfer through the packed bed of spheres. Fig. 10 shows the solid

models for the pebble bed, the graphite walls and the insulation material surrounding the packed pebble bed used in the CFD model (De Beer, 2014).

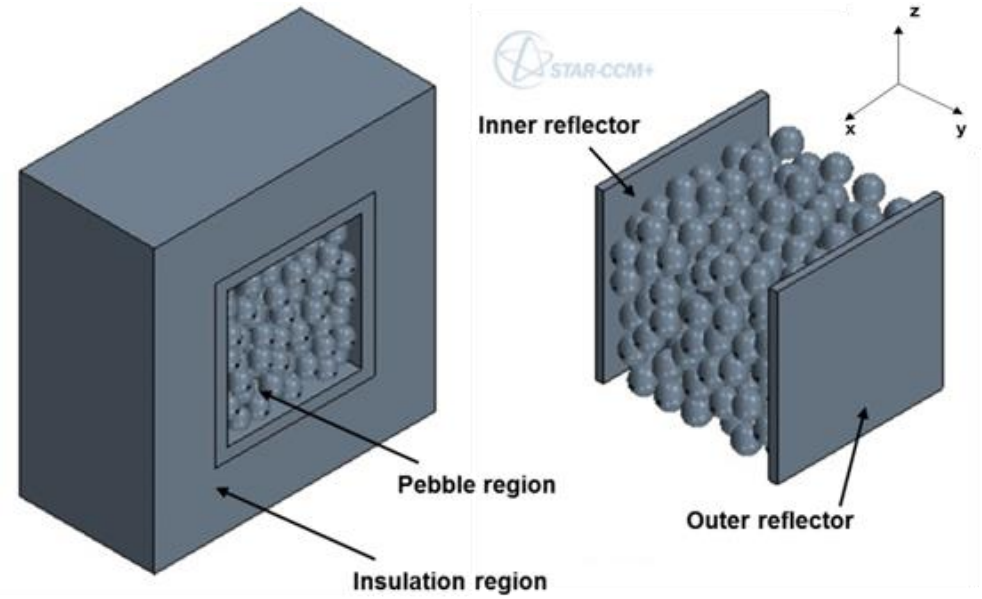

Fig. 10 Solid models of the pebble bed, graphite walls and insulation layers used in the CFD model (De Beer, 2014).

At the pebble-pebble and pebble-wall contact points in the solid model cylindrical fillets were inserted as the contact point treatment, as shown in Fig. 11 (a), in order to obtain a suitable computational grid in this region. The length of the fillet (aligned with the pebble radius) was specified as 0.24 mm based on work presented by Van der Merwe *et al*. (2014). This results in the radius of the fillet cross-section being equal to $r_f = 2.59\ mm$.

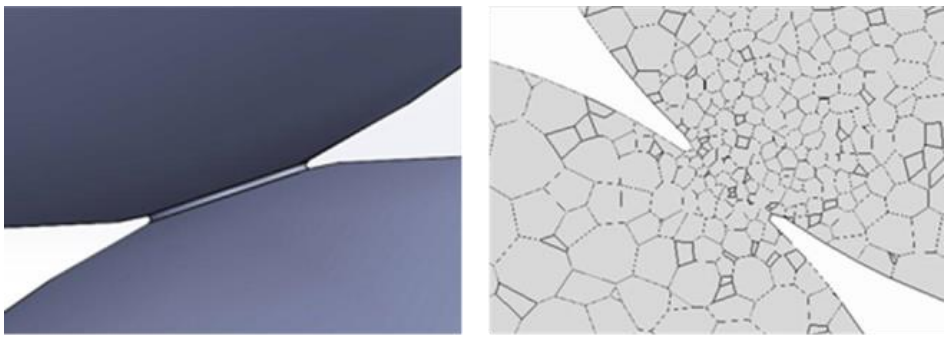

Fig. 11 (a) Close-up of the fillet contact point treatment in the CFD model and (b) the mesh structure at the contact points (De Beer, 2014).

The quality and density of the mesh at the fillet directly influence the results of the conduction heat transfer through the contact point. Therefore, the minimum surface size of the cells required at the contact points to deliver a mesh independent solution was investigated in more detail. For this a separate CFD simulation was set up with a solid

model consisting of two half spheres with a similar fillet inserted at the contact point between the two half spheres. The influence of the mesh density on the conduction heat transfer between the two half spheres was analyzed by solving for various mesh base sizes combined with different minimum surface sizes. The required mesh base size for a mesh independent solution was found to be 3 mm with a minimum surface size of 0.48 mm. The resultant mesh at the contact point is shown in Fig. 11 (b).

An important point to note at this stage is that in order to account for the contact resistance that can be expected at the solid-solid interface an empirical correlation or model will have to be implemented in the CFD model. A model such as proposed by Bahrami *et al*. (2006) can potentially be used to predict the contact resistance that accounts for both the solid and the gas contributions at the solid-solid interface. However, since the test facility is operated under near-vacuum conditions in order to eliminate convection, this model may not be directly applicable.

Wang *et al*. (2016) recently proposed a model to predict the effective thermal conductivity in packed pebble beds. The effective thermal conductivity due to conduction heat transfer was predicted by calculating an equivalent thermal resistance. The total centre-to-centre conduction resistance through the so-called “inner” region consisted of two components in series namely: (1) the resistance of the pebble solid material that is aligned with the solid-solid interface, and (2) the contact resistance at the solid-solid interface. An empirical correlation derived by Chen and Tien (1973) was used as a first approximation for the solid-solid contact resistance. The same approach was also used here to obtain an order of magnitude estimate for the influence of the contact resistance that can be expected for the fillet region in the current CFD model.

The thermal resistance of the pebble material that is aligned with the solid-solid interface is calculated as:

$$R_s = \frac{2r_p}{k_s \pi r_f^2} \tag{3}$$

with $r_p = 30\ mm$ the pebble radius and k_s the thermal conductivity of the solid material. The contact resistance at the solid-solid interface is estimated as (Chen and Tien, 1973):

$$R_{ss} = \frac{0.64}{k_s r_f} \tag{4}$$

The total conduction resistance through the inner region without the contact resistance is therefore equal to R_s, while if the contact resistance is included it becomes $R_s + R_{ss}$. The ratio of the total conduction resistances for the case with the solid-solid contact resistance included and without it is:

$$1+\frac{R_{ss}}{R_s}=1+1.00531\frac{r_f}{r_p} \quad (5)$$

Therefore, for this case, by not including the solid-solid contact resistance, the empirical model used here indicates that the total conduction resistance will be underestimated by approximately 8 %. This means that the impact of the solid-solid contact resistance is not negligible and we will get back to that shortly.

The surface remesher and the polyhedral volume mesher models were selected for the CFD simulations. Two different mesh continua were specified for the CFD simulations; a coarser mesh for the insulation regions and a finer mesh for the pebble, radiator, and reflector regions. A mesh base size of 5 mm and 3 mm were selected based on the results of the mesh independence study for the coarser and the finer mesh respectively. The Segregated Solid Energy and Surface-to-Surface Radiation models were used in the setup of the CFD simulation. The surface emissivity was set to 0.68 for the insulation walls and 0.8 for the graphite reflector, radiator, and pebbles. A curve was fitted through the data shown in Fig. 4 to obtain a function for the dependence of the graphite material thermal conductivity on temperature and was used in the CFD model. It was accepted that the simulations were converged when the residual value was smaller than 10^{-6}.

4.2 Calibration of the CFD model

Fig. 12 (a) shows the temperature distribution calculated with the CFD model compared to the values measured in the NWTCTF. From this it is clear that although the temperature boundary values are the same the agreement between the measured and simulated values is not satisfactory with an average percentage difference of 15%.

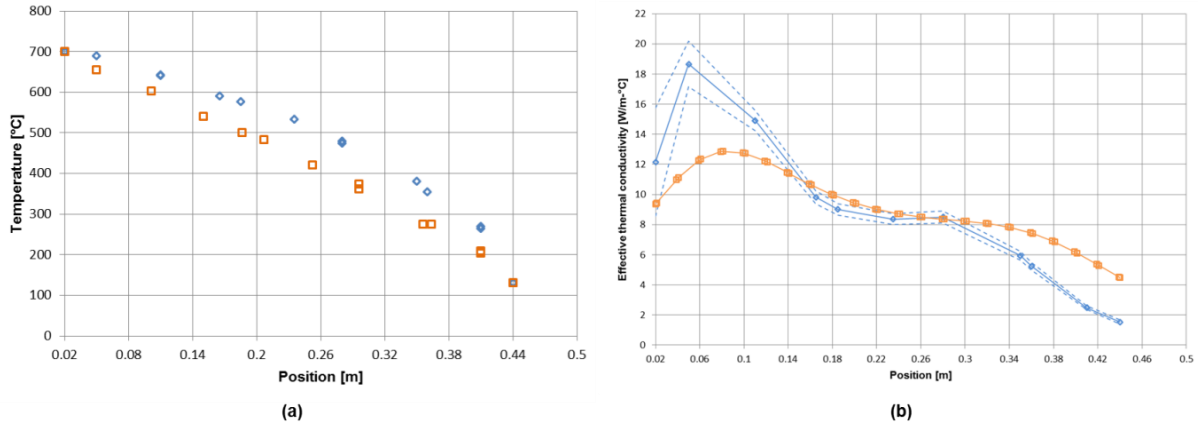

Fig. 12 Comparison between the experimental (◊) and CFD (□) (a) temperature distribution (De Beer, 2014) and (b) effective thermal conductivity results.

Fig. 12 (b) shows the effective thermal conductivity values derived from the experimental and CFD results respectively. The comparison between the effective thermal conductivity

results shows that at high temperatures the CFD effective thermal conductivity is lower than the experimental effective thermal conductivity and at low temperatures the CFD effective thermal conductivity is higher than the experimental effective thermal conductivity. This means that at higher temperatures the resistance in the numerical packed bed in the CFD model should be less (more conduction) and at lower temperatures the resistance should be more (less conduction).

A method similar to that used to obtain the heat flux distribution in the y-direction through the bed for the experimental results was used to obtain the heat flux distribution through the CFD model. For the CFD simulation the heat transfer rate through the cooled outer reflector was found to be 2020.4 W while the corresponding value measured in the experiment is 1657.6 W. This means that the overall conduction resistance of the bed in the simulation is underestimated by approximately 22 %. As shown in section 4.1 an underestimation could be expected due to the solid-solid contact resistance at the pebble-pebble interfaces not being included at present. In the CFD model the total heat loss through all of the insulation layers surrounding the test section was found to be 347.1 W. This is within 5.5 % of the value of 366.7 W obtained from the experimental results. However, the conduction resistance is again underestimated due to the solid-solid contact resistance at the pebble-wall interface not being included.

The analysis above shows that the results obtained with the CFD model are consistent with what can be expected due to the solid-solid contact resistances not being included at present. It is therefore necessary to include the contact resistances at the pebble-pebble and pebble-wall solid-solid interfaces and also to calibrate the empirical constant in the correlation in an appropriate manner. This is the fourth step in the proposed methodology and will involve a direct comparison between the results obtained with the CFD model and those obtained from the experiments. Such a calibration should account for three aspects namely (i) matching the overall heat flux through the bed, (ii) matching the temperature distribution through the bed and (iii) matching the heat losses through the insulation layers. It should also incorporate all the tests conducted at the different boundary temperatures to account for potential temperature dependent effects.

It is quite a complex task to include the contact resistance at each of the fillet regions in the CFD model. Furthermore, the effects of the altered packing due to the walls at the top, bottom and sides of the test section have not yet been eliminated in either the physical test or in the geometry used in the CFD model. This means that even if the contact resistances were included in the current simulations, we could still not yet treat the results obtained as the final archival data. Therefore, it was decided that for the purpose of the current study,

where we aim to demonstrate the qualitative interplay between the phenomena, it is sufficient to use the CFD model without including and calibrating the solid-solid contact resistances. The authors are continuing the work towards obtaining the final archival data that will be presented in future.

The temperatures specified at the various boundaries of the CFD model for the different simulation cases addressed in the current study are shown in Table 3. The temperature values correspond to the experimental measurements of De Beer (2014) for the various test cases up to 800 °C. For the higher temperature simulation cases the temperature of the heated wall was increased and the rest of the boundary values of the 800 °C case were used. In a PBR one would expect higher temperatures for the outer reflector wall; however, for the current study the focus was not to simulate typical PBR conditions but to investigate the effect of the macro temperature gradient on the effective thermal conductivity. From the CFD simulation results the heat extracted at the cooled wall as well as the temperature distribution through the pebble bed can be obtained. By using the methodology proposed by Rousseau *et al*. (2014) the effective thermal conductivity can be determined.

Table 3: Temperature boundary values for the CFD model.

Inner radiator wall	Outer reflector wall	Top insulation	Bottom/Side insulation
400 °C	59.39 °C	33.86 °C	35.29 °C
500 °C	74.65 °C	34.07 °C	35.26 °C
600 °C	103.43 °C	41.02 °C	46.05 °C
700 °C	130.30 °C	48.86 °C	54.17 °C
800 °C	163.00 °C	51.45 °C	58.39 °C
1000; 1200; 1400 & 1600 °C	163.00 °C	51.45 °C	58.39 °C

4.3 Separation of the radiation and conduction components

For the final step of the methodology the conduction and radiation components of the effective thermal conductivity are separated. Fig. 13 shows a detailed outline of the method used to separate the effective thermal conductivity components. For each of the CFD temperature cases two simulations were run namely one for conduction and radiation combined and another for conduction only. This can be done by de-activating the radiation heat transfer model in the CFD simulation. As a result, only the effects of conduction heat transfer will be simulated.

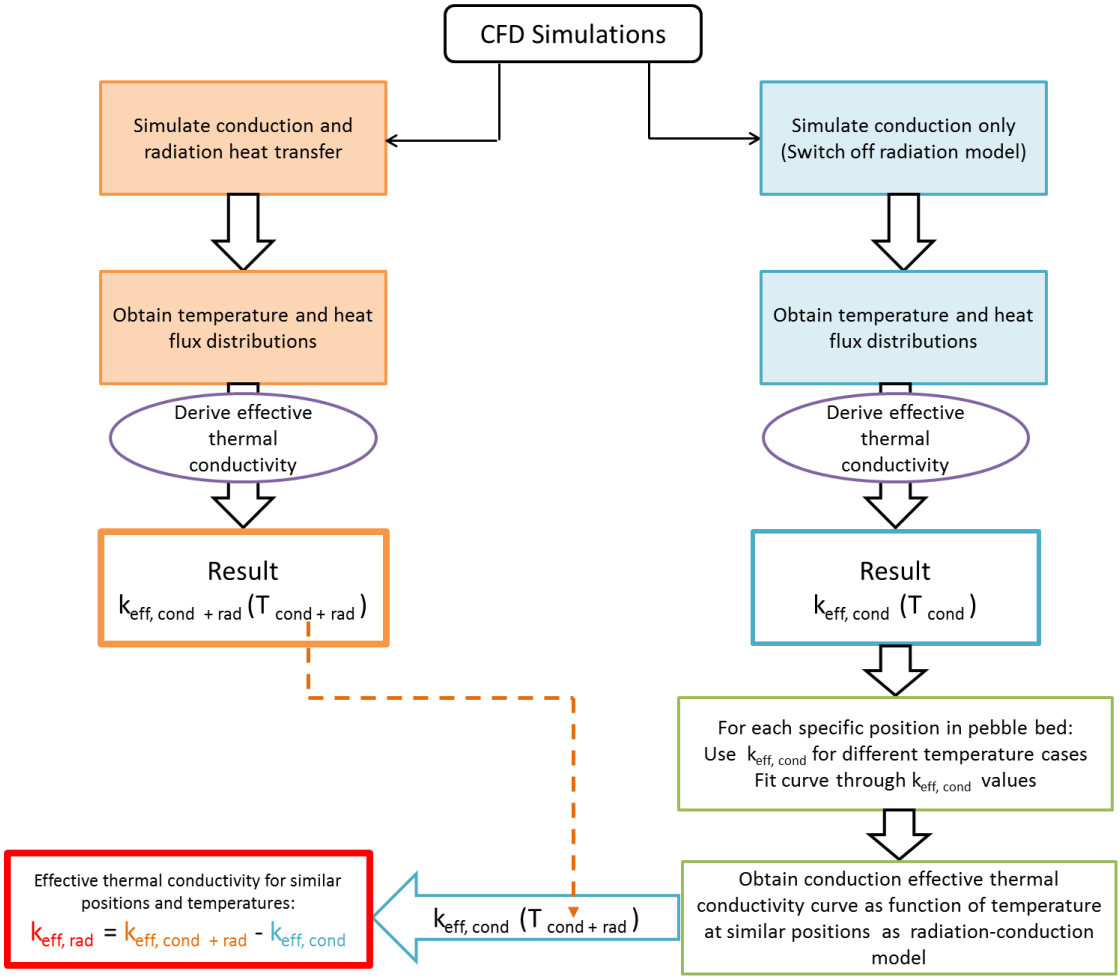

Fig. 13 Outline of method for separation of the conduction and radiation components of the effective thermal conductivity.

Once the effective thermal conductivity is calculated for both the conduction-radiation and conduction-only cases for each of the CFD tests, the contribution of the radiation component can be determined. However, it is important to note that the results of the two cases must be compared at similar positions within the bed, to ensure similar packing structures, and at the same time also at similar temperatures. It is also important to note that for similar boundary values the conduction-radiation case and the conduction-only case will not necessarily result in similar temperatures at corresponding positions in the bed. This means that the required data cannot simply be extracted from the two cases with the same boundary values. The conduction-only effective thermal conductivity values are therefore first determined for the various temperature cases for each position in the pebble bed. Curves are then fitted through the data from which multiple polynomial functions are obtained for the conduction component of the effective thermal conductivity as a function of temperature, with each function applicable to a specific position in the pebble bed. The use of curve fitting in the procedure will of course introduce additional uncertainty in the final

results. This will need to be accounted for in the generation of the final archival results but will not be addressed here.

The conduction-radiation results are considered and the conduction-only values at corresponding positions and temperatures are obtained from the fitted curves. The conduction-only values are then subtracted from the combined conduction-radiation values according to Eq. (2) to obtain the corresponding radiation-only values.

5. Results and discussion

The results obtained with the CFD model for the temperatures, temperature gradients and resultant effective thermal conductivities are presented next.

5.1 Temperature distribution results

The temperature distribution results obtained from the CFD model for the different boundary value cases with combined conduction-radiation and conduction-only are shown in Fig. 14 and Fig. 15 respectively. When the results are compared it is clear that the contribution of radiation becomes more significant for the higher temperature cases. This can be seen in the significant difference between the temperature distributions for the 1600 °C case in Fig. 14 and Fig. 15, at the same overall temperature gradient, as opposed to the small difference for the 400 °C case.

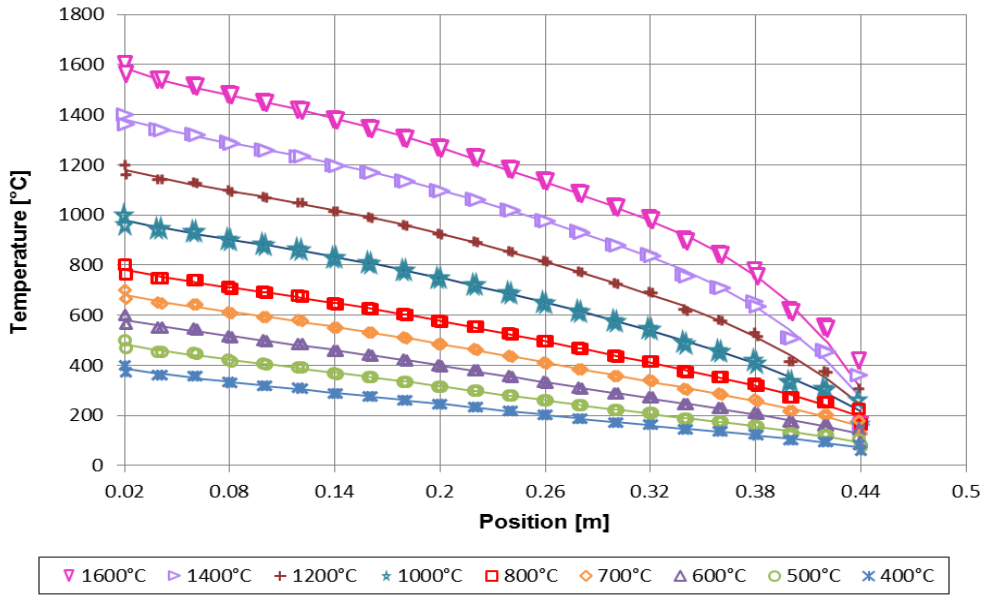

Fig. 14 Temperature distributions derived from the CFD model for combined conduction and radiation for the different simulation cases.

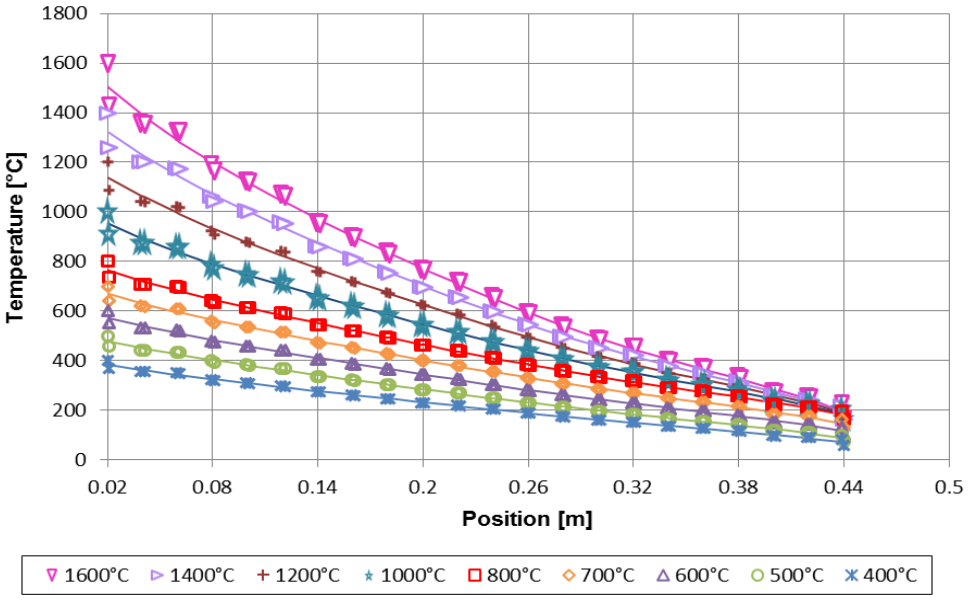

Fig. 15 Temperature distributions derived from the CFD model for conduction-only for the different simulation cases.

5.2 Temperature gradient results

The temperature gradient distribution results derived for the various conduction-radiation and conduction-only cases are shown in Fig. 16 and Fig. 17. The wall effects at the inner radiator as well as the outer reflector can be seen in the results of both the conduction-radiation and conduction-only cases. There is also a significant difference in the absolute magnitude of the temperature gradients for the lower temperature cases compared to the higher temperature cases. This can be expected as the heat flux through the pebble bed is higher for the higher temperature cases than for the lower temperature cases.

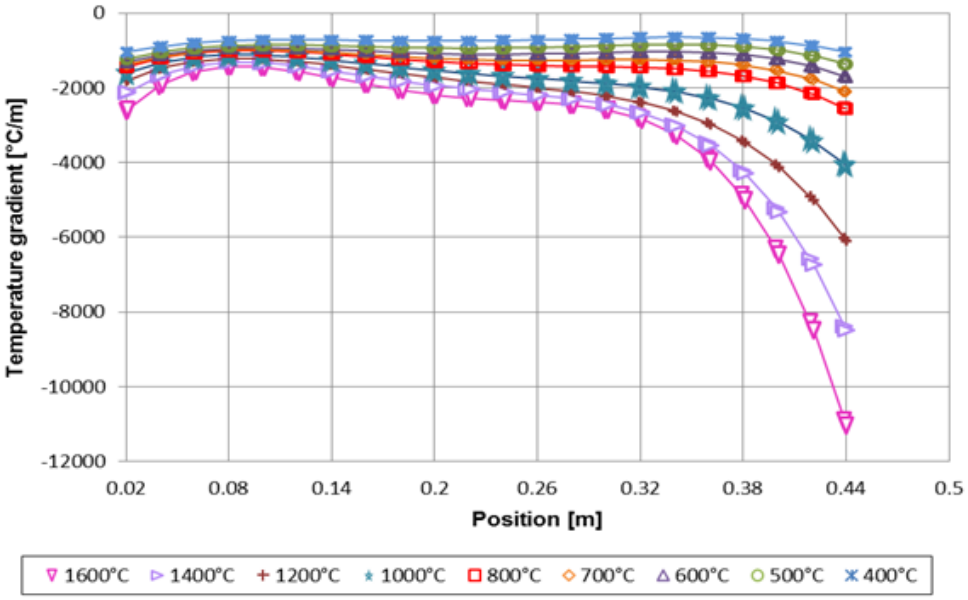

Fig. 16 Temperature gradient distributions derived from the CFD model for combined conduction and radiation for the different simulation cases.

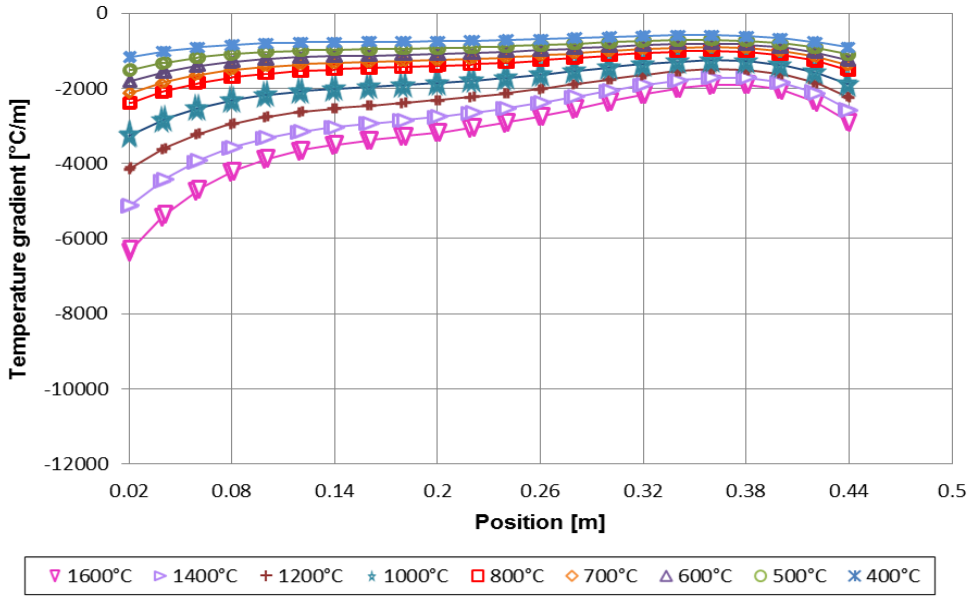

Fig. 17 Temperature gradient distributions derived from the CFD model for conduction-only for the different simulation cases.

5.3 Combined conduction-radiation effective thermal conductivity results

The effective thermal conductivity results as a function of position derived for each of the CFD cases, with combined conduction and radiation heat transfer present, are shown in Fig. 18. The same “peaks-and-dip” trend discussed in sections 2.2 and 3.2 can be seen in the results, marked by an increase followed by a decrease in the effective thermal conductivity in the near-wall region at the inner radiator (hot wall). A similar trend is seen in the near-wall region at the outer reflector (cold wall); however, it is less pronounced.

From Fig. 14 it can be seen that much higher temperatures are present in the near-wall region at the inner radiator than at the outer reflector. This reconfirms the conclusion that the radiation heat transfer mechanism becomes more prominent at higher temperatures and therefore has a larger effect on the effective thermal conductivity in the near-wall regions, especially at the inner radiator wall.

The effective thermal conductivity results as a function of temperature (rather than position) derived for each of the CFD cases are shown in Fig. 19. It can be noted that the effective thermal conductivity values increase with an increase in temperature. A decrease in the effective thermal conductivity value for each of the CFD cases is observed in both the near-wall regions at the inner radiator and outer reflector.

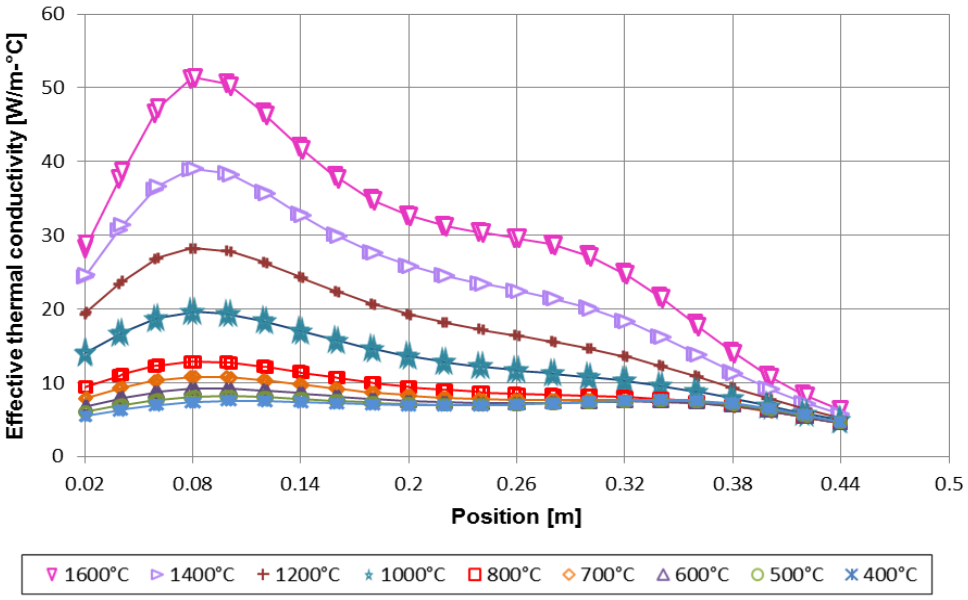

Fig. 18 Effective thermal conductivity distributions derived from the CFD model as a function of position for combined conduction and radiation for the different simulation cases.

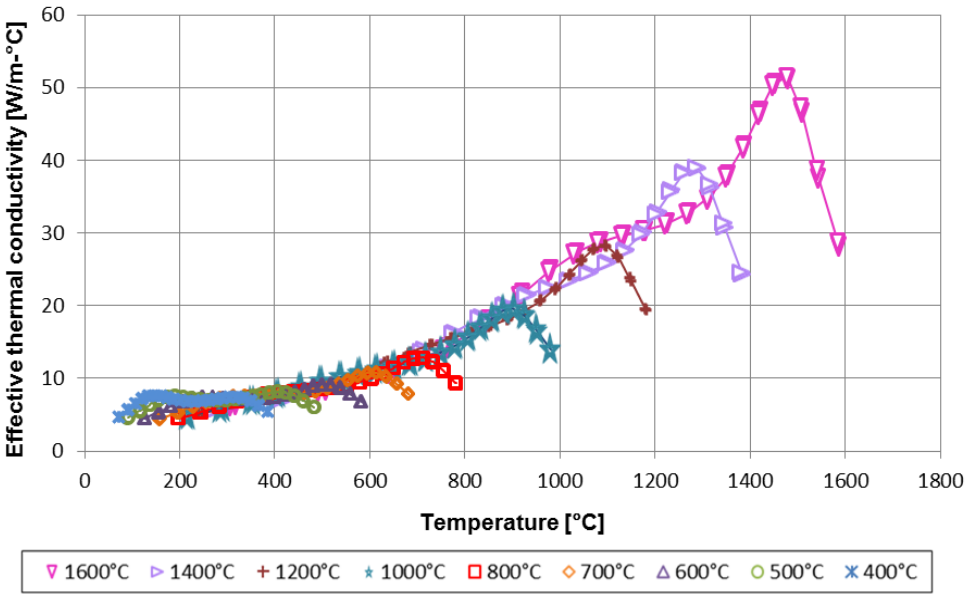

Fig. 19 Effective thermal conductivity distributions derived from the CFD model as a function of temperature for combined conduction and radiation for the different simulation cases.

One would expect the curves for the various CFD cases to form one continuous increasing curve when plotted on the same graph as in Fig. 19. However, deviations can be observed between the different cases. In the near-wall regions the deviations occur due to the altered packing structure of the pebble bed, but in the bulk regions the deviations cannot be attributed to differences in packing structure. From Fig. 16 it is clear that there are differences in the macro temperature gradients of each of the CFD cases that also contribute to the deviations seen in the effective thermal conductivity values in Fig. 19. This confirms the observation made by Rousseau *et al*. (2014) that the effective thermal conductivity of a

packed pebble bed is not only a function of the local temperature, but also a function of the macro temperature gradient.

5.4 Conduction-only effective thermal conductivity results

The conduction component of the overall effective thermal conductivity distributions as a function of temperature for the different cases is shown in Fig. 20. For each of the cases the near-wall effects at both the inner radiator and the outer reflector are clearly visible. The wall effect at the outer reflector, and thus lower temperatures, is much more prominent than at higher temperatures. The effective thermal conductivity value for the 400 °C - 1000 °C cases decreases with an increase in temperature as expected, reflecting the correlation between the thermal conductivity of the graphite pebble material as a function of temperature. The higher temperature cases also show a decrease in the effective thermal conductivity value; however, the results do not align with that of the other cases due to the differences in the macro temperature gradient.

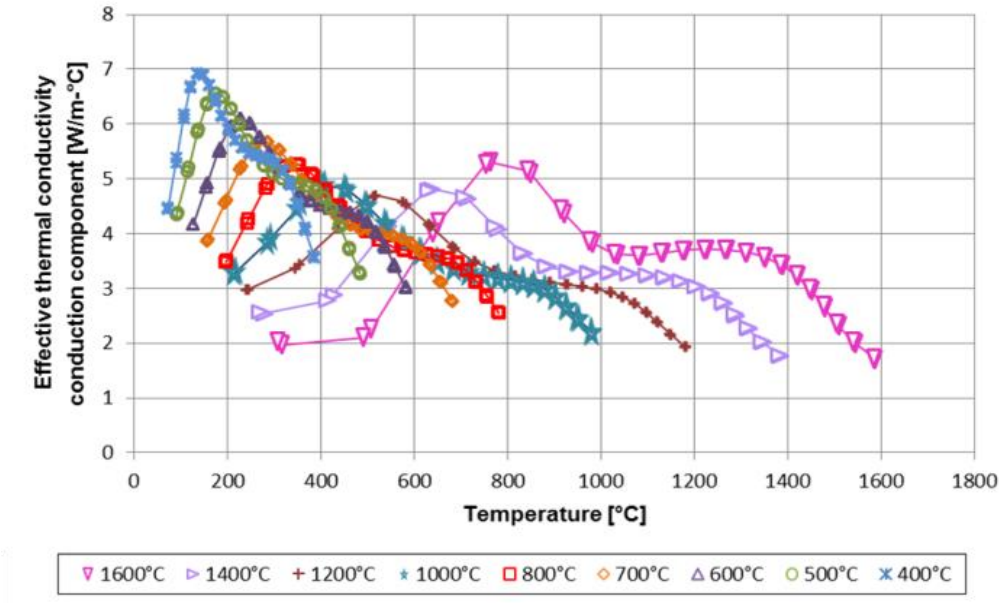

Fig. 20 Conduction components of the effective thermal conductivity distributions derived from the CFD model as a function of temperature for the different simulation cases.

5.5 Radiation-only effective thermal conductivity results

The derived radiation-only components as a function of temperature for the various cases are shown in Fig. 21. For all of the cases the radiation component of the effective thermal conductivity increases with an increase in temperature as the radiation contribution becomes more significant at higher temperatures. The near-wall effect at the inner radiator is clearly visible and a sharp decrease in the effective thermal conductivity values is observed for all of

the cases. The near-wall effect at the outer reflector (cold side) in the bed is less noticeable since the radiation heat transfer mechanism becomes less prominent at lower temperatures.

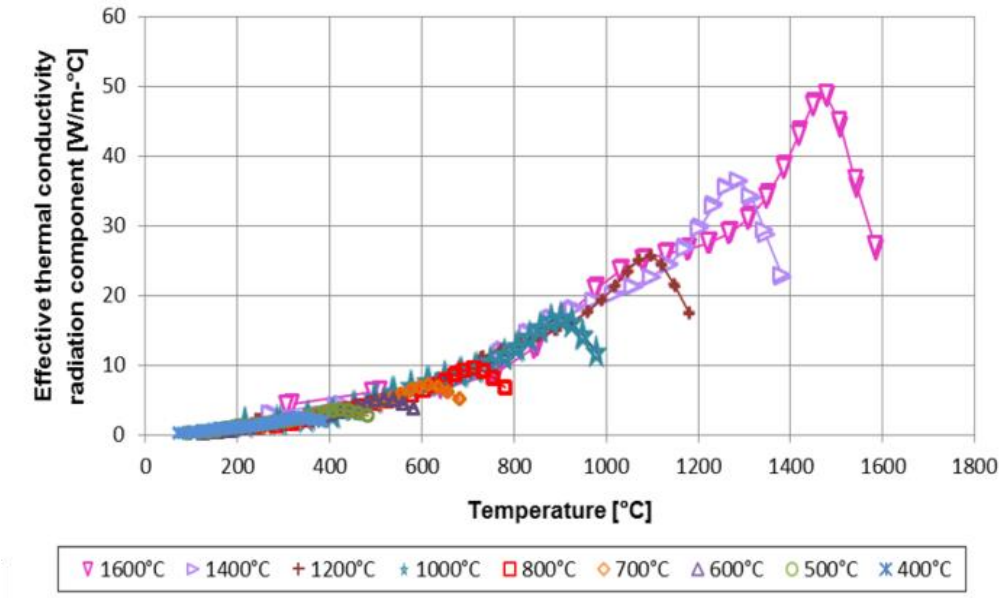

Fig. 21 Radiation components of the effective thermal conductivity distributions derived from the CFD model as a function of temperature for the different simulation cases.

5.6 Separation of the conduction and radiation components

Fig. 22 and Fig. 23 show the overall effective thermal conductivity distributions as a function of position derived from the CFD model, together with its conduction-only and radiation-only components for the 400 °C and 1000 °C cases respectively. The radiation component (△) of the 1000 °C case is significantly larger than that of the 400 °C case and therefore at higher temperatures radiation can be considered as the dominant contributing phenomenon to the overall effective thermal conductivity of the pebble bed.

At lower temperatures conduction becomes the main contributing heat transfer mechanism and the conduction component (□) of the 400 °C case is larger than that of the 1000 °C case. The values of the effective thermal conductivity are lower at the inner radiator (hot wall) for the conduction components, due to the decrease of the thermal conductivity of the pebble graphite material at higher temperatures. The wall effects due to the higher porosity in both near-wall regions are clearly visible in the conduction components of both cases; however, the effect is more prominent at the outer reflector (cold wall). This can be expected as the higher porosity in the near-wall region implies that there is much less pebble material present and also fewer contact points between adjacent pebbles.

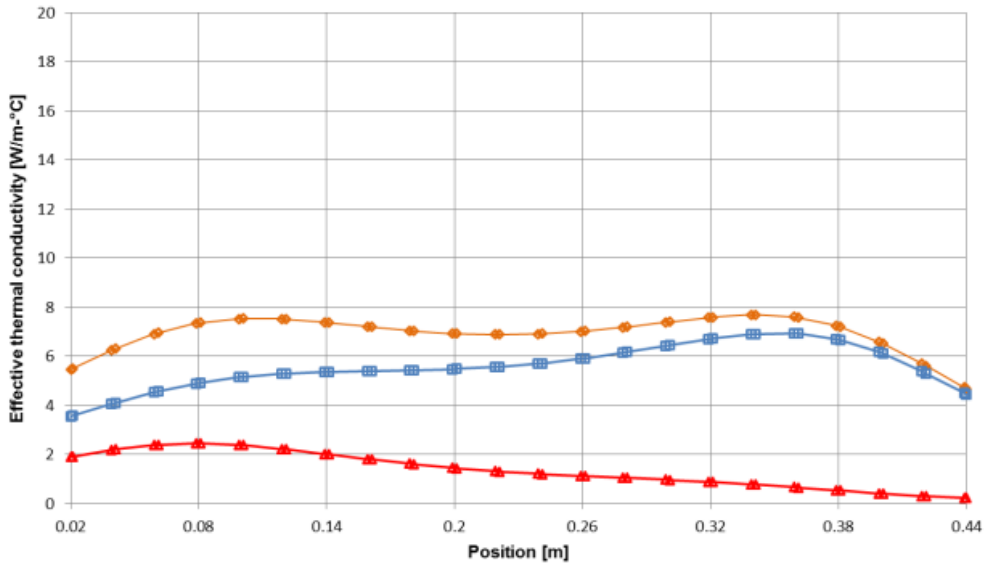

Fig. 22 Effective thermal conductivity distributions derived from the CFD model for combined radiation and conduction (◇), conduction-only (□) and radiation-only (△) for the 400 °C case.

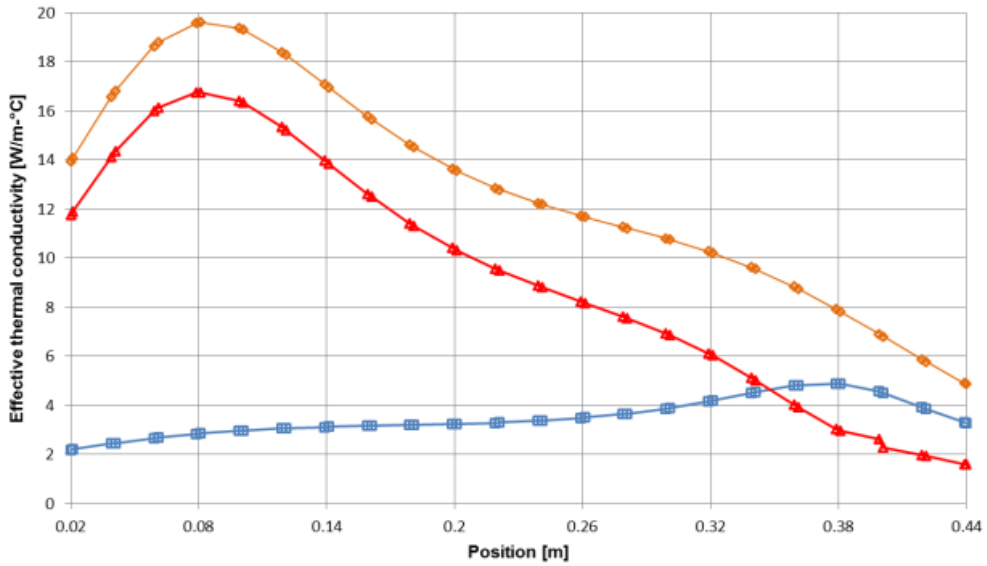

Fig. 23 Effective thermal conductivity distributions derived from the CFD model for combined radiation and conduction (◇), conduction only (□) and radiation only (△) for the 1000 °C case.

The radiation component of both CFD cases increases with an increase in temperature and the wall effects are visible at the inner radiator as well as the outer reflector. The altered packing structure in the wall regions influences the radiation heat transfer as it is not only a short-range effect, but a long-range effect as well. For the 1000 °C case the increase in the radiation component is much more pronounced and a significant reduction in the effective thermal conductivity value can be seen at the inner radiator due to the near-wall effect. The higher porosity in the near-wall region implies that there is much less pebble surface area present. Thus, at higher temperatures, where radiation is more pronounced, the wall effect is more prominent than at the lower temperatures where the contribution of radiation decreases significantly.

The “peaks-and-dip” trend observed in the overall effective thermal conductivity due to combined conduction and radiation can be explained as the result of the interplay between the unique gradients of the radiation-only and conduction-only curves. Both the radiation-only and conduction-only curves are a function of temperature, packing structure and macro temperature gradient in the pebble bed.

6. Conclusions

A custom designed test facility was introduced and an accompanying methodology was proposed to separate the effects of conduction and radiation on the effective thermal conductivity in a packed pebble bed consisting of graphite spheres of uniform size, including the wall effects. Although the absolute values of the results obtained here are not yet archival, it clearly demonstrates the qualitative interplay between the phenomena.

For both heat transfer phenomena, the near-wall effects have a notable influence. The conduction is reduced due to the higher porosity which implies that there is less pebble material and fewer contact points between adjacent pebbles. The radiation is also reduced due to the reduction in pebble surface area exposed to radiation at higher porosity. The conduction increases at lower temperatures due to the characteristic increase in the graphite thermal conductivity and therefore the wall effect is more prominent for conduction on the low temperature side of the bed. The radiation naturally increases at higher temperatures and therefore the wall effect is more prominent for radiation on the high temperature side of the bed. The interplay between these phenomena results in the characteristic “peaks-and-dip” trend in the combined conduction and radiation effective thermal conductivity that is observed in the results obtained from both the HTTU and NWTCTF experiments.

In order to obtain archival results, the effects of the altered packing due to the presence of the walls at the top, bottom and sides of the test section must be eliminated. Furthermore, it is necessary to include the contact resistances at the pebble-pebble and pebble-wall solid-solid interfaces of the CFD model and also to calibrate these contact resistances by comparing with the measured results. The authors are currently working towards obtaining such archival data that will be presented in subsequent papers.

Nomenclature

A	Area [m^2]
k_{cond}	Conduction component of effective thermal conductivity [W/m-K]

k_{eff}	Effective thermal conductivity [W/m-K]
k_{rad}	Radiation component of effective thermal conductivity [W/m-K]
k_s	Thermal conductivity of solid material [W/m-K]
$\dot{Q}$	Heat transfer rate [W]
Δr	Path length [m]
r_f	Radius of fillet cross-section [m]
r_p	Pebble radius [m]
R_s	Thermal resistance of pebble material aligned with solid-solid interface [K/W]
R_{ss}	Contact resistance at solid-solid interface [K/W]
T	Temperature [K] / [°C]
z	Position in terms of sphere diameters [-]

Abbreviations

CFD	Computational Fluid Dynamics
DEM	Discrete Element Modeling
HTTU	High Temperature Test Unit
MSUC	Multi-sphere Unit Cell
NWTCTF	Near-Wall Thermal Conductivity Test Facility
PBR	Pebble Bed gas-cooled reactor
SC	Simple Cubic

References

Abou-Sena, A., Ying, A. & Abdou, M. 2003. Experimental investigation and analysis of the effective thermal properties of Beryllium packed beds. *Fusion Science and Technology*, 44:79-84.

Asakuma, Y., Kanazawa, Y. & Yamamoto, T. 2014. Thermal radiation analysis of packed bed by a homogenization method. *International Journal of Heat and Mass Transfer*, 73(2014):97-102.

Bahrami, M., Yovanovich, M.M. & Culham, J.R. 2006. Effective thermal conductivity of rough spherical packed beds. *International Journal of Heat and Mass Transfer*, 49:3691-3701.

Breitbach, G. & Barthels, H. 1980. The radiant heat transfer in the high temperature reactor core after failure of the afterheat removal systems. *Nuclear Technology*, 49:392-399.

Cheng, G.J. & Yu, A.B. 2013. Particle scale evaluation of the effective thermal conductivity from the structure of a packed bed: Radiation heat transfer. *Industrial & Engineering Chemistry Research*, 52(34):12202-12211.

Chen, C.K. & Tien, C.L. 1973. Conductance of packed spheres in vacuum. *Journal of Heat Transfer*, 95:302-308.

De Beer, M. 2014. Characterization of thermal radiation in the near-wall region of a packed pebble bed. Potchefstroom, South Africa: North-West University. (Masters Dissertation).

Rousseau, P.G., Du Toit, C.G. & De Beer, M. 2015. A methodology for the characterization of the effective thermal conductivity in the near-wall region of a packed pebble bed. (Nice, France: Paper presented at the International Congress on Advances in Nuclear Power Plants.)

Rousseau, P.G., Du Toit, C.G., Van Antwerpen, W. & Van Antwerpen, H.J. 2014. Separate effects tests to determine the effective thermal conductivity in the PBMR HTTU test facility. *Nuclear Engineering and Design*, 271:444-458.

Rousseau, P.G. & Van Staden, M. 2008. Introduction to the PBMR heat transfer test facility. *Nuclear Engineering and Design*, 238:3060-3072.

Slavin, A.J., Arcas, V., Greenhalgh, C.A., Irvine, E.R. & Marshall, D.B. 2002. Theoretical model for the thermal conductivity of a packed bed of solid spheroids in the presence of a static gas, with no adjustable parameters except at low pressure and temperature. *International Journal of Heat and Mass Transfer*, 45:4151-4161.

Stöcker, B. & Niessen, H.F. 1997. The SANA-I experiments for self-acting removal of the afterheat from a pebble bed.

Talukdar, P., Mendes, M.A.A., Parida, R.K., Trimis, D. & Ray, S. 2013. Modeling of conduction-radiation in a porous medium with blocked-off region approach. *International Journal of Thermal Sciences*, 72:102-114.

Tsotsas, E. & Martin, H. 1987. Thermal Conductivity of Packed Beds: A Review. *Chemical Engineering Processes*, 22:19-37.

Van Antwerpen, W. 2009. Modeling the effective thermal conductivity in the near-wall region of a packed pebble bed. Potchefstroom, South Africa: North-West University. (Thesis - Ph.D.).

Van Antwerpen, W., Du Toit, C.G. & Rousseau, P.G. 2010. A review of correlations to model the packing structure and effective thermal conductivity in packed beds of mono-sized spherical particles. *Nuclear Engineering and Design*, 240:1803-1818.

Van Antwerpen, W., Rousseau, P.G. & Du Toit, C.G. 2012. Multi-sphere Unit Cell model to calculate the effective thermal conductivity in packed pebble beds of mono-sized spheres. *Nuclear Engineering and Design*, 247:183-201.

Van der Merwe, W.J.S., Du Toit, C.G. & Kruger, J.H. 2014. Local rise of total pressure in viscous flow through cylindrical packed beds with spherical particles. (Somerset West, South Africa: Proceedings of the 9th SA Conference on Computational and Applied Mechanics (SACAM).)

Wang, X., Zheng, J. & Chen, H. 2016. A prediction model for the effective thermal conductivity of mono-sized pebble beds. *Fusion Engineering and Design*, 103(2016):136-151.

Zhou, J., Yu, A. & Zhang, Y. 2007. A boundary element method for evaluation of the effective thermal conductivity of packed beds. *Journal of Heat Transfer*, 129:363-371.

Zhou, Z.Y., Yu, A.B. & Zulli, P. 2010. A new computational method for studying heat transfer in fluid bed reactors. *Powder Technology*, 197:102-110.

5. Article 4: Effect of contact resistance on the prediction of the effective thermal conductivity in a packed graphite pebble bed

M. De Beer *, C.G. Du Toit, P.G. Rousseau

Abstract

The overall heat transfer in a packed bed of spheres in a stagnant gas environment can be described by the effective thermal conductivity. Conduction and thermal radiation are the two main contributing heat transfer phenomena in the packed bed. At higher temperatures, the contribution of thermal radiation to the overall heat transfer becomes significant. The conduction through the sphere-sphere and sphere-wall contact areas in the packed bed should be considered in detail as these conduction paths will have a significant influence on the effective thermal conductivity trends when conduction becomes the dominant heat transfer mechanism at lower temperatures. The real contact area of a contact point in the packed bed is a summation of its micro-contacts. Heat flow across the contact area is restricted due to the presence of these micro-contacts and can be represented by a contact resistance associated with the contact area. Various approaches exist to predict and model the conduction heat transfer through contact areas in a packed bed. This paper presents the addition of contact resistances to a methodology previously proposed by the authors, which combines physical measurements with Computational Fluid Dynamics (CFD) simulations to separate the contributions of radiation and conduction to the overall effective thermal conductivity, including wall effects. Preliminary results obtained with the CFD model that include contact resistances offer insight into the importance of the inclusion of contact resistances to accurately model the conduction component. A preliminary method that can be used to calibrate the CFD model by adjusting the contact resistances is presented. The calibrated CFD model provides results in agreement with the physical measurements.

Keywords: Effective thermal conductivity, Packed pebble bed, Thermal conduction, Thermal contact resistance, Thermal radiation, Computational Fluid Dynamics

1. Introduction

Packed pebble beds are used in a variety of thermal-fluid applications due to their high solid surface area to volume ratio (Bahrami *et al.*, 2006). Thermal-fluid applications include catalytic reactors, drying processes, thermal insulation, heat storage systems, hydrogen production and generation IV type nuclear reactors (Asakuma *et al.*, 2016; Ren *et al.*, 2017; Van Antwerpen *et*

al., 2010; Zhou *et al.*, 2007). Accurately predicting the bed effective thermal conductivity, which is a parameter representative of the overall heat transfer through the bed, is a complex problem as it is not isotropic.

When considering applications with a packed bed in a stagnant fluid environment, such as the safety case of a pebble bed gas-cooled reactor during a depressurized loss of forced coolant incident, the main contributing heat transfer phenomena becomes conduction and radiation. At higher temperatures, above 650 °C, the contribution of radiation heat transfer to the overall effective thermal conductivity increases significantly (Breitbach & Barthels, 1980; Zhou *et al.*, 2007; Cheng & Yu, 2013; Talukdar *et al.*, 2013; Ren *et al.*, 2017). The conduction component consists of two parts: (1) conduction through the pebble material itself and the stagnant fluid and (2) conduction through the physical contact points and contact surfaces of the solid materials (Van Antwerpen *et al.*, 2010). A thorough understanding of the mechanics of the thermal contact conductance is important as the pebbles are the main carriers of thermal energy throughout the bed. Thus, the heat transfer through the contact points has a direct influence on the bed effective thermal conductivity and is one of the factors that determine the thermal behavior of the packed bed (Asif *et al.*, 2019; Bahrami *et al.*, 2005; Kiani-Oshtorjani & Jalali, 2019).

Contact area refers to the contact region between two particles, which can increase in size due to the elasticity of the particle solid material when an external load is applied to the packed bed. The effective thermal contact area is dependent on the surface roughness, which is a characteristic of the two particles in contact (Van Antwerpen *et al.*, 2010). The real contact area between two spheres is only a small portion of the nominal contact area. The surface roughness of real surfaces causes the contact between surfaces to only occur over microscopic contacts. Thus, the macro-contact area or real contact area is only a summation of the total area of the micro-contacts (Bahrami *et al.*, 2004).

A relatively high temperature drop is observed across the contact interface due to the heat flow that is constricted through the micro-contacts. According to Bahrami *et al.* (2006) conduction is the main mode of heat transfer across the contact area as the contribution of radiation and natural convection in the gaps between the micro-contacts can be neglected. The conduction through the contact area can be divided into two parts: (1) solid-solid conduction through the micro-contacts and (2) conduction through the interstitial gas present in the micro-gaps between the contacting spheres.

In a randomly packed bed the porous structure changes significantly in any region near the wall as the bed geometry is disrupted in this area (Van Antwerpen *et al.*, 2010; 2012). This altered packing structure is known as the wall effect and influences the heat transfer in the wall region. When conduction heat transfer is one of the main contributing heat transfer phenomena in the packed bed, the conduction path between the particle-wall contact point becomes important for an accurate prediction of the overall effective thermal conductivity. Due to the wall effect, it is important to also obtain models which specifically predict the heat transfer for the particle-wall interface (Van Antwerpen *et al.*, 2012; Gan & Kamlah, 2010).

2. Background

The effective thermal conductivity has been investigated in numerous studies which used different analytical, numerical, and experimental methods. Some of these studies take the effect of contact areas into account, while others neglect the conduction through the contact points. Structured packed beds, in which the packing structure of uniform size spheres are repeated throughout the bed, are useful when studying the contact mechanics in packed beds since a typical unit cell can be identified which is representative of the entire bed (Bahrami *et al.*, 2006). Although randomly packed beds are mainly used in real applications, the trends observed in studies of structured beds can provide valuable insights into the characteristics of a random bed. The three packing structures most often considered are simple cubic (SC), body centered cubic (BCC), and face centered cubic (FCC).

Studies that employ numerical models account for contact resistances between particles by specifying the contact resistance values as boundary conditions, thus the contact resistance problem is solved separately. Another common modeling approach used is the Discrete Element Method (DEM). It is a numerical Lagrangian method used to predict the dynamic evolution of a large set of discrete particles over time, tracking the position, velocity, and angular velocity of each of the particles as well as the contact forces exerted between particles (Beaulieu *et al.*, 2021). The Thermal Discrete Element Method (TDEM) is an approach derived from the DEM, in which a local heat balance is established on every particle to also predict its temperature and determine the heat transfer across the packed bed.

If an analytical model is used the bed effective thermal conductivity is determined as a series/parallel combination of individual thermal resistances representative of the various heat transfer contributions. Distinct conduction paths are identified, and the contact resistance is modelled as one of these conduction paths (Bahrami *et al.*, 2006). Relative contributions of each of the conduction paths to the overall bed effective thermal conductivity and trends of each

conduction path as a function of the bed characteristics can be determined when using an analytical approach.

Van Antwerpen *et al*. (2010) presented a thorough review of literature that describes the packing structure as well as the different methodologies used to predict the effective thermal conductivity for random packed beds of mono-sized spherical particles. Important conclusions were made from the review regarding the consideration of the contact area when modeling the conduction component. The models that neglected the effect of contact area resulted in values of the effective thermal conductivity being lower than that of experimental results. However, the models that accounted for contact area provided results that are in good agreement with experimental data for the bulk region of the bed (Van Antwerpen *et al.*, 2010). This illustrates the importance of determining a suitable contact resistance associated with the contact region between pebbles to ensure a more accurate prediction of the bed effective thermal conductivity.

The authors of the current study used a similar categorization as that of Van Antwerpen *et al*. (2010) to provide a review of recently published work on effective thermal conductivity models and correlations for packed beds in a stagnant fluid environment (De Beer *et al.*, 2018a). From the review it was found that several correlations and approaches define the conduction component in the packed bed by only considering a point contact (Dixon *et al.*, 2013; Panchal *et al.*, 2016; Suarez *et al.*, 2017; Wu *et al.*, 2017). Thus, no contact area is included in these approaches and the contact between two spheres is essentially a point contact. This means that the solid-solid conduction through the contact region is neglected.

In the studies conducted by Chen *et al.* (2016), Liang and Li (2014), Liang *et al.* (2016) and Tsory *et al.* (2013) the conduction component of the effective thermal conductivity through the solid and fluid phases is predicted and the contact area is explicitly considered (De Beer *et al.*, 2018a). Studies that predicted the effective thermal conductivity due to conduction and radiation and also accounted for contact area in their models and correlations are Zhou *et al.* (2007), Zhou *et al.* (2010), Gan & Kamlah (2010), Van Antwerpen *et al.* (2012), Yamoah *et al.* (2012), Asakuma *et al*. (2014; 2016), Wang *et al.* (2016a; 2016b) and Ren *et al.* (2017) (De Beer *et al.*, 2018a)

In the following sections the approaches and correlations used in recent literature to define and predict the conduction heat transfer though the contact area in a packed bed will be discussed in more detail. The analytical and numerical approaches and models will be presented in sections 2.1 and 2.2 respectively.

2.1. Analytical approach

The models and approaches discussed in this section predict the conduction component of the effective thermal conductivity through the contact area between two contacting particles by using an analytical method.

Liang and Li (2014) developed a new parallel-column model for the conduction heat transfer through the contact network in a randomly packed pebble bed with varying particle sizes. For the parallel-column model it was assumed that the packed bed can be represented by several particle columns and the contact network throughout the bed consists of several parallel chains. The conduction path between contacting particles was approximated to be a particle column. The results obtained with the analytical expression for the conduction effective thermal conductivity were compared with numerical results and were found to be in good agreement. Thus, it was concluded that the parallel-column model adequately represents the heat transfer through the contact network in a pebble bed.

Further research was conducted by Liang *et al*. (2016) on the parallel-column model of Liang & Li (2014) by incorporating two different contact force models into the existing parallel-column model and considering particle sizes ranging from 4 mm to 8 mm. An expression for the effective thermal conductivity was derived for each of the different contact force models. The coefficient of thermal conductance of the column connecting the ith particle with the jth particle is shown in Eq. (1):

$$k_{ij} = \frac{\pi k_s}{-ln\,2 - ln\,\delta_{ij}^{n} + ln\left(r_{p,i} + r_{p,j}\right) + 3} \tag{1}$$

where k_s is the particle thermal conductivity and r_p is the radius of the each of the connecting particles. The normal relative contact displacement between the interacting particles *i* and *j* is defined as $\delta_{ij}^{n} = F_{ij}^{n} \big/ K_{ij}^{n}$ with F_{ij}^{n} the normal contact force and K_{ij}^{n} the normal contact stiffness coefficient. The first contact model considered was the Hooke model in which the normal contact stiffness coefficient was assumed to be constant for all the contact points. For the second contact force model it was assumed that $K_{ij}^{n} = 2E \, r_i r_j \big/ \left(r_i + r\right)_j$, where E is the Young's modulus of the material.

Gan & Kamlah (2010) focused on the heat transfer at the pebble bed-wall interface in their study by modeling a heat transfer coefficient that is representative of the thermal contact conductance of the interface. The model is based on a basic unit cell of the contact region which includes the wall, a pebble, and the gas in the macro-gap between the pebble and the

wall. Three different heat transfer mechanisms were accounted for in the calculations namely (1) conduction through the solid-solid contact point, (2) conduction through the gas gap between the pebble and the wall and (3) thermal radiation. A thermal resistance network approach was used to determine the heat transfer from the pebble bed through the contact area to the wall. The interfacial heat transfer coefficient can be considered as a resultant thermal resistance that is a combination of the three thermal resistances representing the various heat transfer mechanisms connected in parallel.

The conduction through the contact area only considers the solid-solid conduction while the conduction through the interstitial gas in the micro-gaps, due to surface roughness, is neglected. Gan & Kamlah (2010) used the heat transfer coefficient, h_c, proposed by Madhusudana (1995) to determine the conduction through the contact area, as shown in Eq. (2):

$$h_c = \frac{2ak_s}{\pi L^2} \tag{2}$$

where a is the radius of the contact area, determined by the Hertzian contact theory, $k_s = 2k_w k_p / (k_w + k_p)$ is the combined solid conductivity of the wall, k_w, and the pebble, k_p, and L is the radius of the unit cell which is dependent on the near-wall packing structure of the bed under consideration.

The predicted values for the interfacial heat transfer coefficient were compared with experimental data and the results were in reasonable agreement. A detailed explanation of the differences between the predicted values and the experimental data was provided by Gan & Kamlah (2010). The proposed model can be implemented into a finite element code that can then be used to perform a full thermo-mechanical analysis of a pebble bed.

The Multi Sphere Unit Cell (MSUC) model was developed by Van Antwerpen *et al.* (2012) to predict the effective thermal conductivity in both the bulk and near-wall regions of a packed bed of mono-sized spheres. A thermal resistance network approach was used to predict the conduction component. The conduction path between two contacting spheres were divided into three regions namely an inner, middle, and outer region. Each of these regions accounted for specific heat transfer mechanisms represented by an arrangement of parallel and series thermal resistances. Combining the various thermal resistances resulted in a joint thermal resistance that could be used to predict the effective thermal conductivity due to conduction.

The joint thermal resistance can account for either a rough or a smooth surface thermal resistance depending on the surface roughness of the sphere material. Conduction through the

contact area forms a part of the inner conduction region and consists of three thermal resistances that include (1) the macro-contact constriction/spreading resistance, R_L, (2) the micro-contact constriction/spreading resistance, R_s, and (3) the resistance of the interstitial gas in the micro-gap, R_g. The model developed by Bahrami *et al.* (2006) was used to calculate these thermal resistances. A comprehensive summary of the definitions of these thermal resistances will be provided later in this paper when discussing the study performed by Bahrami *et al.* (2006).

Van Antwerpen *et al.* (2012) followed a similar approach as the one for the bulk region to determine the conduction through the particle-wall contact points of the packed bed. However, due to the presence of the wall the magnitude of the resistances differed. In their study it was assumed that the circumference of the wall is so large compared to the circumference of the sphere that the wall geometry could be approximated as a flat surface. The results obtained with the MSUC model were compared with the experimental data of various studies and were found to be in good agreement.

Bahrami *et al*. (2006) developed a compact analytical model to determine the effective thermal conductivity of packed beds consisting of uniform spherical particles in a stagnant gas environment. The effect of surface roughness, gas pressures ranging from atmospheric to vacuum as well as different mechanical loads were taken into consideration. Packed beds with SC and FCC packing structures were studied. Fig. 1 shows a schematic representation of the contact region used by Bahrami *et al*. (2006). Each contact region consists of a contact area between two portions of spheres surrounded by a gas layer.

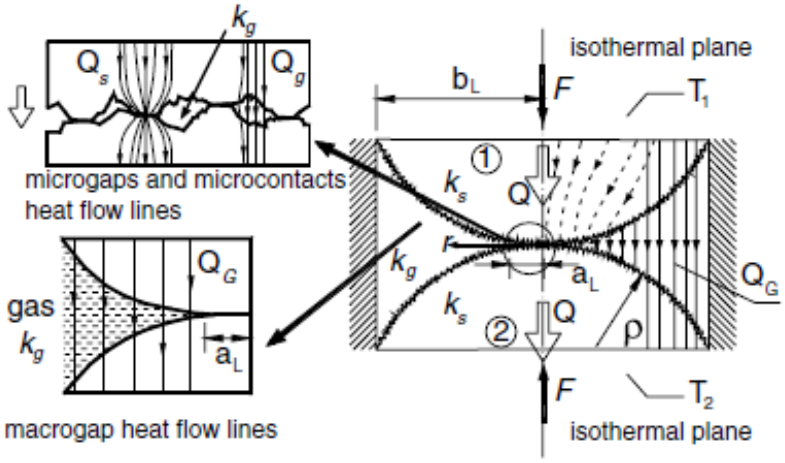

Fig. 1 Contact region between rough spheres (Bahrami *et al.*, 2006).

The heat flow through the interface between two spheres in the contact region is subjected to a relatively large thermal resistance due to the small real contact area and low thermal

conductivity of the gas present in the contact region. As a result of the high joint thermal resistance a relatively high temperature drop is observed across the interface. The interface thermal resistance proposed by Bahrami *et al.* (2006) consists of four components that include (1) the macro-contact constriction/spreading resistance, R_L, (2) the micro-contact constriction/spreading resistance, R_s, (3) resistance of the interstitial gas in the micro-gap, R_g, and (4) the resistance of the interstitial gas in the macro-gap, R_G. The overall joint resistance, R_j, expressed as a parallel combination of the different resistance components is shown in Eq. (3).

$$R_j = \left[\frac{1}{\left(1/R_s + 1/R_g\right)^{-1} + R_L} + \frac{1}{R_G} \right]^{-1} \tag{3}$$

The thermal resistance network for the contact region is shown in Fig. 2. Simple correlations were derived that were used for the calculation of the various thermal resistance components. The resistances for the solid material of the two spheres (R_1 and R_2) are negligible compared to R_G, as the gas thermal conductivity is much smaller than the solid thermal conductivity (Bahrami *et al.*, 2006). Only the resistances R_s and R_g contribute towards the thermal resistance of the contact area pathway due to the physical contact of the two spheres.

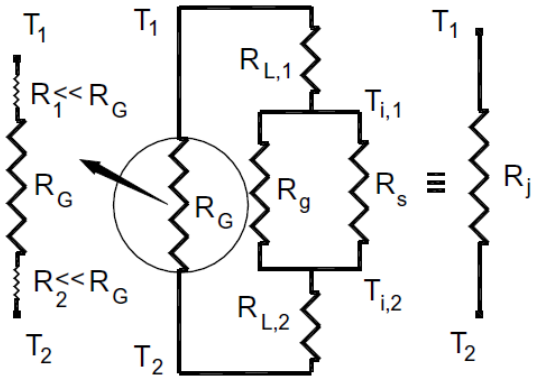

Fig. 2 Thermal resistance network for the contact region (Bahrami *et al.*, 2006).

Bahrami *et al.* (2006) assumed that the surfaces of the spheres are randomly rough and stated that the contact between two Gaussian rough surfaces can be modelled by the contact between a single Gaussian surface (that has the combined roughness characteristics of both surfaces) with a perfectly smooth surface. The combined surface roughness, σ_{RMS}, and surface slope, m_{RMS}, for the two surfaces in contact can be calculated with $\sigma_{RMS} = \sqrt{\sigma_1^2 + \sigma_2^2}$ and $m_{RMS} = \sqrt{m_1^2 + m_2^2}$ respectively. The compact model for the micro-contact constriction/spreading

resistance, R_s, was developed by assuming plastically deformed asperities and is presented in Eq. (4):

$$R_s = \frac{0.565 H^* \left(\sigma_{RMS}/m_{RMS}\right)}{k_s F^n} \tag{4}$$

where F^n is the force between the spheres, k_s is the solid conductivity given by $k_s = 2k_{s1}k_{s2}/\left(k_{s1}+k_{s2}\right)$ and H^* is the equivalent Vickers micro-hardness given by $H^* = c_1\left(\sigma'/m_{RMS}\right)^{c_2}$ with $\sigma' = \sigma_{RMS}/\sigma_0$ and $\sigma_0 = 1$ µm. The correlation coefficients c_1 and c_2 were determined from Vickers microhardness measurements which resulted in the expressions:

$$\begin{aligned} c_1 &= H_{BGM}\left(4.0 - 5.77\kappa + 4.0\kappa^2 - 0.61\kappa^3\right) \\ c_2 &= -0.57 + 0.82\kappa - 0.41\kappa^2 + 0.06\kappa^3 \end{aligned} \tag{5}$$

with $\kappa = H_B/H_{BGM}$, where H_B is the Brinell hardness of the bulk material in GPa and H_{BGM} = 3.178 GPa. The correlations given in Eq. (5) are only valid for the range 1.3 ≤ H_B ≤ 7.6 GPa. If the effective value of the microhardness H_{mic} is known the coefficients will be $c_1 = H_{mic}$ and $c_2 = 0$.

Eq. (6) is used to determine the macro-contact constriction/spreading resistance, R_L, by assuming the macro-contact region is isothermal (Bahrami *et al.*, 2006).

$$R_L = \frac{1}{2k_s a_L} \tag{6}$$

A general contact pressure distribution model was proposed which is applicable to the entire range of spherical rough contacts. The radius of the macro-contact area, a_L, can be determined from a relationship developed based on the maximum contact pressure, P_0, presented in Eq. (7) and Eq. (8):

$$P_0' = \frac{P_0}{P_{0,H}} = \frac{1}{1 + 1.22\alpha\kappa^{-0.16}} \tag{7}$$

$$\frac{a_L}{a_H} = \begin{cases} 1.605/\sqrt{P_0'}, & 0.01 \le P_0' \le 0.47 \\ 3.51 - 2.51P_0' & 0.47 \le P_0' \le 1 \end{cases} \tag{8}$$

where $P_{0,H} = 1.5F^n/\pi a_H^2$ and $a_H = \left(0.75F\rho/E'\right)^{1/3}$ is the Hertzian contact area radius. The equivalent radius of curvature for uniform spheres can be calculated as $\rho = r_p/2$, with r_p the radius of a sphere. Bahrami *et al.* (2006) showed that better agreement with experimental data

were obtained when using $\rho = r_p$. The effective elastic Young's modulus can be found from $1/E' = \left(1-\upsilon_1^2\right)/E_1 + \left(1-\upsilon_2^2\right)/E_2$, where υ is Poisson's ratio for each of the spheres.

The resistance of the interstitial gas in the micro-gap can be calculated by using Eq. (9):

$$R_g = \frac{2\sqrt{2}\sigma_{RMS}a_2}{\pi k_g a_L^2 \, ln\left(1+\dfrac{a_2}{a_1 + M/\left(2\sqrt{2}\sigma_{RMS}\right)}\right)} \tag{9}$$

where $a_1 = erfc^{-1}\left(2P_0/H'\right)$, $a_2 = erfc^{-1}\left(0.03P_0/H'\right) - a_1$ and $H' = c_1\left(1.62\sigma'/m_{RMS}\right)^{c_2}$. The inverse complementary error function, $erfc^{-1}(x)$, can be found from Eq. (10).

$$erfc^{-1}(x) = \begin{cases} \dfrac{1}{0.218 + 0.735x^{0.173}}, & 10^{-9} \le x \le 0.02 \\ \dfrac{1.05(0.175)^x}{x^{0.12}}, & 0.02 < x \le 0.5 \\ \dfrac{1-x}{0.707 + 0.862x - 0.431x^2}, & 0.5 < x \le 1.9 \end{cases} \tag{10}$$

In the studies conducted by Yamoah *et al.* (2012) and Ren *et al.* (2017) they predicted the effective thermal conductivity using similar mathematical models. The existing model of Kaviany (1991), as shown in Eq. (11), was used to predict the conduction through the solid material including the contact area between pebbles:

$$\frac{k_e^c}{k_s} = r_c \cdot \frac{1}{0.531S}\left(\frac{N_A}{N_L}\right) \tag{11}$$

where k_e^c is the effective thermal conductivity component which accounts for solid-contact area-solid conduction, N_A and N_L are the number of spheres per unit area and unit length of the bed, respectively and S is the constant related to the packing structure of the bed. The calculation of the contact area is based on the Hertzian deformation theory, with the contact radius $r_c = \left[\left(3\left(1-\upsilon^2\right)/4E\right)F^n r_p\right]^{1/3}$. Ren *et al.* (2017) concluded from the results obtained that the conduction heat transfer through the contact area contributes significantly to the overall effective thermal conductivity for the lower temperature range.

Asakuma *et al*. (2016) developed a homogenization method to perform a thermal analysis of a packed bed. This method can be used to evaluate exact changes in the microstructure and temperature with the use of a three-dimensional finite element method. In their study,

conduction through the real contact areas as well as the conduction through the interstitial gas in the micro-gaps were considered in their calculation of the thermal contact resistance. Parameters that are accounted for in the calculation of the contact resistance include surface roughness, contact pressure and microhardness of the material. A parallel resistance network was used to calculate the overall contact resistance due to the resistances of each of the conduction paths.

The homogenization method was applied to calculate the effective thermal conductivity for a BCC packed bed including the effect of convection heat transfer. Asakuma *et al*. (2016) noted that the effect of the contact resistance becomes more significant when the contributions of convection and radiation to the overall heat transfer becomes less. The effect of porosity was ignored in this study.

Wang *et al*. (2016a) used the thermal resistance approach of Van Antwerpen *et al*. (2012) to develop an effective thermal conductivity model to predict conduction, radiation, and convection heat transfer in a pebble bed. The minimum unit cell of the packed bed was also divided into an inner, a middle, and an outer region accounting for different conduction heat transfer mechanisms in each of these regions (Van Antwerpen *et al.*, 2012). Two thermal resistance components in parallel were defined for the conduction path through the inner region of two contacting spheres namely the resistance of the conduction through the solid material, R_c , and the contact resistance in the contact region, R_{cont} .

Using Fourier's law and the thermal-electrical analogy the definition of R_c is shown in Eq. (12), where L_r is the conduction thickness. The empirical correlation derived by Chen & Tien (1973) was used to calculate R_{cont} , given in Eq. (13), as it was assumed that the spheres have smooth surfaces, thus the effect of surface roughness was neglected.

$$R_c = \frac{L_r}{A_c k_s} \tag{12}$$

$$R_{cont} = \frac{0.64}{k_s r_0} \tag{13}$$

A method to couple the contact area with bed strain, ε , was presented by Wang *et al*. (2016a) by expressing the radius of the contact area as a function of the bed strain, $r_0 = r_{p,0}\sqrt{2\zeta \cdot \varepsilon}$. The initial sphere radius before radial deformation is $r_{p,0}$ and the correction factor, ζ , can be predicted in detail using a DEM method. Wang *et al*. (2016a) also provided a method to obtain a preliminary estimation of the correction factor.

The results obtained with the model were compared with existing theoretical models, CFD numerical simulations and experimental data, and were found to be in good agreement. It was concluded that the effect of contact areas becomes significant for pebble beds with a high solid to fluid effective thermal conductivity ratio.

2.2. Numerical approach

The models and approaches discussed in this section predict the conduction component of the effective thermal conductivity through the contact area between two contacting particles by using a numerical method.

A one-way coupled CFD-DEM method was used by Chen *et al.* (2016) in which the particle contact points were derived from the DEM model and included in the mesh generation for the CFD model. The original particle diameter was kept for most of the spheres in the packed bed to ensure the contact states derived from the DEM model were conserved. However, some very small gaps or overlaps between particles at the contact points caused difficulty with the mesh generation for approximately 1.5 % of the particles. To overcome this problem the particles causing problems were resized within ± 0.5 % and the mesh could then be rebuilt successfully. Chen *et al.* (2016) assumed that the effect on the overall heat transfer as a result of the changes to the bed's original geometry, due to the resized particles, could be neglected as the changes were only made locally.

Tsory *et al.* (2013) developed a coupled DEM-CFD model to study the conduction through packed beds. Forces exerted on particles due to contact interaction with other particles, the walls, and the fluid (Brosh & Levy, 2010) were accounted for in the DEM model used and various compression loads were considered. Surface roughness as well as the interstitial gas at the contact points were accounted for in the calculation of the conduction through the contact area. Tsory *et al.* (2013) derived Eq. (14) and Eq. (15) to calculate the heat transfer, $\dot{Q}_c$, through a particle-particle contact point and, $\dot{Q}_w$, through a particle-wall contact point respectively:

$$\dot{Q}_c = \frac{A_r}{A_c}\dot{Q}_r + \frac{A_v}{A_c}\dot{Q}_v \tag{14}$$

$$\dot{Q}_{wi} = \frac{4d_{sij}\left(T_i - T_w\right)}{1/k_{s,i} + 1/k_{s,w}} \tag{15}$$

where $\dot{Q}_r$ is the heat transfer through the solid-solid contact points, $\dot{Q}_v$ is the heat transfer through the fluid gaps present in the contact area, $A_c = A_r + A_v$ is the total contact area, A_r is

the area of the point contacts and A_v is the area of the fluid gaps. For the calculation of the particle-wall heat transfer, it was assumed that the wall is a single particle with infinite radius and the wall temperature, T_w, is constant. The overlap surface diameter was calculated using $d_{s,ij} = 2\sqrt{r_{p,i}^2 - s^2}$ with s the distance between the centers of the two adjacent particles. The temperature of the ith particle is represented by T_i and the solid thermal conductivities of the particle and the wall by $k_{s,i}$ and $k_{s,w}$.

Numerical simulations were conducted by Tsory *et al.* (2013) for a packed bed with a particle diameter of 1 mm. The average slope of the surface roughness was used as an adjustable parameter that was varied until a good agreement was achieved between the numerical and experimental results. A parametric study on the influence of average slope of the surface roughness on the effective thermal conductivity were included in the study (Tsory *et al.*, 2013). As the particle surface roughness increases, the thermal resistance increases and as a result the temperature difference also increases. It was found that if the thermal resistance was neglected by setting the surface roughness to zero and in effect neglecting the conduction through the fluid gaps present in the contact area, the effective thermal conductivity almost doubled, and the bed temperature difference was almost halved. It was concluded that the average surface roughness slopes have a significant influence on the heat transfer results and therefore it is not advisable to use a DEM-only model when studying packed beds with high surface roughnesses.

Zhou *et al.* (2007) developed a boundary element method (BEM) to predict the effective thermal conductivity due to conduction-radiation heat transfer in a two-dimensional packed bed. In their study the packed bed is bounded by plates on all sides and an external compression load is applied to the bounding plates, thus the particles undergo deformation at the contact points. The wall effects were neglected in the study by increasing the number of particles in the packed bed. The contact areas were not calculated based on contact mechanics theory and surface roughness was not taken into account, instead Zhou *et al.* (2007) calculated the conduction through the contact areas by defining the void fraction of the structured packed beds as a function of the ratio of contact radius to the particle radius. Various particle deformation ratios were considered, and the BEM model produced good results for square and hexagonal packing structures when compared with existing theoretical models. The heat flux constriction effect due to the contact area between particles could be observed in the temperature distribution results for the local regions in the packed beds.

A coupled DEM and CFD approach was used by Zhou *et al.* (2010) to study the heat transfer in a packed bed on a particle scale level. Zhou *et al.* (2010) stated that due to the sensitivity of the heat transfer through the particle-particle contact points, it is necessary to use an extremely small time step with the real Young's modulus in the DEM-CFD simulation to obtain accurate results, however at a high computational cost. They proposed the use of a correction coefficient, c, in the calculation of the particle-particle contact radius between colliding particles, r_c, to overcome this problem. With the use of the correction coefficient one can account for the overestimation of the particle-particle contact radius due to the use of a lower Young's modulus. The equation for conduction through the contact area derived by Batchelor & O'Brien (1977), which was slightly modified by Cheng *et al*. (1999), was used to determine the conduction through the contact area, as shown in Eq. (16):

$$Q_{ij} = \frac{4r_c^{'}\left(T_j - T_i\right)}{\left(1/k_{si} + 1/k_{sj}\right)} \tag{16}$$

where Q_{ij} is the conduction heat transfer between the contacting particles *i* and *j*, with *T* the surface temperature and k_s the solid thermal conductivity of each of the particles *i* and *j*. The value of the reduced particle-particle contact radius, $r_c^{'} = c \cdot r_c$, is determined by the correction coefficient which varies between 0 and 1. Based on the Hertzian contact theory the correction coefficient is determined as a function of the real value of the Young's modulus of the materials used and the magnitude of the Young's modulus specified in the DEM-CFD simulation.

Zhou *et al.* (2010) used a similar approach to Tsory *et al.* (2013) for the particle-wall contact points, where the wall is seen as a particle with an infinite diameter and mass with similar material properties as those of the other particles. Various simulations were performed for different solid thermal conductivities and a range of Young's modulus values to determine the validity of the calculated correction coefficients. The results obtained with the DEM-CFD approach were compared with the experimental results obtained by Cheng *et al*. (1999) and were found to be in good agreement.

A new TDEM model based on a resistance network in which the surface roughness is considered was proposed by Beaulieu *et al.* (2021). They decoupled the thermal problem from the dynamic one in their study and only the thermal problem was solved. The TDEM model was used to study the conduction heat transfer in a static packed bed of mono-sized spherical particles in a stagnant gas environment.

The contact model of Bahrami *et al*. (2006) was used to predict the conduction through the contact areas in the packed bed. For the macro-contact constriction/spreading resistance and

the resistance of the interstitial gas in the micro-gaps and macro-gap, the exact expressions proposed by Bahrami *et al*. (2006) were used. However, for the micro-contact constriction/spreading resistance, the expression of Van Lew (2016) was used, whose work is also based on the Bahrami *et al.* model. The resistance expression of Van Lew (2016) was preferred as it considers the contact force between particles given in DEM, whereas in the Bahrami *et al.* model a total load is considered on the packed bed. Similar definitions were used for the various resistances at the particle-wall contact points, only the resistance of the interstitial gas in the macro-gap was taken as half of that of a particle-particle contact point.

Beaulieu *et al.* (2021) performed experiments on a packed bed of spherical particles for four different materials. The transient temperature results at three different heights in the packed bed were obtained. The TDEM numerical results were compared with the experimental results and were found to be in reasonable agreement. The effect of particle size and surface roughness on the overall effective thermal conductivity were examined numerically. From the results it was concluded that the heat transfer though a packed bed is indeed hindered due to the real contacts that occur as a result of the surface roughness. The effect of surface roughness was more significant for particles with a higher solid thermal conductivity, as a large fraction of the heat transfer through the packed bed occurs through the solid micro-contacts instead of the stagnant interstitial gas.

In a recent study by Cheng *et al.* (2020) they extended their previous approach to determine the effective thermal conductivity based on the Voronoi-Delaunay tessellation (Cheng *et al.*, 1999) by adding the conduction heat transfer through the voids of a randomly packed bed. The effect of packing structure on the bed effective thermal conductivity was investigated by using DEM simulations combined with the heat transfer models from their previous work. For the conduction path through the contact area, they used their previous model as shown in Eq. (16) (Cheng *et al.*, 1999). From their results they showed that the conduction and radiation through the solid paths in the packed bed decreases with an increase in porosity, whereas the conduction through the fluid voids increases. Thus, the results show that the packing structure plays a significant role when considering heat transfer through packed beds.

A TDEM model was used by Kiani-Oshtorjani & Jalali (2019) to study the conduction heat transfer in a packed bed of spherical particles under various compressive forces with a particle radius of 2 mm. The local heat fluxes and temperatures of particles were determined based on the material thermal conductivity and the deformation of particles at the contact points. In their model the effects of all the contact areas of neighboring particles on the temperature of a central particle were taken into account by using a pipe model. In the pipe model, the

conduction path through the contact area is represented by a pipe stretching between the centers of two contacting spheres and through the contact area. The conduction thermal resistance as a result of the heat flux from particle *i* to particle *j*, $R_{cond,ij}$, is calculated using Eq. (17):

$$R_{cond,ij} = \frac{0.6846}{2k_{s,i}r_{p,i}\Delta\phi_i} \tag{17}$$

with $\Delta\phi_i$ is the deformation angle of particle *i*.

The contact forces and deformation were determined in the DEM simulation based on the Hertzian contact theory. The results of the TDEM model were compared with an analytical solution and were found to be in good agreement. From the results obtained, Kiani-Oshtorjani & Jalali (2019) concluded that an increase in compression pressure on the packed bed resulted in a decrease in the heat conduction rate and thus a decrease in the effective thermal conductivity. However, they stated that a more detailed study is required to determine whether the decrease of the effective thermal conductivity with pressure is related to changes in the contact areas under various compression forces.

In a recent study the authors developed a methodology which combines experimental measurements with CFD simulations to separate the contributions of conduction and radiation heat transfer to the overall effective thermal conductivity in a packed bed of graphite spheres, including the wall effects. From the results a better understanding of the interplay between the heat transfer phenomena was obtained and the effect on the characteristic trend of the effective thermal conductivity was observed (De Beer *et al.*, 2017). At the time of the study contact resistances were not included at the pebble-pebble and pebble-wall solid-solid interfaces of the CFD model. From the results obtained it was found that the heat transfer rate through the bed as well as the heat loss through the insulation walls were higher for the CFD model than the experimental results, thus the overall conduction resistance of the bed in the CFD simulations was underestimated.

It was concluded that the underestimation could be due to the absence of the solid-solid contact resistances at the contact interfaces throughout the bed and that the CFD model can be calibrated to obtain numerical results in good agreement with the experimental results by adjusting the contact resistance values in the packed bed. The aim of this paper is to investigate the effect of contact resistance on the overall effective thermal conductivity and the trends of the conduction and radiation components, and to show that the contact resistance can be used as an adjustable parameter in the CFD model to obtain good agreement between the experimental and numerical results. This will be done by applying an initial contact resistance correlation from

literature to the contact points in the existing CFD model and separating the conduction and radiation components of the numerical results. A preliminary attempt to calibrate the contact resistances will then be presented to determine if the CFD model can be calibrated by adjusting the initial contact resistances to obtain a good agreement between the experimental and CFD results (De Beer *et al.*, 2017; 2018b).

3. Methodology

An outline of the previous proposed methodology is shown in Fig. 3. A summary of the methodology will be provided in section 3.1. For a more detailed description of the methodology the reader can consult our previous study (De Beer *et al.*, 2017). The method used to add a contact resistance correlation to the CFD model will be discussed in section 3.2. The method used for the separation of the conduction and radiation components will be described in section 3.3.

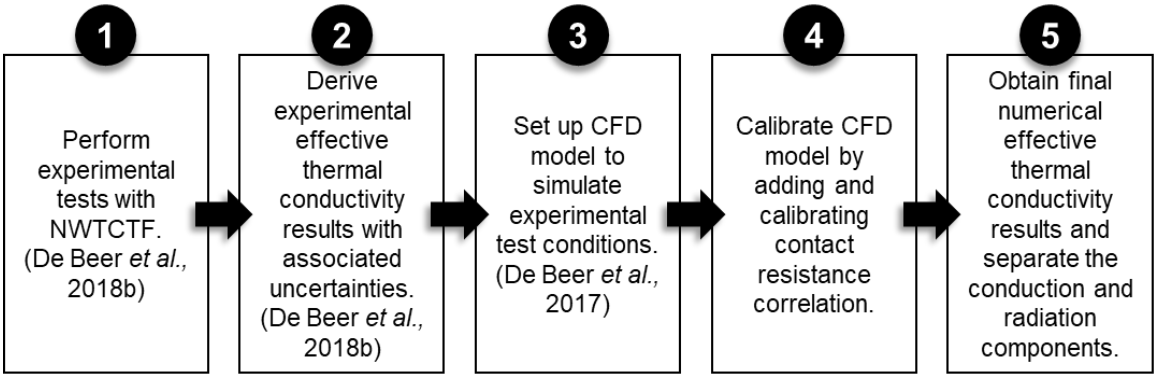

Fig. 3 Outline of method to investigate conduction and radiation contribution to the effective thermal conductivity.

3.1. Overview of methodology

The first step of the methodology entails performing experimental tests with the Near-wall Thermal Conductivity Test Facility (NWTCTF) (De Beer *et al.*, 2018b). The purpose of the NWTCTF is to perform detailed investigations of the conduction and radiation heat transfer in a packed bed of uniform graphite spheres in the near-wall region. The NWTCTF test section has a cubical configuration with side lengths of 420 mm in which spheres with a diameter of 60 mm are placed to form the packed bed. The packed bed has an inner radiator graphite wall (heated wall) and an outer reflector graphite wall (cooled wall) on opposite sides. A temperature gradient is induced through the packed bed between the heated and cooled walls. To minimize losses to the surroundings the packed bed is enclosed in layers of insulation material.

Experimental tests were performed with a near-vacuum nitrogen environment maintained in the NWTCTF test section to ensure that the effects of convection could be neglected. For the experimental tests conducted the heated wall was maintained at a set temperature. Experimental tests were performed for packed beds with SC, BCC, and random packing configurations. Temperature and heat transfer measurements with associated uncertainties were gathered from the experimental tests. In a previous study conducted by the authors a detailed description of the NWTCTF experimental setup and the final experimental data were provided (De Beer *et al.*, 2018b).

The data reduction methodology proposed by Rousseau *et al.* (2014) is used and applied to the NWTCTF experimental data in step two of the methodology to extract the effective thermal conductivity results with associated uncertainties. The experimental effective thermal conductivity results for the three packing structures investigated are reported in the study by De Beer *et al.* (2018b).

The third step of the methodology is to set up a suitable CFD model to simulate the conduction and radiation heat transfer through the pebble bed at the experimental test conditions and thereby numerically determine the effective thermal conductivity. In our previous study, where we proposed the methodology, we used a randomly packed bed whilst in the current study a SC packed bed is used. The reason being that one of the goals of the current study is to add contact resistances at the contact points in the CFD model, which is easier to do for a structured packed bed. In a structured bed the exact positions of the contact points are known, whereas the geometry of a randomly packed bed is more complex. Once the correct contact resistance function for the SC packed bed is obtained it can also be applied to a random packing structure in future studies.

Solidworks was used to create a solid body for each of the spheres forming the SC packed bed geometry that was then used for the CFD heat transfer model. The solid models for the pebble bed, the graphite walls and the insulation material surrounding the packed bed is shown in Fig. 4. Cylindrical fillets were inserted at the pebble-pebble and pebble-wall contact points in the solid model as a contact point treatment to obtain a suitable computational mesh in the contact region. In our previous study (De Beer *et al.*, 2017) the fillets created in the packed bed connected all the pebbles to form one solid mass and a single solid region in the CFD geometry. In the current study, Solidworks was used to cut all the fillet regions in the packed bed along the middle cross section of each fillet, to obtain a contact interface for which a contact resistance could be assigned in the CFD model when calculating the heat transfer. The radius of the contact interface of the fillet region is 2.57 mm. Thus, in the current study each sphere

was defined as a separate solid region in the CFD model, and the spheres were connected by contact interfaces to form the pebble bed.

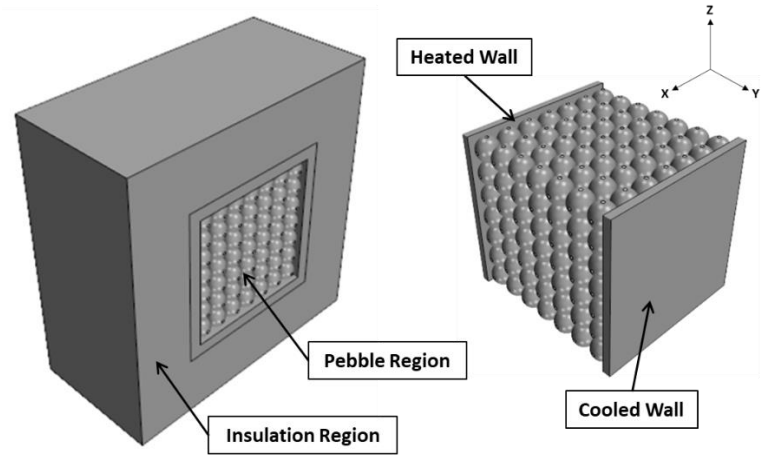

Fig. 4 Solid models of the SC pebble bed, graphite walls and insulation layers used in the CFD model.

The fourth step of the methodology is to calculate the numerical effective thermal conductivity results with STAR-CCM+ and compare the results with the NWTCTF experimental results to calibrate the CFD model. The calibration of the CFD model is done by adding contact resistances to the pebble-pebble and pebble-wall solid-solid interfaces and adjusting the contact resistance correlations to obtain numerical results which are in good agreement with the experimental results. In our previous study the calibration of the CFD model was not completed, as the purpose of the study was to establish the methodology and demonstrate qualitatively the interplay between the heat transfer phenomena (De Beer *et al.*, 2017). The disadvantage of not taking the effect of contact resistances into account and not calibrating the CFD model is that the influence of contact resistances on the trends observed for the conduction and radiation components of the effective thermal conductivity is unknown. Therefore, we will present a first iteration of the calibration of the CFD model in the current study by adding the Bahrami *et al.* (2006) contact resistance correlation to the CFD model to determine the effect of contact resistance on the various heat transfer phenomena and effective thermal conductivity trends. A preliminary calibration method for the contact resistances will be presented in section 5.1.

After the calibration of the CFD model is completed, the CFD results should be in good agreement with the experimental results and the CFD model then becomes representative of the experimental setup. The CFD results can then be used to investigate and explain the characteristic trends observed in the experimental effective thermal conductivity. Thus, the final step of the methodology is to separate the conduction and radiation components of the effective thermal conductivity and determine the interaction between the phenomena.

3.2. Contact resistance in the CFD model

In our previous work we found that the experimental and numerical temperature and heat transfer distribution results were not in good agreement when the contact resistances were neglected, although similar qualitative trends could be identified in the results. We will first consider the results for the 800 °C case (the heated wall temperature was controlled at 800 °C for the experimental tests and the CFD simulations) for the randomly packed bed. Fig. 5 (a) shows the temperature distribution calculated with the CFD model (with no contact resistances) compared to the values measured in the NWTCTF (De Beer *et al.*, 2017). Although the temperature boundary values are the same it is clear from the results that the agreement between the measured and simulated values is not satisfactory with an average percentage difference of 15 %.

The heat transfer rate through the cooled wall for the CFD model was found to be 2020.4 W while the corresponding value measured in the experiment is 1657.6 W. This means that the overall conduction resistance of the random packed bed in the simulation is underestimated by approximately 22 %. For the CFD model the total heat loss through the insulation region surrounding the test section was found to be 347.1 W and the value obtained for the experimental results is 366.7 W, thus the CFD result is within 5.4 % of the experimental measurement. Although the heat loss results are in better agreement with the experimental measurements, the conduction resistance of the bed is again underestimated.

The experimental and numerical effective thermal conductivity results for the 800 °C case of the random packed bed is shown in Fig. 5 (b) (De Beer *et al.*, 2017). We found that at high temperatures the CFD effective thermal conductivity is lower than the experimental effective thermal conductivity, whereas at lower temperatures the CFD values are higher than the experimental values. Thus, the resistance in the numerical packed bed is too high at higher temperatures (not enough conduction) and the resistance is too low at lower temperatures (too much conduction). The authors concluded that the incorrect estimation of the bed conduction resistance in the CFD simulations was due to the absence of solid-solid contact resistances at the pebble-pebble and pebble-wall interfaces in the packed bed.

In the current study we focus on the 800 °C case of the SC packed bed in a first attempt to add and calibrate contact resistances to the CFD model. As a starting point for the inclusion of contact resistances in the CFD model we first obtained the SC CFD results without contact resistances and compared the results to the experimental results to determine whether the bed conduction resistance is also incorrectly estimated for the structured packed bed, as seen in

Fig. 5 (b) for the random packed bed. A comparison of the experimental and CFD temperature distribution and effective thermal conductivity results for the SC packed bed is shown in Fig. 6 (a) and Fig. 6 (b), respectively. The temperature boundary values of the heated and cooled walls were set to 809.88 °C and 149.97 °C, similar to the experimental test conditions. As seen with the temperature distribution results for the random packed bed, the agreement between the measured and simulated temperatures for the SC packed bed is also not satisfactory with an average percentage difference of 17 %.

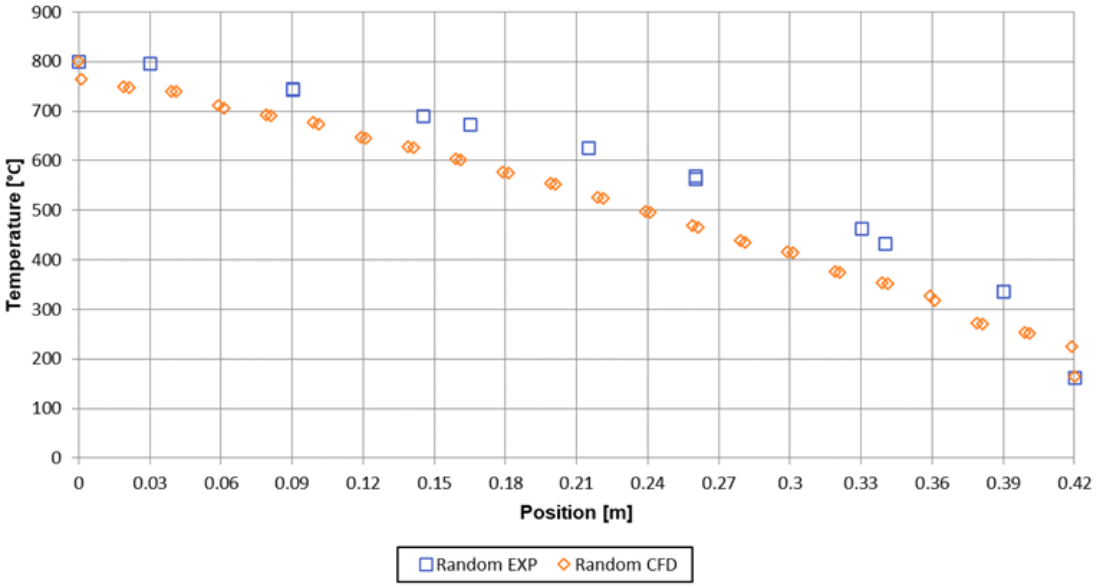

(a)

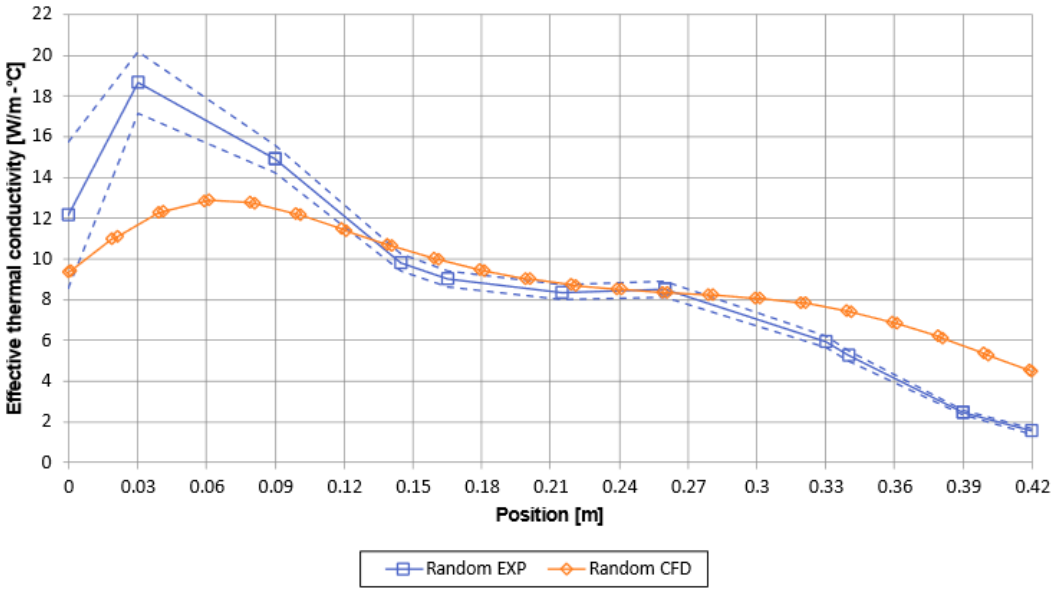

(b)

Fig. 5 Comparison between the experimental (□) and CFD (without contact resistances) (◊) (a) temperature distribution and (b) effective thermal conductivity results for the 800 °C test case of the random packed bed (De Beer *et al.*, 2017; 2018b).

The heat transfer rate through the cooled wall for the SC CFD model was found to be 3557.2 W while the corresponding value measured in the experiment is 1677.5 W. This means that the overall conduction resistance of the random packed bed in the simulation is underestimated by approximately 112 %. The total heat loss through the insulation region surrounding the test section was found to be 338.7 W for the CFD model and 350.7 W for the experimental results, thus the CFD result is within 3.4 % of the experimental measurement.

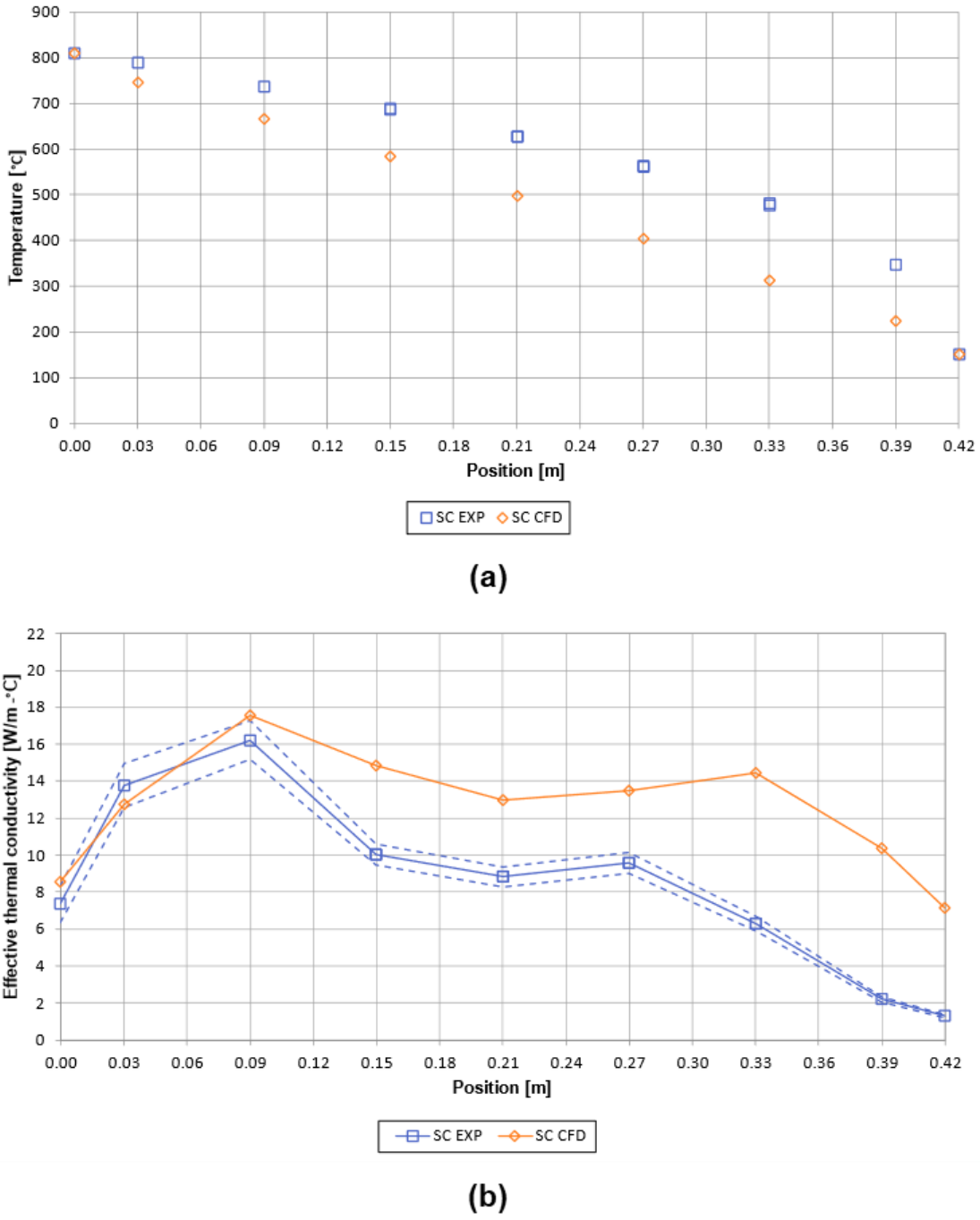

Fig. 6 Comparison between the experimental (□) and CFD (without contact resistances) (◊) (a) temperature distribution and (b) effective thermal conductivity results for the 800 °C test case of the SC packed bed.

For the effective thermal conductivity results, shown in Fig. 6 (b), the CFD values are slightly higher or lower than the experimental values up until the position of 0.06 m, which coincides with the first layer of spheres next to the heated wall. Thereafter the CFD values are higher than the experimental values throughout the rest of the packed bed, with the difference between the values increasing as the temperature decreases. Thus, the resistance in the CFD model is too low with the conduction heat transfer being overestimated, especially at lower temperatures.

The spheres form a solid network of “pure” graphite as the contact points have the same thermal conductivity as the graphite when no contact resistances are considered. Fig. 7 shows the thermal conductivity of the graphite pebble material as a function of temperature. The graphite thermal conductivity increases significantly with a decrease in temperature.

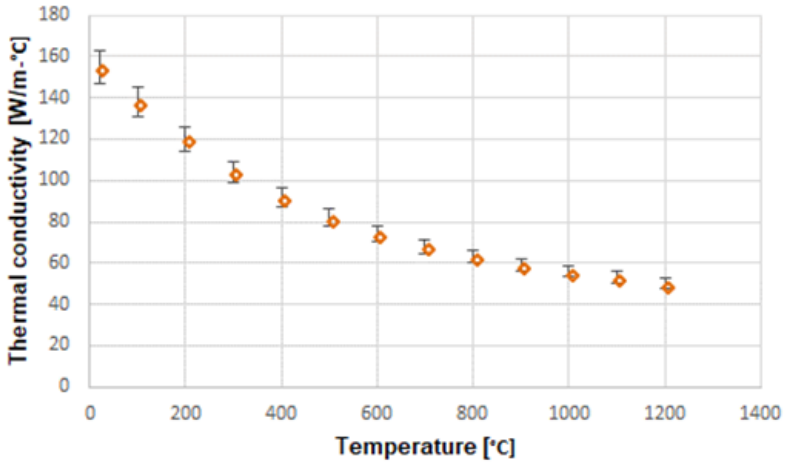

Fig. 7 Thermal conductivity of the virgin graphite pebble material as a function of temperature with associated uncertainties (De Beer *et al.*, 2018b).

The difference between the numerical and experimental results is more notable for the SC packed bed than the random packed bed. The random packed bed consisted of 313 spheres whereas the SC packed bed consisted of 343 spheres. The differences observed between the results for the SC and random packed beds are due to the different packing structures as well as how the packed bed is “viewed” by the wall when considering the contribution of radiation heat transfer. The effect of packing structure on the effective thermal conductivity includes the influence of the porosity variation, coordination number and contact angles (Van Antwerpen *et al.*, 2010; De Beer *et al.*, 2018b). For the SC packed bed, the gaps formed between the pebbles will be much larger and penetrate deeper into the bed than for the random packed bed. As a result, when looking into the pebble bed from the vantage point of the heated wall along the y-coordinate direction, the heated wall will “view” more of the spheres through to the cooled wall for the SC packed bed, as shown in Fig. 8 (a), whereas for the random packed the heated wall will only “view” some of the spheres, as shown in Fig. 8 (b). This will result in different

magnitudes of radiation heat transfer between the wall and the pebbles for the different packed beds as radiation is both a short-range and a long-range effect.

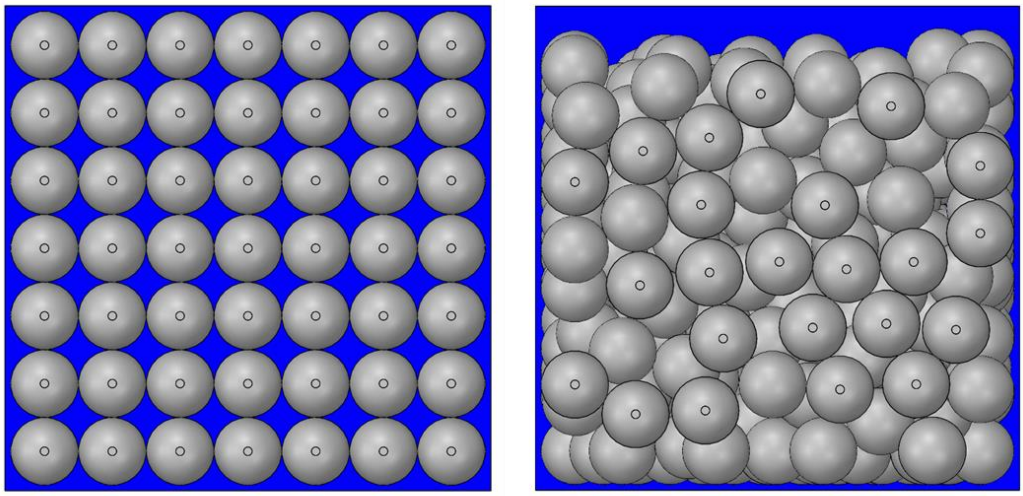

Fig. 8 View of the packed bed of spheres from the vantage point of the heated wall for (a) the SC bed and (b) the random bed.

The model proposed by Bahrami *et al.* (2006) will be used to obtain a first approximation of the contact resistances as a function of temperature. In the CFD model a contact resistance function will be assigned to the contact interfaces at the pebble-pebble and pebble-wall contact points. The Bahrami *et al.* (2006) model was also used in the studies performed by Van Antwerpen *et al.* (2012) and Beaulieu *et al.* (2021).

Fig. 9 (a) shows two spheres in contact and the four thermal resistances used by Bahrami *et al.* (2006) to predict the conduction heat transfer through the contact region (Beaulieu *et al.*, 2021). The corresponding thermal resistance network with each of the conduction pathways are shown in Fig. 9 (b). The conduction resistance of the sphere solid material, R_L, is already accounted for in our existing CFD model as the graphite material thermal conductivity is defined as a function of temperature in the CFD model according to Fig. 7. The NWTCTF experimental tests were conducted in a near-vacuum environment to eliminate the effects of natural convection, therefore the effect of the gas in the macro-gaps between pebbles was not included in the CFD model. Thus, in the current study only the two thermal resistances for the contact area will be considered in the calculation of the overall contact resistance, which include the conduction resistance of the solid-solid micro-contacts, R_s, and the conduction resistance of the interstitial nitrogen gas in the micro-gaps, R_g.

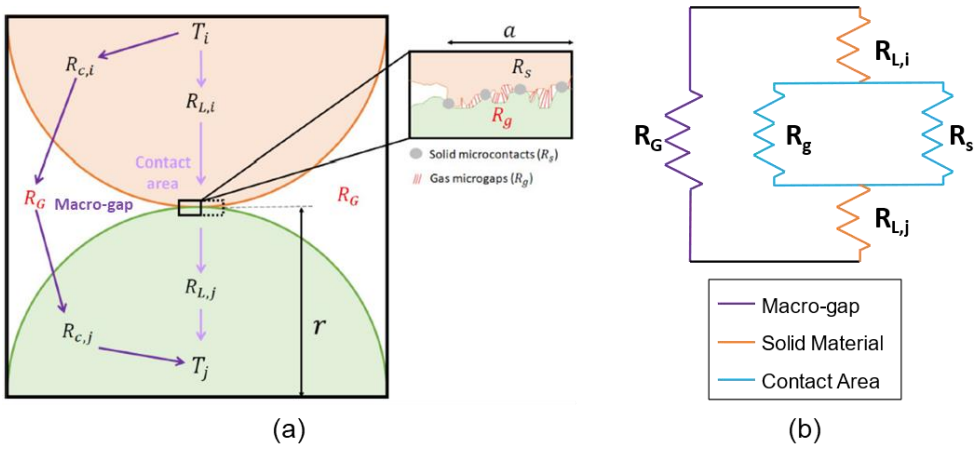

Fig. 9 (a) Thermal resistances for conduction heat transfer in the contact region proposed by Bahrami *et al.* (2006) (Beaulieu *et al.*, 2021) and (b) the corresponding thermal resistance network indicating the different conduction pathways.

The Bahrami *et al.* (2006) model and the combination of the two thermal resistances in parallel, as shown in Eq. (18), was used to determine the contact resistance as a function of temperature for the pebble-pebble and pebble-wall contact points.

$$\frac{1}{R_{cont}} = \frac{1}{R_s} + \frac{1}{R_g} \tag{18}$$

The graphite spheres used in the NWTCTF were inherited from the HTTU test facility (Rousseau & Van Staden, 2008) and were originally supplied by SGL Carbon Group in 2005 with designated grade MLRF1. Van Antwerpen *et al.* (2009; 2012) used the HTTU experimental results to verify and validate the MSUC model, hence the graphite material properties reported by them were used for the calculation of the contact resistance functions. The insulation region is made up of layers of Zircar type SALI-2 followed by layers of AL-45 with a total thickness of approximately 230 mm. The insulation material properties were reported in a previous study by De Beer (2014) and were used in the contact resistance calculations.

The contact resistances as a function of temperature for the pebble-pebble and pebble-wall contact points are shown in Fig. 10. At the contact points of the pebbles with the graphite walls the pebble-pebble contact resistance was used. The pebble-wall contact resistance that can be seen in Fig. 10 is for the contact points between the pebbles and the insulation walls. In STAR-CCM+ the contact resistance is defined as $RA_{cont} = R_{cont} \cdot A_c$, where the fillet radius was used to determine the contact area. It is important to note that the contact area, due to the fillet contact point treatment, in the solid model of the CFD geometry is likely bigger than the real contact area between the pebbles in the NWTCTF packed bed. Although this will result in an overestimation of the contact area, this is an acceptable first estimation as no detailed experiments about the contact region between spheres were available. In the fourth step of the methodology the contact resistance function will also be calibrated further to obtain good

agreement between the numerical and experimental results. Therefore, the overestimation of the contact area can be accounted for in the calibration of the contact resistance function.

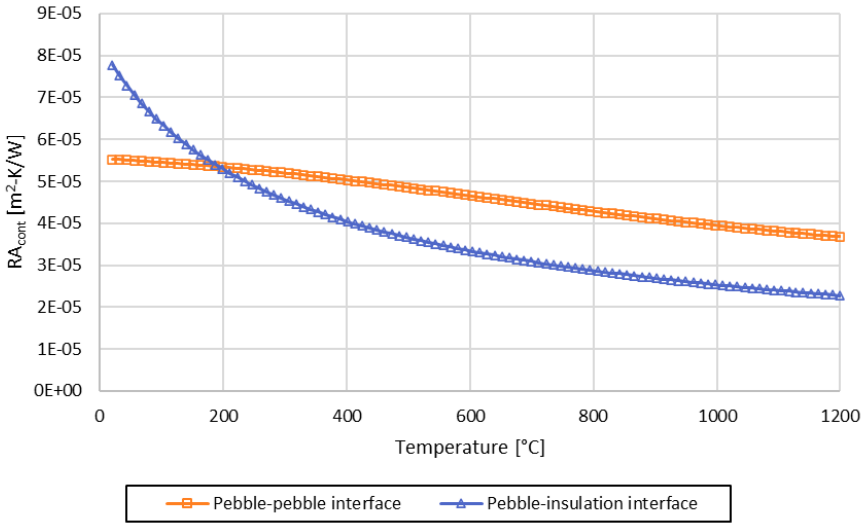

Fig. 10 Contact resistance as a function of temperature for the pebble-pebble contact points (□) and the contact points between the pebbles and the insulation walls (Δ) determined by using the Bahrami *et al*. (2006) model.

3.3. Method for separation of radiation and conduction components

To separate the conduction and radiation components of the effective thermal conductivity, two CFD simulations were completed namely one for combined conduction and radiation and one for conduction only. For the conduction only CFD simulation the radiation heat transfer model is de-activated in the simulation and only the effect of conduction heat transfer is simulated.

Once the effective thermal conductivity is calculated for both the conduction-radiation, k_{eff} , and conduction-only, k_{cond} , cases, Eq. (19) can be used to determine the contribution of the radiation component, k_{rad} (De Beer *et al.*, 2017).

$$k_{eff} = k_{cond} + k_{rad} \tag{19}$$

In our previous study (De Beer *et al.*, 2017) we explained that the required data cannot simply be extracted from the two simulation cases with the same boundary values, but that the results of the two cases should be compared at similar positions in the packed bed (similar packing structures) as well as similar temperatures. To achieve this, conduction-only effective thermal conductivity values must first be determined for various temperature cases at each of the positions in the packed bed. Multiple polynomial functions are then obtained for the conduction component as a function of temperature, with each function applicable to a specific position in the pebble bed.

However, in the current study, due to the ordered or regular packing structure of the SC packed bed, it was not necessary to run multiple conduction-only simulations for various temperature cases to obtain the effective thermal conductivity as a function of temperature and position. It is important to note that even though the packing structure is the same and similar boundary values are used, the two cases will still not necessarily result in similar temperatures at corresponding positions in the bed. Linear interpolation was used to obtain the effective thermal conductivity values for the conduction-only case at the same temperatures as that of the conduction-radiation case. The combined and separated effective thermal conductivity results for the CFD model with the Bahrami *et al.* (2006) contact resistance are presented in section 4.

4. Results and discussion

In this section the results obtained with the CFD model that includes the Bahrami *et al.* (2006) contact resistance will be presented and compared to the results obtained without the contact resistance from our previous study (De Beer *et al.*, 2017).

4.1. Overall effective thermal conductivity results

The temperature distributions and effective thermal conductivity results obtained via the CFD models are shown in Fig. 11 (a) and Fig. 11 (b) respectively without and with the contact resistance included.

For the case with the contact resistance included, the average percentage difference between the numerical and experimental temperature values is 12 %. The heat transfer extracted through the cooled wall in the CFD simulation is 2629.2 W, which means the overall conduction resistance of the bed is still underestimated by 57 %. The total heat losses in the CFD model through the insulation region is 365 W, within 4.1 % of the experimental result.

The addition of the contact resistance improved the agreement of the overall “peaks-and-dip” trend of the numerical results with that of the experimental results. The numerical results also show a marked reduction in the magnitude of the conductivity in the near-wall region followed by a “peak” indicating the maximum value at a position of 0.09 m. The maximum “peak” is followed by a slight dip that can be observed at a position between 0.15 m and 0.27 m. A smaller “peak” is also observed next to the cooled wall at a position of 0.27 m. By adding the contact resistance, the maximum “peak” value determined with the CFD model matches that of the experimental results and the value of the smaller “peak” is also in close agreement with the experimental value. Although the overall characteristic trend of the effective thermal conductivity curve improves with the addition of contact resistances, the values are still underestimated by

the CFD model up to the position of 0.09 m after which the values are overestimated throughout the rest of the packed bed.

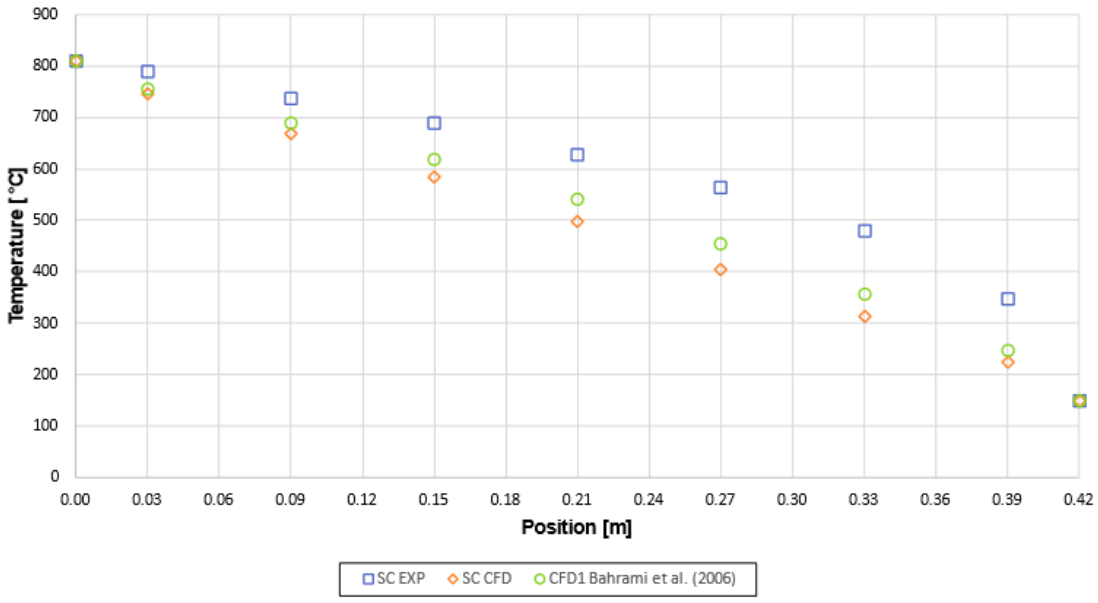

(a)

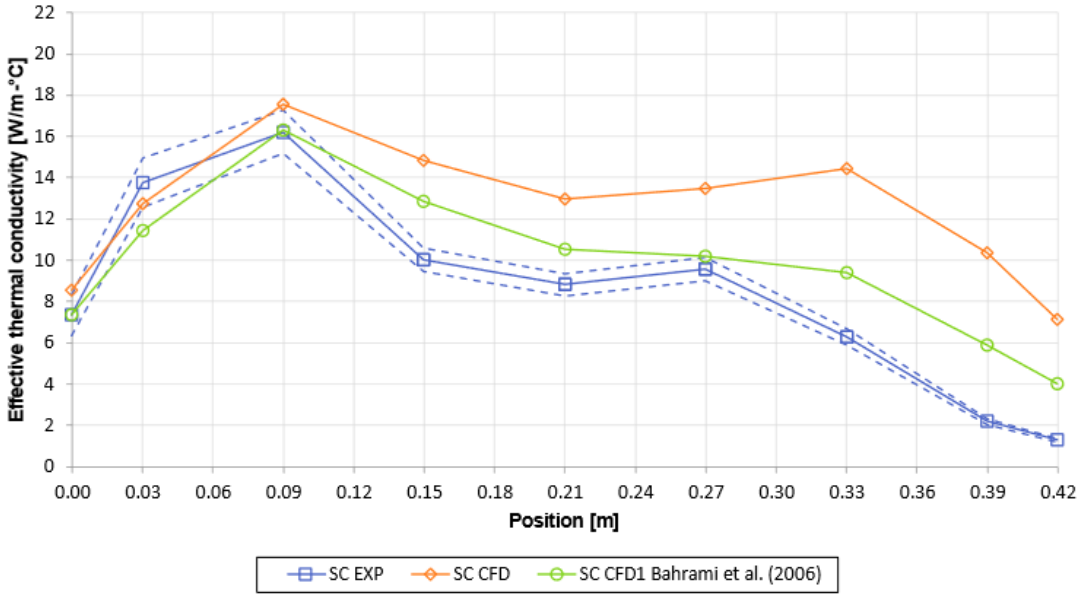

(b)

Fig. 11 Comparison between the experimental (□), CFD with no contact resistance (◊) and CFD with the Bahrami *et al*. (2006) contact resistance (○) (a) temperature distribution and (b) effective thermal conductivity results for the 800 °C test case of the SC packed bed.

The results show that the addition of the contact resistance to the CFD model improved the agreement between the experimental and numerical results. The agreement between the experimental and numerical results is still not satisfactory, but the results demonstrate that the

effect of contact resistance is important and cannot be neglected in a study of the effective thermal conductivity.

4.2. Effective thermal conductivity conduction and radiation component results

In this section the effective thermal conductivity components obtained via the CFD model without contact resistances will be compared with the results with the Bahrami *et al.* (2006) contact resistance included.

Fig. 12 and Fig. 13 show the distributions as a function of position derived from the CFD model with no contact resistances, together with its conduction-only and radiation-only components for the random and SC packed beds, respectively. The distributions as a function of position derived from the CFD model that includes contact resistances, together with its conduction-only and radiation-only components for the SC packed bed are shown in Fig. 14.

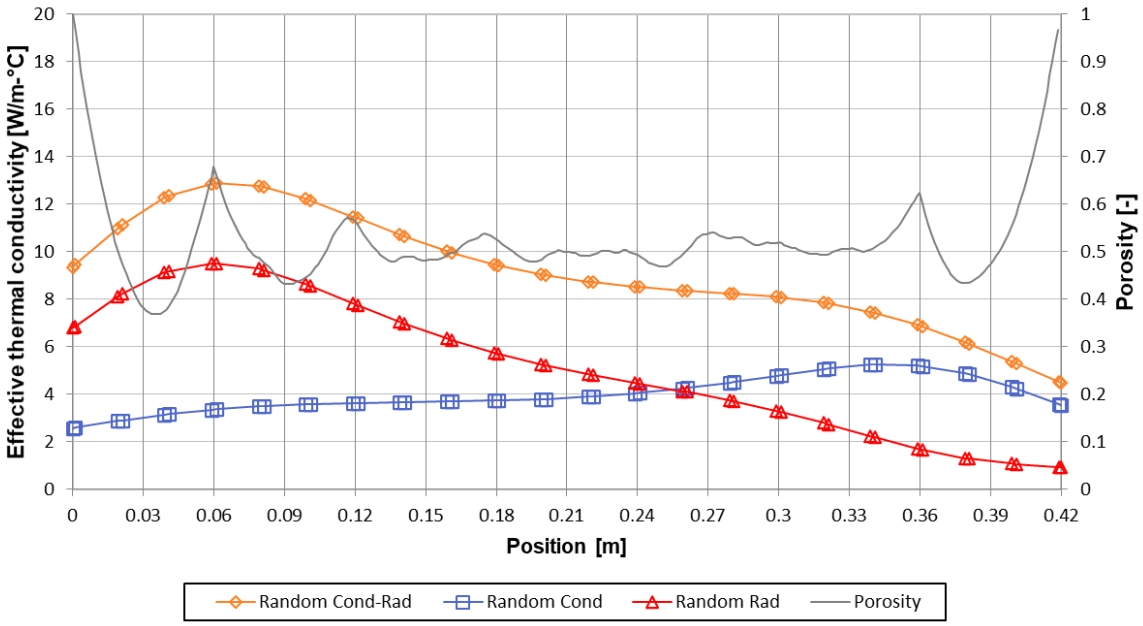

Fig. 12 Effective thermal conductivity distributions derived from the CFD model without contact resistances for combined conduction and radiation (◊), conduction-only (□) and radiation-only (Δ) for the 800 °C case of the random packed bed (De Beer *et al.*, 2017).

The CFD model with contact resistances included produce results with similar overall trends to those where the effect of contact resistances is neglected. The trend of the radiation component is similar with the radiation contribution decreasing with a decrease in temperature. However, it clearly shows that the inclusion of the contact resistances leads to a reduction in the conduction component, with a subsequent increase in the radiation component.

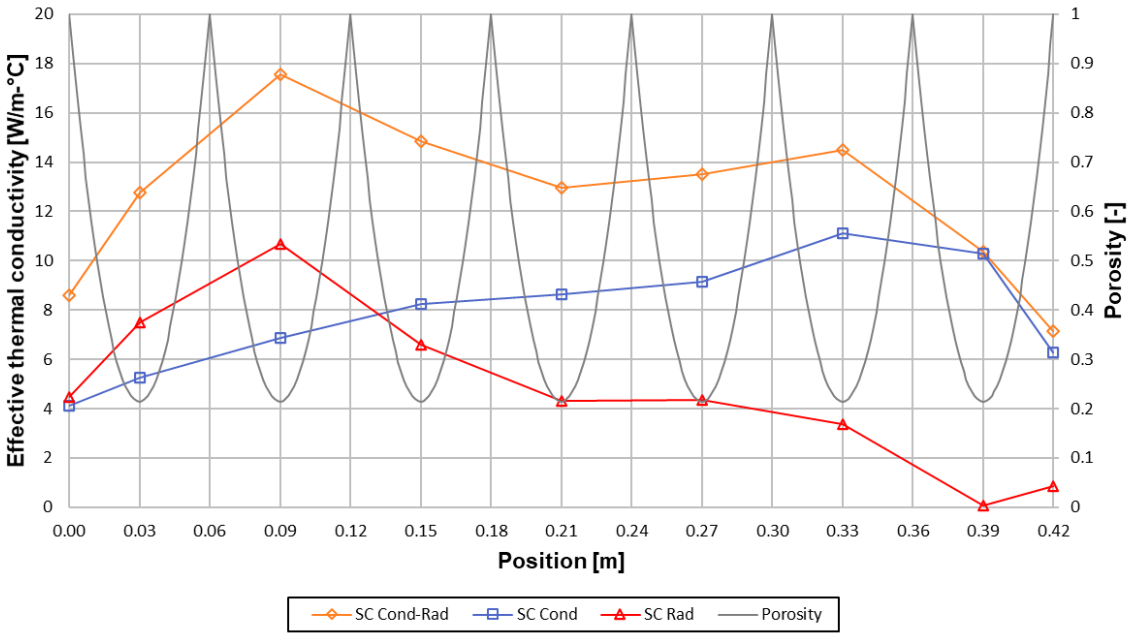

Fig. 13 Effective thermal conductivity distributions derived from the CFD model without contact resistances for combined conduction and radiation (◊), conduction-only (□) and radiation-only (Δ) for the 800 °C case of the SC packed bed.

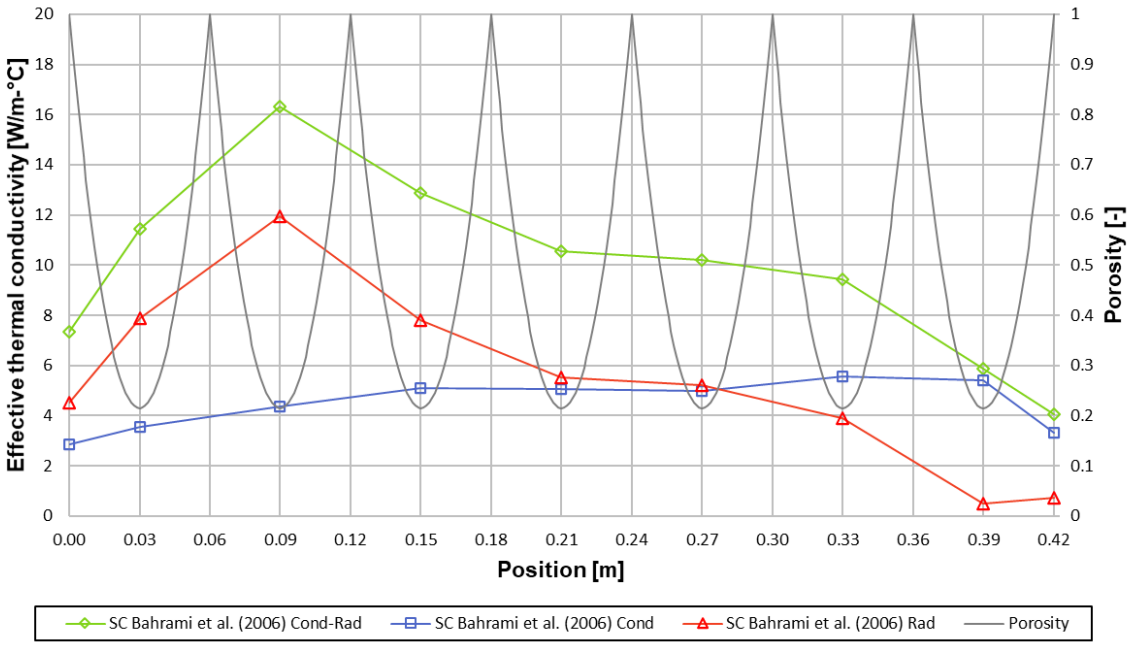

Fig. 14 Effective thermal conductivity distributions derived from the CFD model with contact resistances included for combined conduction and radiation (◊), conduction-only (□) and radiation-only (Δ) for the 800 °C case of the SC packed bed.

At higher temperatures, the wall effect has a more prominent influence on the radiation component, whereas at lower temperatures the wall effect results in the sharp reduction of the conduction component. The results show that with the inclusion of the Bahrami *et al*. (2006) contact resistances, the “peaks-and-dip” trend observed in the overall effective thermal conductivity due to combined conduction and radiation can still be explained as the result of the

interplay between the unique gradients of the radiation-only and conduction-only curves, as concluded in our previous study (De Beer *et al.*, 2017).

5. Calibration of the CFD model

Although the addition of the Bahrami *et al*. (2006) contact resistance to the CFD model improved the agreement between the experimental and numerical results it is still not satisfactory. An important part of the fourth step of the presented methodology is the calibration of the CFD model. In our previous study (De Beer *et al.*, 2017) it was suggested that the CFD model can be calibrated by adjusting the contact resistances. When the CFD model has been calibrated the final numerical results can be calculated and the final conduction and radiation effective thermal conductivity components can be separated to obtain archival data of the conduction and radiation contribution trends throughout the packed bed.

5.1. Calibration method

The results presented in section 4 showed that contact resistance is important and should be taken into consideration to accurately predict the conduction heat transfer in a packed bed. For the purpose of the current study, where we aim to demonstrate that the contact resistance specified in the CFD model of our proposed methodology can be adjusted to calibrate the CFD model, it was decided to perform a preliminary calibration of the CFD model. Through the calibration process we aim to match the overall heat flux and temperature distribution through the SC bed as well as the heat losses through the insulation layers with that of the NWTCTF experimental results. As a first attempt it was assumed that the contact resistance is only a function of temperature. A detailed outline of the preliminary method used for the calibration of the CFD model is shown in Fig. 15. The CFD model with the Bahrami *et al.* (2006) contact resistance is considered as the first CFD iteration in the calibration process.

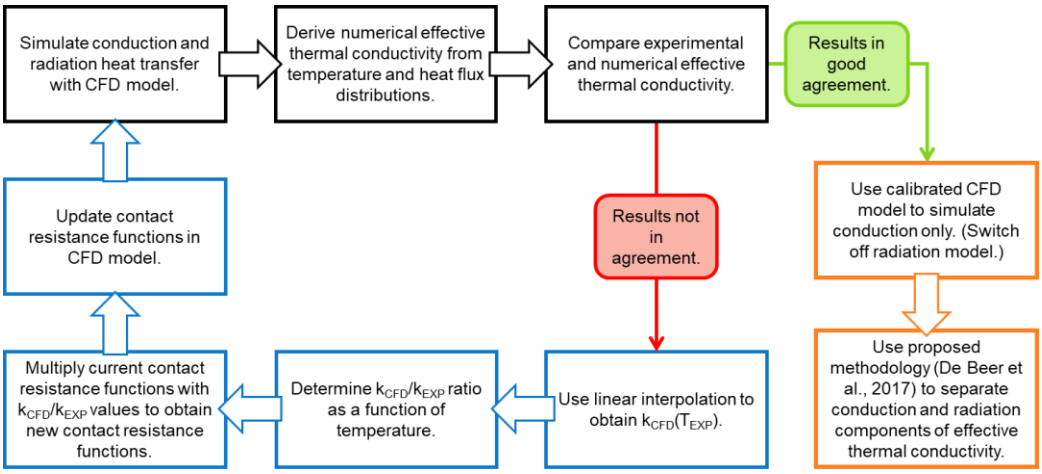

Fig. 15 Outline of method for calibration of the CFD model.

A global iterative process was used for the calibration of the contact resistances. The contact resistance functions were adjusted for each subsequent CFD iteration with the use of a calibration parameter. The ratio of the effective thermal conductivity of the current CFD iteration to the experimental effective thermal conductivity, $k_{CFD,i}/k_{EXP}$, as a function of temperature was used as the calibration parameter to obtain the new contact resistance functions for the following CFD iteration. Linear interpolation was used to obtain the numerical effective thermal conductivity values at the same temperatures as that of the experimental effective thermal conductivity results before the $k_{CFD,i}/k_{EXP}$ ratio was calculated. As the value of the $k_{CFD,i}/k_{EXP}$ ratio approaches one the difference between the numerical and experimental effective thermal conductivity results decreases. A linear function was fitted through the $k_{CFD,i}/k_{EXP}$ ratio for different temperature ranges. Fig. 16 shows the calibration parameter, $k_{CFD,i}/k_{EXP}$, as a function of temperature for the various CFD iterations. The calibration process was repeated for 11 CFD iterations to obtain numerical results in good agreement with the experimental results.

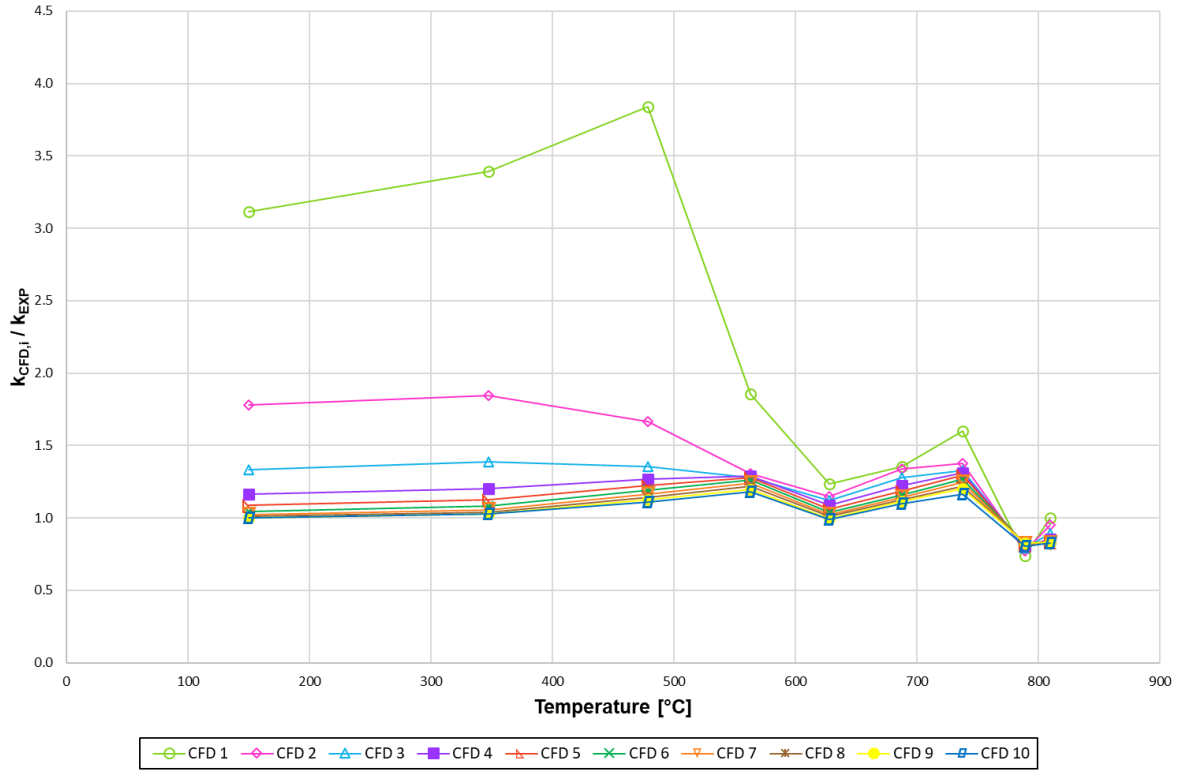

Fig. 16 Effective thermal conductivity ratios as a function of temperature used as the calibration parameter for the various CFD iterations.

The contact resistance values of the latest CFD iteration were multiplied with the calibration parameter to obtain the new adjusted contact resistance functions for the next CFD iteration, $RA_{cont,i+1}(T) = k_{CFD,i}/k_{EXP}(T) \cdot RA_{cont,i}(T)$. A field function and IF-statements were used to

define the new contact resistance function in STAR-CCM+. After the adjusted contact resistance functions were specified, the CFD simulation was solved again to obtain a new set of numerical results that were compared with the experimental results. For the first six CFD iterations only the pebble-pebble contact resistance function was calibrated and for the last five CFD iterations the contact resistance function for the pebble-wall contact points with the insulation region was also calibrated.

The contact resistances as a function of temperature for each of the CFD iterations for the pebble-pebble contact points and the pebble-wall contact points are shown in Fig. 17 and Fig. 18, respectively. The sharp “peaks” observed in the contact resistance functions are a direct result of the global iterative process used to adjust the contact resistance values. The authors recognize that there is no apparent explanation for the trend of the final curve, however the aim of the preliminary calibration of the CFD model is not to obtain the final contact resistance functions for the packed bed or to develop a new contact resistance model, but rather to illustrate that the contact resistance functions can be used as the adjustable parameter to obtain a CFD model in good agreement with the NWTCTF experimental setup. A more detailed study should be performed to investigate the effect of various parameters such as pressure distribution and contact force, gas and solid material thermal conductivity, surface roughness, contact area size and thermal expansion on the contact resistance functions.

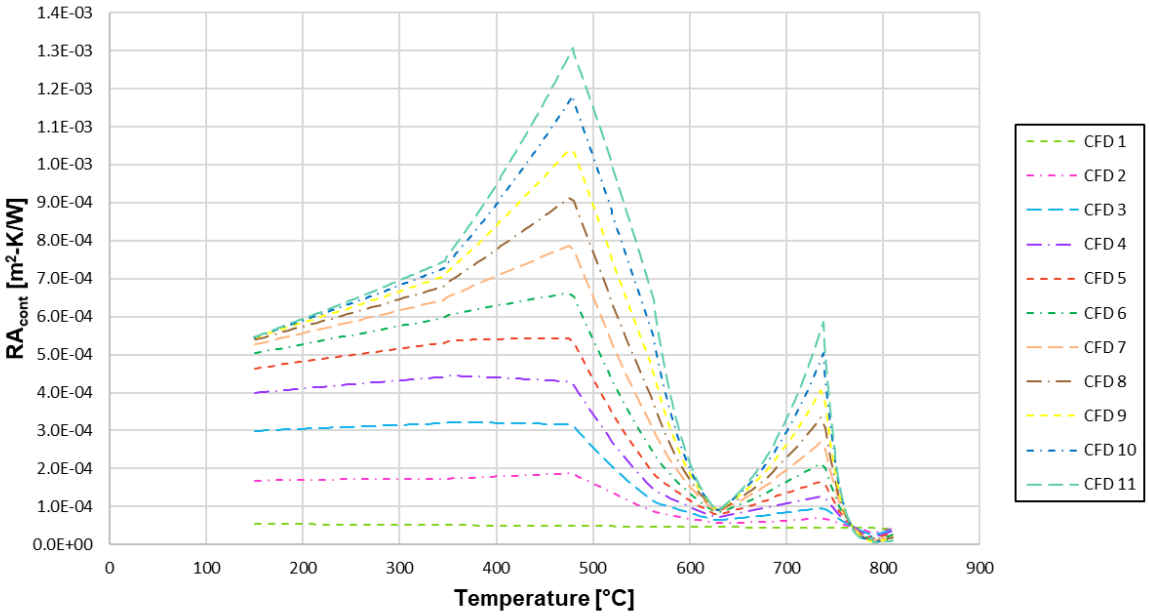

Fig. 17 Contact resistance as a function of temperature for the pebble-pebble contact points for the various CFD iterations.

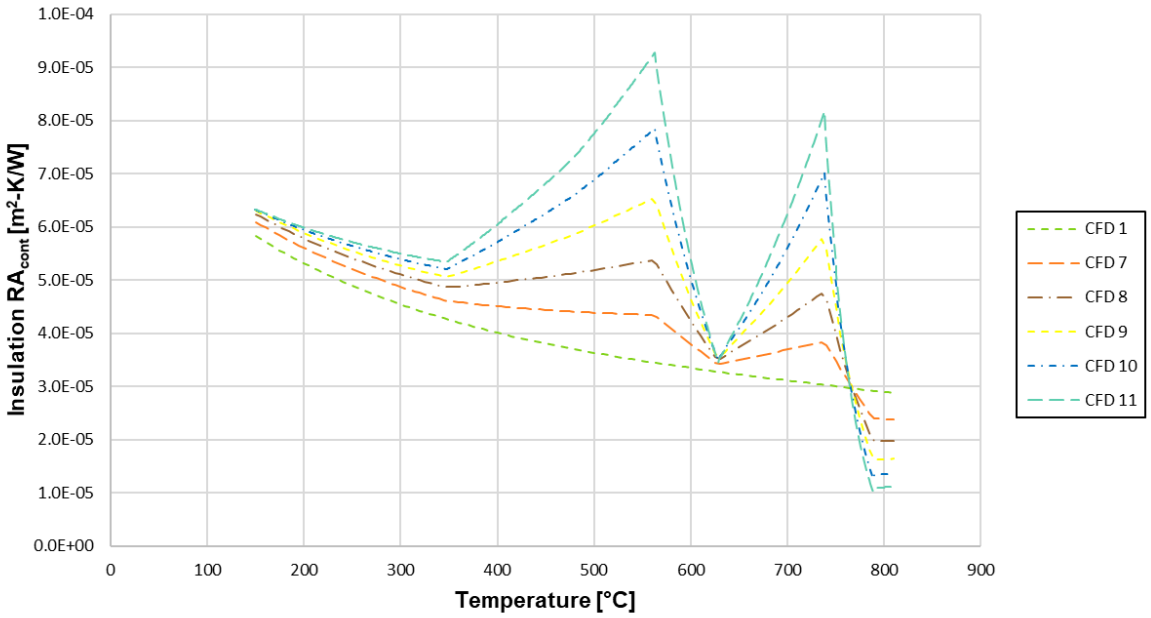

Fig. 18 Contact resistance as a function of temperature for the pebble-insulation wall contact points for the various CFD iterations.

5.2. CFD calibration results

The temperature distribution results obtained for the different CFD calibration iterations compared with the experimental results are shown in Fig. 19. From the results it is clear that the agreement between the measured and simulated values improves with the calibration of the contact resistance functions. The temperature values of the final calibrated CFD model (iteration 11) are in good agreement with the experimental values with an average percentage difference of 1.39 %.

Fig. 20 shows the heat transfer distribution results obtained for the different CFD calibration iterations compared with the experimental results. The agreement of the overall heat transfer through the bed for the CFD model with the experimental result improves with the addition and calibration of the contact resistances to the packed bed. The heat transfer extracted through the cooled wall in the final calibrated CFD simulation is 1665.5 W, within 0.7 % of the experimental value. The total heat loss through the insulation region is 422.2 W for the calibrated CFD model which is not satisfactory when compared to the experimental value with an average percentage difference of 20 %. This shows that the contact resistance for the contact points of the pebbles with the insulation walls are underestimated allowing too much heat loss through the insulation layers surrounding the packed bed.

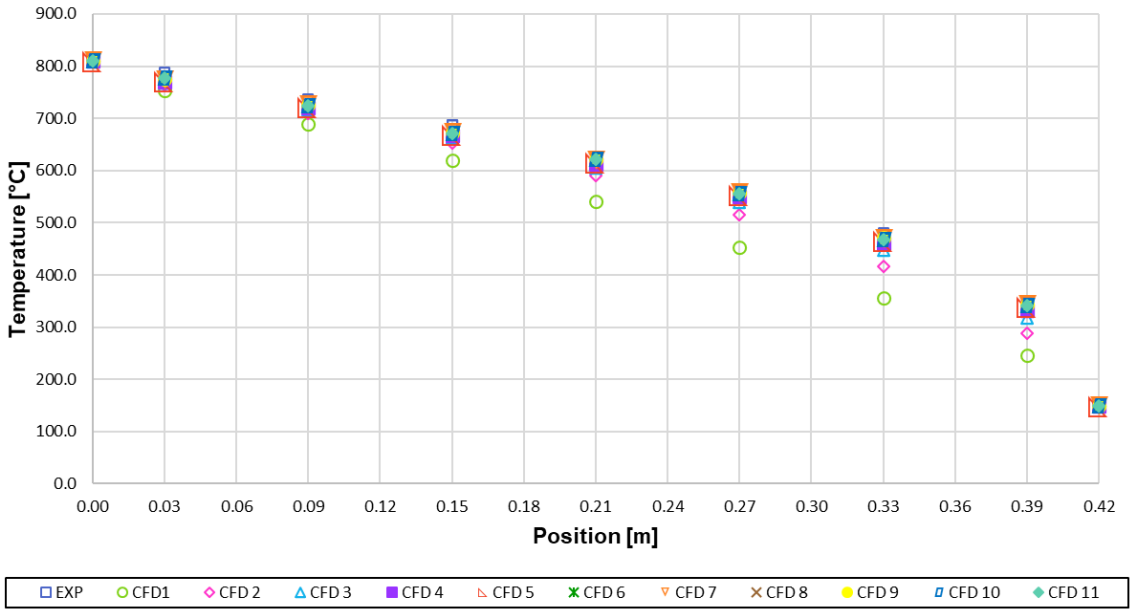

Fig. 19 Comparison between the experimental and CFD temperature distribution results for the various calibration iterations.

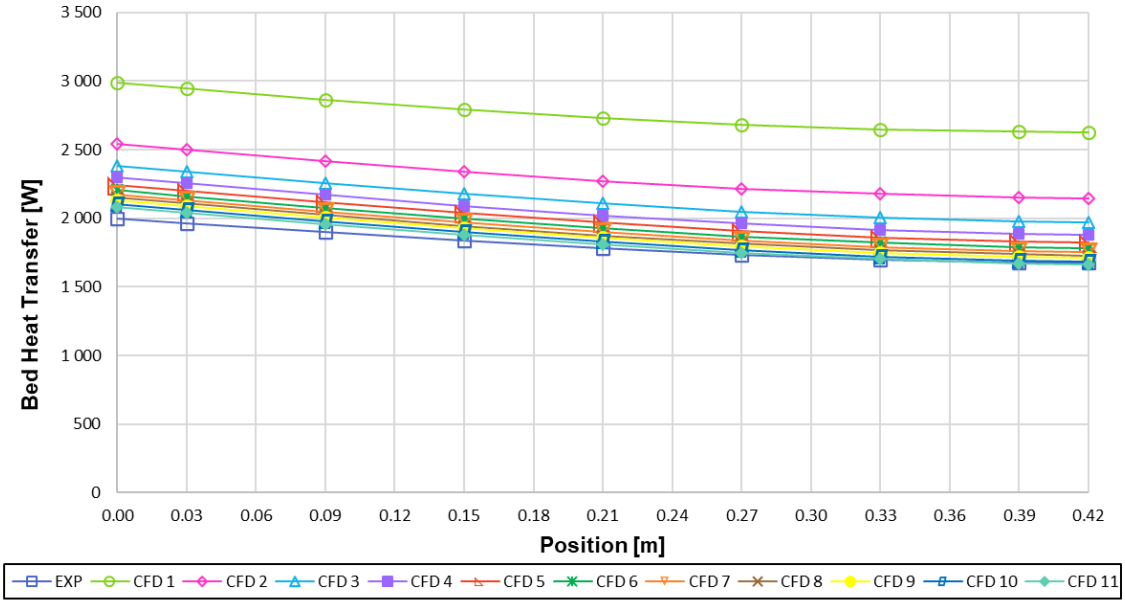

Fig. 20 Comparison between the experimental and CFD heat transfer distribution results for the various calibration iterations.

The temperature gradient distribution results derived for the various CFD iterations are presented in Fig. 21. The temperature gradient values of the calibrated CFD model are in reasonable agreement with the experimental results with an average percentage difference of 7.9 %. Next to the heated wall, up to a position of 0.09 m, the most significant difference between the numerical and experimental values are observed. The temperature gradient for the experiment is steeper than for the CFD model at higher temperatures. In the experimental study conducted by Rousseau *et al.* (2014) they concluded that the influence of the macro

temperature gradient on the effective thermal conductivity will be more pronounced at higher temperatures, therefore we can expect that the difference in the macro temperature gradient will also influence the derived effective thermal conductivity results.

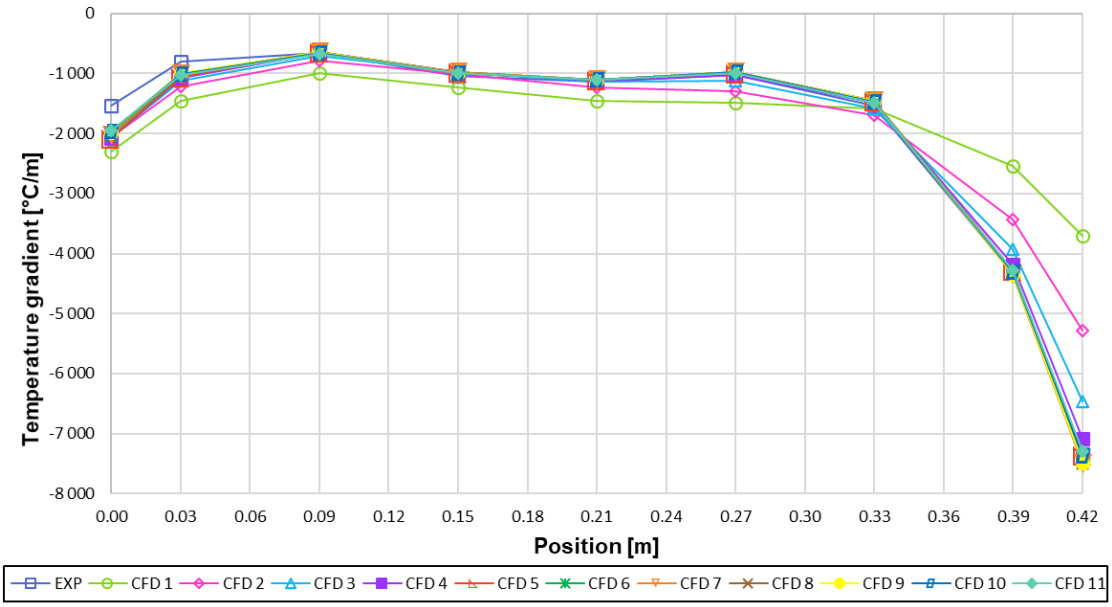

Fig. 21 Comparison between the experimental and CFD temperature gradient distribution results for the various calibration iterations.

The effective thermal conductivity results as a function of position derived for the various CFD calibration iterations are shown in Fig. 22. By adding contact resistances to the SC packed bed, the effective thermal conductivity values are in better agreement with the experimental values compared to the CFD model with no contact resistance as observed in Fig. 6 (b). The average percentage difference between the numerical and experimental effective thermal conductivity is 6.5 %. For the positions 0.09 m ≤ y ≤ 0.42 m the characteristic trend of the calibrated CFD effective thermal conductivity curve is similar to that of the experimental result with values slightly higher than the experimental values. As the temperature decreases towards the cooled wall, y = 0.42 m, the agreement between the numerical and experimental values improves. Next to the heated wall, 0 m ≤ y < 0.09 m, the experimental values are higher than that of the calibrated CFD model. Thus, at higher temperatures in the near-wall region the resistance in the numerical packed bed should be less (more conduction). Note that the higher experimental effective thermal conductivity values coincide with the steeper temperature gradient values observed in Fig. 21, this observation agrees with the conclusion made by Rousseau *et al.* (2014) that a steeper temperature gradient will result in a higher effective thermal conductivity.

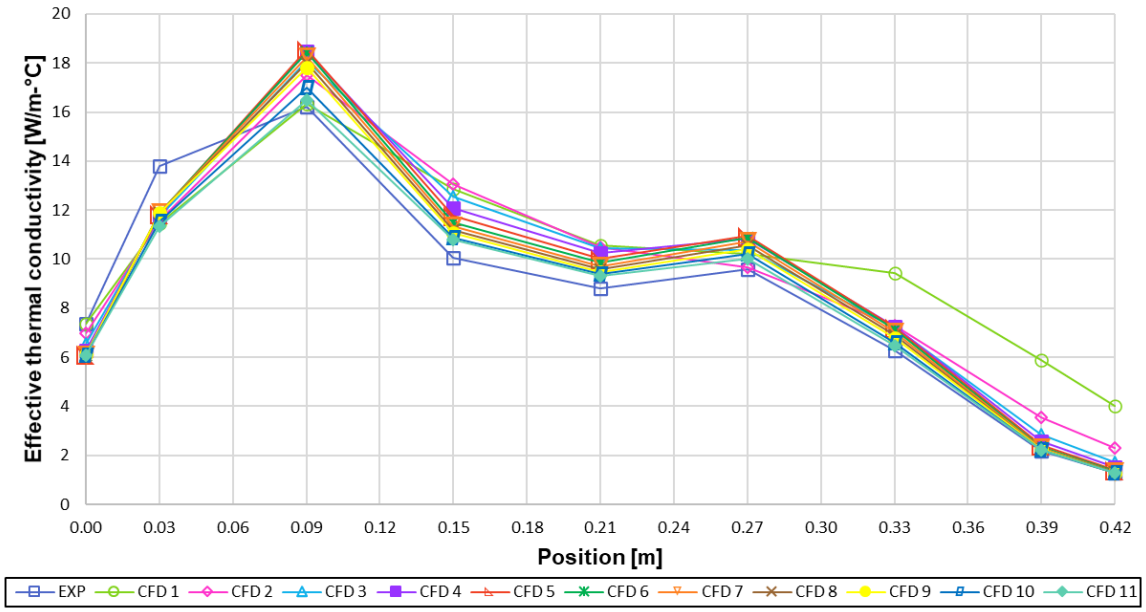

Fig. 22 Comparison between the experimental and CFD effective thermal conductivity results for the various calibration iterations.

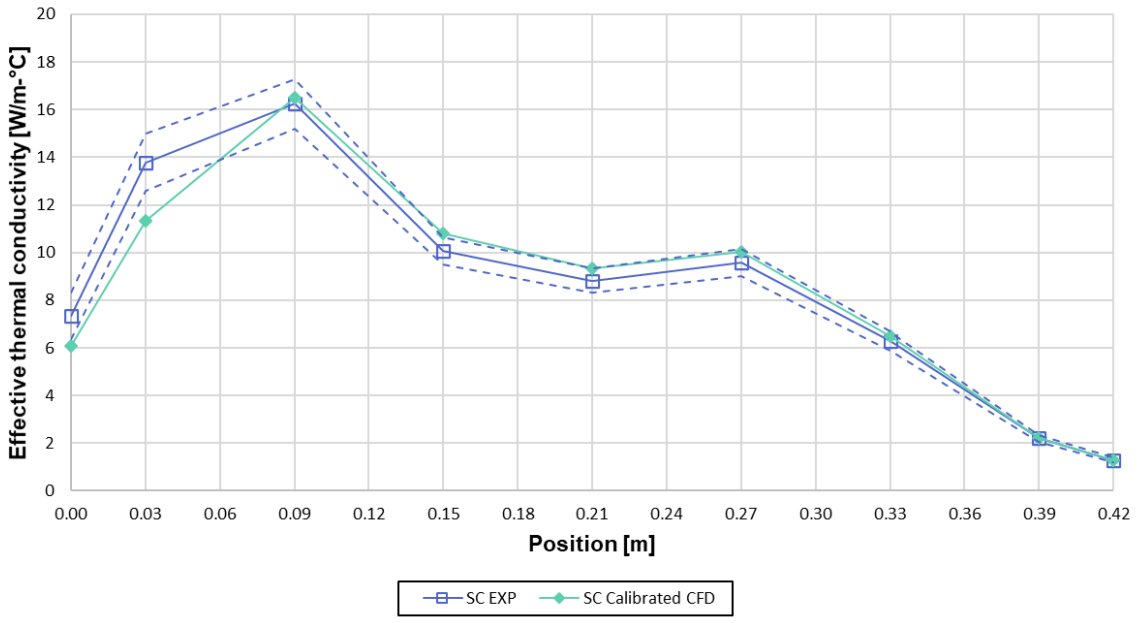

Fig. 23 Comparison between the experimental effective thermal conductivity results with error bands and the results obtained with the final calibrated CFD model (iteration 11).

The contact resistance functions derived through the calibration process did not deliver results in perfect agreement with the experimental test. However, the effective thermal conductivity for the calibrated CFD model falls within the expanded uncertainty with a confidence level of 95 % bands (dashed lines) of the experimental results for most of the packed bed, as can be seen in Fig. 23. The results illustrate that when the contact resistance is adjusted the comparison between the experimental and the CFD results improve. It was decided that for the purpose of the current study, where we aim to add and calibrate preliminary contact resistances to the CFD

model of our proposed methodology and determine if contact resistances influence the effective thermal conductivity trends observed, the current calibrated CFD model is sufficient. However, we know that contact resistance in a packed bed is a complex phenomenon, thus for future work the contact resistances should be studied in more detail and a more comprehensive regression approach should be used to obtain a more accurate description of the contact resistances.

It is also important to note that the calibrated contact resistance takes into account both radiation and conduction, thus at higher temperatures the dominant presence of radiation could influence the contact resistance results. It is therefore necessary to calibrate the contact resistance values for an experimental test case at lower temperatures, where radiation does not play a significant role and conduction is the dominant heat transfer mechanism. In our previous study (De Beer *et al.*, 2017) we observed that for the 400 °C NWTCTF test case, the conduction component was dominant throughout the packed bed when results were obtained with the uncalibrated CFD model. We know that in the experimental test combined radiation and conduction is naturally present and we cannot obtain experimental results which only consider conduction. However, to limit the influence of radiation we can consider experimental results at lower temperatures.

6. Conclusions

The restriction of conduction heat transfer through the contact area between pebble-pebble and pebble-wall contact points due to surface roughness and micro-contacts has a significant influence on the conduction contribution to the overall effective thermal conductivity of a packed pebble bed. For higher material thermal conductivity values and lower temperatures, where the contribution of radiation becomes less significant, the effect of contact resistances becomes more prominent. Various analytical and numerical approaches can be found in the literature to model the conduction heat transfer through the contact area. A thermal resistance network approach is popular in modeling conduction, where each of the conduction paths present in the contact region is modeled as an individual thermal resistance and the overall contact resistance is represented by a series or parallel combination of the individual resistances.

Previously the authors proposed a methodology to separate the contributions of conduction and radiation to the overall effective thermal conductivity, including the wall effects, by using a combination of experimental measurements and CFD simulations. In this study preliminary contact resistance values determined with the model of Bahrami *et al*. (2006) were added to the CFD model. The characteristic “peaks-and-dip” trend was still observed in the results for the SC

packed bed. The characteristic trends of the conduction and radiation components remained similar to the results obtained with the CFD model that did not take contact resistances into account. The conduction contribution increases with a decrease in temperature, whereas the contribution of radiation heat transfer becomes more significant at higher temperatures. The characteristic “peaks-and-dip” trend observed in the combined conduction and radiation effective thermal conductivity is still predominantly as a result of the interplay between the two heat transfer phenomena. The results demonstrate that the presence of contact resistances in the packed bed has a significant influence on the conduction heat transfer and therefore it indirectly also has an influence on the characteristic trend of the radiation component.

The results also demonstrate that the effect of the wall in the near-wall region has a notable influence on the radiation contribution whereas its influence on the conduction contribution is not as prominent. The effect of the wall cannot be associated with an altered packing structure in the near-wall region of the SC packed bed as in the case of a random packed bed, but the presence of the wall and the thermal radiation from the wall to pebbles also play an important role in the observed trend. The contact resistance values were adjusted through an iterative calibration process to obtain results in agreement with the NWTCTF experimental results. Although the contact resistance values specified are preliminary and needs to be refined and described in more detail, the results obtained with the calibrated CFD model demonstrates that the contact resistance can be used as an adjustable parameter to calibrate the CFD model in our proposed methodology. The results also demonstrate that the contact resistance has a significant influence on the effective thermal conductivity results, in particular the conduction contribution, and it can therefore not be neglected in the study of the effective thermal conductivity.

In future studies the conduction heat transfer through the contact area should be studied in more detail. This may require specifically designed experimental tests to develop a detailed model to describe the contact resistance functions, not only for the solid-solid interfaces between adjacent pebbles, but also for the contact areas between pebbles and the wall. The conduction heat transfer through the stagnant gas in the macro-gaps of the packed bed should also be included. At higher temperatures radiation can potentially influence the calibration of the contact resistance function, thus for the calibration of the CFD model experimental tests at lower temperatures should be used to limit the dominant effect of radiation heat transfer on the contact resistance function at higher temperatures. A more comprehensive regression approach should be used to obtain a more accurate description of the contact resistances for the calibration of the CFD model.

Nomenclature

a	Radius of contact area [m]
a_1, a_2	Empirical constants [-]
a_L	Radius of macro-contact area [m]
a_H	Radius of Hertzian contact area [m]
A_c	Total contact area [m^2]
A_r	Total area of point contacts [m^2]
A_v	Total area of fluid gaps in contact region [m^2]
c	Correction coefficient [-]
c_1, c_2	Vickers micro-hardness coefficient [GPa]
d_s	Overlap surface diameter [m]
E	Young's Modulus [Pa]
$E^{'}$	Effective Young's Modulus [Pa]
F^n	Normal contact force [N]
h_c	Conduction heat transfer coefficient for contact area [W/m^2-K]
H^*	$c_1\left(\sigma^{'}/m_{RMS}\right)^{c2}$ [GPa]
H_B	Brinell hardness [GPa]
H_{BGM}	Hardness constant [GPa]
H_{mic}	Vickers micro-hardness [GPa]
k_{CFD}	Bed effective thermal conductivity of the CFD model [W/m-K]
k_{cond}	Conduction component of effective thermal conductivity [W/m-K]
k_e^c	Effective thermal conductivity through solid and contact area [W/m-K]
k_{eff}	Effective thermal conductivity [W/m-K]
k_{EXP}	Bed effective thermal conductivity of the experiment [W/m-K]
k_g	Thermal conductivity of gas [W/m-K]
k_{ij}	Coefficient of thermal conductance of pipe [W/m-K]
k_p	Thermal conductivity of pebble solid material [W/m-K]
k_{rad}	Radiation component of effective thermal conductivity [W/m-K]
k_s	Thermal conductivity of solid material [W/m-K]
k_w	Thermal conductivity of wall solid material [W/m-K]
K^n	Normal contact stiffness coefficient [N/m]

L	Radius of unit cell [m]
L_r	Conduction thickness [m]
m	Surface slope [-]
m_{RMS}	Combined root mean squared surface slope [-]
M	Gas parameter [m]
N_A	Number of particles per unit area [-]
N_L	Number of particles per unit length [-]
P_0	Maximum contact pressure [Pa]
$P_{0,H}$	Hertzian contact pressure [Pa]
Q	Heat transfer rate [W]
$\dot{Q}_c$	Heat transfer through particle-particle contact point [W]
$\dot{Q}_r$	Heat transfer through solid-solid region of contact point [W]
$\dot{Q}_v$	Heat transfer through fluid gaps in contact area [W]
$\dot{Q}_w$	Heat transfer though particle-wall contact point [W]
r_0	Radius of contact area [m]
r_c	Particle-particle contact radius [m]
$r_c^{'}$	Reduced particle-particle contact radius [m]
r_p	Initial sphere radius [m]
$r_{p,0}$	Particle / Sphere radius [m]
R	Thermal resistance [K/W]
R_c	Inner solid resistance [K/W]
R_{cond}	Conduction thermal resistance [W/m-K]
R_{cont}	Contact resistance [K/W]
R_L	Macro-contact constriction/spreading resistance [K/W]
R_g	Resistance of the interstitial gas in the micro-gap [K/W]
R_G	Resistance of the interstitial gas in the macro-gap [K/W]
R_j	Overall joint contact resistance [K/W]
R_s	Micro-contact constriction/spreading resistance [K/W]
RA_{cont}	Contact resistance [m^2-K/W]
s	Distance between centers of two particles / spheres [m]
S	Packing structure constant [-]
T	Temperature [K]

y	Position in the packed bed measured from the heated wall [m]
α	Non-dimensional parameter [-]
δ^n	Normal relative contact displacement [m]
ε	Bed strain [-]
κ	Non-dimensional parameter [-]
ϕ	Deformation angle [rad]
ρ	Equivalent radius of curvature [m]
σ	Surface roughness [m]
σ'	σ_{RMS}/σ_0 , $\sigma_0 = 1$ µm
σ_{RMS}	Combined root mean squared surface roughness [m]
υ	Poisson ratio [-]
ζ	Correction factor [-]

Abbreviations

BCC	Body Centered Cubic
BEM	Boundary Element Method
CFD	Computational Fluid Dynamics
DEM	Discrete Element Method
DPS	Discrete Particle Simulation
FCC	Face Centered Cubic
HTTU	High Temperature Test Unit
MSUC	Multi Sphere Unit Cell
NWTCTF	Near-wall Thermal Conductivity Test Facility
SC	Simple Cubic
TDEM	Thermal Discrete Element Method

Subscripts

i	Particle i
j	Particle j
p	Particle

w	Wall
1	Particle / Surface 1
2	Particle / Surface 2

References

Asakuma, Y., Asada, M., Kanazawa, Y. & Yamamoto, T. 2016. Thermal analysis with contact resistance of packed bed by a homogenization method. *Powder Technology*, 291:46-51.

Asakuma, Y., Kanazawa, Y. & Yamamoto, T. 2014. Thermal radiation analysis of packed bed by a homogenization method. *International Journal of Heat and Mass Transfer*, 73(2014):97-102.

Asif, M., Tariq, A. & Singh, K.M. 2019. Estimation of thermal contact conductance using transient approach with inverse heat conduction problem. *Heat and Mass Transfer*, 55:3243-3264.

Bahrami, M., Culham, J.R. & Yovanovich, M.M. 2004. Modeling Thermal Contact Resistance: A Scale Analysis Approach. *Journal of Heat Transfer*, 126:896-905.

Bahrami, M., Yovanovich, M.M. & Culham, J.R. 2005. Thermal contact resistance at low contact pressure: Effect of elastic deformation. *International Journal of Heat and Mass Transfer*, 48:3284-3293.

Bahrami, M., Yovanovich, M.M. & Culham, J.R. 2006. Effective thermal conductivity of rough spherical packed beds. *International Journal of Heat and Mass Transfer*, 49:3691-3701.

Batchelor, G.K. & O'Brien, R.W. 1977. Thermal or electrical conduction through a granular material. *Proceedings of the Royal Society of London. Series A - Mathematical and Physical Sciences*, 355(1682):313-333.

Beaulieu, C., Vidal, D., Yari, B., Chaouki, J. & Bertrand, F. 2021. Impact of surface roughness on heat transfer through spherical particle packed beds. *Chemical Engineering Science*, 231:116256-116277.

Breitbach, G. & Barthels, H. 1980. The radiant heat transfer in the high temperature reactor core after failure of the afterheat removal systems. *Nuclear Technology*, 49:392-399.

Brosh, T. & Levy, A. 2010. Modeling of Heat Transfer in Pneumatic Conveyor Using a Combined DEM-CFD Numerical Code. *Drying Technology*, 28:155-164.

Chen, L., Chen, Y., Huang, K. & Liu, S. 2016. Investigation of effective thermal conductivity for pebble beds by one-way coupled CFD-DEM methods for CFETR WCCB. *Fusion Engineering and Design*, 106(2016):1-8.

Cheng, G., Gan, J., Xu, D. & Yu, A. 2020. Evaluation of effective thermal conductivity in random packed bed: Heat transfer through fluid voids and effect of packing structure. *Powder Technology*, 361:326-336.

Cheng, G.J. & Yu, A.B. 2013. Particle Scale Evaluation of the Effective Thermal Conductivity from the Structure of a Packed Bed: Radiation Heat Transfer. *Industrial and Engineering Chemistry Research*, 52:12202-12211.

Cheng, G.J., Yu, A.B. & Zulli, P. 1999. Evaluation of effective thermal conductivity from the structure of a packed bed. *Chemical Engineering Science*, 54:4199-4209.

Chen, C.K. & Tien, C.L. 1973. Conductance of packed spheres in vacuum. *Journal of Heat Transfer*, 95(1973):302-308.

De Beer, M. 2014. Characterization of thermal radiation in the near-wall region of a packed pebble bed. Potchefstroom, South Africa: North-West University. (Masters Dissertation).

De Beer, M., Du Toit, C.G. & Rousseau, P.G. 2017. A methodology to investigate the contribution of conduction and radiation heat transfer to the effective thermal conductivity of packed graphite pebble beds, including the wall effect. *Nuclear Engineering and Design*, 314:67-81.

De Beer, M., Du Toit, C.G. & Rousseau, P.G. 2018b. Experimental study of the effective thermal conductivity in the near-wall region of a packed pebble bed. *Nuclear Engineering and Design*, 339:253-268.

De Beer, M., Rousseau, P.G. & Du Toit, C.G. 2018a. A review of methods to predict the effective thermal conductivity of packed pebble beds, with emphasis on the near-wall region. *Nuclear Engineering and Design*, 331:248-262.

Dixon, A., Gurnoon, A., Nijemeisland, M. & Stitt, E. 2013. CFD testing of the pointwise use of the Zehner-Schlünder formulas for fixed-bed stagnant thermal conductivity. *International Communication in Heat and Mass Transfer*, 42:1-4.

Gan, Y. & Kamlah, M. 2010. Thermo-mechanical modelling of pebble bed-wall interfaces. *Fusion Engineering and Design*, 85(2010):24-32.

Kaviany, M. 1991. Principles of heat transfer in porous media. (New York, USA: Springer-Verlag. p. 126-127).

Kiani-Oshtorjani, M. & Jalali, P. 2019. Thermal discrete element method for transient heat conduction in granular packing under compressive forces. *International Journal of Heat and Mass Transfer*, 145:118753.

Liang, Y. & Li, X. 2014. A new model for heat transfer through the contact network of randomly packed granular material. *Applied Thermal Engineering*, 73(2014):984-992.

Liang, Y., Niu, H. & Lou, Y. 2016. Expression for ETC of the solid phase of randomly packed granular materials. *Applied Thermal Engineering*, 109(2016):44-52.

Madhusudana, C.V. 1995. Thermal Contact Conductance. Springer.

Panchal, M.C.P., Van Lew, J. & Ying, A. 2016. Numerical modelling for the effective thermal conductivity of lithium meta titanate pebble bed with different packing structures. *Fusion Engineering Design*, 112:303-310.

Ren, C., Yang, X., Jia, H., Jiang, Y. & Xiong, W. 2017. Theoretical analysis of effective thermal conductivity for the Chinese HTR-PM heat transfer test facility. *Applied Sciences*, 7(1)

Rousseau, P.G., Du Toit, C.G., Van Antwerpen, W. & Van Antwerpen, H.J. 2014. Separate effects tests to determine the effective thermal conductivity in the PBMR HTTU test facility. *Nuclear Engineering and Design*, 271:444-458.

Rousseau, P.G. & Van Staden, M. 2008. Introduction to the PBMR heat transfer test facility. *Nuclear Engineering and Design*, 238:3060-3072.

Suarez, F., Luzi, C.D., Mariani, N.J. & Barreto, G.F. 2017. Effective parameters for conductive contributions to radial heat transfer in fixed beds under stagnant conditions. *Chemical Engineering Research and Design*, 119:245-262.

Talukdar, P., Mendes, M.A.A., Parida, R.K., Trimis, D. & Ray, S. 2013. Modelling of conduction-radiation in a porous medium with blocked-off region approach. *Journal of Thermal Sciences*, 72(2013):102-114.

Tsory, T., Ben-Jacob, N., Brosh, T. & Levy, A. 2013. Thermal DEM-CFD modeling and simulation of heat transfer through packed bed. *Powder Technology*, 244(2013):52-60.

Van Antwerpen, W. 2009. Modelling the effective thermal conductivity in the near-wall region of a packed pebble bed. Potchefstroom Campus, South Africa: North-West University. (PhD Thesis).

Van Antwerpen, W., Du Toit, C.G. & Rousseau, P.G. 2010. A review of correlations to model the packing structure and effective thermal conductivity in packed beds of mono-sized spherical particles. *Nuclear Engineering and Design*, 240:1803-1818.

Van Antwerpen, W., Rousseau, P.G. & Du Toit, C.G. 2012. Multi-sphere Unit Cell model to calculate the effective thermal conductivity in packed pebble beds of mono-sized spheres. *Nuclear Engineering and Design*, 247:183-201.

Van Lew, J.T. 2016. On Thermal Characterization of Breeder Pebble Beds with Microscale Numerical Modeling of Thermofluid and Pebble-pebble Interactions. Los Angeles: University of California. (PhD Thesis).

Wang, X., Zheng, J. & Chen, H. 2016a. A prediction model for the effective thermal conductivity of mono-sized pebble beds. *Fusion Engineering and Design*, 103(2016):136-151.

Wang, X., Zheng, J. & Chen, H. 2016b. Application of a model to investigate the effective thermal conductivity of randomly packed fusion pebble beds. *Fusion Engineering and Design*, 106(2016):40-50.

Wu, H., Gui, N., Yang, X., Tu, J. & Jiang, S. 2017. Numerical simulation of heat transfer in packed pebble beds: CFD-DEM coupled with particle thermal radiation. *International Journal of Heat and Mass Transfer*, 110(2017):393-405.

Yamoah, S., Akaho, E.H.K., Ayensu, N.G.A. & Asamoah, M. 2012. Analysis of fluid flow and heat transfer model for pebble bed high temperature gas cooled reactor. *Research Journal of Applied Sciences, Engineering and Technology*, 4(12):1659-1666.

Zhou, J., Yu, A. & Zhang, Y. 2007. A boundary element method for evaluation of the effective thermal conductivity of packed beds. *Journal of Heat Transfer*, 129:363-371.

Zhou, Z.Y., Yu, A.B. & Zulli, P. 2010. A new computational method for studying heat transfer in fluid bed reactors. *Powder Technology*, 197:102-110.

6. Summary and conclusions

The effective thermal conductivity in the near-wall region of a packed pebble bed reactor forms part of the critical heat flow path during the decay heat removal process. Therefore, for the design of pebble bed gas-cooled and solid fuel molten salt-cooled generation IV reactors, it is imperative to properly understand and assess this phenomenon.

The ZBS (Bauer & Schlünder, 1978) and the IAEA ZS Total (Niessen & Ball, 2000) correlations are commonly used to predict the effective thermal conductivity in packed pebble beds. These widely used correlations are valid for the bulk region but breaks down in the near-wall region. As shown in chapter 2, the comparison between the results of these correlations and experimental results prove that the conclusion of Bauer & Schlünder (1978), that the wall effects can be neglected, is not valid.

From the literature review presented in chapter 2 it is evident that none of the current methods that account for conduction and radiation heat transfer properly addresses the near-wall effects. The MSUC model is the closest to a comprehensive model. However, its long-range radiation component is only applicable to the bulk region and should be developed further. Therefore, a need still exists for a complete model of the effective thermal conductivity that takes into account the effects of the altered packing structure in the near-wall region.

The development of a comprehensive model for effective thermal conductivity should be based on a better understanding of the underlying phenomena and the interplay between them, especially in the near-wall region. Some studies reported in literature do distinguish between the different components, but do not necessarily investigate the underlying phenomena and interactions.

In chapter 3 of this thesis a custom designed test facility with extensive new empirical results were introduced. In chapter 4 an accompanying methodology was proposed to separate the effects of conduction and radiation on the effective thermal conductivity in a packed pebble bed consisting of graphite spheres of uniform size, which includes the wall effects.

For both heat transfer phenomena the near-wall effects have a notable influence. The conduction is reduced due to the higher porosity, which implies that there is less pebble material and fewer contact points between adjacent pebbles. The radiation is also reduced due to the reduction in pebble surface area exposed to radiation at higher porosity. The conduction increases at lower temperatures due to the characteristic increase in the graphite thermal conductivity and therefore the wall effect is more prominent for conduction on the low

temperature side of the bed. The radiation naturally increases at higher temperatures and therefore the wall effect is more prominent for radiation on the high temperature side of the bed.

The interplay between the radiation and conduction phenomena results in the characteristic “peaks-and-dip” trend in the combined conduction and radiation effective thermal conductivity that is observed in the results obtained from both the HTTU and NWTCTF experiments.

In chapter 5 it is shown that the restriction of conduction heat transfer through the contact areas between pebble-pebble and pebble-wall contact points has a significant influence on the conduction contribution to the overall effective thermal conductivity of a packed pebble bed. For higher material thermal conductivity values and lower temperatures, where the contribution of radiation becomes less significant, the effect of contact resistances becomes more prominent. Given this, contact resistance values determined with the model of Bahrami *et al*. (2006) were added to the CFD model.

The characteristic “peaks-and-dip” trend was still observed in the results for the SC packed bed and the characteristic trends of the conduction and radiation components remained similar to the results obtained without the contact resistances taken into account. The conduction contribution increases with a decrease in temperature, whereas the contribution of radiation heat transfer becomes more significant at higher temperatures. The characteristic “peaks-and-dip” trend observed in the total effective thermal conductivity is still predominantly due to the interplay between the two heat transfer phenomena. The results demonstrate that the presence of contact resistances in the packed bed has a significant influence on the conduction heat transfer and therefore it indirectly also has an influence on the characteristic trend of the radiation component.

Recommendations for further research

Recommendations for future investigations of the conduction and radiation heat transfer in the near-wall region of a packed pebble bed using the developed methodology are given in the following points:

- The current design of the NWTCTF test section include the wall effects of the top, bottom and side insulated walls that surround the packed bed. It would be beneficial to eliminate the effects of the altered packing structure due to these walls in future experimental tests. These wall effects can also be eliminated by applying the final methodology to a CFD model with only one near-wall region.

- A larger experimental data set at higher temperatures of up to 1600 °C should be obtained which can be used together with the presented methodology to gather valuable insight into the radiation contribution to the effective thermal conductivity, as the contribution of radiation becomes more significant at higher temperatures.
- The focus of this study was on a packed bed of graphite spheres with a particle diameter of 60 mm as one would find in Pebble Bed Gas-cooled Reactors. By conducting additional experimental tests using pebbles that consist of different materials and particle sizes, the effect of various material thermal conductivities and emissivity values as well as particle sizes on the effective thermal conductivity can be determined and the methodology presented here can be used for different applications.
- The conduction heat transfer through the contact area at the solid-solid contact points in a packed bed should be studied in more detail. Experimental tests should be designed and conducted which focus on gaining a better understanding of the contact resistances by using various applied forces and different surface roughness values for various packing structures in both the bulk and near-wall regions. Experimental tests should be conducted at lower temperatures where the contribution of conduction to the effective thermal conductivity becomes prominent. The conduction through the stagnant gas in the macro-gaps of the packed bed should also be considered.
- A detailed contact resistance model for the bulk and near-wall regions of the packed bed should be developed from the experimental data and applied to the CFD model of the developed methodology. Contact resistance can also be a function of local contact point features such as sphere surface roughness and shape imperfections due to previous use, which can directly influence the contact force between specific spheres throughout the packed bed. Although the influence of these local features on the contact resistance would be impossible to predict precisely, it would be beneficial to account for these effects in future research by introducing an uncertainty range for contact resistance values. A more comprehensive regression approach should be used for the calibration of the CFD model.
- The change in the isotherm pattern of the conductive geometry was not considered in the current study when considering radiation heat transfer across the spaces of the geometry. The isotherm pattern for the radiation-conduction case will differ from the isotherm pattern for the conduction-only case of the packed bed. This change in isotherm pattern should be taken into account in future work when separating the radiation-conduction and conduction-only effective thermal conductivities.
- With additional experimental data that eliminate the effects of the side walls and a detailed contact resistance model applied to the CFD model, the developed methodology can be applied to obtain final archival results that describe the characteristics of the conduction and

radiation contributions to the overall effective thermal conductivity in the near-wall region for different packing structures. The final archival data can then be used to develop detailed effective thermal conductivity models which are specifically applicable to the near-wall region.

Appendix A - Experimental data and uncertainty analyses

The theoretical background of the methods used by Van Antwerpen *et al.* (2010) and Rousseau *et* al. (2014) for the calculation of the temperature distribution and temperature gradient functions for the experimental results of the HTTU test facility, with its associated uncertainties, is presented in the following section. The methodology was applied to the NWTCTF experimental data to extract the effective thermal conductivity results.

A.1 Derivation of temperature gradient function

A method was required to determine the local temperature gradient of the HTTU experimental temperature distribution, without the local temperature variations resulting in large uncertainties in the temperature gradient. Van Antwerpen *et al.* (2010b) proposed the least-squares fitting of a polynomial to the set of temperature data and by differentiating the polynomial the temperature gradient was determined.

A short description of the derivation of the polynomial curve fit is given in the following section. For a more detailed derivation consult Van Antwerpen *et al.* (2010b). The power-series polynomial, $T(x)$, shown in Eq. (6) is fitted to a set of experimental data, (x_i, T_i)

$$\begin{aligned} T(x) &= a_0 x^0 + a_1 x^1 + a_2 x^2 + \ldots + a_m x^m \\ \therefore T(x) &= \sum_{k=0}^{m} a_k x^k \end{aligned} \tag{6}$$

where a_0 to a_m are the coefficients of the polynomial and *m* is the order of the polynomial.

Define the function $f_k(x)$ as $f_k(x) = x^k$ and rewrite Eq. (6) as:

$$T(x) = \sum_{k=0}^{m} a_k f_k(x) \tag{7}$$

The coefficients of the polynomial are determined from the solution of the system of equations shown in Eq. (8).

$$\bar{\beta} = \alpha \bar{a} \tag{8}$$

For a data set with *N* data points $\bar{\beta}$ and α are defined as

$$\beta_k = \sum_{i}^{N} T_i x_i^k \tag{9}$$

and

$$\alpha_{lk} = \sum_{i}^{N} x_i^l x_i^k \tag{10}$$

Let ε be the inverse matrix of α then for the polynomial the fitted function is given in Eq. (11).

$$\mathrm{T}(x) = \bar{\beta}^T \varepsilon^T \bar{f}$$

$$\therefore T(x) = \left[\beta_0, \beta_1, \beta_2, \cdots, \beta_m\right] \begin{pmatrix} \varepsilon_{00} \cdots \varepsilon_{0m} \\ \vdots \\ \varepsilon_{m0} \cdots \varepsilon_{mm} \end{pmatrix} \begin{bmatrix} x^0 \\ x^1 \\ x^2 \\ \vdots \\ x^m \end{bmatrix} \tag{11}$$

The slope of the regression function is determined by differentiating Eq. (11).

$$b(x) = \frac{dT(x)}{dx} = \left[\beta_0, \beta_1, \beta_2, \cdots, \beta_m\right] \begin{pmatrix} \varepsilon_{00} \cdots \varepsilon_{0m} \\ \vdots \\ \varepsilon_{m0} \cdots \varepsilon_{mm} \end{pmatrix} \begin{bmatrix} 0 \\ 1 \\ 2x \\ 3x^2 \\ \vdots \\ mx^{m-1} \end{bmatrix} \tag{12}$$

A.2 Uncertainty of temperature gradient function

The uncertainty of the regression function must be calculated. The pointwise variance in the fit at a point *x*, is described by the function $u^2(x)$ shown in Eq. (13).

$$u^2(x) = \left(\frac{\partial T(x)}{\partial T_1}\right)^2 u_1^2 + \left(\frac{\partial T(x)}{\partial T_2}\right)^2 u_2^2 + \cdots + \left(\frac{\partial T(x)}{\partial T_N}\right)^2 u_N^2$$

$$u^2(x) = \sum_{i=1}^{N} \left(\frac{\partial T(x)}{\partial T_i}\right)^2 u_i^2 \tag{13}$$

Eq. (9) is substituted into Eq. (11) in order to determine the derivative shown in Eq. (14).

$$\frac{\partial T(x)}{\partial T_i} = \left[1, x_i, \mathrm{x}_i^2, \cdots, x_i^m\right] \begin{pmatrix} \varepsilon_{00} \cdots \varepsilon_{0m} \\ \vdots \\ \varepsilon_{m0} \cdots \varepsilon_{mm} \end{pmatrix} \begin{bmatrix} x^0 \\ x \\ x^2 \\ \vdots \\ x^m \end{bmatrix} \tag{14}$$

$$\therefore \frac{\partial T(x)}{\partial T_i} = \sum_{k=0}^{m} \left(x_i^k \sum_{j=0}^{m} \varepsilon_{kj} x^j\right)$$

Substitute Eq. (14) into Eq. (13):

$$u^2(x) = \sum_{i=1}^{N}\left(\sum_{k=0}^{m}\left(x_i^k \sum_{j=0}^{m}\varepsilon_{kj}x^j\right)\right)^2 u_i^2 \tag{15}$$

The data point uncertainty, u_i^2, is the sum of the measurement uncertainty and the scatter uncertainty.

$$u_i^2 = u_{measurement,i}^2 + u_{scatter,i}^2 \tag{16}$$

The measurement uncertainty includes the statistical variance and the instrument and drift uncertainty.

$$u_{measurement,i}^2 = u_{instrument,i}^2 + \frac{\sum_{i=1}^{N}(T_i - \overline{T})^2}{N-1} + u_{drift,i}^2 \tag{17}$$

Initially Van Antwerpen *et al.* (2010b) considered determining the uncertainty in the calculated temperature gradient using a perturbation analysis, but it would have required a significant programming effort with a large margin for error. Therefore analytical methods for the uncertainty calculation were found to be easier and more practical to implement. A detailed derivation of an uncertainty equation for the slope of the polynomial is given by Van Antwerpen *et al.* (2010b). The uncertainty in the slope of the regression function, $b(x)$, is given in Eq. (18).

$$\sigma^2(b(x)) = \sum_{i=1}^{N}\left(\frac{\partial b(x)}{\partial T_i}\right)^2 \sigma_i^2 \tag{18}$$

The derivative shown in Eq. (18) was calculated as:

$$\frac{\partial \mathrm{b}(x)}{\partial T_i} = \left[1, \mathrm{x}_i, \mathrm{x}_i^2, \cdots, \mathrm{x}_i^m\right]\begin{pmatrix}\varepsilon_{00}\cdots\varepsilon_{0m}\\ \vdots \\ \varepsilon_{m0}\cdots\varepsilon_{mm}\end{pmatrix}\begin{bmatrix}0\\1\\2x\\3x^2\\\vdots\\mx^{m-1}\end{bmatrix}$$

$$\therefore \frac{\partial b(x)}{\partial T_i} = \sum_{k=0}^{m}\left(x_i^k \sum_{j=0}^{m}\varepsilon_{kj} j x^{j-1}\right) \tag{19}$$

Substitute Eq. (19) into Eq. (18) to obtain the uncertainty in the slope of the fitted curve:

$$\sigma^2(b(x)) = \sum_{i=1}^{N}\left(\sum_{k=0}^{m}\left(x_i^k \sum_{j=0}^{m}\varepsilon_{kj} j x^{j-1}\right)\right)^2 \sigma_i^2 \tag{20}$$

Other methods for the calculation of the temperature gradient were also considered by Van Antwerpen *et al.* (2010b). The point-by-point finite difference method did not work due to the combination of varying space between measurement points and measurement uncertainty. Piecewise least-squares fitting of straight lines to the data presented better results than that obtained by the point-by-point difference method as it has a better capability of handling scattered data. However, the uncertainty results were still much bigger than that given by the polynomial method.

It is important to note that the uncertainty in the polynomial fit is proportional to the order of the polynomial (Van Antwerpen *et al.*, 2010), thus higher-order polynomial terms will magnify the uncertainty in the input parameters as well as roundoff errors. If only the goodness-of-fit is assessed, higher polynomial orders will always be better than lower polynomial orders. Therefore, it is important to find the polynomial order which delivers results with the best balance between goodness-of-fit and output uncertainty.

A.3 Uncertainty of effective thermal conductivity

Van Antwerpen (2009) used Eq. (21) to determine the effective thermal conductivity values once the heat flux distribution and temperature gradient were known as functions of the radial position in the packed pebble bed.

$$k_{eff} = -\frac{Q_{bed}}{A\,dT/dr} \tag{21}$$

The uncertainty associated with the effective thermal conductivity values was calculated using Eq. (22):

$$u(k_{eff}) = \sqrt{\left[\frac{\partial(k_{eff})}{\partial Q_{bed}} \cdot u(Q_{bed})\right]^2 + \left[\frac{\partial(k_{eff})}{\partial(dT/dr)} \cdot u(dT/dr)\right]^2} \tag{22}$$

with the partial derivatives shown in Equations (23) and (24) respectively.

$$\frac{\partial(k_{eff})}{\partial Q_{bed}} = \frac{-1}{A\,dT/dr} \tag{23}$$

$$\frac{\partial(k_{eff})}{\partial(dT/dr)} = \frac{Q_{bed}}{A(dT/dr)^2} \tag{24}$$

A detailed description of the method used to obtain the uncertainty associated with the effective thermal conductivity values is provided by Van Antwerpen (2009).

References

Rousseau, P.G., Du Toit, C.G., Van Antwerpen, W. & Van Antwerpen, H.J. 2014. Separate effects tests to determine the effective thermal conductivity in the PBMR HTTU test facility. *Nuclear Engineering and Design*, 271(2014):444-458.

Van Antwerpen, H.J., Rousseau, P.G. & Du Toit, C.G. 2010. The extraction of the temperature gradient from measured temperature profiles with uncertainty propagation as applied to the High Temperature Test Unit. (*In* Seventh South African Conference on Computational and Applied Mechanics. Pretoria.)